ROLE OF MITOCHONDRIAL PYRUVATE CARRIER IN OVARIAN CANCER PROGRESSION

Mohamed Rufaik Yasim Farook

Submitted to Swansea University Medical School in fulfilment of the requirements for the degree of Doctor of Philosophy

Swansea University
Prifysgol Abertawe

2021

Declarations & Statements

This work has not previously been accepted in substance for any degree and is not being concurrently submitted in candidature for any degree.

Signed ...[redacted]

Date: 31-07-2021

STATEMENT 1

This thesis is the result of my own investigations, except where otherwise stated. Where correction services have been used, the extent and nature of the correction is clearly marked in a footnote(s).

Other sources are acknowledged by footnotes giving explicit references. A bibliography is appended.

Signed ..[redacted]

Date : 31-07-2021

STATEMENT 2

I hereby give consent for my thesis, if accepted, to be available for photocopying and for inter-library loan, and for the title and summary to be made available to outside organisations.

Signed .[redacted]

Date: 31-07-2021

NB: *Candidates on whose behalf a bar on access has been approved by the University (see Note 7), should use the following version of Statement 2:*

I hereby give consent for my thesis, if accepted, to be available for photocopying and for inter-library loans **after expiry of a bar on access approved by the Swansea University.**

Signed .....[redacted]

Date: 31-07-2021

Abstract

Ovarian cancer is the sixth most common cause of cancer deaths in females in the UK. High-grade serous ovarian cancer (HGSOC) comprises 75% of ovarian epithelial carcinomas. Patients with HGSOC initially respond well to platinum-based chemotherapy, but most relapse with the therapy-resistant disease. Cancer cells that adapt to their metabolic microenvironment, known as "metabolic flexibility", are more likely to proliferate, metastasise, and be resistant to therapy. Mitochondrial pyruvate carrier (MPC) is responsible for transporting pyruvate, generated through glycolysis, into mitochondria to enable oxidative phosphorylation (OXPHOS). Up to 80% of ovarian cancers have deleted *MPC1* expression, which correlates strongly with poor prognosis across a wide variety of cancers. Here, I hypothesised that depletion of MPC might force ovarian cancer cells to use glutamine as a fuel source enabling their survival in glucose-limited environments.

Using ovarian cancer cell lines characterised as MPC1 lacking PEO1 and PEO4 (derived from the same patient), glutamine-addicted (SKOV3) or glutamine-independent (OVCAR3) as exemplars, the role of MPC1 on ovarian cancer cell metabolism was investigated by stable isotope tracing analysis, quantitative real-time PCR, Western blotting, and metabolic assays. This study revealed, innately MPC1-lacking PEO4 cells are able to utilise OXPHOS from glycolytic pyruvate via MPC2 homodimer. However, MPC1 knockdown in OVCAR3 cells is capable of re-purposing amino acid metabolism and yield TCA cycle intermediates from non-carbohydrate precursors for cancer cell survival and metastasis. Moreover, OVCAR3 cells are able to use proline to compensate for the loss of glutamine under the MPC1-depleted state. Exogenous proline availability to MPC1-depleted cells not just rescued cells under nutrient starvation but also enhanced the ECM development in OVCAR3 cells. It is now evident that the observed >80% deletion of *MPC1* in HGSOCs mediates not just cancer proliferation but possibly therapy-resistant tumours via upregulating ECM proteins. Here, I show ovarian cancer cells delete MPC1 to increase amino acid metabolism for the dual advantage of conquering carbon and nitrogen limitations and to exhibit an aggressive phenotype while maintaining a quiescent state TCA cycle.

Table of Contents

List of figures

List of Tables

Acknowledgements

Where should I start? Perhaps I should start with the most satisfying story title, "Three Little Pigs", which helped me plan my work, not just in PhD but also in day to day life. Thank you, Professor Martin Sheldon for introducing me to the story. The past four years have been the most challenging part of my life so far. But, honest to God, I enjoyed every single second of my PhD research, including the laboratory gossips which kept me entertained. Firstly, this PhD wouldn't have been possible without my supervisors Dr James Cronin and Professor Martin Sheldon. I would like to thank Dr James Cronin for allowing me to obtain the PhD degree and PUTTING UP with me. When I say, "I promise to", he knows what it means. I was so lucky during my PhD to be personally trained by my primary supervisor Dr Cronin. He taught me every technique he learned, and inspired me to shadow fellow colleagues to learn useful experimental methods for future. I appreciate the advice from Prof. Sheldon and Dr Cronin which will help me throughout my career. Both of them have been excellent.

I would like to thank all the members of Professor Martin Sheldon's group. Mainly Dr Sian Owens and Dr Matthew Turner, who helped me a lot with specific laboratory techniques. The results highlight my research wouldn't have been possible without Dr Nick Jones, Dr Emma Vincent (Bristol University) and the chemistry department of McGill University, Canada. Dr Nick Jones played a major role in my PhD, and I am forever grateful for his help and guidance. Not sure why students think he is scary, but he is not. I take this opportunity to thank Professor Venkat Kanamarlapudi, Dr Salman Jahromi, and Dr Ben Skalkoyannis for their support. To all the fourth-floor laboratory research students and staff who helped on my project, a big thank you to you all. Most of you have been excellent with me. Of course, late-night laboratory work wouldn't have been possible if some of you weren't there. I would like to apologise to Dr Martin Clift for putting up with my banter in Dr Cronin's office, and again, I am grateful for his advice and support.

Some of the data were generated with the help of mentoring students and the PhD students. I would like to sincerely thank Zack Croxford (MSci. student) and James Hamer (PhD student) of Dr Cronin's group for their help in generating some of the

data for my PhD. I would like to take this opportunity to thank Dr Cronin's group for their help and support, and I wish you all the very best for your future. Being the first PhD student of Dr Cronin and welcoming new students to the group, I feel too attached to all of you. It's unfortunate to leave the group after all the fun we had during the PhD.

I owe my life to my parents for sending me to the UK to pursue the degree. Me being an international student was not easy for my parents nor me. Every single moment in my life, I pray to God for their good health and long-lasting life. The backbone of this PhD is my proud Dad, who worked hard way more than my input to the PhD for paying all the tuition fees and my daily expenses. Forever in debt to him. I finally thank all my family members and friends who were there for me in my good and bad times. Especially the friends who answered my phone call to listen to my drama regardless of their time zone. I would like to thank Joana Moura who played a key role during the PhD. Her support during my health-related problems were incredible. I wish her all the very best to pursue her degree and success in life.

I dedicate my thesis to my grandparents, mum, dad, and my family members who are proud of me. I am delighted to see them happy as their son is the first member of the family to achieve a PhD.

Abbreviations

ADP – Adenosine diphosphate

ALD – Aldolase

ALDH – Aldehyde dehydrogenase

ALT – Alanine aminotransferase

AMP – Adenosine monophosphate

AMPK – AMP-activated protein kinase

APC – Antigen presenting cell

ARID – AT-rich interaction domain

ATP – Adenosine triphosphate

BRCA – Breast cancer gene

CDK12 – Cyclin dependent kinase 12

CTTNNB1 – Catenin beta 1

DMEM – Dulbecco's Modified Eagle medium

ECAR – Extra cellular acidification rate

ERBB2 (or HER2) – Erythroblastic oncogene B

ETC – Electron transport chain

FBS – Fetal bovine serum

GAPDH – Glyceraldehyde-3-phosphate dehydrogenase

GLS – Glutaminase

GLUT – Glucose transporter

GSH – Glutathione

HER – Human epidermal growth factor receptor

HIF-1α – Hypoxia inducible factor 1-alpha

HK – Hexokinase

IFN – Interferon

IDH – Isocitrate dehydrogenase

IL – Interleukin

KRAS – Kirsten rat sarcoma viral oncogene homologue

LDH – Lactate dehydrogenase

MMP – Matrix metalloproteinase

MPC – Mitochondrial pyruvate carrier

mTOR – mammalian target of rapamycin

MYC – MYC Proto oncogene

NADH – Nicotinamide adenine dinucleotide

NADPH – Nicotinamide adenine dinucleotide phosphate

NEAA – Non-essential amino acid

NF1 – Neurofibromatosis type 1

OAT – Ornithine aminotransferase

OCR – Oxygen consumption rate

OXPHOS – Oxidative phosphorylation

P5CS – Pyrolline-5-carboxylate synthase

PALB2 – Partner and localizer of BRCA2

PC – Pyruvate carboxylase

PDH – Pyruvate dehydrogenase

PEP – Phosphoenolpyruvate

PFK – Phosphofructokinase

PI3K – Phosphoinositide 3-kinase

PPP – Pentose phosphate pathway

PPP2R1α – Protein phosphatase 2 regulatory subunit 1-alpha

PTEN – Phosphatase and tensin homolog

P5C – Pyrolline-5-carboxylase

PYCR – Pyrolline-5-carboxylate reductase

RB1 – Retinoblastoma 1

ROS – Reactive oxygen species

RPL19 – Ribosomal protein L19

RPMI – Roswell Park Memorial Institute medium

STIC – Serous tubal intraepithelial carcinoma

TP53 – Tumour protein p53

TCA – Tricarboxylic acid cycle

TCGA – The cancer genome atlas

VDAC – Voltage dependent anion channel

Conferences

- Farook M.R., Sheldon I.M., Gonzalez D., and Cronin J. G. Loss of the mitochondrial pyruvate carrier drives 'glutamine addiction', a hallmark of metastatic ovarian cancers. European Association for Cancer Research. Amsterdam. **Abstract accepted for the Poster presentation.**
  Abstract published online: https://doi.org/10.1136/esmoopen-2018-EACR25.289

- Farook M.R., Sheldon I.M., Gonzalez D., and Cronin J. G. Role of mitochondrial pyruvate carrier in ovarian cancer progression. Medical School Postgraduate Research conference. **Poster presentation.**

- Farook M.R., Sheldon I.M., Gonzalez D., and Cronin J. G. Depletion of mitochondrial pyruvate carrier 1 re-purpose amino acid metabolism for cancer survival and metastasis. Medical School Postgraduate Research conference. **Poster presentation.**

- Attended the CR@B 2017, UK. 1st Cancer Research at Bath Symposium, 20th -21st April 2017.

- Attended the EACR-2020 virtual congress, 18th – 19th June 2020.

Chapter One

General introduction

1. Introduction

1.1 Outline

The ovaries are part of the female reproductive system and are responsible for the formation of gametes and the production of sex hormones. The ovaries develop at the mesonephric region and terminate at the pelvic region. The surface of the ovary is covered by germinal epithelium (ovarian surface epithelium; OSE). The epithelial integrity of the OSE is maintained by partial tight junctions, integrins and cadherins (Epifano and Perez-Moreno, 2012). The OSE is involved in ovulatory ruptures and repair by rapid proliferation, synthesizing both epithelial and connective tissue-type components (Auersperg et al., 2001).

The ovary has two important functions; generating oocytes for fertilization and secretion of sexual hormones to regulate the process of fertilization and reproduction. The ovaries have a functional unit called follicles which hold the oocytes surrounded by granulosa cells. Ovulation is triggered in the ovary; the process is characterized as the rupture of OSE for extrusion of an ova. Following the ovulation, the OSE has a wound that is naturally healed by the immune response. However, this wound can also play a critical role in high-grade serous ovarian cancer (HGSOC), by incorporating serous tubal *in-situ* carcinoma (STIC) that arise from the fallopian tube (Lee et al., 2007; Shaw et al., 2009).

While ovarian cancer is the sixth most common cancer in women in the UK, it is characterised as one of the most advanced stage gynaecological malignancies in women (Landen et al., 2008). Ovarian cancer has the highest death rate of all female reproductive cancer (Hu et al., 2013). Statistical analysis in the United Kingdom showed an estimated new ovarian cancer diagnosis of 20 patients per day in 2014, with 4100 deaths per year (Siegel et al., 2016). At the initial stage of diagnosis, most patients show an overall survival rate of 5 years while at the latter stages only about 5% of the patients survive for 5 years or more (Langyel, 2010). Due to the lack of reliable screening methods and advanced stage diagnosis, ovarian cancer patients often have a poor prognosis. Therefore, discovery of screening methods for detection of early ovarian cancer is vital and it is one of the most challenging subjects in ovarian

cancer research. The future perspective of ovarian cancer diagnosis and treatments need to be addressed. Defining the role metabolic pathways (metabolites involved) play in cancer cells and tumours is important in order to understand how cancer cells adapt to their harsh microenvironment. Metabolic flexibility is important for survival and proliferation during cancer progression. Therefore, targeting how cancer cells adapt to utilise limited energy sources might highlight new therapeutic targets in ovarian cancer (Figure 1.1). The current study intends to explore how metabolic flexibility of ovarian cancer cells contribute to cancer progression and an aggressive phenotype.

Figure 1.1 Current flow of research to find a therapeutic target in clinical research.

1.2 Ovarian cancer

1.2.1 Cancer biology and metastatic ovarian cancer

The term ovarian cancer is a collective term for different invasive cancers, most of which metastasize to or from the ovary. Ovarian tumours regardless of their clinical stage can originate from epithelial cells, stromal cells, and germ cells. However, 90% of the ovarian tumours are from the epithelial surface of the ovary and there are various histological subtypes of epithelial ovarian cancers, namely high-grade serous ovarian carcinoma (HGSOC), low-grade serous ovarian carcinoma (LGSOC), endometrioid carcinoma, clear-cell carcinoma, and mucinous invasive carcinoma (Fig 1.2) (Mangili et al., 2012; Matulonis et al., 2016). Although the HGSOC and LGSOC subtypes were originally thought to be derived from the surface of the ovary, ovarian cancer may be a misnomer as recent genomic studies have shown that the primary cancer cells arise from the distal fallopian tube which then metastasize to the ovary as a STIC (Folkins et al., 2009; Vaughan et al., 2011). Whereas, the endometrioid and clear-cell

carcinomas are derived from endometrium, and mucinous invasive carcinoma are mostly derived from colon, appendix or stomach (Fig 1.2) (Vaughan et al., 2011).

The HGSOC make up most (around 70-80%) epithelial ovarian cancer. Women who are diagnosed with HGSOC have lower survival rates and poorer prognoses than other subtypes due to advanced stage disease at diagnosis; less than 5% of the patients are diagnosed at stage 1 (Seidman et al., 2004). Due to chromosomal instability, HGSOC tumours exhibit a higher rate of gene mutations resulting in damage to genes controlling DNA repair and tumour suppressors. The HGSOC tumours are characterized by the presence of papillary or solid growth of the tumour with abundance of proliferation and poor differentiation (abnormal nuclei and varying cell size and shape). Furthermore, HGSOCs can exhibit solid mass in intra-abdominal locations triggering the accumulation of ascites, the build-up of abnormal fluid in the abdomen (Ahmed and Stenvers, 2013). When the metabolic environment of circulating tumour cells in ascites was analysed, ascites was shown to be rich in lactate (>5 mM; compared to blood <1 mM) and lactate dehydrogenase (>400 mU/mL, blood > 140-280 mU/mL) (Schneider et al., 1997).

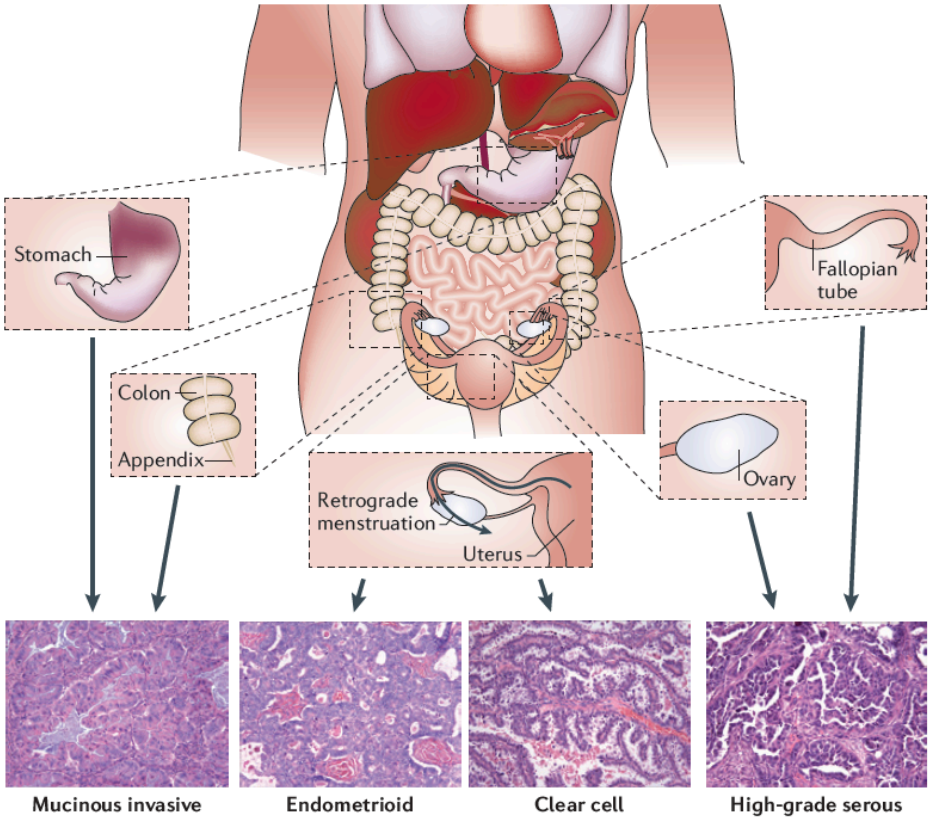

Figure 1.2 Diagram representing the classification of ovarian cancer subtypes. Mucinous carcinomas are typified by goblet cells that secretes mucin, which results in mucin-filled tumours. The HGSOC cells are characterized by abundant cell division (mitosis) and high nuclear to cytoplasmic ratio, while clear cell carcinomas are characterized by large, unusual tumours and clearing of the cytoplasm. Unlike other cancer types, clear cell carcinomas have stromal cells that deteriorate to homogenous and translucent nature. Adapted with permission from (Vaughan et al., 2011).

The aetiology of ovarian carcinomas is poorly understood. The ovary is surrounded by peritoneal mesothelium, which has the potential to undergo metaplasia (Auersperg et al., 2001). During the formation of malignant tumours, cancer cells can differentiate towards other cell types in the female reproductive system, like fallopian tube and ovarian stroma (Naora, 2005). The clinical findings suggest ovarian cancers develop from exposure of surface epithelium and corpus luteum cysts to chemokines resulting from inflammation (Wang et al., 2020). In 1971, a hypothesis was proposed for ovarian cancer stating that "increased rate of ovulation increases the risk for ovarian cancer" (Fathalla, 1971, 2013). During ovulation, the ovum leaves a wound in the ovary. The internalized ovarian surface was thought to provide the space for fallopian carcinoma cells to metastasize into the ovary whilst the wound heals. Also, the damage repair mechanism of the ovarian surface epithelium is thought to increase the risk of developing mutations and malignancies (Landen et al., 2008). Together with these hypotheses, a case control study spanning 30 years in the US, with 2197 ovarian cancer patients and 8893 control patients, showed multiple pregnancies, oral contraceptives and increased lactation time reduce the risk of epithelial ovarian cancer. The Gene mutations, age, post-menopausal hormonal therapy use, infertility and null-parity are some of the known risk factors of ovarian cancer (Matulonis et al., 2016).

Most lethal ovarian cancer malignancies are diagnosed after peritoneal metastasis has already occurred. Almost all cancer cells have driving gene mutations. The mutations can either be inherited (hereditary) or from an environmental cause, e.g., smoking, or poor lifestyle. Around 30% of all ovarian cancer gene mutations are inherited while remaining could be attributed to age, obesity and exposure to environmental carcinogens (Prat et al., 2005). Furthermore, impact of environmental factors on cancer is still an ongoing research. Gene mutations can be associated with the risk of developing ovarian cancer alone or coupled with increased risk of breast or colon

cancer, for example. Ovarian cancers that have been found to arise from precursor sites in the fallopian tubes, such as HGSOCs, are associated with *BRCA1* or *BRCA2* gene mutations in a substantial proportion of women (Carlson et al., 2008; Erickson et al., 2013). Recent clinical studies have also shown that familial history of breast cancer increase risk of women developing ovarian cancer depending on germline *BRCA1* or *BRCA2* gene mutation in the individual (Bergfeldt et al., 2002; Gangi et al., 2014). Table 1.1 indicates the chance of developing various cancer types associated with either *BRCA1* or *BRCA2* gene mutations. Furthermore, various germline mutations involved in DNA repair (*RAD51C, RAD51D, BRIP1* and *PALB2*) are also correlated with increased risks of ovarian cancer. This includes inherited mutant genes that contribute to DNA repair such as *HER2, ATM* and *TP53* (known as the guardian of the genome) (Bergfeldt et al., 2002; Cass et al., 2005; Gangi et al., 2014; Liu et al., 2012a; Prat et al., 2005; Zhang et al., 2011). Almost all cancers have mutant *TP53* and this mutation is almost ubiquitous in HGSOC (Bell et al., 2011; Patch et al., 2015).

Inherited diseases can lead to ovarian cancer. Patients with Lynch syndrome (associated with colorectal cancer) are shown to also have a 50% chance of developing stage 1 ovarian cancer at around the age of 48 years, whereas non-Lynch syndrome patients develop ovarian cancer around the age of 68 years (Ryan et al., 2017).

Table 1.1 Summary of *BRCA* gene related mutations that can correspond to other cancer types.

Gene mutation	Type
BRCA1	Serous endometrial cancer
BRCA1 and *BRCA2*	Breast cancer
BRCA2	Pancreatic cancer
BRCA2	Melanoma
BRCA2	Prostate cancer

Ovarian cancers in women with *BRCA* mutations are linked with STIC precursors in the fimbriae. Furthermore, studies in mice lacking components of the PI3K pathway (*Pten* mediated), coupled with *Dicer*, developed serous carcinoma in the fallopian tube (Kim et al., 2012). Gene expression studies on these Double knockout (DKO) mouse

models suggest that the tumour resembles the human serous carcinoma phenotype and genotype at the molecular level. Moreover, the tumours possessed a stromal origin in the fallopian tube indicating mesenchymal origin not epithelial lineage (Kim et al., 2012). Table 5.2 summarizes the mutated genes associated with histological subtype of epithelial ovarian cancer (Banerjee and Kaye, 2013; Bell et al., 2011; Singer et al., 2003). Cancer cells undergo epithelial mesenchymal transition (EMT), an opportunity for cancer cells to metastasize and resembles stem-cell like property. Further studies revealed the carcinoma cells to have metastasized to the abdominal cavity including pancreas and omentum, a fat-rich pad that encases the intestines and other abdominal organs (most of the cancer cells metastasize and reside near adipocytes) causing development of ascites (reflecting ascites observed in human ovarian cancers) (Kim et al., 2012; Landen et al., 2008). The tumour cells were characterized as HGSOC from their appearance with complex papillae, gland forming solid sheets of tumour and high mitotic activity (Kim et al., 2012). The cancer cells that arise from STICs demonstrate high levels of mutated *TP53*. The mutation in the *TP53* gene results in the production of non-functional p53 protein that accumulates in the tumour, whilst staining of *BRCA* gene mutated STIC cells showed overexpression of *TP53,* suggesting STIC as a precursor lesion of HGSOC (Lee et al., 2007). Cancer cells' increased mutations promote oncogenic activities and cancer progression called gain of function (GOF) independent of wild type *TP*53.

Further to the research carried out by Kim et al., 2012, research was carried out on DKO mouse lacking ovaries but not fallopian tubes and a DKO mouse with both ovaries and fallopian tubes intact. The mice lacking ovaries but not fallopian tubes developed serous carcinoma in 90% of the mice, showing similar result to the DKO mouse with ovary and fallopian tube intact (Kim et al., 2012). When the mouse lacked a fallopian tube (unilateral removal of fallopian tube) despite the presence of ovary, progression of the cancer was not seen. Another study carried out by Kindelberger et al., 2007, investigated pathology samples of 55 women with pelvic cancer cells for immunostaining of *TP53*. Nearly 75% of the pelvic samples contained STIC and 93% of the STIC identified samples were in the distal tubal fimbriae (Erickson et al., 2013; Kindelberger et al., 2007). The *TP53* staining identified similar mutations to *TP53* mutation in metastatic ovarian cancer in all the samples. Further studies revealed the

absence of STIC in other histological subtypes of ovarian cancer, suggesting the uniqueness of STIC in HGSOC (Erickson et al., 2013; Przybycin et al., 2010).

Table 1.2 Commonly mutated genes associated with epithelial ovarian cancer

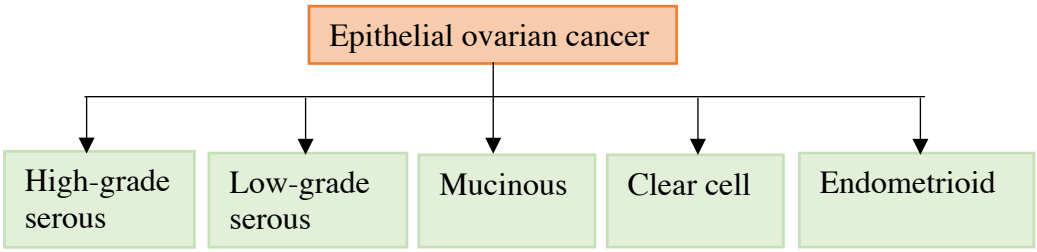

High-grade serous	Low-grade serous	Mucinous	Clear cell	Endometrioid
P53	*BRAF*	*KRAS*	*ARID1A*	*ARID1A*
BRCA1	*KRAS*	*HER2*	*PIK3CA*	*PIK3CA*
BRCA2	*NRAS*		*PTEN*	*PTEN*
RB1	*ERBB2*		*CTNNB1*	*PPP2R1α*
CDK12			*PPP2R1α*	
NF1				

1.2.2 Current therapies

Understanding metabolic and molecular mechanisms of any cancer is crucial for the development of a therapeutic target, particularly in cancers that frequently undergo metabolic reprogramming. Ovarian cancer cells reprogram their metabolism to meet their survival potentials. The screening strategies for women who are at risk of developing ovarian cancer monitors CA125 antigen levels in the serum (CA125 is a putative cancer biomarker encoded by the *MUC16* gene which is found in higher concentrations in ovarian cancer tumours) and transvaginal ultrasonography (monitors the female reproductive organs using ultrasound). If a woman is found to have an increased genetic risk for ovarian cancer, then surgery to remove the fallopian tube and the ovaries (bilateral salpingo-oopheractomy) is performed to reduce the risk of ovarian cancer (Kim et al., 2012; Xiang and Kong, 2013).

Although 70% of ovarian cancer patient normally receive first line therapy combined treatment of cyto-reductive (removal of visible tumours in patients with intraabdominal metastasis) surgery followed by a platinum-based chemotherapy, most of the women with advanced stage disease relapse within 12-18 months with recurrence of disease, particularly HGSOC patients (Langyel, 2010; Salani et al., 2011). Since the introduction of platinum-based chemotherapy more than three decades ago, survival rate for women with epithelial ovarian cancer has improved. Unfortunately, the relapsed patients develop a tumour possessing aggressive phenotype and are highly metastatic. At this stage patient is given neoadjuvant chemotherapy to shrink the tumours. However, the recurrent tumour can often become resistant to platinum-based chemotherapy. Fortunately, new therapeutics have been introduced to target the chemo-resistant carcinoma cells. Chemotherapy- resistant tumours can be treated by angiogenesis inhibitors like bevacizumab (binds to vascular endothelial growth factor (VEGF), to prevent VEGF receptor activation) or poly(ADP-ribose) polymerase (PARP) inhibitors, which prevent the repair of DNA damage (Matulonis et al., 2016). The PARP inhibitors were known to work on *BRCA* gene mutated ovarian cancer cells and lately they were found to work on *BRCA* wild type cancers when combined with antiangiogenic agents (Evans and Matulonis, 2017). Discovery of PARP inhibitors partially overcome the challenges associated with HGSOC and platinum resistant tumours. Moreover, ovarian cancers which were often fatal have improved with advanced therapeutic options including immunotherapy and heated intraperitoneal chemotherapy (HIPEC) substantially increasing the hopes of patient survival.

1.3 Cellular metabolic pathway

1.3.1 **Overview**

The classification of hallmarks of cancer has focussed cancer research over the last two decades. Since genetic alterations and metabolic flexibility in HGSOC cells has been shown to drive tumour progression and resistance to chemotherapy, we looked at hallmarks of cancer. Because genomic instability, reprogramming energy metabolism and evading growth suppressors etc. were major functions carried out by HGSOC cells. The first hallmarks of cancer paper was published in 2000 (Hanahan and Weinberg, 2000), and an updated version of hallmarks of cancer was published in

2011, which further included "Reprogramming energy metabolism" (Fig. 1.3) (Hanahan and Weinberg, 2011).

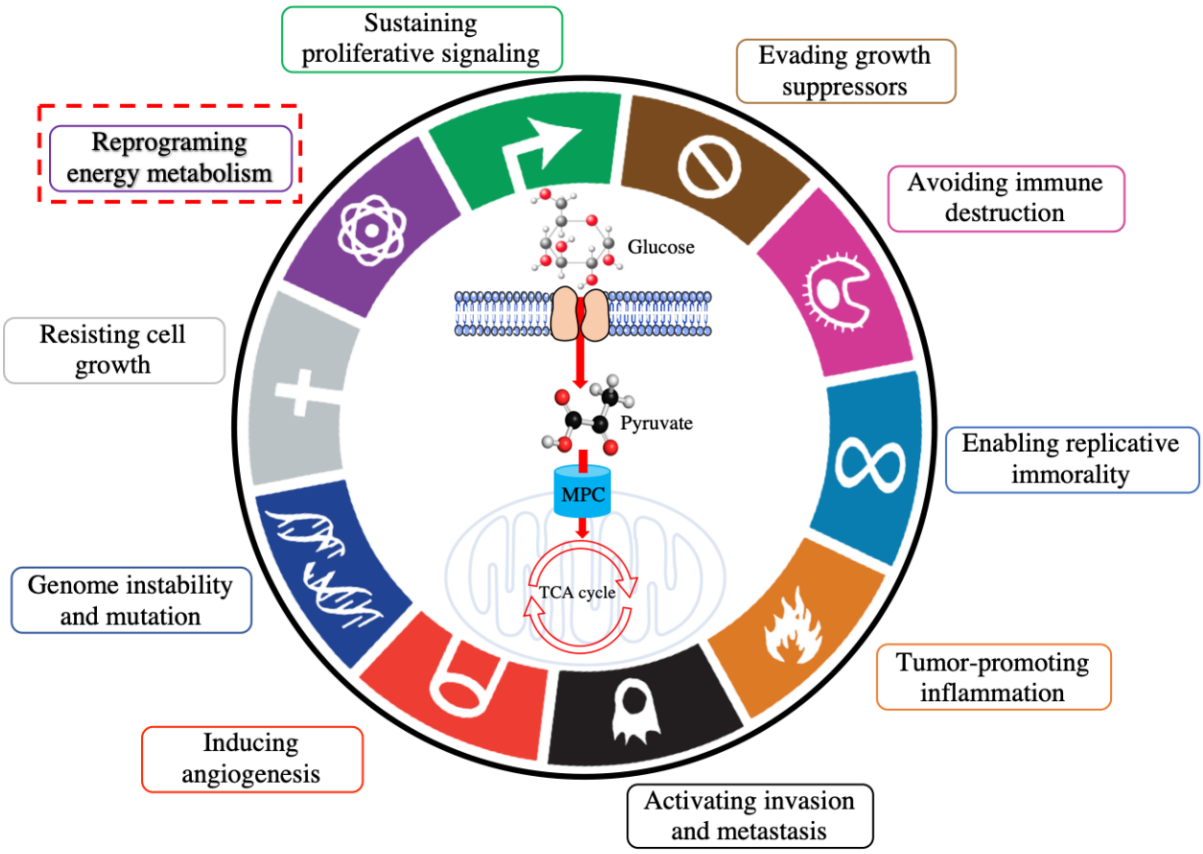

Figure 1.3 Hallmarks of cancer.
The diagram shows an updated ten important hallmarks of cancer. The red dotted lines indicate the important hallmark of cancer concerned within this thesis: reprogramming energy metabolism. Adapted from (Hanahan and Weinberg, 2011).

Deregulated cancer cell metabolism is further classified in a review by Pavlova and Thompson as "Emerging hallmarks of cancer metabolism" (Pavlova and Thompson, 2016),

I. Deregulated uptake of glucose and amino acids
II. Opportunistic modes of nutrient acquisition
III. Use of glycolysis/NADPH production
IV. Increased demand for nitrogen
V. Alterations in metabolite driven gene regulation
VI. Metabolic interactions with tumour microenvironment.

Cells employ various metabolic reprogramming to produce energy for growth and proliferation. A common theme of research over the past few years is metabolic reprogramming of the cancer cells. The major central carbon compounds utilized by cancer cells are glucose and glutamine, and their metabolism is reprogrammed by mutations in *MYC, TP53, Ras*-related oncogenes and signalling pathways like LKB1-AMP kinase (AMPK) and PI3 kinase (PI3K) (Boroughs and DeBerardinis, 2015).

1.3.2 **Glycolysis**

Glycolysis is the first step of glucose breakdown for cellular metabolism, yielding a net of two ATP molecules and two molecules of pyruvate along with two NADH + H^+ molecules. Glycolysis comprises a series of reversible and irreversible enzymatic reactions which occur in the cytosol. The initial step of glycolysis starts with the phosphorylation of a glucose molecule to produce glucose-6-phosphate by the enzyme hexokinase (HK) which involves consuming one molecule of ATP. The glucose-6-phosphate is then converted to fructose-6-phosphate by the phosphoglucose isomerase. The enzyme phosphofructokinase (PFK) phosphorylates fructose-6-phosphate to fructose 1,6-bisphosphate, which is considered an irreversible reaction contributing to glucose precursors for glycolytic by-product. This is the final energetically expensive reaction in glycolysis. The enzyme aldolase (ALD) converts fructose 1,6-bisphosphonate to two three carbon compound glyceraldehyde-3-phosphate (G3P) and dihydroxyacetone phosphate (DHAP). The DHAP is then converted back to G3P by triose phosphate isomerase (TPI). At this point each molecule of glucose yields two molecules of G3P, any molecules from now on are duplicated. Then glyceraldehyde-3-phosphate dehydrogenase (GAPDH) catalyses the phosphorylation G3P to 1,3 bisphosphoglycerate (1,3 BPG) using NAD^+ as a co-substrate (yields two molecules of NADH + H^+). Conversion of two 1,3 BPG molecules to two 3-phosphoglycerate (3PG) by phosphoglycerate kinase (PGK) yields two molecules of ATP. The phosphoglycerate mutase (PGM) catalyses transfer of a phosphate group from 3rd carbon to 2nd carbon, yielding 2-phosphoglycerate. At this stage metalloenzyme enolase plays an important role catalysing the conversion of 2-phosphoglycerate to phosphoenol pyruvate (PEP) and producing water as a by-product. The enzyme

pyruvate kinase produce pyruvate from PEP yielding two molecules of ATP. Glycolysis is critical for hypoxic tumours due to intricate roles for glycolytic intermediates and enzymes. The demand for energy differs between quiescent state and differentiated state of cancer cells. Under a glucose deficient environment, cancer cells are able to utilise pyruvate to lead to gluconeogenesis (generation of glucose from non-carbohydrate precursors) which can also lead to the pentose phosphate pathway (PPP) or serine biosynthesis via glucose-6-phosphate and 3-phosphoglycerate (figure 1.4) (Cho et al., 2018).

The PPP contributes to production of energy for metabolism by recruiting other metabolites, fructose-6-phosphate (F6P) and glyceraldehyde-3-phosphate (G3P). The role of PPP also includes production of nicotinamide adenine dinucleotide phosphate (NADH) which is involved in fatty acid synthesis and maintaining the intracellular redox by removing reactive oxygen species (ROS). However, the pivotal role of PPP is contributing to the nucleotide (RNA and DNA) synthesis that has an important role in any cancer (Patra and Hay, 2014). The level of PPP in proliferating cancer cells is high due to increased expression of carbon metabolites F6P and G3P driving the high glycolytic activity regardless of the level of ATP production (Cho et al., 2018).

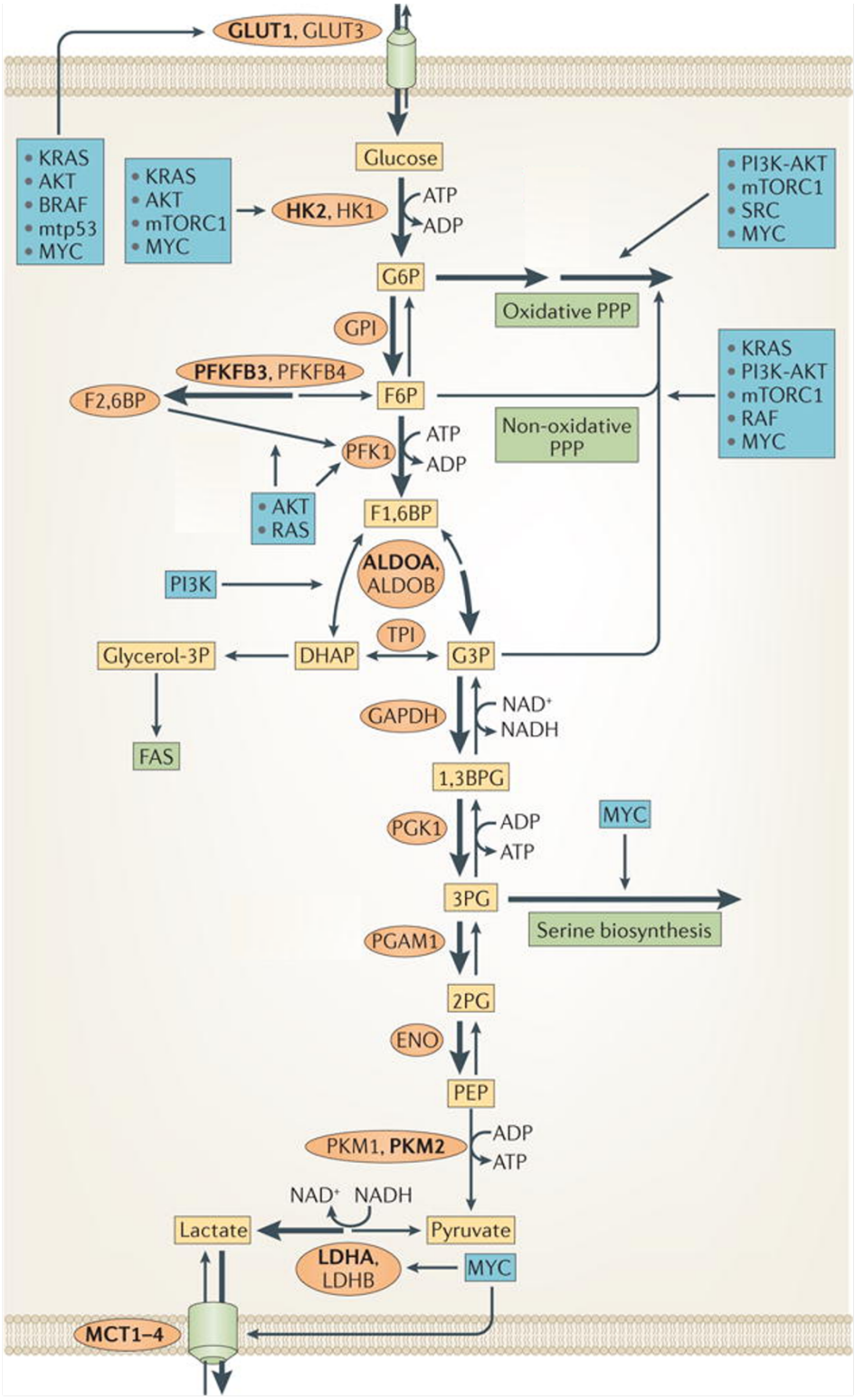

Figure 1.4a Overview of glucose metabolism and oncogenes involved in glucose utilization.
Oncoproteins that induce the activity of cancer promoting enzymes are shown in blue. Adapted from (Hay, 2016)

1.3.2.1 **Pyruvate sources in cancer cells**

Apart from via glycolysis, pyruvate can be also reformed from various sources to drive energy cycle, for example pyruvate can be re-formed from malate by cytosolic malic enzyme. This formation of pyruvate plays a key role in synthesis and regulation of tricarboxylic acid (TCA) cycle intermediates citrate, malate, and oxaloacetate. Lactate dehydrogenase (LDH) has two isoforms LDH-A and LDH-B; LDH-A converts pyruvate to lactate whereas certain amounts of pyruvate are also produced from the oxidation of lactate by LDH-B (Dawson et al., 1964). Lastly, pyruvate can be formed from alanine transaminase (ALT). ALT has a role in transporting alanine to mitochondria at the mitochondrial matrix where alanine can be catalysed by ALT to produce glutamate and pyruvate (Mendesmourao et al., 1975). Pyruvate acts as a central metabolite between the cytoplasm and the mitochondria (Bowman et al., 2016). The fate of pyruvate is important in eukaryotic cells in order to produce enough energy. Cancer cells display accelerated glycolysis and pyruvate accumulation in the cytoplasm. Excessive pyruvate gets converted to lactate by LDH even under aerobic condition. The idea was named the "Warburg effect" after Otto Warburg observed it for the first time (Warburg et al., 1927). In Warburg's experiment, he observed cancer cells cultured in 13 mM glucose had an increased concentration of lactate accumulation, despite replete oxygen (Otto, 2016). Since cancer cells can alternatively use lactate to provide energy, lactate is known to as one of the major fuel sources and gluconeogenic precursors. However, increased lactate concentrations can cause a drop in pH in the cells acidifying the extracellular microenvironment and lowering drug efficacy when targeting cancer cells, which is advantageous for cancer cells for immune evasion, invasion and metastasis (Doherty and Cleveland, 2013; Faubert et al., 2017; Kane, 2014; Metallo et al., 2012; Morais-Santos et al., 2015).

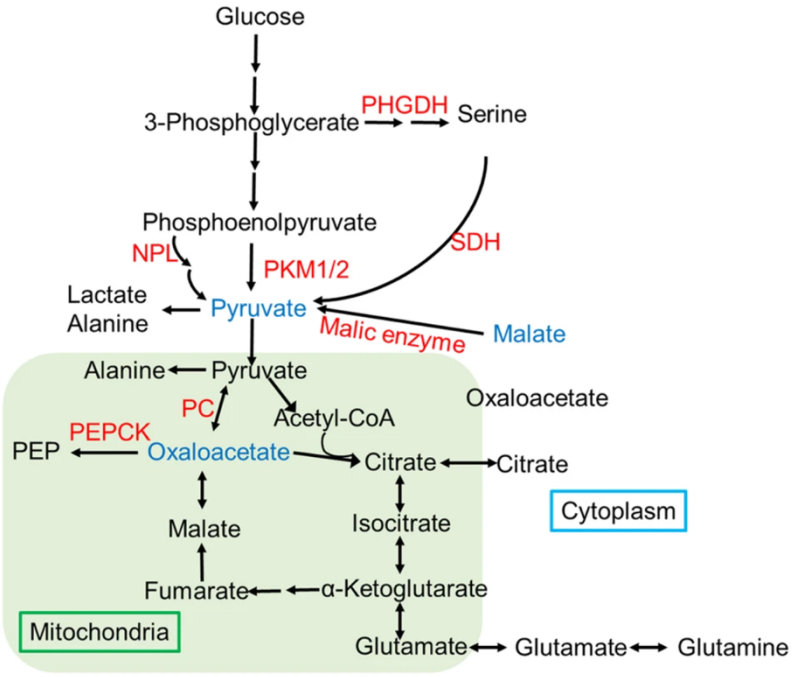

Figure 1.4b An overview of pyruvate sources in cells.

The lactate produced by cancer cells can be transported in and out of the cell bidirectionally; transport of lactate into the cell is mediated by monocarboxylate transporter 1 (MCT1) and cellular lactate export mediated by MCT4. However, the transport of lactate into the cell will not exceed the concentration of extracellular lactate to maintain equilibrium. The drop in pH difference due to intracellular and extracellular lactate levels is maintained by the anion and cation gradient of lactate (Usher-Smith et al., 2006).

The end product of glycolysis, pyruvate fate is most important in cancer cell metabolism. Ultimately, pyruvate transport into the mitochondria is vital for oxidative phosphorylation to proceed by feeding the TCA cycle. Originally, pyruvate was thought to freely cross the inner mitochondrial membrane (Klingenb.M, 1970). However, later studies using rat liver mitochondria and radiolabelled pyruvate provided evidence for the presence of a specialized transporter for pyruvate. The pyruvate transporter for mitochondria was recently found to be a specialized carrier "Mitochondrial pyruvate carrier" formed of subunits MPC1 and MPC2 (Bricker et al., 2012).

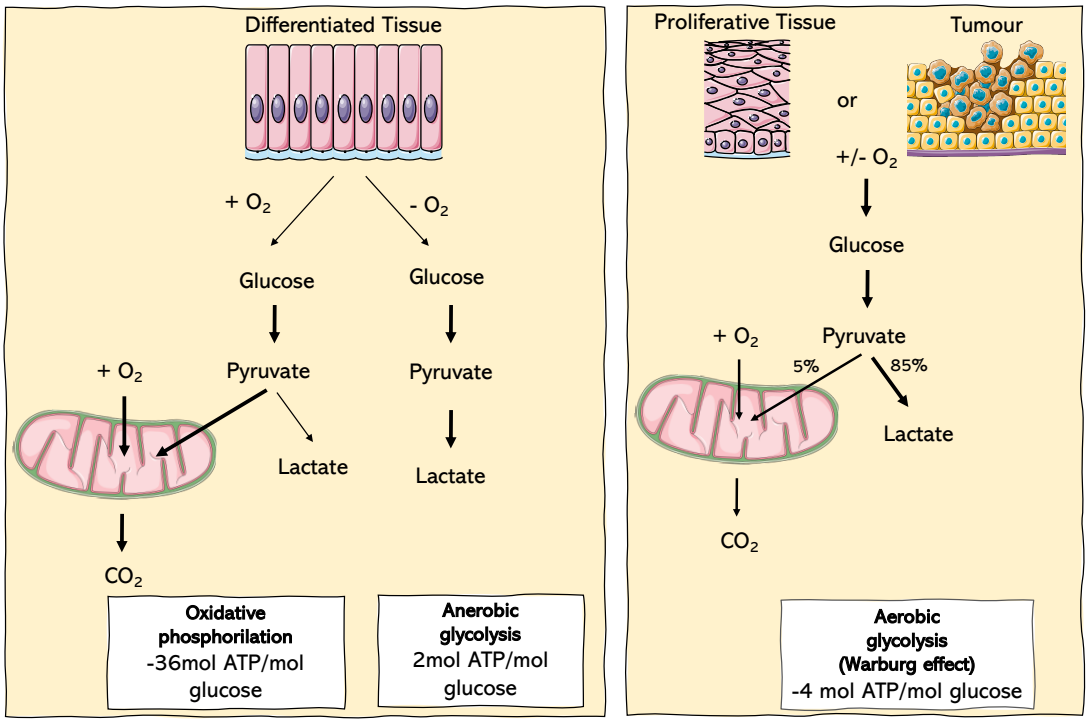

Figure 1.5 Schematic representation of differences between oxidative phosphorylation and aerobic glycolysis (also known as the Warburg effect).

1.3.3 Mitochondrial pyruvate carrier (MPC)

The *MPC1* and *MPC2 genes* encode for the mitochondrial pyruvate carrier 1 (MPC1), and mitochondrial pyruvate carrier 2 (MPC2) proteins respectively. The mitochondrial pyruvate carrier is a 150 kDa oligomeric protein complex composed of hetero-oligomers of MPC1 and MPC2 proteins, which is found in the inner mitochondrial membrane (Bricker et al., 2012). The structural features of MPC1 and MPC2 are predicted but not yet proven (Fig. 1.6). MPC1 has two predicted domains of approximately 12 kDa, whilst MPC2 has three predicted domains of approximately 14 kDa (Li et al., 2017b). MPC1 and MPC2 together form the pyruvate transporter complex, where loss of either one will results in destabilization of the other, hence restricting its ability to transport pyruvate across the mitochondrial membrane (Compan et al., 2015b). Originally the human MPC proteins were known as BRP44L (brain protein 44-like) and BRP44 (brain protein 44), until their names were changed to MPC1 and MPC2 after their function was determined in a study of pyruvate transport into the mitochondria in yeast, *Drosophila*, and humans (Bricker et al., 2012;

Jiang et al., 2009). Although, the idea of a special transport mechanism for pyruvate was first introduced in 1971 in a study of pyruvate transport in rat liver mitochondria (Papa et al., 1971). The results from the experiment showed that pyruvate exchange is not inhibited when other TCA cycle intermediate transporters were inhibited (like inorganic phosphates and malate), showing an evidence for a unique transporter for pyruvate (Papa et al., 1971).

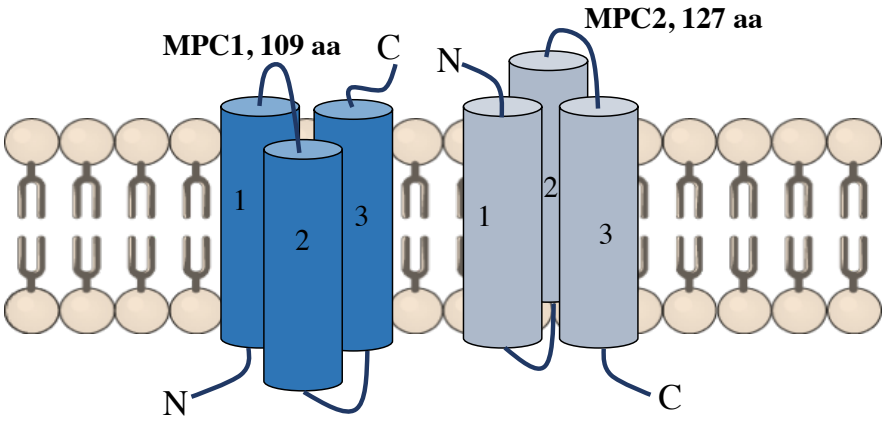

Figure 1.6 Schematic diagram of a predicted MPC1 and MPC2 monomers.
The MPC1 (109 amino acids) helices are shown in blue while MPC2 helices are shown in grey (127 amino acid). MPC1 and MPC2 together form the 150 kDa transport complex in the inner mitochondrial membrane.

Mitochondrial mutations were thought to be linked to various types of fatal medical conditions. A defective or deficient MPC contributes to diseases like lactic acidosis, hepatomegaly, cancer, epilepsy and encephalopathy (Ruiz-Iglesias and Manes, 2021). The genetic deletion of *MPC1* has been shown to result in complete loss of pyruvate transport in yeast mitochondria and human cells (Bricker et al., 2012). Knockdown of *MPC1* or *MPC2* genes by siRNA reduced mitochondrial respiration mediated by pyruvate (Bricker et al., 2012). Recent studies suggest that *MPC* may be a key point altered in metabolic regulation of cancer. Numerous cancer types, including, colon, kidney, lung, bladder, brain, and ovarian cancer, correlate deleted *MPC1* with a low survival and poor prognoses (Aguirre-Gamboa et al., 2013; Schell et al., 2014b). Around 80% of epithelial ovarian cancers are known to have a deleted chromosomal region 6q27 (corresponding loci D6S149 and D6S93), which has been determined to include the *MPC1* gene locus (Cai et al., 2014; Tibiletti et al., 1998). In a study of

twenty benign ovarian tumours most of them presented with terminal deletion in chromosome 6 of 6q region, while ten cases were defined with interstitial deletion in chromosome 6 (Tibiletti et al., 1998). Further studies revealed MPC1 inhibition or downregulation has been shown to correlate with poor prognosis of multiple cancer types, while re-expression of MPC1 *in vitro* suppressed the Warburg effect in colon cancer (Schell et al., 2014b). Further studies also have shown that MPC1 inhibition or downregulation has increased cell proliferation, cancer progression in prostate cancer while giving them a stem-like phenotype (Wang et al., 2016; Zhong et al., 2015). Cancers with deleted *MPC1* uses amino acids as an alternative fuel source to glucose, primarily glutamine (Gonsalves et al., 2020). Although MPC1 and MPC2 are proposed to function as a complex, a recent study showed MPC2 can operate independently of MPC1 (Nagampalli et al., 2018). The MPC2 was not regarded as necessary until it was shown to form a homodimer and the efficiency of pyruvate transport into the mitochondria via an MPC2 homodimer is much less compared to the MPC1-MPC2 heterodimer complex. Increased pyruvate transport efficiency was demonstrated by Herzig et al., where co-expression of mpc1 and mpc2 in *Lactococcus lactis* induced a four-fold increase in pyruvate uptake (Herzig et al., 2012).

The expression of MPC plays a key role in determining the fate of certain signalling pathways. The tumour suppressor genes *Notch* and *Apc* (adenomatous polyposis coli) determine cell fate and regulation of the WNT signalling pathway, respectively, and are influenced by Mpc expression (Bensard et al., 2020). Both *Notch* and *Apc* signalling pathways are critical in normal cellular function. Deleting or silencing *Mpc* has shown to promote intestinal tumour formation in mice and flies while overexpression of *Mpc* has shown to block the *Notch and Apc* function in intestinal stem cells of *Drosophila,* preventing them from undergoing hyperplasia (Bensard et al., 2019). There is numerous evidence to confirm *MPC1* deleted cells exhibiting glycolytic phenotype and increased expression of stem cell markers suggesting a critical role for glycolytic intermediates, amino acid metabolism and fatty acid biosynthesis (Bensard et al., 2019; Li et al., 2017a; Nieman et al., 2011; Wei et al., 2018).

1.4 Inhibitors of mitochondrial pyruvate carrier

1.4.1 Thiazolidinedione compounds

Thiazolidinediones (TZD) are well known for their role in treating hyperglycaemia of type 2 diabetes by actively blocking complex I. Recent studies have shown that certain TZD are potent inhibitors of pyruvate transport into the mitochondria. The TZDs are involved in increased fatty acid oxidization and promote insulin sensitization in the skeletal muscle (Divakaruni et al., 2012). The TZD compounds rosiglitazone and troglitazone inhibited pyruvate oxidation in both mouse and human myocytes while having no effect on the oxidation of complex 1 and pyruvate dehydrogenase activity. Even though the mechanism behind pyruvate transport inhibition by TZDs were still unclear, the comparison of inhibition by TZD and UK-5099 (an analogue of α-cyano-4-hydroxycinnamate) indicated the similar mechanisms for MPC inhibition (Divakaruni et al., 2012).

Furthermore, the TZD compounds GW450863X and GW604714X were found to be potent inhibitors of MPC complex with much lower inhibitory constant values compared to UK-5099 (Hildyard et al., 2005). The compounds GW450863X and GW604714X didn't have any effect on MCTs until the concentration is four orders of the IC_{50} for UK-5099 (50 nM) while UK-5099 bound to MCTs at twice the concentration for MPC complex (Fig. 1.7) (Hildyard et al., 2005).

The compounds GW450863X and GW604714X were tested against pyruvate transport in rat and yeast mitochondria (Hildyard et al., 2005). The inhibition of MPC was seen in both the rat liver and yeast and different concentrations (inhibitory constant for GW450863X is 56 nM and GW604714X is 57 nM in rat liver), whilst MPC inhibition in yeast is lower with these compounds, due to slow pyruvate oxidation (Hildyard et al., 2005). Thiazolidine compounds that inhibit MPC bear no structural resemblance to MCTs.

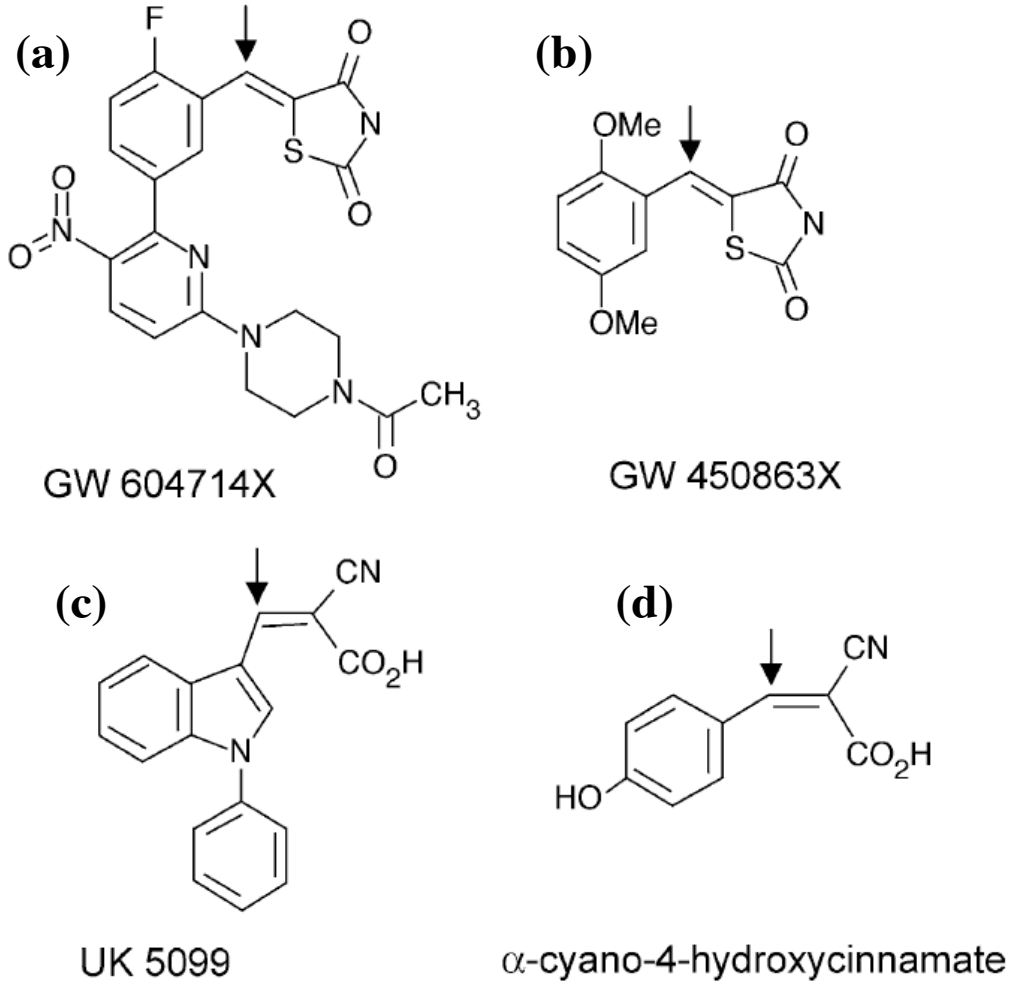

Figure 1.7 Chemical structure of inhibitors used to block MPC complex.
The inhibitors block the MPC via Michael's addition. The non-competitive inhibitors (a) and (b) covalently binds to the carrier protein and reaction is reversible. The arrow shows the potential site for modification of thiol group. Adapted from: (Halestrap, 1976)

1.4.2 α-cyano-4-hydroxycinnamate and UK-5099

Since the 1960s pyruvate dependent oxygen consumption has been extensively studied. In 1971, a metabolic study on rat liver mitochondria and erythrocytes revealed the presence of a specialised carrier protein for pyruvate transport in mitochondria (Papa et al., 1971). The research was conducted in the presence of an inhibitor α-cyano-4-hydroxycinnamate which successfully blocked the transport of pyruvate into the mitochondria. Then in 1974 a plasma protein inhibitory study on α-cyano-4-hydroxycinnamate and its analogue, UK-5099 (α-cyano-ß-(1-phenylindol-3-yl)-acrylate) confirmed the presence of this specialised carrier protein as this inhibitor

blocked the pyruvate intake across the mitochondrial membrane, whereas, enzymes like pyruvate dehydrogenase, pyruvate carboxylase or pyruvate kinase involved in pyruvate metabolism were not affected (Halestrap, 1975; Halestrap and Denton, 1974). The compounds UK-5099 and α-cyano-4-hydroxycinnamate are powerful inhibitors of MPC complex. However, compared to α-cyano-4-hydroxycinnamate (IC_{50} 0.2 μM), UK-5099 was more effective with an IC_{50} of 50 nM (Fig 1.6) (Halestrap, 1975; Halestrap and Denton, 1974). The kinetics behind the inhibitory process involved in the transport of pyruvate shows that inhibition is non-competitive and reversible. The reversible process behind this mechanism indicates the formation of inhibitor-carrier complex covalently bound by modifying a thiol group (Michael addition) in the carrier between α-carbon and ß-carbon atoms of α-cyano-4-hydroxycinnamate derivatives (Halestrap, 1975).

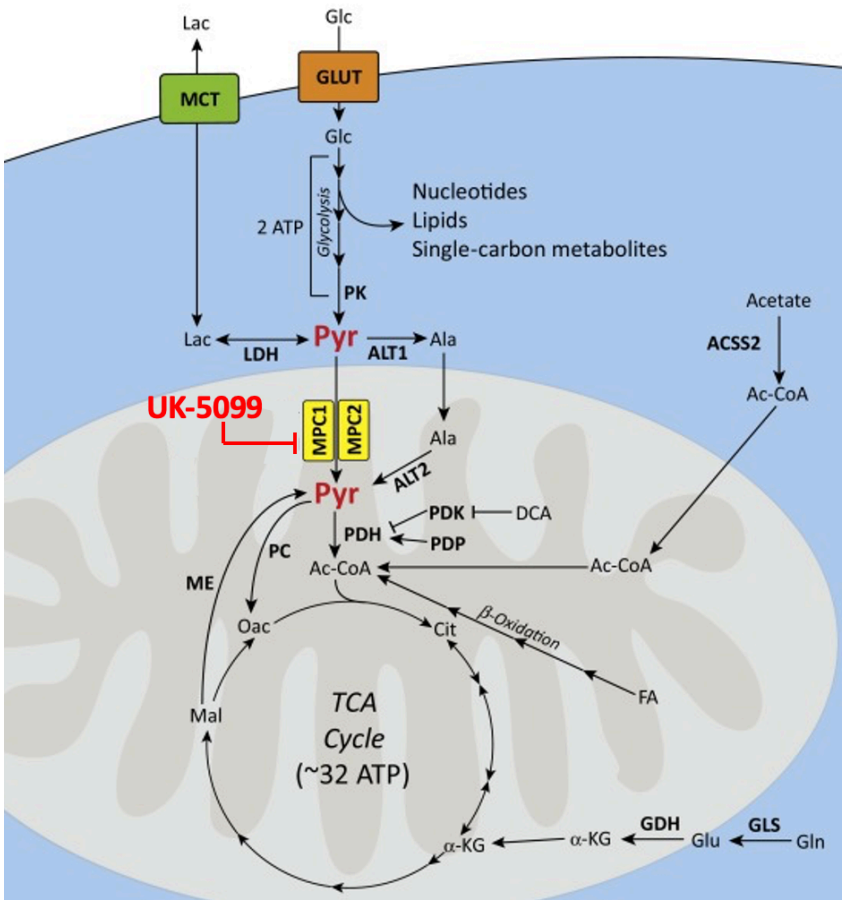

Figure 1.8 A schematic diagram displaying pyruvate utilization.
Blocking MPC complex with UK-5099 results in pyruvate accumulation in the cytosol, which may then get converted to lactate by LDH. The diagram also shows the utilization of ALT to transport pyruvate to feed the TCA cycle (Olson et al., 2016).

1.5 Crosstalk between amino acid metabolism and cancer

The amino acids are the backbone for protein and nucleotide biosynthesis. In normal cells, most essential amino acids are gained through dietary intake, while non-essential amino acids are produced from intracellular biosynthetic reactions. The amino acid biosynthesis is majorly from glycolysis and glutaminolysis. Some of the non-essential amino acids that are known to be important in cancer are alanine, serine, aspartate, and glycine, while conditionally essential amino acid proline has also been shown to be important for cancer proliferation (Tanner et al., 2018). Apart from glutamine contribution to amino acids, carbohydrate precursors leading to amino acid metabolism have been poorly studied in ovarian cancer. For example, the glycolytic intermediate 3-phosphoglycerate leads to serine biosynthesis via enzyme 3-phosphoglycerate dehydrogenase (PHGDH). Multiple cancers, including breast and melanoma cancer cells, have shown increased expression of PHGDH *in vitro* (Locasale, 2013; Possemato et al., 2011a). In the study of Possemato et al. 2011, complete ablation of PHGDH resulted in increased cell death while PHGDH expressing cells contributed to α-KG from glutamate via glutamate dehydrogenase (Possemato et al., 2011a). Serine has a role in glutathione synthesis via the biosynthesis of glycine and cysteine. Glutathione is a scavenger of ROS, which protects the cell from oxidative damage. The majority of the amino acid abundancies depends on glutaminolysis (Vincent et al., 2015; Wise and Thompson, 2010). The glutaminolysis has shown to be important in glucose deficient cancers, including epithelial ovarian cancer (Vacanti et al., 2014b; Yang et al., 2014c; Yang et al., 2017).

1.5.1 Glutamine metabolism

Glutamine, one of the most abundant amino acids in the body plays several major physiological roles due its naturally occurring structure (containing an amide and amino side chain) (Souba, 1993). Mammalian blood has a glutamine concentration of around 0.6 mM, and in tissue can reach up to 20 mM. Glutamine is a NEAA and in normal cell metabolism it participates in the TCA cycle, glutathione synthesis (GSH) and biosynthesis of other amino acids. Glutamine acts as the primary source of α-ketoglutarate (KG) to feed the tricarboxylic acid (TCA) cycle, whilst its intermediate glutamate is involved as an exchange factor for essential amino acids (EAA) (Butler

et al., 2021). Glutamine enters the cells via solute carrier family 1 member 5 (SLC1A5) or the alanine-serine-cysteine transporter 2 (ASCT2). Glutamine was thought to be one of the most advantageous alternative fuel sources for cancer cells, as tumour cells consume glutamine from circulating blood and studies have shown glutamine regulation is crucial in multiple cancers for cellular energy production and proliferation (DeBerardinis and Cheng, 2010; Vincent et al., 2015). The first event of glutamine utilization is the conversion of glutamine to glutamate by the enzyme glutaminase (phosphate dependent) producing ammonia as a by-product. This deamination reaction could be a reason why increased glutaminolysis in patients with malignant carcinoma cells indicate hyperammonaemia. The glutaminolysis provides substrates for nucleotide and protein biosynthesis for the growth and survival of carcinoma cells (Souba, 1993). Glutamate is then converted to alpha-ketoglutarate (α-KG) by glutamate dehydrogenase (GDH) (figure 1.9). The α-KG can be used for ATP production and also as a substrate for the TCA cycle intermediates for mitochondrial respiration. This phenomenon of using glutamine as an alternative source to feed the TCA cycle is called glutamine anaplerosis. In normoxic and hypoxic tumours, α-KG can be converted to citrate by isocitrate dehydrogenase 2 (IDH2). The citrate leaves the mitochondria via tricarboxylate anion carrier system to synthesise fatty acids and amino acids, while generating the electron donor NADPH for anabolic reactions and redox homeostasis.

In the mitochondria α-KG dehydrogenase converts α-KG to succinate. Succinate is further reduced to fumarate and then to malate by fumarase and malate dehydrogenase, respectively. This series of reactions formulates the by-product oxaloacetate which can then drive the TCA cycle by producing pyruvate via regulating phosphoenolpyruvate carboxykinase 2 (PCK2) located in the mitochondria. The enzyme pyruvate dehydrogenase oxidizes pyruvate to Acetyl-CoA by recruiting Coenzyme A (Vincent et al., 2015). Previously it was believed that glucose deprivation is enough to induce cancer cell death via AMPK activation (Chuang et al., 2014; Sandulache et al., 2011). Cancer cells have shown to utilise glutamine under a glucose depleted environment where highly invasive ovarian carcinoma displayed glutamine addiction (Wise and Thompson, 2010; Yang et al., 2014c). During glucose starvation, the PCK2 enzyme generates glycolytic intermediates to promote the biosynthetic intermediates required

for tumour cell proliferation. The elevated expression of PCK2 was shown in non-small cell lung carcinoma cells (Vincent et al., 2015). The lung carcinoma cell line A549 was capable of proliferating under glucose depletion. During this study, a significantly high level of oxaloacetate was converted to both aspartate and phosphoenolpyruvate (Vincent et al., 2015). Studies on the serine biosynthesis pathway also revealed the upregulation of phosphoglycerate dehydrogenase in coupling of serine and glycine induced nucleotide biosynthesis (Locasale, 2013). Collectively the data from Vincent at al., 2015 and Locasale, 2013, concludes the contribution of amino acid metabolism as both carbon and nitrogen sources through the malate–aspartate shuttle under glucose deprivation (Locasale, 2013; Vincent et al., 2015).

Cancer cells utilizing glutamine and fatty acids have been shown to protect themselves from immune attack (Jiang et al., 1998; Yang et al., 2014c).This may explain why cancer cells lacking or having a dysfunctional MPC1 seemed to display an aggressive phenotype when they were glutamine addicted. Research on glutamine addiction using glioblastoma cells revealed, glucose withdrawal induced glutamine dependent pyruvate formation (Yang et al., 2009). In this experiment, all five carbons in the glutamine were heavy labelled with ^{13}C and glucose deprived cells illustrated pyruvate production from TCA intermediates, as succinate, fumarate and malate were fully labelled from the ^{13}C glutamine, indicating glutamine was used as the precursor. Furthermore, glucose deprivation indicated citrate was labelled with ^{13}C atoms. This indicates that both oxaloacetate and acetyl-CoA were generated from glutamine. Glutamine induced citrate by reduced pyruvate was seen in both HeLa and Huh-7 cells (Yang et al., 2014c). Mostly, glutamine addiction in cancer cells has shown to be *MYC* dependent. Mutations in *MYC* are extensively studied and thought to be a target for anti-cancer drug. Increased expression of *MYC* is advantageous for cancer cells depending on glutamine as it promotes the glutamate synthase enzyme which converts glutamine to glutamate. Glutamine addiction is thought to be more efficient compared to fatty acid oxidation, as fatty oxidation in cancer cells produces acetyl-CoA to drive the TCA cycle but there are no oxaloacetate intermediates formed during the process (discussed later). The impairment of pyruvate transport by MPC inhibition depletes citrate availability for the TCA cycle. Glutamine dependent respiration was also

proved by the research group who first named MPC1 and MPC2 (Bricker et al., 2012). However, the results for glutamine addiction via MPC inhibition were not consistent with different inhibitors used. The use of MPC inhibitors thiazolidinedione and Zaprinast behaved differently to MPC inhibition by UK-5099 (Divakaruni et al., 2013; Du et al., 2013). A possible explanation could be the use of different cellular types, which differ in the rate of metabolic activity. As mentioned before, not all cancer cells are glutamine addicted but inhibition or deletion of MPC1 in some cancer cells has been shown to induce fatty acid oxidation.

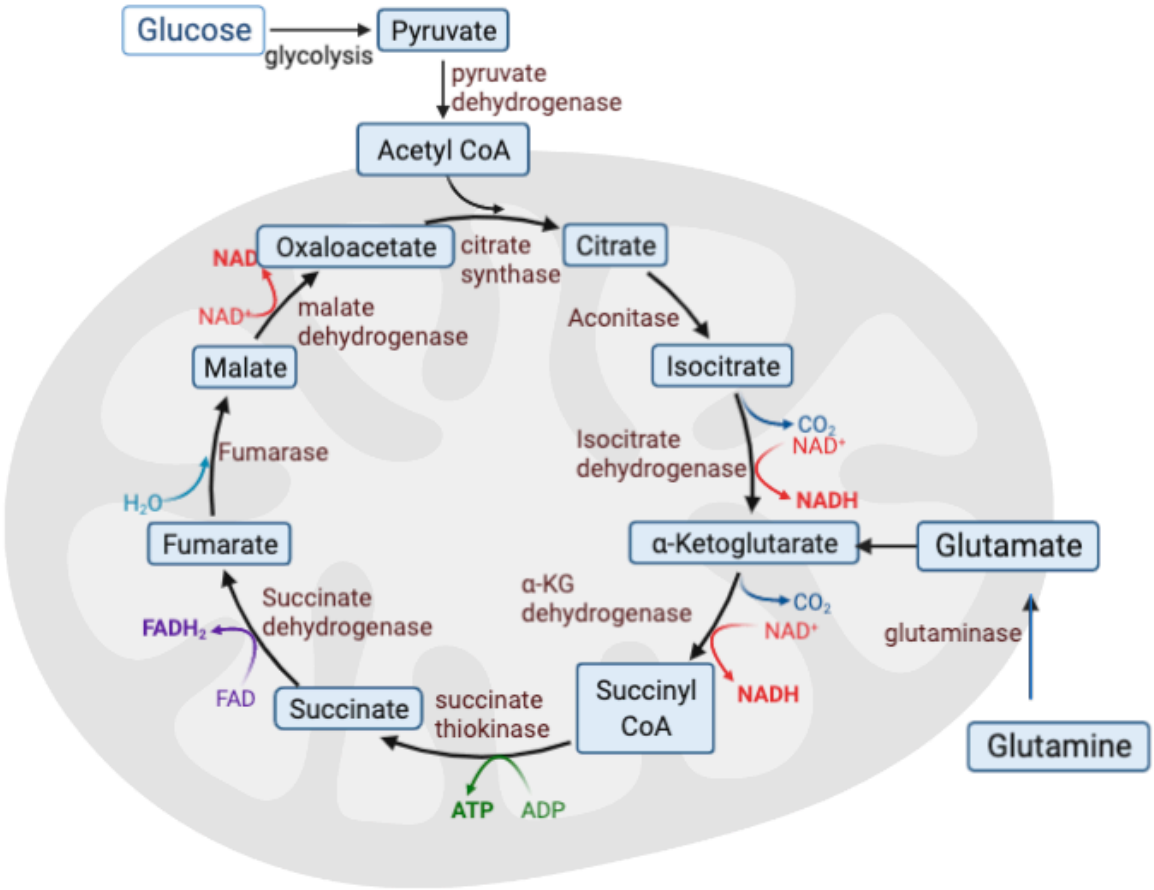

Figure 1.9 The tricarboxylic acid cycle showing the enzymes involved in catalysing the reaction.
The enzyme names are in brown while red, green, and purple letters denote energy utilisation. The diagram was drawn with the help of Bio Render database.

1.5.2 Proline metabolism in cancer

Determining the contribution of proline to cancer metabolism is challenging because of its underexplored role in cancer cell proliferation and metastasis. Proline is

beneficial to cancer cells, either through its biosynthesis or its degradation, depending on the cancer type. Biosynthesis of proline occurs in the cytoplasm, while degradation occurs in the mitochondria (Adams and Frank, 1980a; Phang, 1985). While proline is classified as a special amino acid, the conformation of proline makes it harder to be metabolised by decarboxylation or racemisation (Adams and Frank, 1980a). Proline has a unique structure compared to other amino acids, where its functional group (R-group) is bonded to both its central carbon atom and the amine group (COOH-R-C=NH). A few of the key enzymes that contribute to altered metabolism in cancer cells are proline dehydrogenase or proline oxidase (PRODH/POX) and the pyrroline-5-carboxylate (P5C) reductase (P5CR/PYCR) isoenzymes (PYCR1, PYCR2, PYCR3; also known as PYCRL) (D'Aniello et al., 2020; Tanner et al., 2018).

Proline has an essential role in stress maintenance and redox balance of prokaryotic and eukaryotic cells. Also, genes involved in cancer cell proliferation, c-MYC and PI3K signalling, increase the expression of P5C synthase and PYCR isoenzymes (Liu et al., 2015; Liu et al., 2012c). Proline also has a connection with glutamine metabolism via the urea cycle. Proline is synthesized from glutamate or ornithine via glutamate-gamma-semialdehyde (GSAL)/P5C, which is then reduced by PYCR to produce proline. Depending on the origin of reduction, the PYCR isoforms involved are energy-dependent or energy independent. The NADPH dependent PYCR1 and PYCR2 (energy independent in the cytosolic form) have a role in making proline in the mitochondria, whilst energy independent PYCR3 reduction to proline from P5C is carried out in the cytosol. However, the degradation of proline is strictly localized to mitochondria. Proline interconversion between proline and P5C is reversible and leads to proline-P5C cycling. Hagedorn and Phang, in 1986, reported proline-P5C cycling for the first time where proline oxidation to P5C by PRODH and P5C reduction to proline by PYCR contributes to energy production (Hagedorn and Phang, 1986). The proline-P5C cycle mediated by PRODH/POX and PYCR isoenzymes link mitochondria and the cytosol to maintain redox homeostasis (Adams and Frank, 1980a; D'Aniello et al., 2020; Hagedorn and Phang, 1986; Phang, 2019). If the P5C reduction to proline is outside the mitochondria (mediated by PYCR3), the reducing equivalents are transferred to the electron transport chain (ETC) to maintain a proton gradient and generate ATP. Moreover, proline has been shown to involve in nutrient

sensitizing pathways mTOR and Gcn2-Atf4 (nutrient starvation pathway) (D'Aniello et al., 2015).

Proline has a plethora of other functions which are crucial for cancer cells. Proline contributes to protein synthesis (where together with hydroxyproline leading to collagen proteins to form an extracellular matrix (ECM)) generating ROS, which leads to activation of other cell signalling pathways and generation of macromolecules (Elia et al., 2017a; Nazemi and Rainero, 2020; Tanner et al., 2018). The ECM plays a crucial part in cancer cell migration and other oncogenic transformations. ECMs are a mesh of secreted proteins that provide strength and support to cells. Likewise, degradation of ECM during cancer metastasis provides proline to generate ATP and protein synthesis via matrix metalloproteinase enzymes (MMPs) (Dixit et al., 1977; Huynh et al., 2020). Various studies have shown MMP upregulation as a critical event in cancer progression which resulted in an increased quantity of endogenous proline (Dashevsky et al., 2009; Kakkad et al., 2010; Lafleur et al., 2005; Stallings-Mann and Radisky, 2007). Furthermore, glucose starvation in colorectal cancer has been shown to activate MMP-2 and MMP-9, resulting in intracellular proline accumulation (Pandhare et al., 2009).

In certain cancers, proline is a limiting amino acid where the under expression of *PYCR1* results in impaired cell proliferation *in vivo* (Loayza-Puch et al., 2016b). Moreover, where *PYCR1* is overexpressed in some cancers, knocking down *PYCR1* affected cell growth and metastasis (Cai et al., 2018a). Recent studies show increased levels of proline biosynthesis in IDH1 mutant human anaplastic oligodendroglioma (HOG) cells compared to the wild type (Hollinshead et al., 2018b). This study showed increased proline synthesis in IDH1 mutant cells via increased PYCR1 activity following a central carbon metabolite tracing experiment. Interestingly redox potential of mitochondrial PYCR1 leads to the synthesis of anabolic precursors aspartate and citrate. Indeed, aspartate has a role in the respiration of proliferating cells under normal and hypoxic conditions while supporting purine and pyrimidine metabolism (Birsoy et al., 2015a; Sullivan et al., 2015).

1.5.3 Aspartate metabolism

Aspartate is a precursor for most of the TCA cycle substrates and is a limiting metabolite in many tumours. Overcoming these limitations is a key mechanism carried out by cancer cells. Like most of the non-essential amino acids, aspartate too is derived from glutamine. Enzymes aspartate aminotransferase 1/glutamate oxaloacetate transaminase 1 (GOT1; Cytoplasmic) and aspartate aminotransferase 2/glutamate oxaloacetate transaminase 2 (GOT2; mitochondrial) facilitate the metabolite exchange between cytosol and mitochondria while playing a key role in NADH redox balance (Son et al., 2013; Vacanti et al., 2014b). Aspartate is synthesized from intermediate oxaloacetate and glutamate via a transamination reaction producing α-KG as a by-product. The transamination reaction is bidirectional and facilitated by GOT1/GOT2 via malate-aspartate shuttle to recycle TCA cycle substrates (Vacanti et al., 2014b; Yoo et al., 2020).

An impaired ETC limits the availability of aspartate in proliferating cancer cells. However, various tumour xenograft study shows evidence of aspartate import from exogenous sources via SLC1A3 (a glutamate – aspartate transporter located on the plasma membrane) feeding the TCA cycle in low oxygen environments and under impaired ETC activity (Birsoy et al., 2015a; Garcia-Bermudez et al., 2018; Sullivan et al., 2015). Furthermore, aspartate is a precursor for arginosuccinate synthesis which leads to arginine synthesis (Cheng et al., 2018). Interestingly, epithelial ovarian cancer cells express high levels of arginosuccinate synthase (ASS) compared to normal OSE and arginine deprivation or silencing ASS in ovarian cancer resulted in cell death *in vitro* (Nicholson et al., 2009; Szlosarek et al., 2007).

1.6 Lipid metabolism

In normal tissue, the cells rely on lipids from the body itself for oxidation of fatty acids. Fatty acids play major part in supplying energy when the body staves for nutrition. Fatty acids are long hydrocarbon chain molecules composed of a carboxylic acid group and are precursors for sphingolipids, phospholipids, diglycerides and triglycerides (Koundouros and Poulogiannis, 2020). Fatty acid biosynthesis from citrate via reductive carboxylation of glutamine produces α-KG. The IDH2 enzyme mediates the

α-KG to citrate conversion. Fatty acid biosynthesis is a cytosolic process and citrate is transported to cytosol via SLC25A1.

Around 90% of epithelial ovarian cancer cells detach from their origin and metastasize to the omentum. The omental structure is formed by the folding of a multi-layered peritoneum lining the cavity and organs (Singh et al., 2015). Metastasizing ovarian cancer cells prefer tumour growth in the omentum due to an abundance of adipocytes. The objective of cancer cells preference to reside in the adipose tissue was still unclear until their metabolic mechanism was revealed in the last decade (Nieman et al., 2011). Research from *in vitro* studies suggests that ovarian cancer cells specifically localize and invade as omental milky spots which consist of immune cells, stromal cells and capillary beds (Clark et al., 2013; Khan et al., 2010); another *in vitro* data also suggested that adipocytes donate lipids to ovarian cancer cells and adipokines, including interleukin (IL)-8, produced by adipocytes promote invasion and migration of ovarian cancer cells (Nieman et al., 2011). Findings from omental metastasis in clinical research have led to the interest of studying the role of lipid metabolism in ovarian cancer and the advantage gained from fatty acid metabolism to ovarian cancer cells. One of the major findings in lipid metabolism is that ovarian cancer cell co-cultured with adipocytes resulted in the transfer of lipids from adipocytes to ovarian cancer cells which induced *in vitro* tumour growth (Nieman et al., 2011). Moreover, the ovarian cancer cells ability to undergo epithelial-mesenchymal transition (EMT) during metastasis provided an invasive phenotype by modifying the expression of E-cadherin, vimentin and integrins (Davidson et al., 2012). To be able to reside in the omentum for colonisation, the ovarian cancer cells underwent mesenchymal-epithelial transition (MET), permitting cells to adhere and proliferate with an abundant supply of energy (Langyel, 2010). Similar effect was seen in Erb-B2 receptor tyrosine kinase-negative growth regulatory protein 1 (ERBB3-NGR1) or (Her3-NGR1) active cancer cells, which promoted secondary metastasis following an omental colonization (Pradeep et al., 2014). The constant supply of energy during energy starvation is achieved by the release of fatty acids and the release of adipokines TNF-alpha, IL-8 and IL-6 attract cancer cells for localisation at the omentum (Clark et al., 2013; Nieman et al., 2011). Fatty acid binding protein 4 (FABP4), also called aP2, is a lipid protein expressed in adipocytes which functions as both cellular and systemic metabolic

process. Previous studies have shown that FABP4 as glucose regulator in mice while it contributes to insulin resistance linked to obesity in humans (Cao et al., 2013; Uysal et al., 2000). Moreover, FABP4 has been shown to promote cancer metastasis and mediated to therapy resistant cancer in epithelial ovarian cancer (Mukherjee et al., 2020).

This project hypothesises that *MPC1* deletion in epithelial ovarian cancer cells drives cancer proliferation and metastasis leading to an aggressive phenotype. Metastatic ovarian cancer cells are susceptible to becoming resistant to therapy. Previous understandings of gene mutations and metabolic flexibility in ovarian cancer led us to determine whether *MPC* could be a major switch in orchestrating metabolic needs. Gene mutations (e.g.: *TP53*) in various ovarian cancer cells have been previously studied (Coscia et al., 2016), hence this thesis does not focus on the role of *TP53*. Metabolic instability and adapting to TME is an important function carried out by cancer cells. How *MPC1* deleted ovarian cancer cells re-purpose amino acid and fatty acid biosynthetic pathways is important in order to look at the role of *MPC1* in epithelial ovarian cancer progression due to lack of in-depth knowledge of MPC1 deletion in ovarian cancer. Therefore, the following work is focused on MPC1 influence on glycolytic intermediate pyruvate and amino acids (glutamine, proline, serine, and aspartate)

1.7 Thesis Aims and Objectives

The aim of this thesis is to determine the metabolic advantage gained by MPC1-deleted ovarian cancer cells that reprogram metabolic pathways for cancer survival and resistant to therapy.

The objectives were to determine:

1. The role of mitochondrial pyruvate carrier and effect of its inhibition in high-grade ovarian cancer cell proliferation.
2. Whether MPC expression levels are altered in nutrient-depleted environment.
3. Whether MPC1-deletion drives glutamine addiction in ovarian cancer cells.
4. The role of amino acid metabolism in MPC1-deleted ovarian cancer cells.

Chapter Two

General materials and methods

2. General Materials and methods

2.1 Cell culture

2.1.1 Ovarian epithelial cell culture

The PEO1 (#10032308, European Collection of Authenticated Cell Cultures, England) and PEO4 (#10032309, European Collection of Authenticated Cell Cultures, England) cell lines (isolated from same patient) under express or partially deleted MPC1 used as negative control. The OVCAR3 (#HTB-161, American Type Culture Collection. England) express MPC1 and used all the way through in this research thesis. All cell lines are representative of HGSOC (Bell et al., 2011; Coscia et al., 2016a). In addition, PEO4 and OVCAR3 cell lines are cisplatin resistant whilst the PEO1 cell line is sensitive to cisplatin (Langdon et al., 1988). As a control for glutamine addiction, previously characterised glutamine addicted cell line, SKOV3 (#HTB-77, American Type Culture Collection. England) was used (Yang et al., 2014c). For routine culture, PEO1 and PEO4 cells were cultured in RPMI 1640 growth medium (#31870, ThermoFisher-Scientific, UK), supplemented with 10% foetal bovine serum (FBS) (#FB-1550, Bio sera, USA), 1% glutamine (2mM) (#25030081, ThermoFisher-Scientific, UK), 1% antibacterial antimycotic solution (ABAM) (#A5955, Sigma-Aldrich). For the routine culture of OVCAR3 cells, RPMI 1640 growth medium was supplemented with 20% FBS (#FB-1550, Bio sera, USA), 1% glutamine (2 mM) (#25030081 ThermoFisher-Scientific, UK), 0.1% insulin (#10516, Sigma-Aldrich) and 1% ABAM (#A5955, Sigma-Aldrich, UK). For the routine culture of SKOV3 cells, McCoy's 5a growth medium (#16600082, ThermoFisher-Scientific, UK), was supplemented with 10% FBS (#FB-1550, Bio sera, USA), 1% glutamine (2mM) (#25030081, ThermoFisher-Scientific, UK) and 1% ABAM (#A5955, Sigma-Aldrich, UK). All cells were cultured in T25 - T175 cm^2 cell culture flasks and incubated at 37˚C in a humidified chamber containing 5% CO_2. Growth medium was replaced every 2 - 3 days and cells were sub-cultured at 70 - 80% confluency.

For sub-culturing, media was aspirated from the flask and cells were gently washed with 5 mL (per T75 cm^2) phosphate buffered saline (PBS) (#10010023, ThermoFisher-Scientific, UK) and detached with 2 mL Accutase enzyme (#A6964, Sigma-Aldrich,

UK). Following detachment cells were transferred to a 15 mL centrifuge tube and centrifuged at 800 x g for 5 min. Cell pellets were re-suspended in 1mL growth media and counted using a Countess (Invitrogen Cell counter, ThermoFisher-Scientific, UK) for further culturing or seeding (6-well or 96-well plates) purposes. For any amino acid studies and conditioned media studies, cells were grown in high glucose phenol-red-free DMEM (#A1443001,) re-suspended in no glucose or glutamine phenol red-free DMEM (#31053044, Gibco technology, UK) to achieve 11.1 mM glucose concentration. All cell lines were maintained at 37°C in a humidified chamber at 5% CO_2. For preparing the complete growth media of DMEM, the 11.1 mM glucose containing medium was give 20% foetal bovine serum (FBS) (#FB-1550, Bio sera, USA, USA) for OVCAR3 and 10% foetal bovine serum (FBS) (#FB-1550, Bio sera, USA) for PEO1, PEO4 and SKOV3. For all cell lines DMEM media, 1% glutamine (2 mM) (#25030081, ThermoFisher-Scientific, UK), 1% antibacterial antimycotic solution (ABAM) (#A5955, Sigma-Aldrich) was given. Further details are discussed within relevant Chapters.

2.1.2 MPC inhibitor – UK-5099 / 2 α-cyano-ß-(1-phenylindol-3-yl)-acrylate

To inhibit the pyruvate transport into the mitochondria, a potent inhibitor for MPC1, UK-5099 (#4186. Tocris, UK) was used. The inhibitor UK-5099 has a half maximal inhibitory concentration; IC_{50} of 50 nM (Halestrap, 1975). Reports indicate 5 μM UK-5099 is sufficient to successfully inhibit MPC1 activity (Hildyard et al., 2005). A UK-5099 stock solution of 20 mM was made with dimethyl sulfoxide (DMSO) (#01934, Sigma-Aldrich. UK). The UK-5099 was aliquoted and stored in the freezer for further use (as per company reference, compound is stable for a year at -80°C). In this study concentration ranges from 0.625 μM to 10 μM were used for preliminary studies and 5 μM was chosen for further experiments.

2.2 Quantitative real time polymerase chain reaction (q-PCR)

2.2.1 RNA extraction and quantification

The cells were washed with PBS and harvested for RNA using the RNeasy mini kit (#74106, Qiagen, UK) following the manufacturer's protocol. Prior to RNA

extraction, a calculated volume of 70% ethanol (Sigma-Aldrich, #E7023-500) was freshly made with deionised water. Briefly, the washed cells were scraped with 350 µl of RLT lysis buffer using a cell scraper (Fisher Scientific, #08100241). The lysate was collected in a 2 ml Eppendorf tube (Eppendorf, #0030120094) and a similar volume (1:1) of freshly prepared 70% ethanol was added to the cell lysate and mixed well by gentle pipetting. The lysate was then transferred to a spin column and centrifuged at 800 x g for 15 sec and the flow through was discarded. Then, 700 µL of RW1 buffer was added to the spin column, followed by centrifugation (800 x g for 15 sec) and the flow-through discarded. Then RPE buffer (500 µL) was added to the spin column and the column centrifuged at 800 x g for 15 sec to remove the flow-through. The step was repeated with a similar volume of RPE buffer and centrifuged at 800 x g for 2 min and the flow-through discarded and replaced with a new collection tube. The column was then centrifuged at maximum speed 17000 x g (~13000 rpm) for 1 min to further dry the membrane. The spin column was then transferred to a labelled 1.5 mL Eppendorf (sterile) and 35 µL of RNase-free water (Ambion, #AM9937) was added to the membrane. The sample was centrifuged at 800 x g for 1 min to elute the RNA. To maximise the yield, the RNA elution was repeated by pipetting the eluted RNA on to the spin column following the centrifugation.

The purity and total RNA concentration was determined using the NanoDrop ND-100 spectrophotometer (Labtech international, Uckfield, UK). The spectrophotometer was cleaned, pat dried with sterile water and paper cloth. Then 1 µL of sterile water was loaded onto the spectrophotometer to blank the instrument. The purity of the sample was determined at 260/280 nm and 260/230 nm range ratios, values varying between 1.8 and 2.3 to exclude any contamination. The concentration of RNA used for reverse transcription was required to be maximum of 1000 ng/µL. The RNA samples were aliquoted accordingly and stored at -80˚C.

2.2.2 Reverse transcription

The cDNA synthesis was performed using QuantiTect reverse transcription kit (#205311, Qiagen, UK), according to manufacturer's protocol. Template RNA and Reverse transcriptase enzyme were thawed on ice whilst the rest of the reagents were

thawed at room temperature. All the reagents and samples were briefly vortexed (Vortex-Genie 2, SLS Ltd. UK) and centrifuged prior to use. The cDNA was synthesized from 1 µg (1000 ng) of total RNA, initially eliminating any genomic DNA (gDNA). The total RNA (up to 1 µg) was diluted in nuclease free water to a total volume of 12 µL in a PCR tube. A genomic DNA elimination step was performed by adding 2 µL of gDNA wipe out buffer. The sample tube was vortexed and centrifuged briefly, incubated at 42˚C for 2 min on an iCycler (Bio-Rad, Hemel Hempstead,UK) then immediately kept on ice. A master mix of reverse transcription was assembled as shown Table 2.1.

Table 2.1 Reverse transcription master mix.

Reagent	Volume (μl)
Reverse transcriptase enzyme	1
Quantiscript RT buffer	4
Primer mix	1
Template RNA (gDNA elimination reaction sample)	14
Total volume	20

Then 6 µL of master mix was added to each sample followed by gentle vortexing and brief centrifugation. Samples were incubated at 42˚C for 15 min for cDNA synthesis, followed by 95 ˚C for 3 min to inactivate the reverse transcriptase enzyme. The samples were kept on ice for immediate experiments or stored at -20˚C for future work.

2.2.3 Real-time PCR

The Real-time PCR was carried out using QuantiFast SYBR Green PCR kit (#204054, Qiagen, UK), following the manufacturer's protocol. All buffers were thawed at room temperature, while the samples and primers were thawed on ice. Samples and reagents were mixed by vortexing followed by a brief centrifugation prior to use. All the primers were obtained from Merck, UK unless stated otherwise. Primers were either previously designed from the published journals or custom-designed, as indicated. Primers from published journals were checked for specificity using NCBI BLAST

(National Centre for Biotechnology Information, United States). Custom-designed primers were aligned on NCBI BLAST and validated for specificity against the human genome. The house keeping gene oligonucleotide primers were previously designed and validated in the laboratory.

2.2.3.1 Primer dilution

The lyophilised primers were diluted in an appropriate volume of nuclease free water to obtain a 100 μM stock. Primers were then aliquoted and stored at -20°C. For each gene of interest, the qPCR reaction mix was comprised as in Table 2.2. The primer volume was calculated to obtain 1 μM final concentration for forward and reverse primer.

Table 2.2 Quantifast SYBR green PCR master mix and primer dilution

Reaction mix	Volume (μl)
2x QuantiFast SYBR green master mix	12.5
Forward primer (1 μM)	0.25
Reverse primer (1 μM)	0.25
RNase-free water	10.5
cDNA template	1.5
Total volume	25

2.2.3.2 Reference RNA

A control cell line was selected using the NCBI gene data base, that abundantly expressed the gene of interest. Cell lines used for RNA reference in this study were isolated from hepatocellular carcinoma HepG2 cells. The HepG2 cells were cultured in Minimal essential medium (ThermoFisher Scientific, #12561056) supplemented with 10% FBS (Bio sera, USA #FB-1550). The HepG2 cells were grown to 80% confluency in a T175 cell culture flask and prepared for RNA extraction as mentioned under Chapter 2, section 2.2.1. Then the cDNA was synthesized from reference cell's total RNA following the steps under Chapter 2, section 2.2.2.

2.2.3.3 Standard curve

Reference RNA (section 2.2.3.2) was used to construct cDNA for a standard curve per gene of interest. The standard curve consisted of serially diluted reference cDNA at dilutions of Neat (undiluted), $\frac{1}{10}$, $\frac{1}{100}$ and $\frac{1}{1000}$. The first step of dilution was made by adding 4 μl of neat cDNA to 36 μl of nuclease free water and a serial dilution was followed thereafter to achieve the final dilution. The diluted samples were prepared into individual PCR tubes. PCR tubes were vortexed and centrifuged briefly prior to use and maintained on ice.

2.2.3.4 Plate set-up

The reaction master mix was made with an extra 10% volume. The non-template controls (NTC) were prepared by replacing cDNA template and adding 1.5 µL of nuclease free water to the reaction mix above. Each reaction mix was made from the master mix in individual PCR tubes and relevant cDNA was added individually to each primer mix. PCR tubes were gently vortexed and centrifuged and samples pipetted in triplicate into a 96-well PCR plate (Bio-Rad, #MLL9651) and sealed with a plate sealer (Greinerbio-one, #676001). The plate was then briefly centrifuged at 800 x g for 1 min and transferred to a CFX connect™ Real-time PCR detection system (Bio-Rad, UK). The PCR cycle was performed according to cycling parameters mentioned in Table 2.3, using the Bio-Rad CFX manager, version 2.1 programme. All the primer sequence designed to measure gene expression is shown in Table 2.4.

Table 2.3 Cycling parameters for q-PCR

Step	Cycle	Temperature (˚C)	Time	Notes
1	(1X)	95	5 min	Enzyme activation
2	(1X)	95	10 sec	Template denaturation
Repeat step 2	(39X)	60	30 sec	Annealing of primers
	(1X)	65 – 95 (0.5 increment)	5 sec each	Melt curve a analysis

2.2.3.5 Data analysis

The data were collected and analysed using the CFX connect software system (version 2.1). The relative quantity ΔΔCq was calculated according to the (Livak and Schmittgen, 2001) method. The amount of amplified target is directly proportional to the input target at the exponential phase, hence it's vital to quantify the gene at the exponential phase. Briefly, the mean Cq values from genes of interest were obtained and subtracted from the relevant housekeeping gene (*RPL19* and *ACTB*) Cq value to obtain the normalised change in relative quantity (ΔCq). The exponential was calculated using the equation $2^{-(\Delta Cq)}$. Similar calculations were applied for NTC wells. Finally, to obtain the relative expression in ΔΔCq, each gene's exponential value was divided by the NTC exponential value. Once the ΔΔCq was calculated for each replicate, an average for each set of samples was plotted as a graph to compare the gene expression. Standard deviation was calculated to manually obtain data for error bars.

Table 2.4 Genes of interest and relevant primers selected for Real-time qPCR

Gene	Primer sequence (5'-3')	
MPC1	forward	ATAACAGGACGGCACTTCTGG
	reverse	AACAGAAGCCAGTTCCGAGG
MPC2	forward	ACCTTTTCCTCACGTCCCAC
	reverse	ACACACCAACCCCCATTTCAT
PYCR1	forward	CATGACCAACACTCCAGTCG
	reverse	CCTTGGAAGTCCCATCTTCA
PYCR2	forward	ATAGCCAGCTCCCCAGAAAT
	reverse	CTCCACAGAGCTGATGGTGA
PYCR3/L	forward	GCCTCATCAGAGCAGGAAAA
	reverse	CACGGACACCAAGATGTGTT
OAT	forward	GACTGCCTGTAAACTAGCTCG
	reverse	AACGTCCTACCCCAGAAGTTC
P5CS / ALDH18A1	forward	CTGAGTATGGGGACCTGGAA
	reverse	GCGGTAACCATCAGAAAAGC
P5CDH / ALDH4A1	forward	GTACGGTGGCCAGAAGTGTT
	reverse	TCTTGATACGGGCAAAGGAC
MYC	forward	ACCACCAGCAGCGACTCTGA
	reverse	TCCAGCAGAAGGTGATCCAGACT
PHGDH	forward	TGCAAATCTGCGGAAAGTGGC
	reverse	TAAGGCCTTCACAGTCCTGC
PSAT1	forward	AAAAACAATGGAGGTGCCGC
	reverse	CCTCCCACAGACACGTAGAA
PSPH	forward	TAGAAAGCTGCAGGACTGGTG
	reverse	TGCAAGTGCTTCTGTAAACTTAAAA
GOT1	forward	CAACTGGGATTGACCCAACT
	reverse	GGAACAGAAACCGGTGCTT
GOT2	forward	GTTTGCCTCTGCCAATCATATG
	reverse	GAGGGTTGGAATACATGGGAC
RPL19	forward	GCGAGCTCTTTCCTTTCGCT
	reverse	TGCTGACGGGAGTTGGCATT
β-Actin	forward	GATGGCCACGGCTGCTTC
	reverse	TGCCTCAGGGCAGCGGAA

2.3 Gene silencing using short-interfering RNA transfection

Gene silencing studies were carried out using short-interfering (si)RNA (RNAi) (Horizon Discovery. UK) duplexed with Lipofectamine (RNAiMAX) (#13778075, ThermoFisher. UK). The RNAi sequences were designed using the Dharmacon siDESIGN centre (Horizon Discovery. UK) and custom siRNA sequences were verified using NCBI nucleotide BLAST. Upon the arrival of RNAi, the tubes were briefly centrifuged to collect the RNA at the bottom of the tube. Following the manufacturer's guideline, 1 mL of 1X siRNA buffer was added to each tube (solution made from 200 µL of 5X siRNA buffer (#NC1338268, Fisher-Scientific. USA) diluted in 800 µL RNase-free water). Manufacturer's RNAi concentration was verified using NanoDrop ND-100 spectrophotometer as described in 2.2.1. The RNAi stock was split into 20 µL aliquots and stored at -20˚C and strictly limited to no more than three freeze thaw cycle. Prior to setting up any gene knockdowns, all the siRNA reagents were thawed on ice and briefly vortexed and centrifuged. The siRNA experiments were performed under a sterile tissue culture laminar flow hood cleaned with 70% ethanol and wiped down with RNaseZap. All Eppendorf tubes were DNase/RNase-free including filter tips. The siRNA cocktail was made with RNAi and RNAiMAX duplex as shown in the Table 2.5. The volume of siRNA mix made according to the Table is optimised for 250,000 cells per well of a 6-well plate. For transfection control or the scramble ON-TARGET plus non-targeting siRNA was used (Horizon Discovery, UK).

Table 2.5 Transfection reagents and dilutions used for siRNA knockdown.

Transfection		
Component	**Scramble (µL)**	**siRNA (µL)**
Opti-MEM I	500	500
RNAiMAX	7.5	7.5
RNAi	5	5

RNAiMAX-RNAi duplexes were made in a Bijou tubes (#369123, Fisher-Scientific. UK) with reduced serum Opti-MEM 1 (#11058021, ThermoFisher-Scientific. UK) and carefully mixed by swirling the tube. Then, 500 µL siRNA mix was pipetted into

each well of a 6-well plate and incubated for 10-15 min, then 1 mL of cell suspension (250,000 cells/mL in growth media without any antibiotics) was pipetted into the siRNA mix wells followed by 1 mL growth media topped up to achieve a final volume of 2.5 mL per well. The siRNA cells were incubated for 48 h or 72 h at 37˚C and 5% CO_2. Following a Real-Time qPCR to assess the efficacy of siRNA target knockdown, 72 h was chosen as the optimal time point to achieve 80% or more efficient gene knockdown. The Real-Time qPCR for gene knockdown data was analysed as described in Chapter 2, section 2.2.3.5. The siRNA sequence designed for specific gene are shown in Table 2.6.

Table 2.6 Target genes and siRNA sequence

Gene	Custom siRNA duplex	
MPC1	Sense	5' U.C.A.A.A.C.A.C.G.A.U.G.A.C.U.A.A.U.U 3'
	Antisense	5' U.U.A.G.U.C.A.U.C.U.C.G.U.G.U.U.U.G.A.U.U 3'
MPC2	Sense	5' G.A.G.A.U.A.U.U.A.A.C.C.A.A.G.A.A.C.U.A.U.U 3'
	Antisense	5' U.A.G.U.U.C.U.U.G.G.U.U.A.U.A.U.C.U.C.U.U 3'
PYCR1	Sense	5' G.C.A.C.G.G.A.G.G.U.G.G.A.A.G.A.G.G.A.U.U 3'
	Antisense	5' U.C.C.U.C.U.U.C.C.A.C.C.U.C.C.G.U.G.C.U.U 3'
PYCR2	Sense	5' G.C.A.A.C.A.A.G.G.A.G.A.C.G.G.U.G.A.A.U.U 3'
	Antisense	5' U.U.C.A.C.C.G.U.C.U.C.C.U.U.G.U.U.G.C.U.U 3'
PYCR3	Sense	5' C.C.A.A.G.G.A.G.C.U.C.A.G.C.A.G.A.A.A.U.U 3'
	Antisense	5' U.U.U.C.U.G.C.U.G.A.G.C.U.C.C.U.U.G.G.U.U 3'

2.4 Western blotting

2.4.1 Sample preparation

2.4.1.1 Mitochondrial isolation

The mitochondrial isolation was carried out using a Pierce mitochondrial isolation kit (ThermoFisher, #89874), following the manufacturer's protocol. All reagents and samples were maintained on ice throughout the process. Volumes needed for reagent A and C were calculated and aliquoted into Eppendorf tubes. To prevent protein

degradation, 1 µL/mL of protease inhibitor cocktail (Thermo-Scientific, #87785) was added to reagent A and C. The pelleted cells were suspended in 800 µL of reagent A and incubated on ice for 2 min (do not incubate more than 2 min). Samples were supplemented with 10 µL of reagent B, incubated on ice for 5 min followed by a brief vortex every minute. Then, 800 µL of reagent C was added and mixed well by inverting the tube a few times (do not vortex), followed by centrifugation at 700 x g for 10 min at 4 ˚C and the supernatant was collected into a labelled tube. Samples were then centrifuged at 3000 x g for 15 min at 4 ˚C to remove any lysosomes and peroxisomes. The remaining pellet (almost transparent) was washed with 500 µL of reagent C and centrifuged at 12000 x g for 5 min at 4 ˚C. The mitochondrial pellet was lysed with 60 µL of RIPA buffer (Sigma-Aldrich, #R0278) on ice for 15 min. The lysate was then centrifuged at 12000 x g for 5 min and the supernatant collected for protein quantification.

2.4.1.2 Whole cell lysis

All samples were maintained on ice throughout the process. Cell samples were initially pelleted by centrifuging at 800 x g for 5 min at 4˚C. The pellet was resuspended in 100 µL of RIPA buffer and kept on ice for 15 min to lyse the cells. During this incubation, the cell lysates were briefly centrifuged every 3 min. Samples were then centrifuged at 5000 x g for 7 min to remove any cell debris. Supernatants were transferred to a new labelled Eppendorf tube and placed on ice for protein quantification. Following the protein quantification, samples were carefully aliquoted and stored at -20 ˚C for future use. Prior to use of any new aliquot, amount of protein was quantified using a detergent compatible protein assay (DC assay; Bio-Rad).

2.4.2 Protein quantification

Protein quantification was performed in a 96-well plate using the DC protein assay kit (Bio-Rad, #5000116). All the samples were thawed on ice prior to the experiment. Samples were then vortexed followed by a brief centrifugation. A standard curve was constructed by preparing several dilutions of bovine serum albumin (BSA) (2.5 mg/ml stock) to obtain a range from 0.5 mg/mL–2.5 mg/mL at 0.5 mg/mL intervals. Dilution

of the standards were made from the same buffer as for the samples. A working solution (A') was obtained by mixing 20 µL of Reagent S in each 1 mL of reagent A. Then 5 µL of standards, samples and blanks were pipetted onto a 96-well plate in duplicates. To each well, 25 µL of working reagent A' and 200 µL of Reagent B was added. The plate was covered by aluminium foil and incubated for 15 min at room temperature with gentle agitation. The absorbances were read at 750 nm using a POLARstar omega plate reader (BMG Labtech, Ortenberg, Germany). The protein concentrations were determined by plotting a standard curve. Protein loading volume was determined by dividing the desired mass (5µg of protein loaded) by stock concentration (mg/mL) of each protein sample.

2.4.3 Sodium dodecyl sulphate polyacrylamide gel electrophoresis (SDS PAGE)

Proteins were separated according to their size on a polyacrylamide gel. The gel composition to make a 12% separation gel is shown in Table 2.7. The resolving gel was loaded onto the casting stand and left for 30-40 min to set followed by adding 1 mL of propanol on top to create a smooth interface. Following aspiration of propanol, the top layer of the gel was washed five times with ddH_2O to remove any excess alcohol. The stacking gel was loaded and left for 20 min to set. While waiting for the stacking gel to set, samples were prepared to load into the gel.

Table 2.7 Recipe for making Polyacrylamide gels

	Stacking Gel	Resolving Gel
	4%	12%
30% Acrylamide	800 µL	4 mL
ddH2O	2.7 mL	3.4 mL
1.5 M Tris (pH 8.8)	N/A	2.5 mL
1 M Tris (pH 6.8)	500 µL	N/A
10% SDS	40 µL	100 µL
10% APS	40 µL	100 µL
TEMED	4 µL	10 µL

The cell lysates were added in 1:1 ratio to 2x loading/Laemmli buffer (#38733, Sigma-Aldrich) (10% w/v SDS, 10 mM β-mercaptoethanol, 20% v/v glycerol, 0.2 M Tris-

HCl (pH 6.8) and 0.05% w/v bromophenol blue) and heated at 95˚C for 5 min. The gel stack was carefully arranged into the Mini-Protean Tetra system and the tank was filled with sufficient 1x running buffer (25 mM Tris-HCl, 200 mM glycine and 0.1% SDS). The gel electrophoresis was performed on an ice tray to minimise any protein degradation due to heat produced. The first well of each gel was loaded with 5 µL precision plus Dual colour standard (Bio-Rad, #1610374) as a marker. Then calculated sample volumes (from DC assay) were loaded carefully into each well. The gel electrophoresis was performed at 120 V for 40 min or until the loading buffer dye almost reached the bottom of the gel. To equilibrate the gel, it was carefully removed from the casting glass mould and dipped in 1x transfer buffer (20 mM Tris (pH 8.3), 200 mM glycine and 20% (v/v) methanol) for 15 min with gentle agitation.

2.4.4 Semi-dry Transfer

Prior to protein transfer, the polyvinylidene difluoride (PVDF) (GE healthcare, Chicago, USA) membrane was activated in methanol for 20 sec and soaked in 1x transfer buffer for 10 min along with filter paper pads. The transfer stack sandwich was assembled by placing a filter paper pad on the bottom and placing the PVDF membrane on top. The gel was carefully transferred to the top of the PVDF membrane followed by placing another filter paper pad on top. Any air bubbles were gently removed between the transfer sandwich using a blot roller (Bio-Rad, UK). A Trans-blot turbo transfer system (Bio-Rad, UK) was used to transfer any proteins from the gel to the PVDF membrane at 25 V and 1.0 A for 7 min (self-optimised).

To avoid non-specific binding of antibodies, the PVDF membrane was blocked using 5% BSA dissolved in 1x Tris buffered saline and 0.1% Tween20 (TBS/ 0.1% Tween20) for 1 h at room temperature with gentle agitation. The blocking buffer was removed and PVDF membrane was washed with TBS/ 0.1% Tween20 for 5 min intervals and washing was repeated 3 times. The PVDF membrane was cut to the protein size of interest and transferred to four compartmented plates to probe with different antibodies.

2.4.5 Immunoblotting

All primary antibodies (raised in rabbit) were used at 1:1000 dilution and diluted in either in 5% BSA or non-fat milk in TBS/ 0.1% Tween20 according to the antibody data sheet. The primary antibody solutions were added to the relevant PVDF membranes and incubated overnight at 4˚C. The antibody solution was removed, and the membranes were washed for 5 min with TBS/tween20 followed by 3 more washings of 5 min each. Secondary antibody, anti-rabbit IgG HRP-linked (#7074S, Cell signalling, UK) was diluted in 5% non-fat milk in TBS/0.1% tween20 at 1:1000 dilution and added to all the membranes. Membranes were incubated at room temperature for 1 h with gentle agitation. The antibody solutions were aspirated, and the membranes were washed for 5 min with TBS/0.1% Tween20 followed by 3 more washings of 5 min each. For protein detection, the protein levels were developed using enhanced chemiluminescent, ultra-western HRP substrate (#WBULS0100, Merck, UK). Membranes were carefully arranged on the imaging tray of ChemiDoc XRS system (Bio-Rad, UK) to acquire the band images for further analysis, ensuring bands were not saturated.

2.4.6 Densitometry

Densitometry of Western blot bands was determined using Quantity One version 4.6.3 software (Bio-Rad, UK). Target/housekeeping protein bands were developed to ensure saturation of bands was not reached. The target protein band densities were then normalised against the corresponding housekeeping protein (VDAC as a mitochondrial marker or Tubulin or β-Actin as cytosolic marker). The target protein band densities were divided by control protein band densities to obtain a fold change.

Table 2.8 Antibodies used in this research study

Antibody	Clonality	Host	Dilution factor	Weight (KDa)	Supplier	Catalogue number	Lot number
MPC1	mAb	Rabbit	1:1000	~12	Cell signaling	14462S	1
MPC2	mAb	Rabbit	1:1000	~14	Cell signaling	46141S	1
VDAC	mAb	Rabbit	1:1000	~32	Cell signaling	4661S	7
α-Tubulin	mAb	Rabbit	1:1000	~52	Cell signaling	2144S	5
β-Actin	mAb	Mouse	1:1000	~42	Cell signaling	Ab8227	GR3255590-1
HRP-linked anti rabbit IgG	N/A	Goat	1:2000	N/A	Cell signaling	7074S	21

2.5 Metabolic substrate assay

2.5.1 Glucose assay

Extracellular glucose was measured using the glucose assay kit 1 (#1200032002, Eton Bioscience, USA) as per the manufacturer's instruction. Briefly, the glucose standard (2x) was thawed to room temperature and the glucose assay enzyme solution was thawed on ice in the dark. Cell supernatants were thawed to room temperature prior to use and diluted in ddH_2O, 1:25 and 1:50 to a final volume of 1 mL to ensure the readings are within the standard curve. Calculated volumes of glucose standard (2x) were diluted with ddH_2O to obtain the working standard solution (1x). The standard curve ranged from glucose concentration 0 μM to 400 μM (0, 8, 40, 80, 160, 240, 320, 400 μM). Standards, diluted samples, and media to blank wells were pipetted in duplicate into a 96-well plate (50 μL final volume). Standards and sample wells, including blanks, were pipetted with 50 μL glucose assay enzyme solution and incubated for 15 min at 37°C in a non-CO_2 incubator. To stop the reaction, 50 μL of 0.5 M acetic acid was added to each well with a gentle agitation. Absorbance was measured at 490 nm on POLARstar Omega microplate reader (BMG Labtech, Ortenberg, Germany). The glucose concentration in samples were obtained by plotting a linear regression fit and corrected to dilution factor before plotting the data set.

2.5.2 Pyruvate assay

Extracellular pyruvate was measured using the pyruvate assay kit (#1200041002, Eton Bioscience. USA) as per the manufacturer's instruction. Briefly, all buffers except for pyruvate assay enzyme mix (thawed on ice) were thawed at room temperature. Cells were cultured in pyruvate free media as indicated in *Results*. Cell supernatants were thawed to room temperature prior to use and diluted in dH_2O, 1:10 to a final volume of 0.5 mL to ensure the readings are within the standard curve. Calculated volumes of pyruvate standard (10x) were diluted in dH_2O with pyruvate assay buffer to generate a standard curve ranged from pyruvate concentration 0 μM to 200 μM. Standards, diluted samples and media to blank wells were pipetted in duplicate into a 96-well plate (50 μL final volume). Reaction solution master mix was prepared by adding 977 μL pyruvate assay buffer, 15 μL pyruvate assay enzyme, 3 μL pyruvate assay pre-

reaction mix and 8 µL assay probe. Then 50 µL of reaction master mix was added to each well and the plate incubated for 30 min at 37°C in a non-CO_2 incubator. Absorbance was measured at 570 nm on POLARstar Omega microplate reader (BMG Labtech, Ortenberg, Germany). Sample pyruvate concentrations were extrapolated by plotting a linear regression fit and correcting for dilution factor before plotting the data set.

2.5.3 Glutamine assay

Extracellular glutamine was determined using the glutamine assay kit (#ab197011, Abcam) as per the manufacturer's instruction. Briefly, all the buffers except for assay enzymes (thawed on ice) were thawed at room temperature. Freshly made glutamine stock (1 mM) was used in the range of 0 to 10 nmol/well to generate a standard curve. Samples underwent brief homogenization/deproteinization by adding perchloric acid to a final concentration of 1 M. Following the deproteinization step, sample recovery steps followed the manufacturer's instruction. Homogenized samples were diluted 1:10 with dH_2O. Standard and samples were pipetted into the wells to a final volume of 40 µL. calculated volume of hydrolysis buffer and hydrolysis enzyme mix were combined to obtain hydrolysis master mix for the standards and samples (10 µL/well) and hydrolysis buffer alone was added to the background control wells (10 µL/well). The plate was incubated for 30 min at 37°C in a non-CO_2 incubator. A glutamine reaction master mix was obtained by mixing development buffer (46 µL), development enzyme mix (2 µL) and developer (2 µL) to achieve 50 µL volume per well of reaction. The plate was incubated for 60 min at 37°C in a non-CO_2 incubator with gentle agitation and protected from light. Absorbance was measured at 450 nm on POLARstar Omega microplate reader (BMG Labtech, Ortenberg, Germany). Sample glutamine concentration were extrapolated by plotting a linear regression fit and correcting for dilution factor before plotting the data set.

2.6 CyQUANT cell proliferation assay

2.6.1 Sample preparation and CyQUANT dye Master mix

The CyQUANT cell proliferation assay kit was used to quantify the DNA content following the manufacturer's protocol (#C7026, Thermo Fisher scientific). The standard DNA with a concentration of 100 μg/mL in Tris/EDTA buffer (provided with the kit) and CyQUANT GR dye in DMSO (400X) were thawed on ice. Lysis buffer (20X) was thawed to room temperature.

DNA standard and GR dye were aliquoted into PCR tubes and stored at -20˚C. Briefly, the assay was performed on 96-well cell culture plates. The cells were seeded at 2000 cells/well of a 96-well plate and incubated for different time intervals. Each of the sample conditions had minimum of 4 technical replicates on the plate. Supernatant was carefully aspirated, and cells were washed with 100 μL of ice-cold PBS twice. The plate was then covered with aluminium foil and stored at -80˚C for a minimum of 4 h (maximum 96 h). The volume needed for the CyQuant GR dye master mix was calculated on the basis of a 200 μL volume per well. Prior to making up the maser mix solution, the plate was taken out of the freezer and thawed to room temperature.
The CyQUANT 1X Master mix was obtained by diluting 20X lysis buffer and 400X CyQUANT GR dye in RNase free water. The solution was made in a 50 mL centrifuge tube. The tube was vortexed at medium speed and briefly centrifuged and covered with aluminium foil.

2.6.2 Standard curve

Initially 20x lysis buffer was diluted RNase free water to obtain 1x lysis buffer. Calculated volume of CyQUANT GR dye (400x) was diluted in 1x lysis buffer to obtain 1x CyQUANT GR buffer master mix. The volume needed for DNA standard was calculated as per Table 2.9. To obtain 1 μg/mL of DNA working concentration, calculated volume of standard DNA (100 μg/mL) was mixed with 1x CyQUANT GR buffer master mix. Then 200 μL of CyQUANT GR buffer master mix was added to each sample well. The plate was wrapped in aluminium foil and incubated for 20 min at room temperature with gentle agitation. The standard curve was generated in duplicate according to Table 2.9 in a new 96-well clear bottom black plate (#CLS3603, Sigma-Aldrich. UK). The CyQUANT GR master mix was added to each sample to a final volume of 200 μL. The plate was covered in foil until fluorescence was ready to

be measured on a microplate reader. The fluorescence was measured using POLARstar Omega plate reader (BMG Labtech, Ortenberg, Germany) at 480 nm excitation and 520 nm emission range.

Table 2.9 Volumes and final concentration for generating standard curve for CyQUANT DNA quantification.

CyQUANT GR buffer master mix (µL)	1 µg/mL DNA in CyQUANT GR buffer master mix (µL)	Final DNA concentration (ng/mL)
200 (blank well)	0	0
198	2	10
190	10	50
180	20	100
160	40	200
120	80	400
80	120	600
40	160	800
0	200	1000

Data analysis

Data were analysed by substituting the fluorescent value (y) in the equation $y = mx + c$ obtained from standard curve (r^2 is equal or closer to 1) to find the value of x (concentration of DNA). A graph was plotted DNA concentration (ng/mL) against the sample names.

2.7 Cell proliferation study with proline supplementation

2.7.1 Cell culture and proliferation assay

The OVCAR3 cells were treated with 5 µM UK-5099 containing growth media for 24 h. Following 24 h incubation, both control and UK-5099 treated cells were counted and checked for 95% viability using Countess™ cell counter. The high glucose DMEM media (#31053044, ThermoFisher Scientific. UK) was mixed with no glucose, no glutamine, no phenol red and no sodium pyruvate DMEM media (#A1443001, ThermoFisher Scientific. UK) to achieve 11.1 mM glucose serum-free growth media. The cells were pelleted at 800 x g for 5 min and resuspended in 10 mL of freshly

prepared DMEM growth media (11.1 mM glucose, no glutamine or proline, 20% FBS). Then 200 µL of cell suspension (10,000 cells/well) were seeded on a 96-well plate, five technical replicate wells for each condition. Cells were incubated for 2 h at 37 ˚C and 5% CO_2. After 2 h, the media was aspirated and changed to conditioned media for control cells and MPC1 pharmacologically blocked cells. The conditions for the DMEM media were, complete growth media with glutamine, no proline, then complete media without glutamine and proline. Finally, complete media with 2 mM proline but no glutamine. The 96-well plate was further incubated for 16 h at 37 ˚C and 5% CO_2. Following the incubation, media was aspirated and cells were briefly washed with 200 µL of PBS. Plates were immediately frozen at -80 ˚C for 8 h.

For CyQuant DNA quantification assay frozen cell culture plates were defrosted to room temperature. The assay was performed according to Chapter 2, section 2.6.

2.8 Collagen Invasion Assay

2.8.1 Collagen coating

The experiment was carried out on a 12-well trans-well plate. 24 h prior to the experiment 8.0 µm pore sized inserts (#353182, Falcon® Corning. UK) were coated with Matrigel (#354277, Corning, UK) diluted in serum-free and phenol red-free DMEM (#A1443001, ThermoFisher Scientific) to achieve 1% solution. Inserts were carefully placed on a 12-well plate under sterile conditions. Then 100 µL of Matrigel suspension was pipetted into each insert for a homogenous coating. The plate was incubated at 37 ˚C in a humidified chamber containing 5% CO_2 overnight.

2.8.2 Assay set-up

The OVCAR3 cells were treated with siRNA media as described in Chapter 2, section 2.3 for MPC1 knockdown. Following 72 h knockdown, both scramble and *siMPC1* cells were counted and checked for 95% viability using countess™ cell counter. The high glucose DMEM media (#31053044, ThermoFisher Scientific. UK) was mixed with no glucose, no glutamine, no phenol red and no sodium pyruvate DMEM media (#A1443001, ThermoFisher Scientific. UK) to achieve 11.1 mM glucose serum-free growth media. The cells were pelleted at 800 x g for 5 min and resuspended in freshly

prepared DMEM growth media (11.1 mM glucose, no glutamine). Then 200 µL of 250,000 cells/mL cell suspensions were seeded on Matrigel coated inserts (both scramble and *siMPC1*) and 750 µL of DMEM (11.1 mM glucose) growth media with serum was added to the bottom wells. Six wells of OVCAR3 cells (3 wells each for scramble and *siMPC1* were seeded). Cells were incubated for 2 h at 37 ˚C and 5% CO_2. After 2 h, the scramble control cells received 250 µL complete serum-free growth media (with 2 mM glutamine), no glutamine or proline and 2 mM proline to each wells as shown is template below.

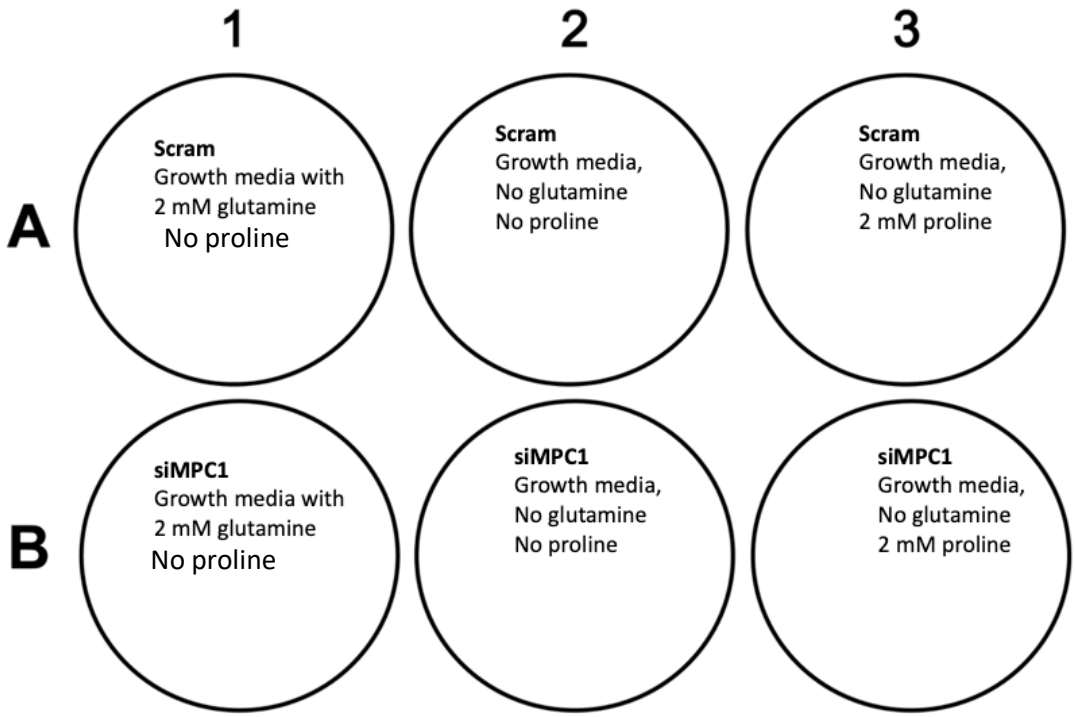

2.8.3 Cell staining

Cell culture inserts were carefully transferred to a clean unused well. Medium was carefully aspirated, and inserts were washed twice with PBS. Cells were fixed with 4% formaldehyde in PBS (#158127, Sigma-Aldrich. UK) at room temperature for 5 min (chamber and the bottom of the membrane). The inserts were washed twice with PBS. Then 100% methanol was used to permeabilize cells at room temperature for 20 min. Following the permeabilization, inserts were washed twice with PBS. Giemsa

stain (#G5637, Sigma-Aldrich. UK) diluted in ddH_2O (20%) was added to the top and bottom (to look for any invaded cells) of the insert and kept in the dark (or wrapped in foil) for 15 min at room temperature. The cells were washed twice with PBS and inserts were ready for analysis.

2.9 Clonogenic Assay

An *in vitro* cell survival assay to measure the ability of a single cell to grow into a colony. Only a fraction of cells is seeded after a desired pre-treatment (post-treatment can also be done after cells adhere to the plate) and cells are left for 2-3 weeks to form colonies.

2.9.1 Plating cells

The experiment followed the protocol described by (Franken et al., 2006) . The siRNA treated cells or UK-5099 treated cells were harvested and pelleted by centrifuging at 800 x g for 5 min. The cell pellet was re-suspended in PBS to remove any excess accutase and pelleted again. The pellet was then resuspended in RPMI 1640 media with supplements mentioned for OVCAR3 (section 2.1.1). The cells were counted and diluted in media accordingly to achieve 800 cells/mL. Cells were seeded in 6-well plates at 800 cells per well in a final volume of 2.5 mL and incubated for 21 days at 37 $^{\circ}$C in a humidified chamber containing 5% CO_2. Every 3 - 4 days cells were given fresh media (for siRNA cells) or media with UK-5099 (for UK-5099 treated wells).

2.9.2 Colony fixation and staining

Following the aspiration of media from the wells, the cells were gently rinsed twice with PBS. To fix and stain, 2 mL of 0.5% crystal violet in 6% glutaraldehyde was added to the cells. The plate was left covered in foil for 30 min at room temperature. The staining mixture was removed carefully (harsh pipetting could remove the colonies from the plate), and the wells were rinsed with water by gently sinking the plate in a wash basin filled with water (direct washing in tap water could end up in

colonies being detached from the plate). The plates were left to dry at room temperature.

2.9.3 Data Analysis

The stained colonies were photographed using a Sony α7 digital camera. Colonies were manually counted using Murgaa Clicker counter (**www.Murgaa.com/mac-mouse-click-counter**) considering 20 cells or more as a colony.

2.10 Bioenergetic studies

The Seahorse XFe96 analyzer (Seahorse Bioscience) was used to measure extracellular flux upon MPC inhibition. The metabolic pathways of oxidative phosphorylation (OXPHOS) were measured as oxygen consumption rate (OCR; pmole/min) and glycolysis measured as the extracellular acidification rate (ECAR; mPH/min) in real-time.

2.10.1 Procedure

The day prior to the assay, cartridge hydration was performed. Briefly, the sensor cartridge was placed upside down and 200 µL of XF calibrant was pipetted into the utility plate (all wells). The sensor cartridge was carefully placed back onto the utility plate containing the calibrant fluid and incubated at 37 ˚C in a humidified non-CO_2 oven overnight. Cells were seeded at 30,000 cells per well to form a uniform monolayer on a XFe96 cell culture plate. The cells were pre-incubated in UK-5099 (5 µM) or vehicle 24 h before analysis. The cells were incubated at 37 ˚C and 5% CO_2 in a humidified chamber.

On the day of assay pre-warmed Seahorse media was adjusted to pH 7.35 at 37 ˚C. Supernatants from cell culture plate were gently aspirated and cells were carefully washed gently with 200 µL PBS. Then 150 µL of serum-free seahorse media was pipetted into each well and incubated for 1 h at 37 ˚C in a non-CO_2 oven. Glucose (11.1 mM) and glutamine (2 mM) solution were diluted in Seahorse media and pH adjusted to 7.35 with sodium hydroxide (#S2770, Sigma-Aldrich). The sensor cartridge was completely removed from the utility plate and replaced immediately to eliminate any air bubbles formed during the incubation. The sensor cartridge was then injected with

25 µL of glucose containing media (port A) or glutamine media (port C) and placed in the Seahorse XFe96 analyzer for calibration. Following the calibration, the utility plate was replaced with a cell culture plate and XFe96 protocol was setup to measure the basal rate for 30 min then simultaneously measure OCR and ECAR for a further 2 h. Upon completion of the Seahorse XFe96 analyzer, the supernatant was carefully removed, and cells were wash gently with PBS. The cell culture plate was frozen at -80˚C for 3 h before carrying out a CyQuant DNA quantification assay for normalisation.

2.10.2 Data Analysis

The data obtained were normalised to the DNA content of each well determined by the CyQuant assay (section 2.5). The respiratory parameters OCR and ECAR were calculated using the data obtained from the Seahorse XFe96 analyzer after normalisation. Basal respiration values were set to 1 (before the injection). Further calculations to generate OCR and ECAR are detailed within *Results* Chapters.

2.11 Stable isotope tracing analysis (SITA) by GC-MS

The stable isotope tracing study sample preparation was done by me but the mass spectrometry analysis was done as a paid service at McGill university, Canada. For sample preparation, OVCAR3 scramble control or *siMPC1* treated cells were seeded at 4 x 10^4 cells/cm^2 in a T25 flask. For heavy labelled glucose SITA, cells were incubated with universally labelled ^{13}C glucose (11.1 mM; #CLM-1396. Cambridge isotope, USA) in glucose free RPMI 1640 (ThermoFisher-Scientific, #11879020) growth media. For labelled glutamine or lactate, cells were incubated with universally labelled ^{13}C glutamine (2 mM; #CLM-1822. Cambridge isotope, USA) or ^{13}C Lactate (10 mM; #CLM-1579. Cambridge isotope, USA) in glutamine free RPMI 1640 (ThermoFisher Scientific, #31870) growth media. The labelled lactate media was supplemented with 2 mM unlabelled glutamine (ThermoFisher scientific, #25030081). Cells were incubated for a period of 72 h and then washed with ice cold saline solution and lysed in 80% methanol. Lysates were centrifuged to remove any cell debris and cell extracts were dried down at 4 ˚C using a speed vacuum concentrator. Cellular

metabolites were extracted and analysed by gas chromatography-mass spectrometry (GC-MS) using a previously described protocol (Vincent et al., 2015).

Metabolite extracts were derived using N-(*tert*-butyldimethylsilyl)-N-methyl trifluoroacetamide (MTBSTFA) as described previously (Faubert et al., 2013). D-myristic acid (750 ng/sample) was added as an internal standard to metabolite extracts, and metabolite abundance was expressed relative to internal standard and normalized to cell number. GC-MS analysis was performed using an Agilent 5975C GC/MS equipped with a DB-5MS + DG (30 m x 250 μm x 0.25 μm) capillary column (Agilent J and W, Santa Clara, CA, USA). For SITA experiments, mass isotopomer distribution was determined using a custom algorithm developed at McGill University (McGuirk et al., 2013). Initially matrix values for each samples were normalized for myristic acid internal standard. Then myristic acid normalized values were normalized for cell number (MID enrichment). Finally, all the MID enrichment values were arranged as a pint glass model (as mentioned by McGill University) to obtain total pool of ^{12}C and ^{13}C abundance.

2.12 Statistical analysis

Raw data were handled using Microsoft Office Excel 365. The arranged data were exported to GraphPad Prism to generate graphs and statistical analyses (GraphPad Prism, version 8.3.1, USA). The Kolmogorov-Smirnoff test was used to check for normality, and data sets that deviated from normality resulted in a non-parametric test and were transformed to achieve normality. Parametric data were analysed using analysis of variance (ANOVA) for two or more groups. One-way ANOVA with either Bonferroni or Tukey's post hoc test was used to compare the treatments group with the control. For multiple comparisons, two-way ANOVA was used with Dunnett's multiple comparison test. Data are presented as the mean ± standard error of the mean (SEM) unless stated otherwise. All replicates have a sample size of at least n = 3 from independent biological replicates/cell passages. Significance values were taken when $p < 0.05$, graphically denoted as *$p < 0.05$**, $p < 0.01$, ***$p < 0.001$.

Chapter Three

The effect of mitochondrial pyruvate carrier inhibition in ovarian cancer cell lines

3 Cell response to MPC inhibition by UK-5099 in ovarian cancer cell lines

3.1 Introduction

Genetic and epigenetic modifications can alter cellular metabolism initiating differences in normal and abnormal cells (cancer cells). Cancer cells often reprogram their metabolism to increase the supply of energy and metabolites to maintain their highly proliferative phenotype (Hanahan and Weinberg, 2011). Energy production in cells involves cascades of pathway reactions starting with the utilisation of a glucose molecule. Glucose generates the central carbon metabolite pyruvate via glycolysis. Pyruvate feeds into the tricarboxylic acid (TCA) cycle and becomes oxidised to acetyl-CoA. The generated acetyl-CoA is used in downstream processes of oxidative phosphorylation (OXPHOS) to generate energy within the mitochondria. However, even under aerobic conditions, some cancer cells are reprogrammed metabolically to increase the rates of glycolysis. In contrast, normal cells favour OXPHOS, which Otto Heinrich Warburg first observed in the 1920s. Aerobic glycolysis was later named the Warburg effect (Compan et al., 2015b; Heiden et al., 2009; Warburg et al., 1927). Here, the pyruvate generated during glycolysis is usually converted to lactate instead of transported into the mitochondria, which can also be converted back to pyruvate, known as the reverse Warburg effect (Fu et al., 2017; Wilde et al., 2017). The metabolic switch to favour glycolysis in cancer cells is yet unknown. However, glycolysis is an efficient option for cancer cells to make precursors for the *de novo* biosynthesis of nucleotides, amino acids and lipids (Ruiz-Iglesias and Manes, 2021).

Around 70–80% of ovarian cancer deaths arise from high grade serous ovarian carcinoma (HGSOC) (Bell et al., 2011; Lisio et al., 2019; Reid et al., 2017). Ovarian surface epithelial cells and secretory epithelial cells of the distal fallopian tube are the main progenitors of HGSOC. Metabolic flexibility in HGSOC cells has been shown to drive tumour progression and resistance to chemotherapy (Anderson et al., 2014; Yang et al., 2014c). Whilst looking at metabolic alterations in HGSOC cells, 80% of the epithelial ovarian cancer cells were revealed to have a deleted chromosomal region 6q27 which has now been realised to include the *MPC1* gene loci (Tibiletti et al., 1998).

In 1971, a metabolic study on rat liver mitochondria revealed the importance of a specialised carrier protein for pyruvate transport into the mitochondria (Papa et al., 1971). Three years following the finding, a plasma protein inhibitory study, using α-cyano-4-hydroxycinnamate, confirmed the presence of a pyruvate carrier protein as this inhibitor blocked the pyruvate intake across the mitochondrial membrane while pyruvate dehydrogenase, pyruvate carboxylase or pyruvate kinase involved in pyruvate metabolism were not affected. This particular carrier protein was identified in 2012 and was named the mitochondrial pyruvate carrier (MPC) complex (Bricker et al., 2012). The MPC complex is a 150 kDa heterodimer formed from MPC1 and MPC2 subunits (Herzig et al., 2012). Pyruvate transport into mitochondria is promoted by MPC1 and MPC2 heterodimer complex that resides in the inner mitochondrial membrane (Bowman et al., 2016; Bricker et al., 2012; Herzig et al., 2012). Lack of *Mpc1* in Yeast and *Drosophila* was found to have reduced concentration of acetyl-CoA and lower TCA cycle intermediates, while *MPC1* silencing in mammalian cells leads to impaired pyruvate oxidation (Bricker et al., 2012). Following the discovery of MPC cooperation demonstrated in mammals, co-expression of MPC1 and MPC2 resulted in a four-fold increase of pyruvate transport in contrast with cells that under express MPC1 (Bricker et al., 2012; Herzig et al., 2012).

For a long time, the impairment of pyruvate transport into the mitochondria has been connected with different cancers (Eboli et al., 1977; Paradies et al., 1983). Following the discovery of a pyruvate carrier, MPC inactivation or its low expression has been shown to promote tumour growth in numerous cancers, whilst overexpression of MPC1 has been shown to successfully reduce tumour growth in colon cancer, oesophageal cancer and gastric cancer cells (Bricker et al., 2012; Schell et al., 2014b; Zhou et al., 2017). Moreover, intestinal stem cells that lack tumour suppressor adenomatous polyposis coli (*APC*) has been shown to fully reduce cancer progression upon MPC overexpression (Bensard et al., 2019). Likewise, re-expressing *MPC1* in colon cancer cells exhibited reduced cell growth and tumorigenicity in mouse models (Rauckhorst and Taylor, 2016; Schell et al., 2014b). However, MPC1 downregulation in renal carcinoma was associated with suppression of proliferator-activated receptor gamma co-activator-1 alpha (PGC-1α) (Li et al., 2018). Upregulation of PGC-1α induced MPC1 expression in breast cancer cells while *MPC1* transcription mediated

by oestrogen-related receptor alpha (ERRα) seemed to be required for tumour growth (Li et al., 2018; Park et al., 2019). As discussed previously, one of the key events observed in breast, lung, prostate, intestinal and colon cancer are employing alternative sources to fuel the TCA cycle and continuing to support nucleotide and lipid biosynthesis. A major finding to date is that MPC1 lacking cells use glutamine as an alternative source to feed the TCA cycle, and *MPC1* deletion has been shown to promote cell proliferation and migration in multiple cancers (demonstrating non-small cell lung carcinomas under glucose depleted environments are dependent on glutamine (Gonsalves et al., 2020; Hudson et al., 2016; Le et al., 2012; Vincent et al., 2015; Yang et al., 2014c; Yoo et al., 2020; Zhao et al., 2019)). This phenomenon of dependency on glutamine and glutaminolysis is called "glutamine addiction", and we believe glutamine addicted ovarian cancer cells are more invasive and have a more aggressive phenotype.

3.2 Hypotheses

The present study tested the hypothesis that epithelial ovarian cancer cells have altered MPC expression, which is influenced by nutrient availability in the tumour microenvironment and drives cancer cell proliferation, migration, and invasion. Furthermore, pharmacological inhibition of MPC in HGSOC cells initiate glutamine addiction.

3.3 Experimental Procedures

3.3.1 Cell culture

Cell lines used for this study were the chemotherapy-sensitive PEO1 and chemotherapy-resistant PEO4 and OVCAR3 cell lines. All cell lines are representative of HGSOC (Coscia et al., 2016a). The cell lines were selected due to (i) PEO1 and PEO4 being reported to have low MPC1 protein expression whilst OVCAR3 are reported to overexpress MPC1 (Coscia et al., 2016a). The SKOV3 cell line was also initially included in studies, but is not thought to phenotypically or genotypically represent HGSOC tumour cells (Coscia et al., 2016a). The cell culture methods for these cell lines are described in Chapter 2, section 2.1.1. Each biological replicate (at least three) is an independent passage of that particular cell line. Any media used for growth studies were consistent (e.g., concentration of glucose or glutamine etc.), except for differential media conditions (e.g., high glucose or low glucose). Cells were seeded at 2,500 cells/cm^2 adjusted to the area of cell culture plates.

3.3.2 Cell proliferation assay

The proliferation rate of ovarian cancer cells was measured by the CyQUANT™ proliferation assay. At each time point, the supernatant was aspirated, cells were briefly washed with PBS and the plate immediately frozen at -80°C for DNA quantification. The data for a 24 h period is shown in the *Results* section (48 and 72 h are shown in the Appendix). Generation of standards and concentration calculations are detailed in Chapter 2, section 2.6

3.3.3 α-cyano-ß-(1-phenylindol-3-yl)-acrylate (UK-5099) - MPC inhibitor

To inhibit the pyruvate transport into the mitochondria, a potent inhibitor for MPC1, UK-5099, was purchased as a powder, and a stock solution of 20 mM was made with DMSO. The UK-5099 solution was aliquoted and stored in the freezer for further use (stable for more than one year at -80°C). The concentration range and serial dilution of UK-5099 are detailed in Chapter 2, section 2.1.2.

3.3.4 Quantitative real-time polymerase chain reaction (qPCR)

The qPCR for gene expression studies were performed using Quantifast SYBR Green (Qiagen, UK) and the CFX connect Real-time PCR detection system (Bio-Rad, UK).

All consumables were DNase/RNase-free, and the laminar flow hood was cleaned using RNaseZAP wipes. The general experimental setup, including RNA extraction and cDNA synthesis, is explained in detail in Chapter 2, section 2.2. Purity of total RNA quantification was measured on the Nano-drop, and 260/280 nm and 260/230 nm values were between 1.8 and 2.3. This Chapter investigated the role of *MPC1* and *MPC2* genes. The starting quantity of mRNA from experimental samples was determined using standard curves generated from serial dilutions of pooled reference RNA with Quantifast SYBR green (Qiagen). Sample and reference genes were analysed in triplicate, and mRNA expressions were normalised to *RPL19* and *ACTB*. The gene expression data relative quantity was calculated according to Livak & Schmittgen's method (Livak and Schmittgen, 2001) and data expressed as ΔΔCq.

3.3.5 Immunoblotting for MPC

To examine the localisation of MPC complex components and any alteration in protein abundance in response to nutrient availability, MPC1 was assayed by Western blotting using an anti-MPC1 antibody (#14462, Cell Signaling Technology, UK). The PEO1, PEO4, OVCAR3 and SKOV3 cell lines were grown in 6-well plates at 24,000 cells/well in complete growth media for whole-cell lysis. For differential media conditions, cells were grown in custom made DMEM (Gibco Technology) where normal glucose (11.1 mM), low glucose (1 mM) and/or glutamine (2 mM or no glutamine) were supplemented. Media preparation and essential supplements recommended for culturing the cell lines to comply with ATCC are explained in Chapter 2, section 2.1.1. The detailed immunoblotting procedure is described in Chapter 2, section 2.4.

3.3.6 Bioenergetic analysis

I. OXPHOS and Glycolysis

The oxidative phosphorylation and glycolysis of MPC1 inhibited cells were measured on the Seahorse XF analyzer as previously described in Chapter 2, section 2.10. Data obtained was normalised to the DNA content of each well before further analysis.

3.3.7 Metabolic substrate measurements

I. Glucose assay

The glucose consumption by MPC inhibited cells over 24 was measured using a glucose assay kit as previously described in Chapter 2, section 2.5.1. Supernatants were collected to labelled cluster tubes (#4410, Corning, UK) and maintained on ice before further use.

II. Pyruvate assay

The extracellular pyruvate level was measured using a pyruvate assay kit as previously described in Chapter 2, section 2.5.2.

III. Glutamine assay

The glutamine concentration was measured using a glutamine assay kit as previously described in Chapter 2, section 2.5.3.

3.3.8 Statistical analysis

Data are presented as mean ± SEM, with statistical analyses performed using GraphPad Prism version 8.4.1. One-way ANOVA with Tukey's multiple comparison test was used to compare treatment groups with the control, and one-sample Kolmogorov-Smirnoff was used to test for normality. Any data deviated from normality; non-parametric test was used.

3.4 Results

3.4.1 Determining MPC1 and MPC2 expression levels in representative HGSOC cell lines

To investigate MPC status, *MPC1* expression was determined in PEO1, PEO4 and OVCAR3 cells under complete growth media conditions. The human hepatoma cell line HepG2 was used as a control for qPCR and Immunoblotting, as they abundantly express *MPC* (NCBI Gene database). Ribosomal protein L19 (*RPL19*) and Beta-actin (*ACTB)* were used as housekeeping reference genes. According to qPCR data, *MPC1* expression was significantly higher in OVCAR3 compared to PEO1 or PEO4 cells (Figure 3.1a). Under the same basal media conditions, no difference was seen in *MPC2* expression in PEO1 or OVCAR3 cells. However, PEO4 cells showed significantly higher expression of *MPC2* compared to the other cell lines (Figure 3.1b).

In order to determine MPC1 expression at the protein level, total protein from cells was extracted by whole-cell lysis, and MPC1 expression was monitored using an anti-MPC1 rabbit monoclonal antibody. The protein voltage-dependent anion channel (VDAC) was used as a mitochondrial loading control. Evidence from Immunoblotting supports the qPCR data where OVCAR3 cells show higher MPC1 protein expression compared to PEO1 or PEO4 cells (blot Figure 3.1c and corresponding densitometry Figure 3.1d), total protein from HepG2 cell line was used as a positive control for MPC1.

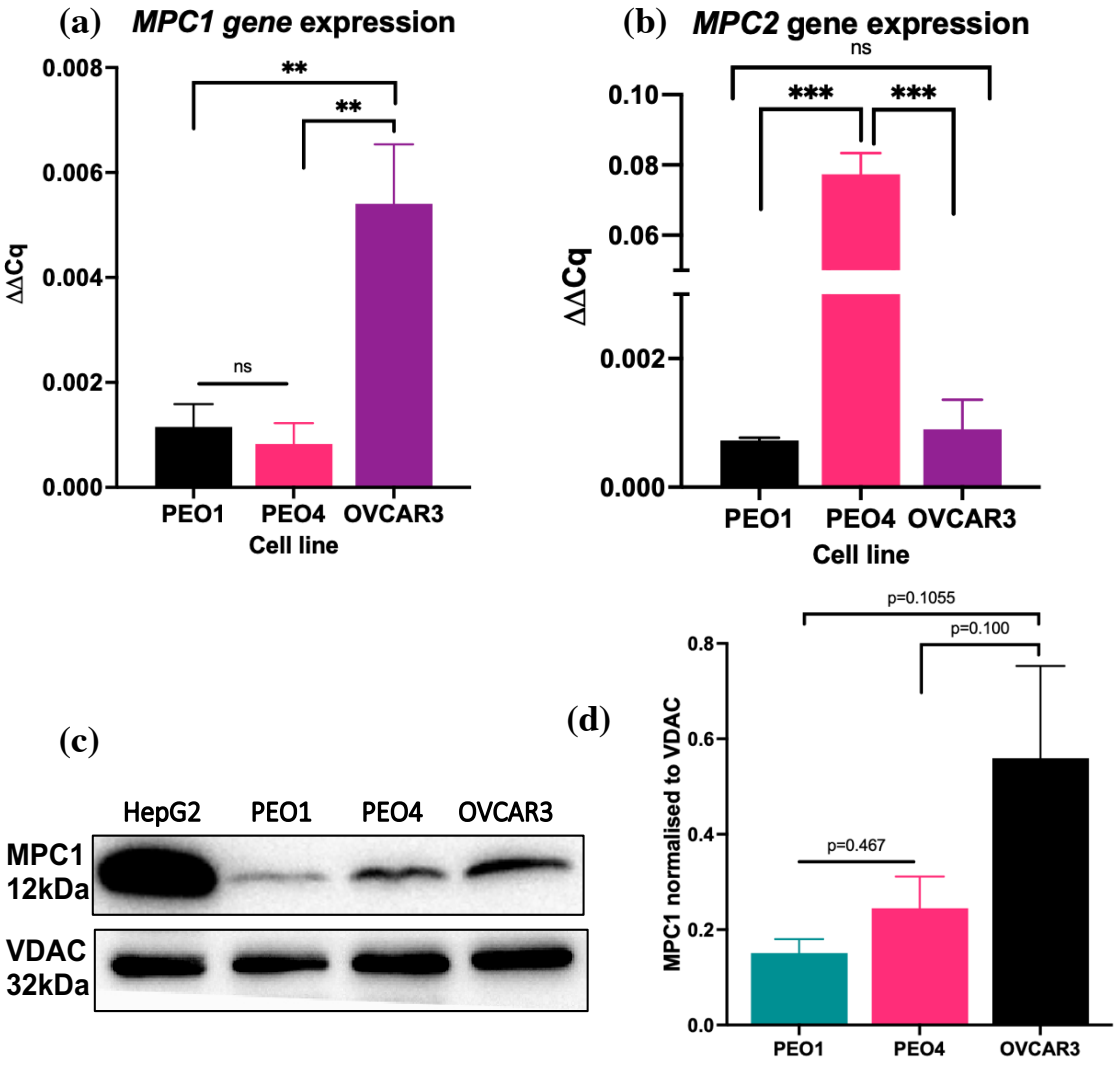

Figure 3.1 Expression levels of MPC1 and MPC2 under complete growth media conditions

Quantitative real-time PCR data of (a) *MPC1* (n = 6), (b) *MPC2* (n = 3) and (c) immunoblotting for MPC1 (n = 3) and corresponding densitometry data (d) are shown. HepG2 cells were used as an MPC1 positive control. Statistical significance was evaluated using one-way ANOVA with Tukey's multiple comparison test. Data was obtained from independent biological replicates for each experimental set-up. Data expressed as mean ± SEM; * $p \leq 0.05$, ** $p \leq 0.01$, *** $p \leq 0.001$.

3.4.2 Inhibition of the mitochondrial pyruvate carrier by UK-5099 induces cell proliferation

The role of MPC in cell proliferation was studied in ovarian cancer cell lines during inhibition of MPC with UK-5099. Epithelial ovarian cancer cell lines PEO1, PEO4, OVCAR3 or SKOV3 cells were treated with 2.5 μM or 5 μM UK-5099 whilst vehicle controls were treated with equivalent volumes of DMSO for 24 h, 48 h or 72 h (48 h and 72 h data are shown in appendix). The UK-5099 drug concentration was chosen based on previous research and preliminary studies. A concentration rage of 0.625 μM to 20 μM UK5099 was used (data not shown). Recent findings showed UK-5099 needs to be changed every 24 h due to its structural instability. The idea behind supplementing fresh growth media with UK-5099 does not fit the experimental design, hence 48 h and 72 h data were used for reference purposes only. Later in this research study, siRNA techniques were used to look at 48 h and 72 h. Inhibition of MPC with UK-5099 (5 μM) resulted in increased cell proliferation over 24 h in PEO1 (Figure 3.2a; $p = 0.01$), OVCAR3 (Figure 3.2c; $p = 0.05$) and SKOV3 (Figure 3.2d; $p = 0.03$) cell lines. Although increased proliferation was not observed in PEO4 cells (Figure 3.1c; $p = 0.27$). This data indicates overall that UK-5099 (5 μM) treatment to target MPC of following cell lines resulted in increased ovarian cancer cell proliferation.

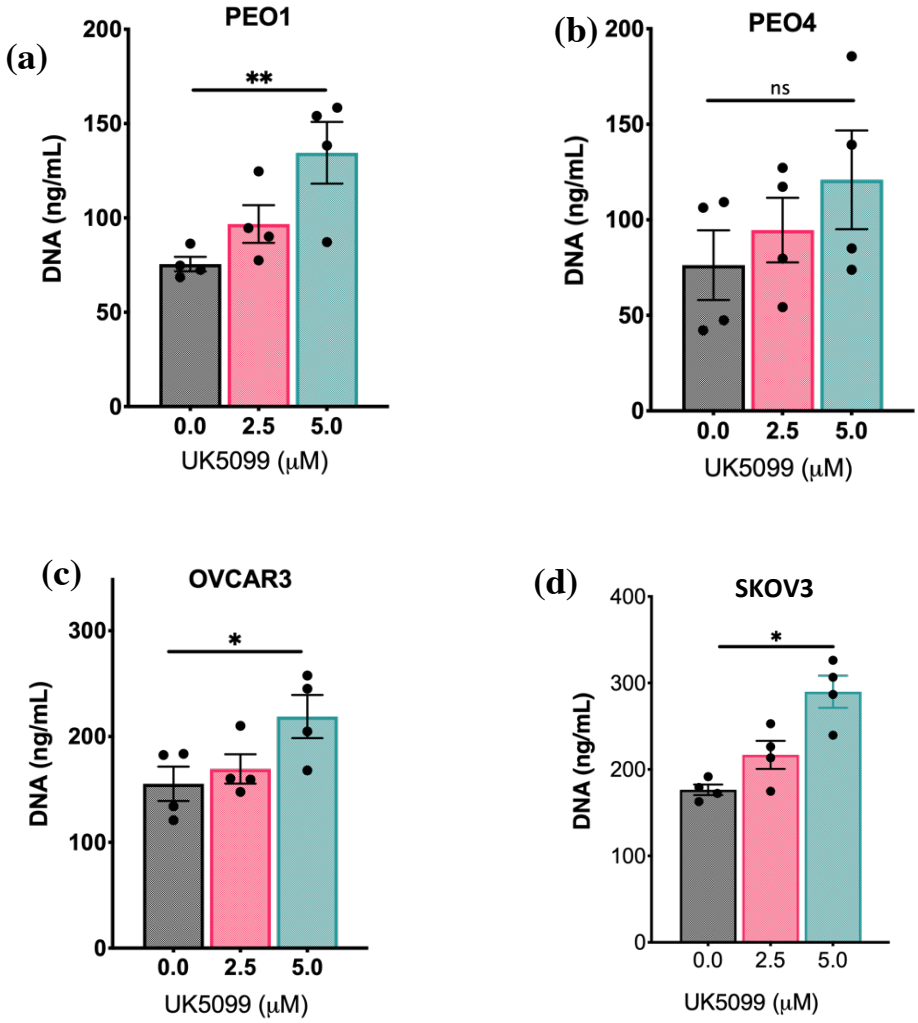

Figure 3.2 MPC inhibition by UK-5099 induced cell proliferation in ovarian cancer cell lines.

Graphs represent the DNA concentration measured by CyQuant in (a) PEO1, (b) PEO4, (c) OVCAR3 and (d) SKOV3 cells after treatment with UK-5099 or vehicle control for 24 h. Statistical significance was evaluated using one-way ANOVA with Tukey's multiple comparison test. Data was obtained from n=4 independent biological replicates for each experiment. Data expressed as mean ± SEM; * $p \leq 0.05$, ** $p \leq 0.01$.

3.4.3 MPC inhibition altered pyruvate concentrations whilst glucose consumption was not affected

Glucose is considered to be the primary fuel source for cells, and the limitation of glucose has been shown to slow cancer progression unless cancer cells rewire their metabolic networks. Therefore, it is important to understand the level of glucose consumption within a short period. Glucose consumption whilst inhibiting MPC was investigated over 24 h. Cells were pre-incubated in growth media containing 5 μM UK-5099 for 24 h. Glucose concentration was then measured in cell supernatants and cell-free media. Vehicle control treated PEO1, PEO4, OVCAR3 and SKOV3 cells on average metabolised ~8 mM glucose in 24 h (Figure 3.3). However, during this period no significant differences in glucose consumption were observed in PEO1 or SKOV3 cells treated with UK-5099 when compared to vehicle (PEO1; $p = 0.685$, SKOV3; $p = 0.686$), while PEO4 or OVCAR3 cells consumed less glucose when MPC1 was inhibited (PEO4; $p = 0.200$, OVCAR3; $p = 0.349$)

UK-5099 inhibits pyruvate transport into the mitochondria via reduced MPC complex activity. Therefore, ovarian cancer cells were exposed to UK-5099 in pyruvate-free media and the concentration of pyruvate in cell supernatants was measured. The UK-5099 did not significantly alter pyruvate concentrations in the reportedly low MPC1 expressing cell lines (Coscia et al., 2016a), PEO1 ($p = 0.98$), PEO4 ($p = 0.67$) and SKOV3 ($p = 0.39$) cells compared with vehicle controls (Figure 3.4). However, the MPC1 positive OVCAR3 cells showed a four-fold increase (~400 μM) in extracellular pyruvate accumulation (OVCAR3; $p \leq 0.0001$) compared to vehicle control upon MPC inhibition (Figure 3.4). This significant increase in extracellular pyruvate levels suggests OVCAR3 cells may lack alternative pathways for the metabolism of pyruvate.

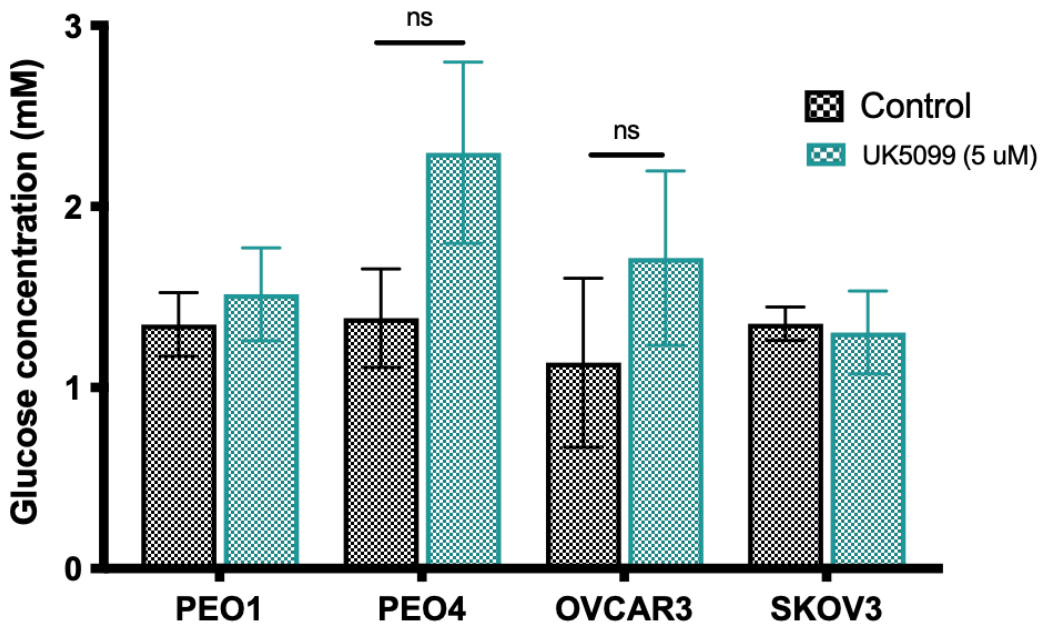

Figure 3.3 Glucose consumption in MPC inhibited ovarian cancer cells.
Control (black) and UK-5099 treated (green) represent supernatants glucose concentrations, and the average concentration of glucose consumed across all cell lines are 8 - 9 mM (Control media 11.1 mM). Data obtained from n = 4 independent biological replicates for each cell line. Data expressed as mean ± SEM; * $p \leq 0.05$, ** $p \leq 0.01$, *** $p \leq 0.001$ and statistical significance were analysed by two-way ANOVA using the šidák's multiple comparison test.

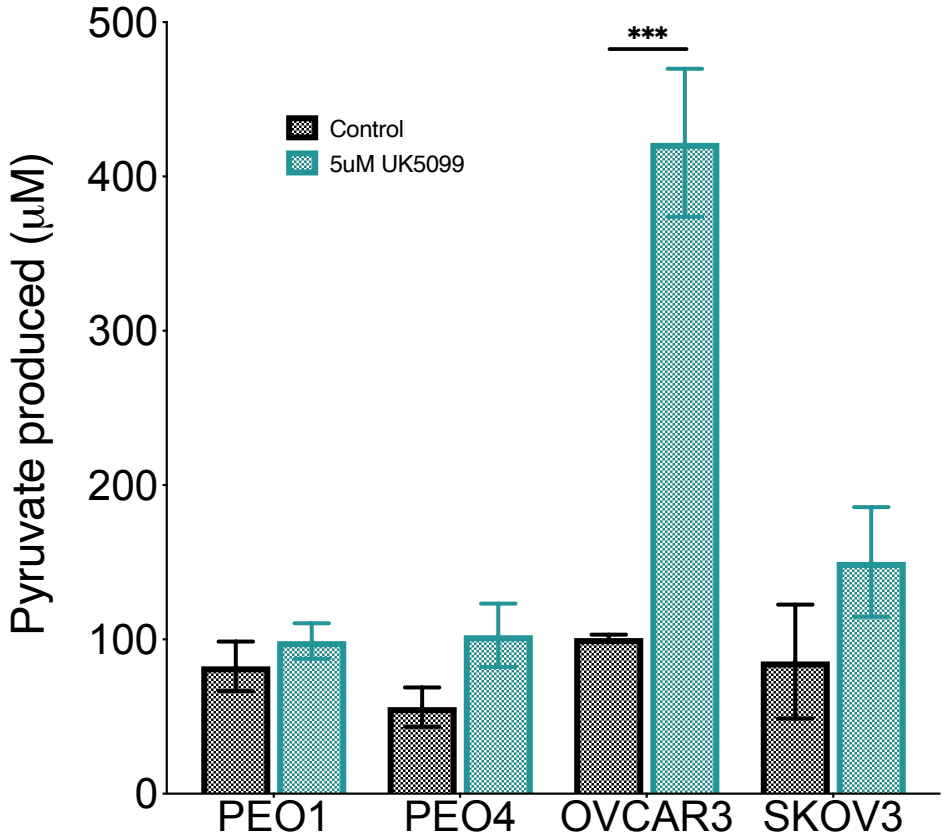

Figure 3.4 Pyruvate production is increased in UK-5099 inhibited OVCAR3 cells Control (black) and UK-5099 treated (green) pyruvate concentrations in cell supernatants. Data defined after correcting for background pyruvate present in cell-free media (blank media). Data was obtained from n=3 independent biological replicates for each cell line. Data expressed as mean ± SEM; * $p \leq 0.05$, ** $p \leq 0.01$, *** $p \leq 0.001$ and statistical significance were analysed by two-way ANOVA using the šidák's multiple comparison test.

3.4.4 MPC inhibition has no significant effect on glutamine consumption

Glutamine plays a major role as an anaplerotic precursor. Glutamine has previously been shown to compensate for the loss of pyruvate transport into the mitochondria in various cancers (Vacanti et al., 2014b). Therefore, glutamine consumption by ovarian cancer cell lines during inhibition of MPC complex was investigated. The data showed moderate changes in glutamine consumption in UK-5099 treated cells over 24 h compared to vehicle controls (PEO1; $p = 0.71$, PEO4; $p = 0.35$, OVCAR3; $p = 0.66$, SKOV3; $p = 0.89$; Figure 3.5)).

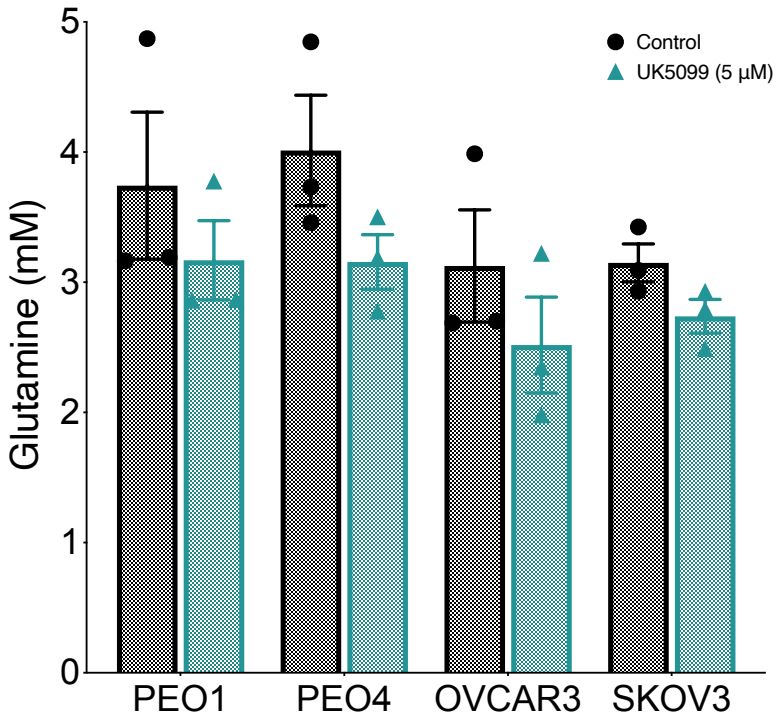

Figure 3.5 Glutamine concentrations in ovarian cancer cell supernatants
Glutamine concentration was determined in cell supernatants with vehicle controls or UK-5099. Data is obtained from n=3 independent biological replicates for each cell line. Data expressed as mean ± SEM; * $p \leq 0.05$, ** $p \leq 0.01$, *** $p \leq 0.001$ and statistical significance were analysed by two-way ANOVA using the šidák's multiple comparison test.

3.4.5 Bioenergetic profile of ovarian cancer cell lines upon MPC inhibition.

Cancer cells generate energy and maintain redox homeostasis via glycolysis and OXPHOS. MPC links glycolysis and the TCA cycle via its central metabolite, pyruvate. As previous studies showed impaired pyruvate transport into the mitochondria can be compensated by glutamine oxidation feeding the TCA cycle, the cellular energy expenditure in MPC inhibited cells was next investigated using the Seahorse Bioanalyzer. On the day of experimental assay, cells that were seeded on Seahorse XF analyzer plates were starved of glucose or glutamine by incubating the cells in serum-free Seahorse media (no glucose or glutamine). This step is important in order to understand the metabolic flexibility of these cell lines. For MPC1 inhibition, cells were incubated with serum-free Seahorse media containing 5 μM UK-5099 for 1 h. Then the cells were loaded into the XF analyzer and the basal readings were taken before injecting with glucose or glutamine for both control and UK-5099 treated cells. The oxygen consumption rate (OCR), which represents OXPHOS, and the extracellular acidity rate (ECAR), which represents glycolysis, was monitored.

The OCR increased in PEO1 and PEO4 cell lines in response to glutamine injection whether or not cells were treated with UK-5099 (Figure 3.6a and 3.6b). Glutamine addicted SKOV3 cells (Yang et al., 2014b) exhibited low OCR under glutamine depleted or basal conditions (Figure 3.6d). However, when glutamine was injected, an increase in OCR was displayed by SKOV3 vehicle control cells, whilst a steady rise in OCR in UK-5099 treated SKOV3 cells ($p = 0.0015$) was observed. MPC1 positive OVCAR3 cells displayed increased OCR in response to glutamine ($p < 0.001$) only when MPC was inhibited (Figure 3.6c), suggesting loss of MPC may drive a glutamine dependent phenotype. These data for MPC1 positive OVCAR3 and glutamine assay suggests that glutamine addiction could be a long term advantage for these cell types.

The glycolytic rate was monitored in PEO1, PEO4, OVCAR3 and SKOV3 cell lines in response to glucose (10 mM) injection, which is represented by changes in extracellular acidity rate (ECAR) from lactate production (pH). The PEO1 cells, when treated with UK-5099, showed a minor decrease in the ECAR (2 mpH/min/cells) in response to glucose injection (Figure 3.7a). Untreated PEO1 cells and PEO4 cells (whether or not treated with UK-5099) showed a moderate increase in ECAR (3

mpH/min/cells) in response to glucose (Figure 3.7a and Figure 3.7b). Interestingly OVCAR3 cells exhibited increased ECAR in MPC inhibited cells in response to glucose (Figure 3.7c), and the ECAR was higher compared to any cell line used in this study (OVCAR3; about 5 mpH/min/cells). Whereas SKOV3 cells displayed no difference in ECAR in response to glucose (Figure 3.7d).

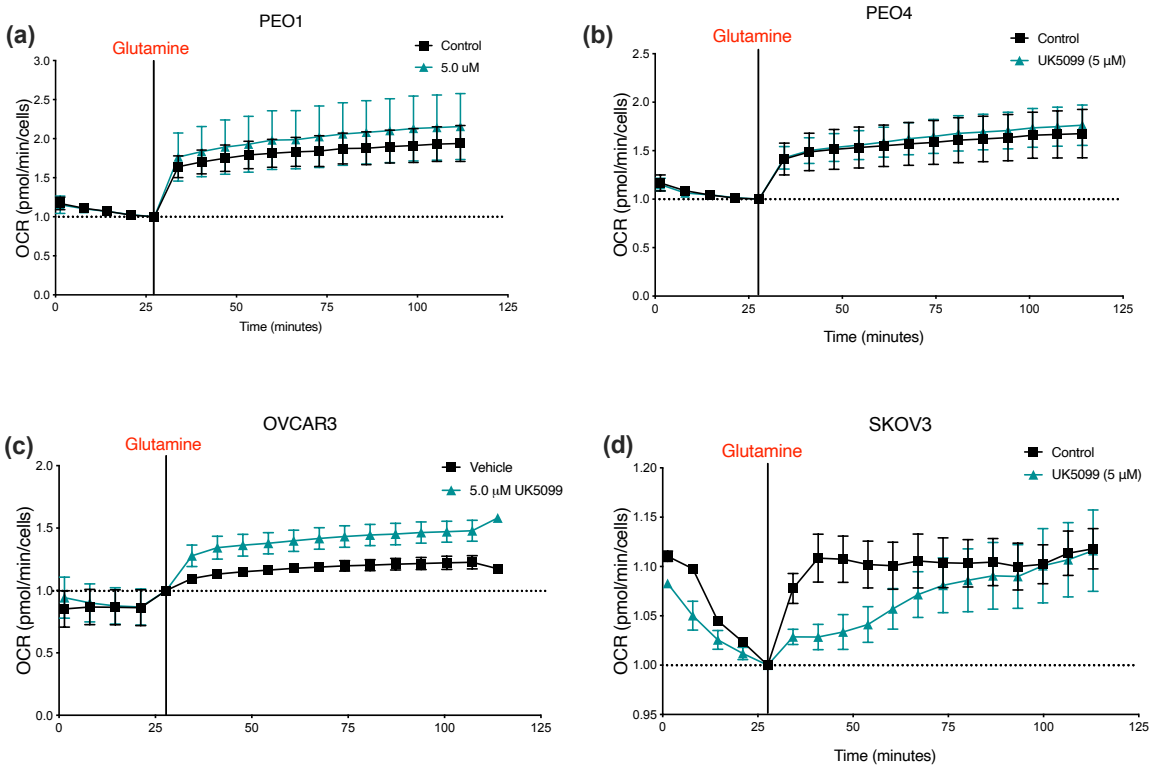

Figure 3.6 Measuring the oxygen consumption rate of ovarian cancer cell lines in response to glutamine

Cells were treated with UK-5099 or vehicle control for 24 h prior to analysis on the Seahorse Bioanalyzer. Cells were then incubated for one hour in Seahorse medium, and a series of basal measurements were taken before injection of glutamine (2 mM). Data were corrected for numbers of cells and was obtained from n=3 independent biological replicates for each cell line. Data expressed as mean ± SEM; * $p \leq 0.05$, ** $p \leq 0.01$, *** $p \leq 0.001$ and statistical significance was analysed by t-test using Mann-Whitney comparison test.

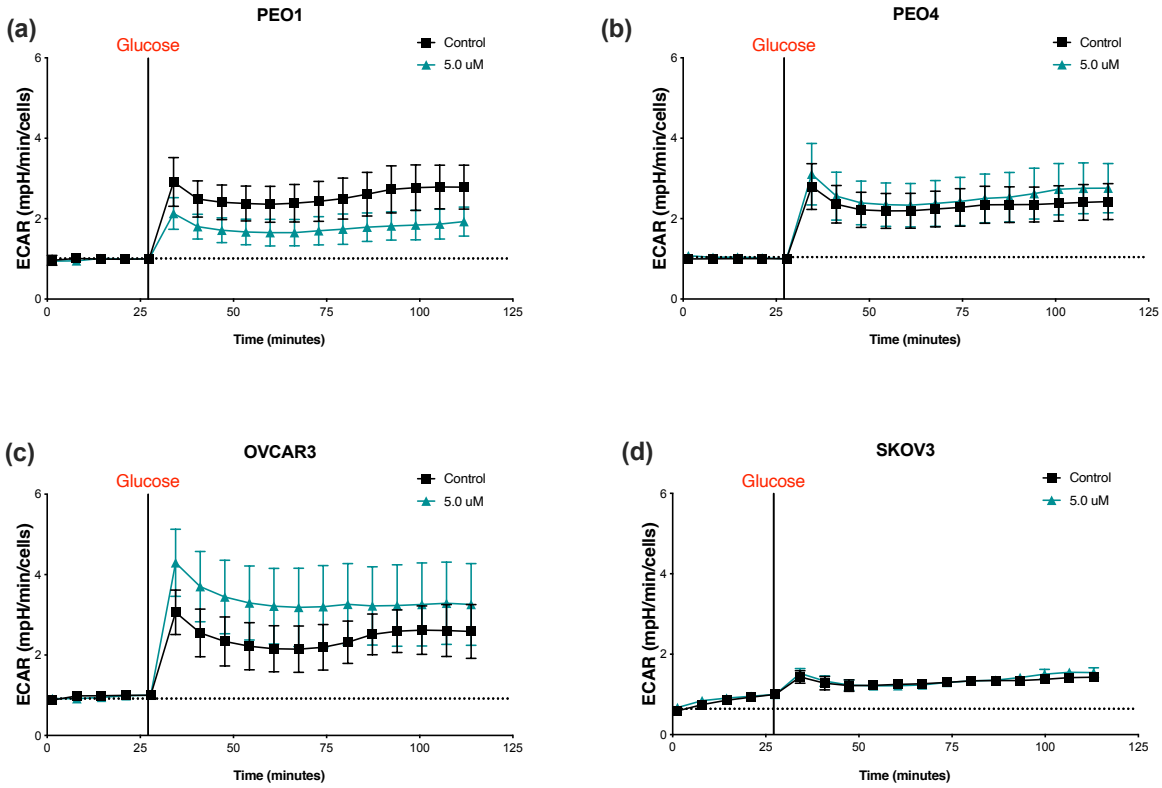

Figure 3.7 Measuring the extracellular acidity rate of ovarian cancer cell lines in response to glucose
Cells were treated with UK-5099 or vehicle control for 24 h prior to analysis on the Seahorse Bioanalyzer. Cells were then incubated for one hour in Seahorse medium, and a series of basal measurements were taken before injection of glucose (10 mM). Data were corrected for numbers of cells and was obtained from n=3 independent biological replicates for each cell line. Data expressed as mean ± SEM; * $p \leq 0.05$, ** $p \leq 0.01$, *** $p \leq 0.001$ and statistical significance was analysed by t-test using Mann-Whitney comparison test.

The HGSOC subtype of ovarian cancer is the most lethal subtype of all ovarian carcinomas and the focus of this study. As SKOV3 cells were shown to be unlikely to represent HGSOC, they were not used in further experiments (Coscia et al., 2016a; Domcke et al., 2013).

3.4.6 MPC expression is influenced by nutrient availability in cancer cells

The availability of nutrients in the TME influences metabolic alterations in cancer. To further investigate the effect of nutrient depletion, the abundance of MPC1 or MPC2 was determined. PEO1, PEO4 and OVCAR3 cells were grown under differing glucose concentrations with or without glutamine supplementation (e.g., NG; normal glucose but no glutamine). PEO4 and OVCAR3 cells grown under nutrient-depleted conditions showed significant differences in *MPC1* expression. PEO4 cells exhibited comparatively high *MPC1* expression under normal glucose and glutamine replete conditions, while *MPC1* expression was not influenced by the availability of glucose in PEO4 cells. However, when glucose and glutamine were both depleted, *MPC1* expression increased considerably (Figure 3.8). In MPC1 positive OVCAR3 cells, depletion of glutamine resulted in significantly increased expression of *MPC1*, but the availability of glutamine under glucose depleted conditions did not induce or affect *MPC1* expression (Figure 3.8).

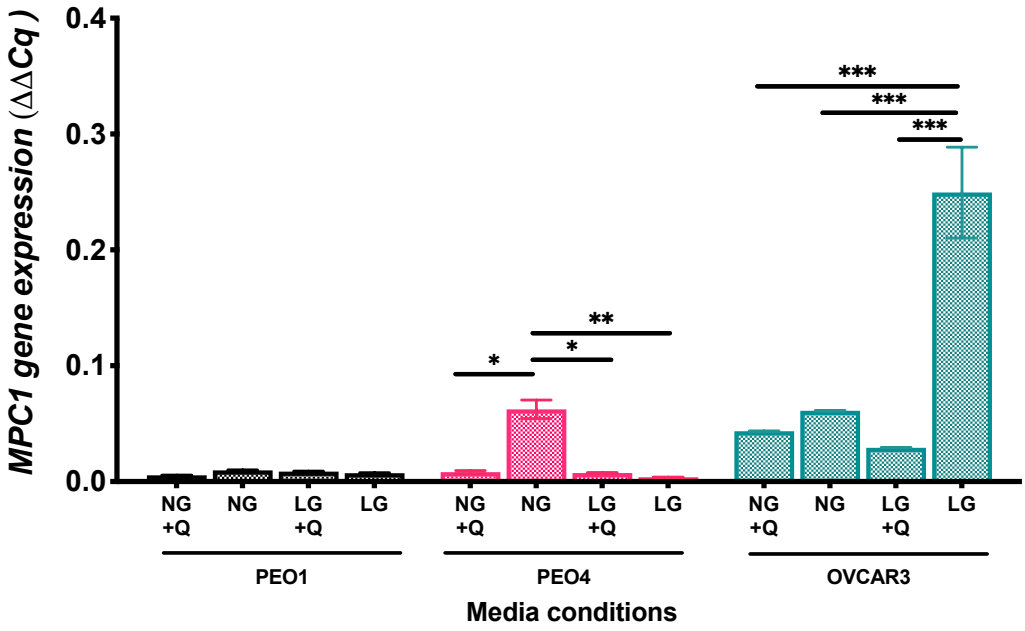

Figure 3.8 Expression of *MPC1* under differential growth media
MPC1 expression was monitored under normal glucose (NG; 10 mM), low glucose (LG; 1 mM) and glutamine (Q; 2mM) conditions. Statistical significance was evaluated using two-way ANOVA with Tukey's multiple comparison test. Data were obtained from independent biological replicates for each experimental set-up and each cell line data n = 3. Data expressed as mean ± SEM; * $p \leq 0.05$, ** $p \leq 0.01$, *** $p \leq 0.001$.

Evidence from the literature suggests MPC is localised to the mitochondria (Herzig et al., 2012). Mitochondria were isolated from cells cultured under differential media conditions over 24 h (11 mM glucose, 2 mM glutamine; NG+Q or 1 mM glucose, no glutamine; LG). Total mitochondrial protein was immunoblotted for MPC1 or MPC2; VDAC was used as a mitochondrial loading control. When glucose was limited in these cell lines, OVCAR3 cells upregulated MPC1 and MPC2 protein expression to presumably maximise the pyruvate transport into the mitochondria (figure 3.9a). The data obtained support the qPCR results for *MPC* expression at the genetic level. The MPC positive OVCAR3 cell lines express more MPC1 and MPC2 than PEO1 or PEO4 (Figure 3.9b).

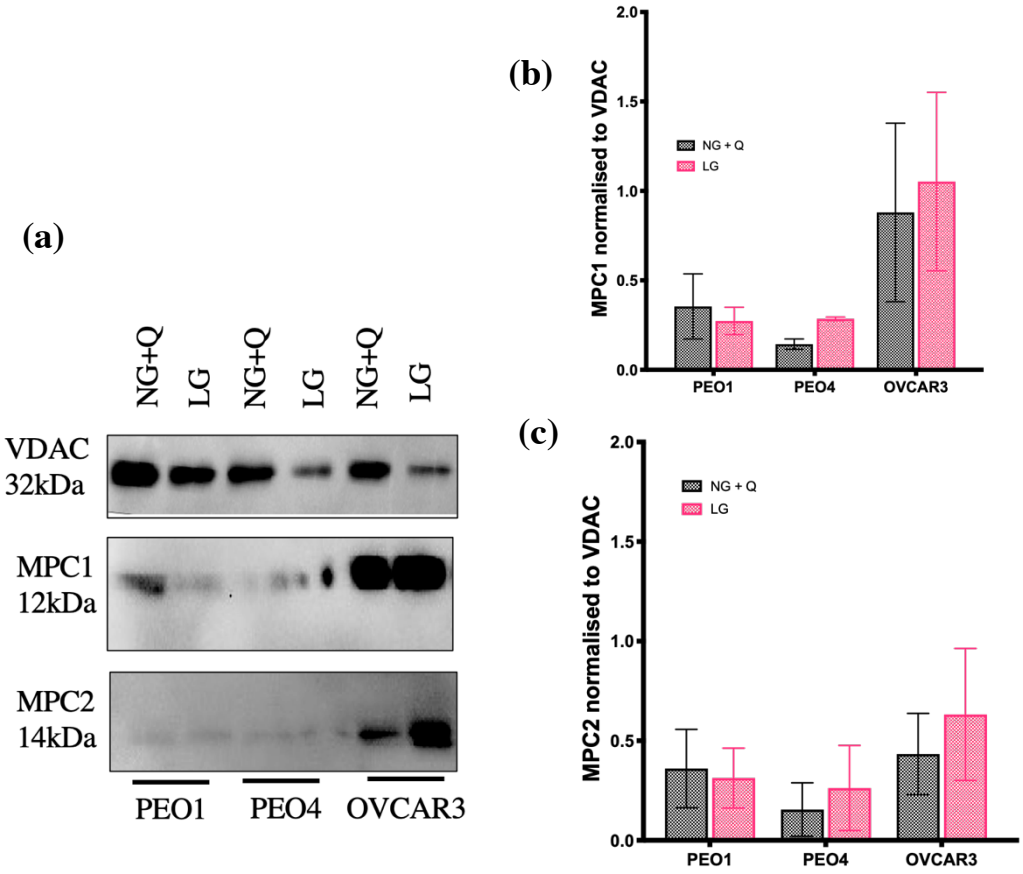

Figure 3.9 Immunoblot analysis for MPC proteins under differential media conditions

Mitochondrial MPC1 and MPC2 expression was measured under normal glucose (NG; 10 mM), low glucose (LG; 1 mM) and glutamine (Q; 2mM) varied conditions. (a) representative MPC1 and MPC2 blot followed by corresponding densitometry for (b) MPC1 and (c) MPC2, respectively. Data were normalised to the housekeeping protein

VDAC and n = 3 independent biological replicates for each cell line. Data is expressed as mean ± SEM; * $p \leq 0.05$, ** $p \leq 0.01$, *** $p \leq 0.001$.

In PEO1 and OVCAR3 cells, no difference in *MPC2* expression was seen. However, PEO4 cells showed relatively high levels of *MPC2* expression (Figure 3.10). However, the expression of *MPC2* was reduced upon depletion of glutamine (glutamine dependent, NG + Q and LG + Q) whether glucose was restricted or not. These data suggest, while OVCAR3 cells rely on MPC1 for OXPHOS, PEO4 cells may utilise MPC2 homodimer for pyruvate transport into mitochondria (Nagampalli et al., 2018). However, the protein data for differential media condition does not reflect on mRNA data obtained for MPC2 expression while MPC1 correlation is seen between the mRNA and protein. The MPC2 elevated levels in PEO4 could also mean that mRNA expression is elevated but a functional protein is not made by these cells.

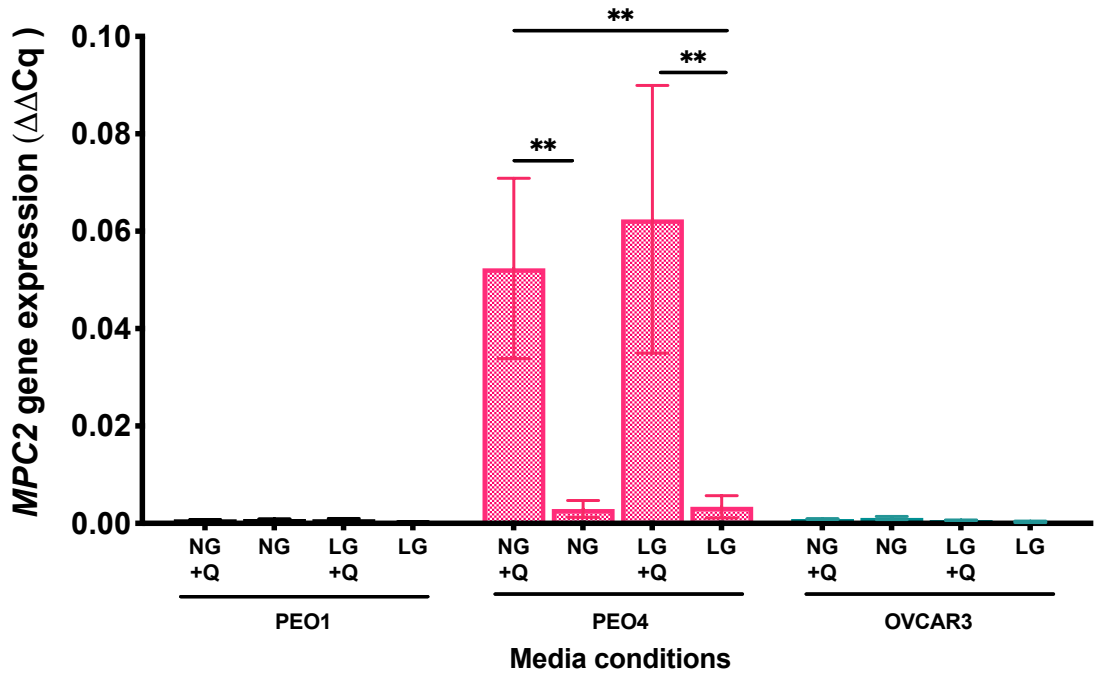

Figure 3.10 Expression of *MPC2* under differential media conditions
Changes in *MPC2* expression were measured under normal glucose (NG; 10 mM), low glucose (LG; 1 mM), with or without glutamine (Q; 2mM). Statistical significance was evaluated using two-way ANOVA with Tukey's multiple comparison test. Data was obtained from n=3 independent biological replicates for each experimental set-up. Data expressed as mean ± SEM; * $p \leq 0.05$, ** $p \leq 0.01$, *** $p \leq 0.001$.

3.5 Discussion

It is becoming increasingly evident that opportunistic modes of nutrient acquisition by cancer cells in the tumour microenvironment are driven by genetic alterations (Pavlova and Thompson, 2016). The tumour suppressor p53 (*TP53*) is commonly mutated in most cancers. Paradoxically, wild type *TP53* is expressed at a relatively low level in some cancers to permit nutrient acquisition in a generally nutrient restricted environment. A recent study on liver cancer tissues showed increased p53 upregulated modulator of apoptosis (PUMA), induced by wild type *TP53,* inhibited pyruvate driven OXPHOS by blocking MPC, resulting in increased glycolysis (Kim et al., 2019). However, according to The Cancer Genome Atlas, over 96% of HGSOC were found to be *TP53* mutated (Corney et al., 2008). The TP53 expression levels in PEO1, PEO4 and OVCAR3 are mentioned in table 3.1. It has been previously shown, tumour suppressor TP53 negatively regulates MPC function in liver cancer cells (Kim et al., 2019). In my model of cell lines, all three cell lines express similar levels of TP53. Moreover, increased glycolysis in HGSOC is modulated by copy number variation (CNV) loss of >80% 6q27, which includes *MPC1* gene locus. Based on the following discoveries of *MPC1*, the current study investigated the role of MPC1 in ovarian cancer progression.

The data in this Chapter indicates deregulation of MPC1 acts as a metabolic switch between glycolysis and OXPHOS in ovarian cancer cells to maximise the efficiency of energetic cellular pathways and increase cell proliferation. Inhibition of MPC1 using UK-5099 in nutrient replete or restricted nutrient environs, replicating the *in vivo* tumour microenvironment, altered rate of glycolysis, OXPHOS and the proliferation rate of HGSOC cells.

In a study by Coscia et al., around thirty different ovarian cancer cell lines were characterised by proteomic profiling (Coscia et al., 2016a). In this study, most HGSOC cancer cell lines were shown to have reduced MPC1 expression (Table 3.1 shows the reported protein expression levels of TP-53, MPC1 and MPC2 for the cell line models used in this study). Reduced expression or deletion of *MPC1* correlates with poor prognosis in several carcinomas (Bensard et al., 2019; Li et al., 2016; Schell et al., 2014b).

Table 3.1 Proteomic study of ovarian cancer cell lines using high-performance liquid chromatography (HPLC) (Coscia et al., 2016a). The data obtained is calculated as binary logarithm (Log_2).

	Protein levels (Log_2)		
Protein	PEO1	PEO4	OVCAR3
TP53	30.18	29.06	30.02
MPC1	n/a	n/a	24.07
MPC2	24.89	23.89	25.25

Previous studies have shown *MPC1* loss affects glucose consumption and initiates glutamine anaplerosis in various carcinoma cells (Vacanti et al., 2014b; Yang et al., 2014c). In this study, inhibition of MPC1 resulted in dose-dependent increases in cell proliferation. Evidence from bioenergetic studies using the Seahorse Bioanalyzer indicated that the proliferation of cells in response to MPC1 inhibition could lead to glutamine dependency. Moreover, it is important to understand whether the glutamine dependency or MPC1 depletion mechanism originated at the primary site or cancer cells reprogrammed during their genetic alteration during the EMT to MET. This is an important episode to investigate since clinically treating MPC1-depleted cells could very well be different from following the same treatment of tumour in the primary site which express MPC1. This glutamine dependency upon inhibition of MPC1 was verified by cells grown under nutrient restricted environments. Although, the reportedly low *MPC1* expressing PEO4 cells showed minor changes in *MPC1* expression under a glutamine depleted environment. Data from the Seahorse Bioanalyzer indicates that PEO1 and PEO4 cells are adapted to utilise glutamine for OXPHOS. However, *MPC1* expressing OVCAR3 cells were only able to switch to metabolise glutamine under glucose depleted conditions when MPC was inhibited. In the OVCAR3 cells, *MPC1* expression was significantly increased when glutamine was removed, and the availability of glucose was limited. Potentially suggesting these cells are trying to increase pyruvate transport efficiency.

Glucose depleted conditioned cells were analysed for MPC1 protein expression via Immunoblotting. Mitochondria were isolated from all three cell lines to analyse the expression and cellular localisation of MPC1. Under low glucose conditions, MPC1

and MPC2 protein expression were significantly higher in OVCAR3 cells, while no changes were seen in the reportedly low MPC1 expressing PEO1 or PEO4 cells. The observed differences between the expression of MPC1 and MPC2 in whole-cell protein fractions vs isolated mitochondrial fractions may indicate that despite MPC1 and MPC2 being expressed in these cells, the localisation of MPC1 and MPC2 to the mitochondria may be affected.

Glutamine plays a dual role in cells as a carbon or nitrogen donor. One of the most important metabolic pathways for glutamine is feeding the TCA cycle through the generation of α-KG. Although α-KG can be produced by other means (i.e., oxidative decarboxylation or reductive carboxylation), TCA cycle substrates are crucial under certain conditions like a hypoxic TME or impaired pyruvate transport into mitochondria (Le et al., 2012; Still and Yuneva, 2019). Studies have shown in the past, maintaining TCA flux under glucose depleted conditions occurs via malic enzymes and pyruvate dehydrogenase in lung and hepatocellular carcinoma cells (Vacanti et al., 2014b). In the present study, *MPC2* expression was demonstrated to be dependent on glutamine in the PEO4 but not in OVCAR3 cells. However, OVCAR3 cells with low *MPC2* expression accumulated pyruvate, which was not evident in PEO4 cells, which expressed a significantly higher level of *MPC2*. Although MPC1 and MPC2 are proposed to function as a complex (Bricker et al., 2012), a recent study shows MPC2 can operate independently of MPC1 (Nagampalli et al., 2018). MPC2 was not regarded as necessary until it was shown to form a homodimer. However, the efficiency of pyruvate transport into the mitochondria via an MPC2 homodimer is much weaker compared to the MPC1-MPC2 heterodimer complex. Increased pyruvate transport efficiency was demonstrated by Herzig et al., where co-expression of mpc1 and mpc2 in *Lactococcus lactis* induced a four-fold increase in pyruvate uptake (Herzig et al., 2012).

The data shown here may identify *MPC2* as a therapeutic target for ovarian cancer. However, the level of MPC2 upregulation in ovarian cancer is not clearly understood. Although, complete ablation of *Mpc2* in a knockout mouse model showed the death of the foetus on the 18th day (Vigueira et al., 2014). Furthermore, in a patient where impaired pyruvate transport was evident, defects in *MPC2* led to the risk of life for

both mother and her foetus (Brivet et al., 2003). These examples suggest the importance of MPC2 in normal cellular metabolic activities, which could be the reason why cancer cells commonly delete MPC1 but not MPC2.

The data here implies that ovarian cancer cells can adapt to their TME by altering metabolic regulatory genes centred on *MPC1* expression as a nodal switch. Further to this, it is evident that MPC1 inhibition not only leaves glutamine as an option for TCA flux but also for nucleotide biosynthesis in cells limited to fatty acid oxidation. Conversely, malate-aspartate shuttle can facilitate the TCA cycle by transporting cytosolic malate to mitochondria where it is converted to OAA which then is converted to aspartate to transport back into the cytosol maintain the redox. Glutamine intermediates together with pyruvate orchestrate major amino acid pathways to create carbon and nitrogen backbones for substrate utilisation. Pyruvate produced from lactate (intracellular) can bypass the mitochondrial matrix without the need for MPC. The intracellular lactate shuttle is an important event in cancer to maintain the pH of the tumour microenvironment. The cytosolic lactate dehydrogenase A (LDHA), which has a high affinity for pyruvate, catalyses the reduction of pyruvate into lactate. The lactate dehydrogenase B (LDHB), on the other hand, has a high affinity for lactate and oxidises lactate to pyruvate in the mitochondrial intermembrane space. However, LDHB function is a more complex and efficient function is seen in cancers with upregulated aerobic glycolysis (McCleland et al., 2012).

Furthermore, lactate can be directly co-transported along with H^+ into the mitochondrial matrix by monocarboxylate transporter 1 (MCT1), where it gets converted back to pyruvate by LDHB in the mitochondrial matrix. Pyruvate is then converted to acetyl-CoA by pyruvate dehydrogenase (PDH) to feed into the TCA cycle to generate ATP. This process bypasses the need for MPC in cancer cells (Dennison et al., 2013; McCleland et al., 2012). Mitochondrial pyruvate carrier 1 inhibition accumulated pyruvate. Cancer cells may be utilising some of the pyruvates to employ alanine metabolism. Pyruvate is converted to alanine by a transamination reaction catalysed by alanine transaminase 1 or alanine aminotransferase 1 (ALT1). Alanine enters the mitochondria via an alanine transporter, which converts back to pyruvate by alanine transaminase 2 (ALT2) inside the mitochondria. Cancer cells achieve a dual

advantage by employing alanine since alanine with α-KG produces glutamate while transporting pyruvate into the mitochondria without the need for MPC (Bowman et al., 2016; McCommis and Finck, 2015). The multifaceted pyruvate, associated with MPC1 loss, acts as a central carbon metabolite and is advantageous to the metabolic plasticity of cancer cells. To further investigate pyruvate flux in HGSOC, along with pharmacological inhibition of MPC by UK-5099, it would be useful to study knockdown of *MPC1* and *MPC2* with short interfering RNA (siRNA) in HGSOC cells while looking at flux phenotypes.

Chapter Four

The metabolic effect of MPC knockdown on ovarian cancer cells

4 The metabolic effect of *MPC* knockdown on ovarian cancer cells

4.1 Introduction

Mitochondrial metabolism acts as the core energy site for most eukaryotic cells. Most tumours reach a point where the nutrients in the microenvironment become severely limited. To maintain bioenergetic demands, cells adapt metabolic pathways by upregulating key metabolic genes to make best use of nutrient availability. Depending on the needs of nutrient biosynthesis, cancer cells activate signalling pathways that involve several glycolytic enzymes. For example, mutant oncogenes such as *PI3K/Akt* induce the expression of glucose transporters (GLUT1 and GLUT4) and hexokinase 2 (HK2), whilst MYC and HIF-1α also induce the expression of HK2 and Phosphofructokinase 1 (PFK1), Pyruvate Kinase M1/2 (PKM), Lactate dehydrogenase A (LDHA), and the glutamine transporter SLC1A5 (Doherty and Cleveland, 2013; Doherty et al., 2014). Hypoxic tumours have limited nutrient and oxygen availability, displaying decreased mitochondrial metabolism and increased LDHA activity (Wilde et al., 2017). Whereas, in normoxic cancer cells, due to increased LDH activity, lactate can be utilised for aerobic glycolysis. The major source of lactate is glucose, and cancer cells are able to use lactate not just as an energy source but also as a signalling molecule for tumour angiogenesis (Doherty et al., 2014). Furthermore, cells utilising lactate display a more aggressive phenotype in multiple cancers (Faubert et al., 2017; Morais-Santos et al., 2015; Schneider et al., 1997). Some ovarian cancer patients have peritoneal metastases causing accumulated ascites in the abdomen. When the nutrient content of these ascites was analysed, it was found to be rich in lactate (>5 mM; compared to blood <1 mM) and lactate dehydrogenase (>400 mU/mL, blood > 140-280 mU/mL) (Schneider et al., 1997). The majority of High-grade serous ovarian cancer (HGSOC) cells which are of epithelial origin, lack *MPC1*, resulting in increased glycolytic intermediates (Bricker et al., 2012). Hence, metabolic vulnerabilities can be exploited to improve treatment options for therapy-resistant cancers. From previous studies carried out on these cell lines by students in our group, research have shown PEO1 and PEO4 to be more glycolytic compared to OVCAR3 cells (data not shown), which was shown by differential media conditions and a lactate secretion assay.

Metabolic diversity within tumours shows the cells' ability to utilise OXPHOS whilst maintaining glycolytic phenotype. While aerobic glycolysis moderately explains tumour metabolism, recent studies show cells' interaction with the tumour microenvironment induces aerobic glycolysis in stromal cells and employs glycolytic end products for oxidative phosphorylation (OXPHOS) by cancer cells, hence the phenomenon was named as the "Reverse Warburg effect" (Danhier et al., 2017; Wilde et al., 2017). This metabolic interaction between stromal cells and cancer cells maintains a metabolically active tumour for cancer proliferation and metastasis with a continuous availability of nutrients under starvation (Wilde et al., 2017). Hence it is crucial to recognise and trace the fate of metabolites involved in the cancer cell's progression. To achieve this, here, I use stable isotope tracing analysis (SITA) to trace the fate of major cellular metabolites.

For SITA studies, usually ^{13}C, ^{2}H, ^{18}O, ^{15}N or ^{32}S are used, depending on the scope of the experiment (Bruntz et al., 2017; Choudhury et al., 2020; Jang et al., 2018). For example, to trace carbons metabolised from glucose, glutamine or lactate during metabolic utilisation, ^{13}C-glucose, ^{13}C-glutamine, or ^{13}C-lactate are selected. The number of labelled isotopes carried forward is denoted by **m+n**, where n is the number of labelled carbon added at each cycle (figure 4.1). Labelled glucose or lactate contribution to OXPHOS is shown by the abundance of labelled TCA cycle intermediates, including citrate, malate, fumarate, and succinate. Glucose is metabolised to the three-carbon compound pyruvate, an end product of glycolysis which is then converted to acetyl-CoA (two carbon). Therefore, the first cycle would be the generation of M+2 intermediates from the labelled glucose. At each cycle, the intermediates would show either an increase or decrease in M+4 and M+6 for mass isotopomer distribution (Choudhury et al., 2020). However, cells lacking MPC1 metabolism would purportedly affect the contribution of labelled carbon to TCA cycle intermediates, thereby reducing the abundance of substrates (e.g., citrate). If lactate can bypass the need for MPC1, it should be evident from the data, as most of the TCA cycle substrates would display ^{13}C from labelled lactate. Here, I investigate the adaptation of primary metabolic pathways to loss of *MPC1*, via glucose or lactate SITA, in ovarian cancer cells lines.

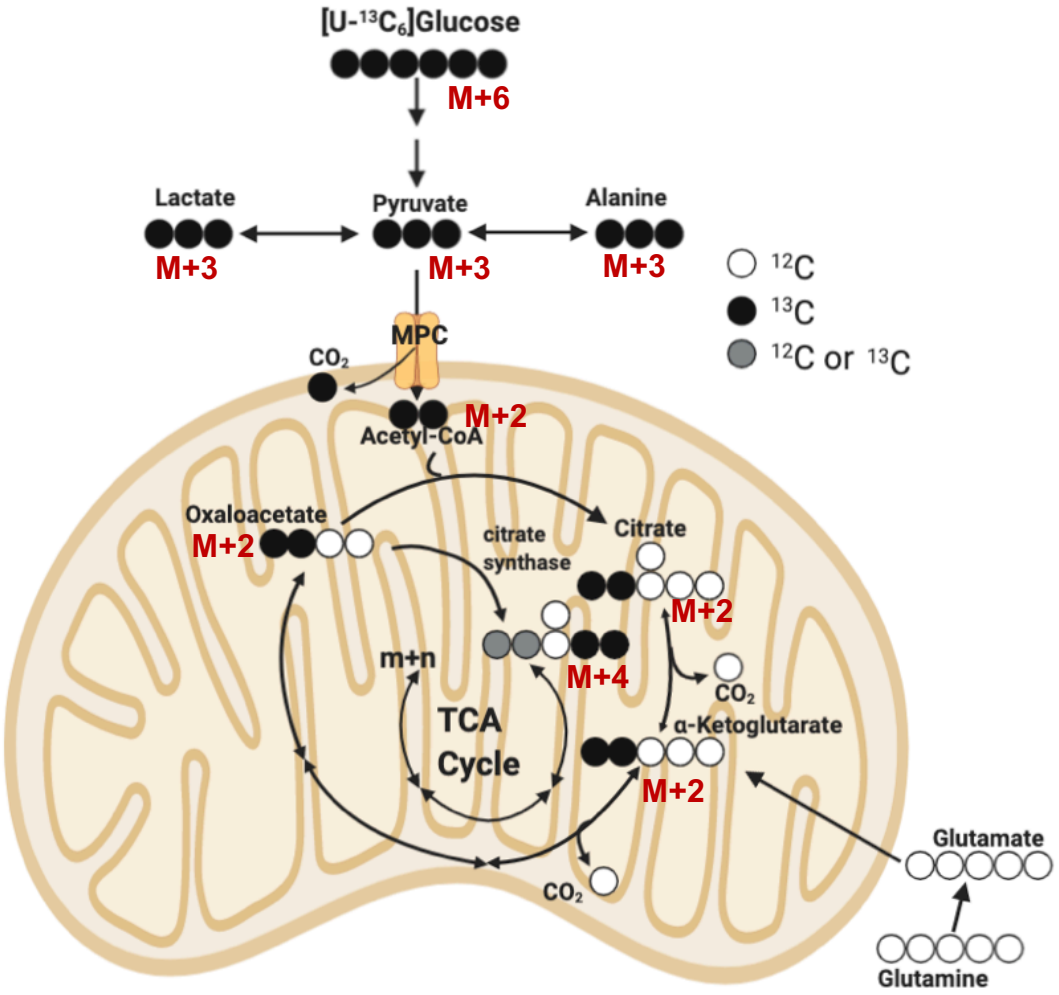

Figure 4.1 A schematic diagram of labelled glutamine ($^{13}C_5$-glutamine).
The pathway above predicts the labelled carbon transferred at each cycle. The letters denoted in red represents the number of labelled carbon carried forward.

4.2 Hypothesis

The present study tested the hypotheses that by forfeiting MPC1, epithelial ovarian cancer cells adapt glycolysis and OXPHOS to sustain growth and metastasis. Furthermore, the reverse Warburg effect provides substrates for the TCA cycle without the need for MPC1 transport of pyruvate into the mitochondria, thereby supporting cancer cell proliferation and metastasis.

4.3 Experimental Procedures

4.3.1 Cell culture

The cell lines used in the following chapter are PEO1 (chemo-sensitive), PEO4, and OVCAR3. The cell culture methods for these cell lines are explained in Chapter 2, section 2.1.1. Each biological replicate (at least three) is an independent passage of that cell line. Any media used for growth studies are the same as mentioned in Section 2.1.1 except for siRNA culture, which was antibacterial, antimycotic (ABAM) free.

4.3.2 siRNA cell culture

To model, the loss of mitochondrial pyruvate carrier, *MPC1*, *MPC2* or both *MPC1* and *MPC2* were depleted in ovarian cancer cells. The siRNA was set up, and the experimental design was arranged as explained in Chapter 2, section 2.3. Briefly, the cells were cultured in the recommended growth media until cells reached the desired confluency (~70% to ensure exponential growth). For siRNA depletion, 0.5 mL of Opti-MEM was added to each well of a 6-well plate. Then, 7.5 µl of RNAimax (lipofectamine) was added to each well, followed by 5 µl of targeting siRNA or scrambled control and plates incubated for 10 min at RT. Meanwhile, cells were washed with 5 mL PBS, detached using 2 mL Accutase (Merck, UK), and live cells counted using the Countess (Invitrogen Cell counter, ThermoFisher Scientific, UK). Cells were then resuspended in growth media without ABAM solution at 1 x 10^5 cells/mL. Then, 2.5 mL of cell suspension was added to the 5 mL Opti-MEM/lipofectamine/siRNA complex. Cells were incubated undisturbed for 72 h at 37˚C and 5% CO_2. Cells were then used immediately or reseeded as stated in the *Results*. Real-time qPCR was used to determine the efficacy of siRNA; 72 h was chosen as the optimal time point to achieve >70% gene knockdown (preliminary data for 48 h knockdown efficiency not shown).

4.3.3 siRNA proliferation study

Following a 72 h incubation in siRNA, cells were gently washed with PBS and detached with Accutase. Cell counts were recorded with a minimum of 95% viability measured using Trypan blue method on Countess™ cell counter. For proliferation studies over time, cells were seeded at 2,000 cells/well in a 96-well plate with 200 µl complete growth media and plates were incubated at 37˚C and 5% CO_2. After each

time point, cells were gently washed with PBS and immediately frozen at -80˚C for DNA quantification (CyQUANT). Prior to performing the CyQUANT proliferation assay, cells were thawed to room temperature. The assay was performed as described in Chapter 2, section 2.6. A standard curve was generated for each plate.

4.3.4 Quantitative real-time polymerase chain reaction (qPCR)

For gene expression studies, qPCR was performed using Quantifast SYBR Green (Qiagen, UK) and the CFX connect Real-time PCR detection system (Bio-Rad, UK). All consumables were DNase/RNase-free, and the laminar flow hood was cleaned prior to using RNaseZAP wipes. The general experimental set-up included RNA extraction and cDNA synthesis, as explained in detail in Chapter 2, section 2.2. The purity of total RNA quantification was measured by Nano-drop, and 260/280 and 260/230 values were determined to be between 1.8 and 2.3. The following Chapter investigated the role of *MPC1* and *MPC2* genes in ovarian cancer cell metabolism. The starting quantity of mRNA from the experimental sample was determined using standard curves generated from serial dilutions of pooled reference RNA with Quantifast SYBR green (Qiagen). Sample and reference genes were analysed in triplicate, and mRNA expression was normalised to housekeepers *RPL19* and *ACTB*. The gene expression data relative quantity was calculated according to Livak & Schmittgen's method (Livak and Schmittgen, 2001) and data was expressed as ΔΔCq.

4.3.5 Stable isotope tracing analysis

The current Chapter used heavy-labelled glucose or lactate to investigate key metabolic pathways affected by the loss of the mitochondrial pyruvate carrier. The experimental set-up for SITA is described in detail in Chapter 2, section 2.11. For stable isotope labelled glucose tracing, cells were incubated with universally labelled ^{13}C6-glucose (11.1 mM; #CLM-1396. Cambridge isotope, USA) in glucose-free RPMI (#11879020, Gibco, UK) basal growth media, supplemented with dialysed FBS, glutamine (2 mM) and ABAM. For labelled lactate, cells were incubated with universally labelled sodium ^{13}C3-lactate (10 mM; #CLM-1579. Cambridge isotope, USA) in glutamine free basal RPMI containing 10 mM unlabelled glucose(#31870, Gibco, UK) growth media. The labelled lactate media lacked glutamine; hence, it was supplemented with 2 mM unlabelled glutamine (ThermoFisher scientific, #25030081). Following 72 h exposure to siRNA, cells were reseeded in heavy-labelled media and

incubated for a further period of 72 h (without siRNA reagents) at 37˚C and 5% CO_2 in a humidified chamber. Prior to intracellular metabolite extraction, cells were washed with ice-cold saline solution and lysed in 80% methanol. Lysates were centrifuged at 12,000 x g for 10 min to remove any cell debris, and cell extracts were dried to pellets at 4°C using a speed vacuum concentrator.

Cellular metabolites were extracted and analysed by GC-MS following a previously described protocol (Faubert et al., 2014; Vincent et al., 2015). Metabolite extracts were derived using N-(*tert*-butyldimethylsilyl)-N-methyl trifluoroacetamide (MTBSTFA) as described previously (Faubert et al., 2013). D-myristic acid (750 ng/sample) was added as an internal standard to metabolite extracts, and metabolite abundance was expressed relative to internal standards and normalised for the number of cells. GC-MS analysis was performed by a commercial service (Metabolomics Core Facility, Metabolomics Goodman Cancer Research Centre Platform, McGill University, Montreal, Canada), using an Agilent 5975C GC-MS equipped with a DB-5MS + DG (30 m x 250 μm x 0.25 μm) capillary column (Agilent J and W, Santa Clara, CA, USA). For SITA experiments, mass isotopomer distribution was determined using a custom algorithm developed at McGill University (McGuirk et al., 2013).

4.3.6 Clonogenic assay

Single-cell cloning of *MPC1*-depleted ovarian cancer cells was observed by a clone formation assay as described in Chapter 2, section 2.9. *MPC1* was knocked down in OVCAR3 cells for 72 h using siRNA. Cells were then washed and counted to achieve 800 cells/mL seeding density on a 6-well plate for both scramble and *siMPC*1 conditions. For UK-5099 treated cells, cells were previously incubated with 5 μM UK-5099. Cells were then prepared for seeding as for siRNA. Fresh UK-5099 was given to the media while seeding to ensure continuous inhibition of MPC function. Following the cell seeding, cell culture plates were incubated for 21 days with a new media change every 3-4 days whilst ensuring cells were not contaminated via observation by light microscopy. For UK-5099 treated cells, the inhibitor was replenished at each media change. Colonies were then stained manually and counted under a compound microscope.

4.3.7 Statistical analysis

Data are presented as mean ± SEM, with statistical analyses performed using Prism version 8.4.1. One-way ANOVA with post-hoc Tukey's multiple comparison test or Two-way ANOVA Sidak's multiple comparison test was used to compare treatment groups with the control. A paired or unpaired *t*-test was used to compare the two groups unless otherwise mentioned for specific data set.

4.4 Results

4.4.1 MPC1 knockdown revealed s*iMPC1* dependent cell rescue in ovarian cancer cells

From the analysis of TCGA data, around 80% of the ovarian cancer patients show deleted *MPC1* while 85% CNV gain for *MPC2* (The Cancer Genome Atlas). To investigate how MPC inhibition reprograms cell metabolism, MPC was depleted in PEO1, PEO4 and OVCAR3 cells using siRNA targeting *MPC1*, *MPC2* or *MPC1* + *MPC2*. The efficacy of stable knockdown at transcriptional levels of HGSOC cells was confirmed using qPCR, and the percentage efficiency is shown in **Table 4.1**.

Table 4.1 Average percentage of mRNA knockdown using *MPC* specific siRNA

Cell lines	**Average percentage knockdown (%)**			
	MPC1 (siMPC1)	*MPC2 (siMPC2)*	***MPC1*** *(siMPC1+siMPC2)*	***MPC2*** *(siMPC1+siMPC2)*
PEO1	85	91	88	82
PEO4	89	85	84	75
OVCAR3	79	96	85	83

Although MPC1 seems to be loss in PEO1 and PEO4 according to proteomics study by Coscia et al., 2016a, siRNA was used in all three cell lines to be consistent and a non-targeting control was used compare the control vs knocked down of MPC. The use of siRNA targeting *MPC1, MPC2* or a combination of *MPC1+2* exhibited a significant difference in cell viability over time compared to scramble control in all three cell lines. A considerable increase in cell proliferation was seen in siRNA targeting of *MPC1* in OVCAR3 cells at 24 h and 48 h (figure 4.2a) and in PEO1 at 72 h (figure 4.3a; $p = 0.02$). However, in PEO4 and OVCAR3, cell growth was significantly reduced (at 72 h: PEO4; $p < 0.0001$, OVCAR3; $p = 0.0007$) under *siMPC1* conditions compared to scramble control, but the DNA concentration was the same as at 48 h (figure 4.2a and figure 4.3a), suggesting no cell death or replication but cells may be metabolically active.

Interestingly, as expected and reported by (Brivet et al., 2003; Vigueira et al., 2014) in the foetus, *MPC2* knockdown in HGSOC cells significantly reduced cell growth compared to the control at all time points, and data is significant at 72 h (PEO1; $p < 0.0001$, PEO4; $p < 0.0001$ and OVCAR3; $p < 0.0001$). The following data demonstrates that *MPC2* is vital for cellular function. When both *MPC* complexes were targeted with siRNA, cellular DNA abundance increased in OVCAR3 after 72 h, when compared *MPC2* only depleted cells (figure 4.2a). While PEO1 and PEO4 cells under-express MPC1 in its physiological state, siRNA targeting of MPC1, resulted in over 80% ablation of mRNA.

Considering cancers have been shown to have a deleted *MPC1* gene locus, including 60-80% of ovarian cancers (Cai et al., 2014; Tibiletti et al., 1998), these data suggest *MPC1* deletion could lead to a more aggressive phenotype of cancer to promote cell survival and metastasis by orchestrating metabolic pathway to synthesise nucleotide precursors. Therefore, we next evaluated the intracellular metabolite pool using GC-MS in *MPC1* depleted OVCAR3 cells to determine which major metabolic pathways were adapted.

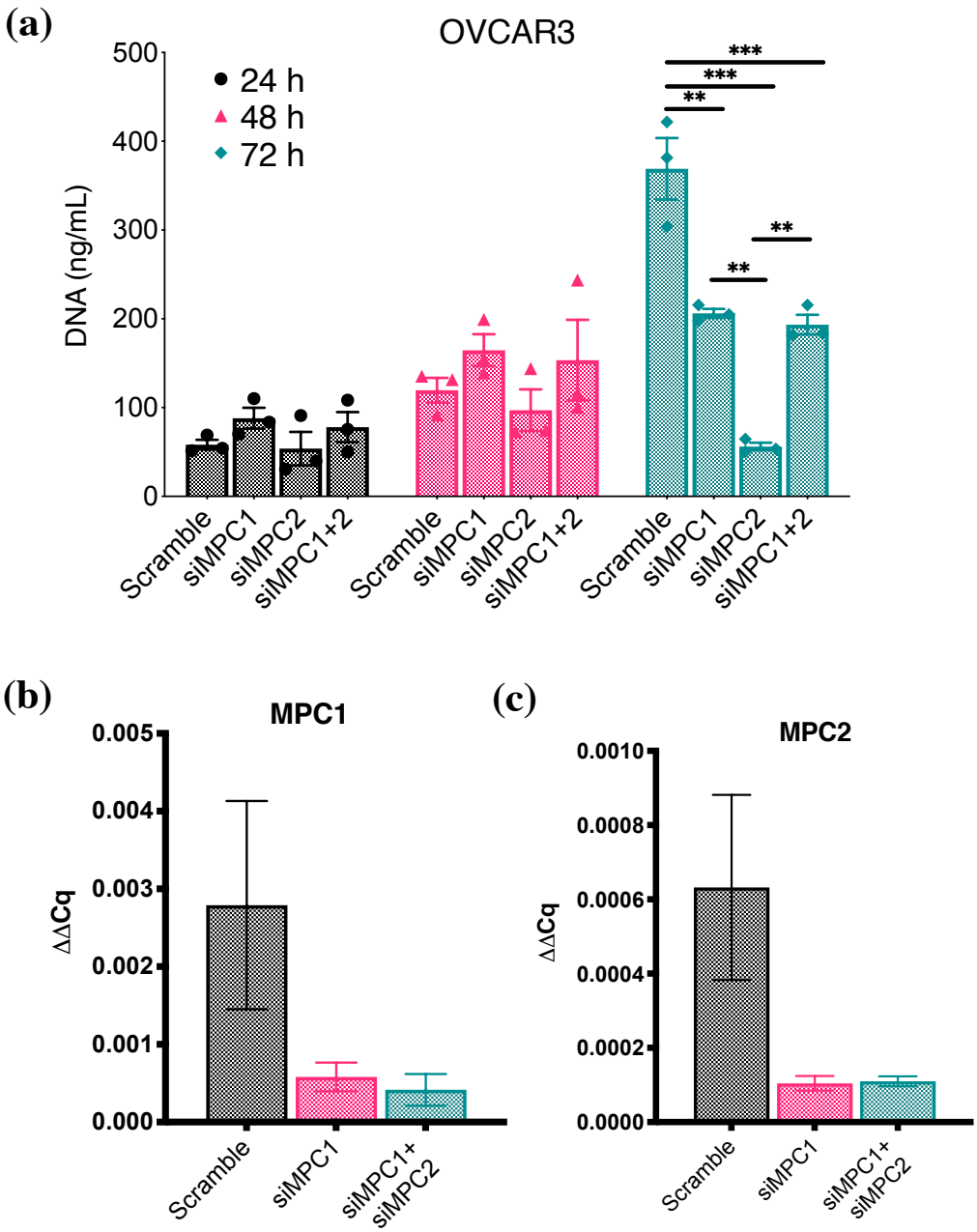

Figure 4.2 Effect of *MPC* knockdown on OVCAR3 cell viability using siRNA. **(a)** Cell viability over 72 h measuring DNA concentration for Scramble versus *MPC1*, *MPC2* or a combination of *MPC1+2*, **(b)** and **(c)** represent qPCR data showing over 70% knockdown efficiency. Statistical significance was evaluated using one-way ANOVA with Dunnett's multiple comparison test. Data were obtained from n=3 independent biological replicates for each experiment. Data expressed as mean ± SEM; * $p \leq 0.05$, ** $p \leq 0.01$, *** $p \leq 0.001$.

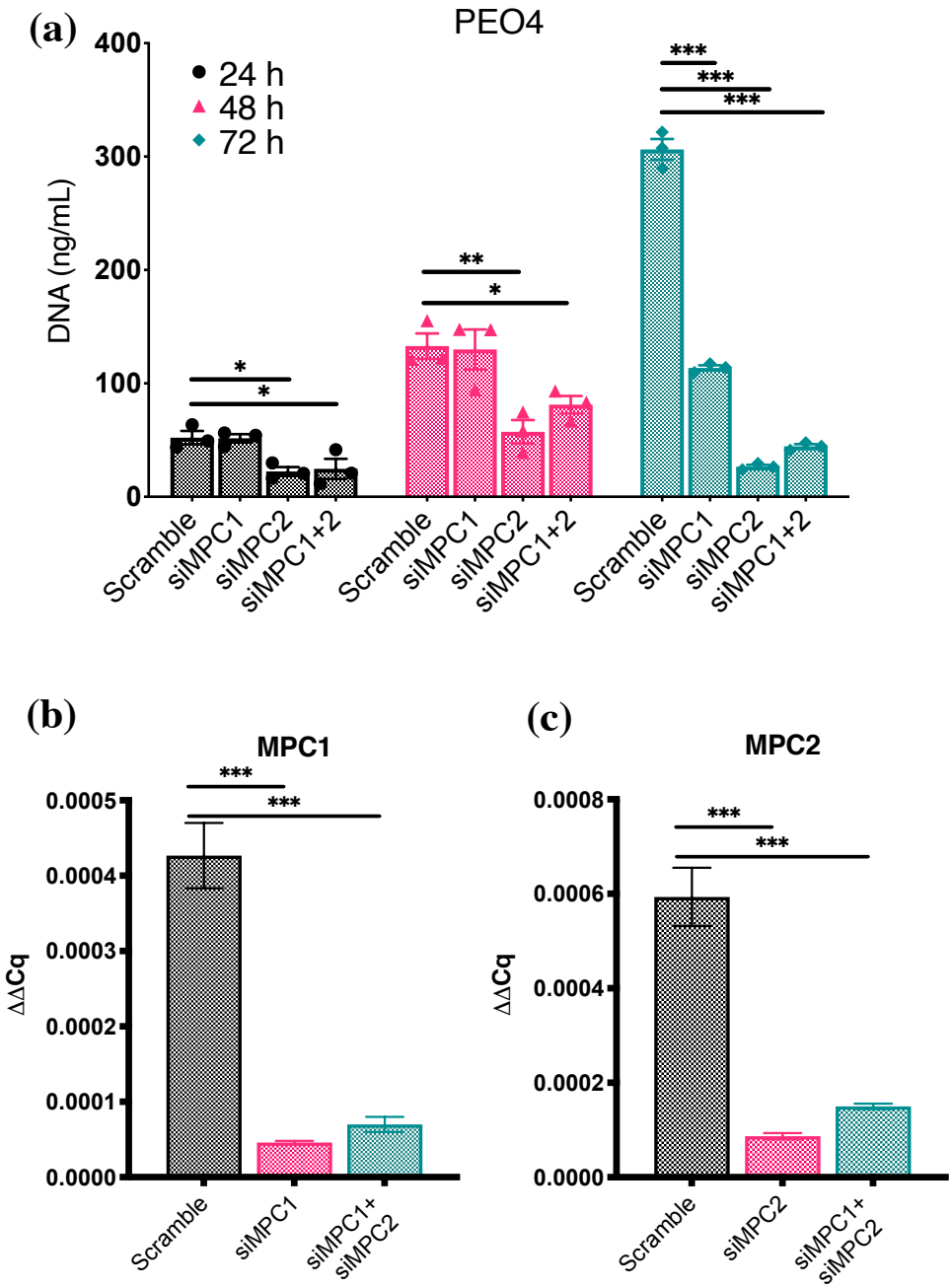

Figure 4.3 Effect of *MPC* knockdown on PEO4 cell viability using siRNA.
(a) Cell viability over 72 h measuring the DNA concentration for Scramble versus *MPC1*, *MPC2* or a combination of *MPC1+2*, **(b)** and **(c)** represent qPCR data showing over 70% knockdown efficiency. Statistical significance was evaluated using one-way ANOVA with Dunnett's multiple comparison test. Data were obtained from n=3 independent biological replicates for each experiment. Data expressed as mean ± SEM; * $p \leq 0.05$, ** $p \leq 0.01$, *** $p \leq 0.001$.

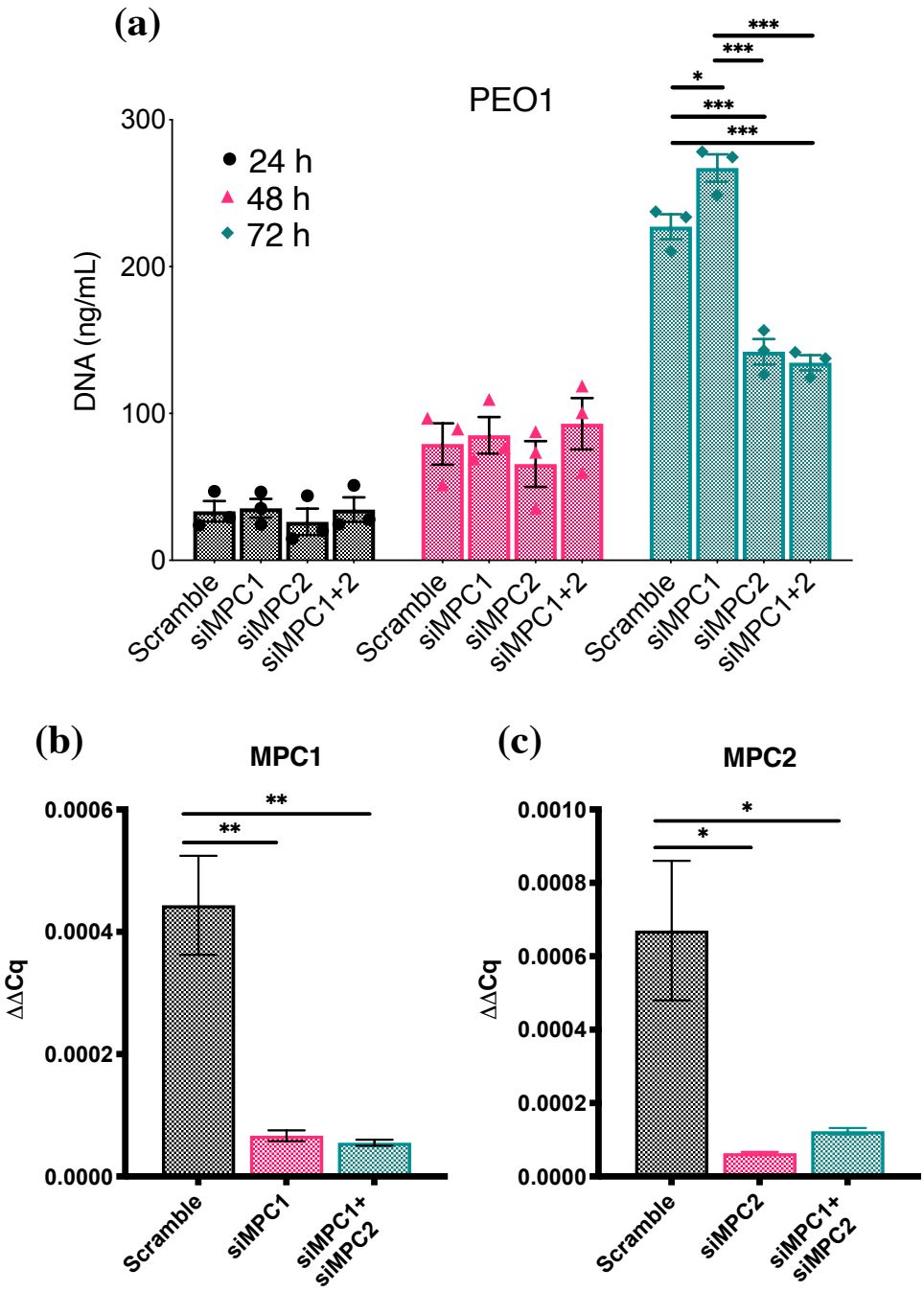

Figure 4.4 Effect of *MPC* knockdown on PEO1 cell viability using siRNA.
(a) Cell viability over 72 h, measuring the DNA concentration for Scramble versus *MPC1*, *MPC2* or a combination of *MPC1+2*, **(b)** and **(c)** represent qPCR data confirming over 70% knockdown efficiency. Statistical significance was evaluated using one-way ANOVA with Dunnett's multiple comparison test. Data were obtained from n=3 independent biological replicates for each experiment. Data expressed as mean ± SEM; * $p \leq 0.05$, ** $p \leq 0.01$, *** $p \leq 0.001$.

4.4.2 Pharmacological inhibition or genetic depletion of MPC1 affects colony formation by OVCAR3 cells

Unfortunately, the majority of ovarian cancer patients present with the late-stage disease when cancer has already metastasised throughout the abdomen. The ability of a single cell to form a colony is a crucial characteristic of metastasising cancer cells that undergo mesenchymal-epithelial transition (MET). Clonogenic assays *in vitro* have been carried out for decades to study cytotoxic agents and treatment involving ionising radiation. Here, we used MPC1 expressing OVCAR3 cells to model MPC1 deletion in HGSOC cells by treating with either an MPC inhibitor UK-5099 or using siRNA depletion of *MPC1*. Considering ten cells or more as a clone the colonies were manually counted under a light microscope. Pharmacological inhibition (figure 4.5a) or gene knockdown (figure 4.5b) of MPC1 resulted in impaired colony formation by OVCAR3 cells (figure 4.5). Furthermore, regardless of the number of colonies formed, colony sizes were different in the siRNA experimental set-up compared to pharmacological inhibition.

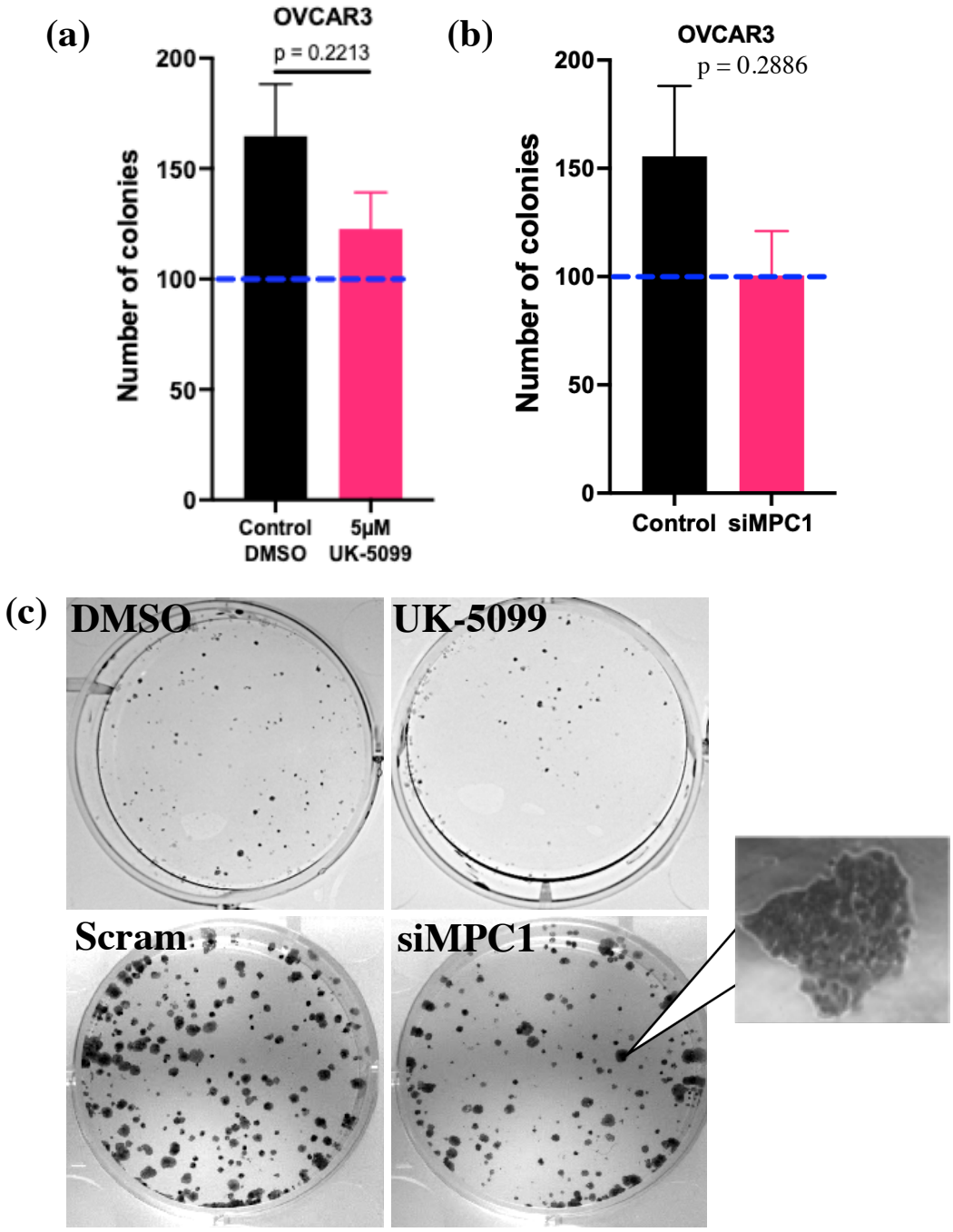

Figure 4.5 single cell colony formation by OVCAR3 cells over 21 days.
(a) graph showing the number of colonies formed from pharmacological inhibition of MPC or **(b)** showing the number of colonies formed from siRNA depletion of *MPC1*. Statistical significance was evaluated using a *t*-test (figure 4.4a). Data were obtained from n=3 (figure 4.4a) and n=2 (figure 4.4b) of independent biological replicates for each experiment. Data expressed as mean + SEM.

4.4.3 Mitochondrial pyruvate carrier 1 regulates mitochondrial substrate utilization.

Previous observation of OVCAR3 cells show 50% reduction in cell growth MPC1-deleted cells. To determine the changes in metabolic substrate utilization during the loss of MPC, stable isotope was carried out by culturing siRNA targeted OVCAR3 cells in the presence of uniformly labelled glucose [U-$^{13}C_6$] or lactate [U-$^{13}C_3$] over 72 h. Cell extracts were then analysed by GC-MS as explained in section 4.3.5. Mass isotopomer distribution (MID) data was collected from a custom algorithm developed at McGill University (McGuirk et al., 2013) to fully understand how labelled carbons were distributed among the metabolic substrates. The M+n for any substrate demonstrates the number of labelled carbons carried over (n denotes the number of labelled carbon). For instance, the three-carbon compound pyruvate is M+3 if all carbons came from a labelled source, whilst M+2 for pyruvate shows only two labelled carbons have been carried forward. The m+2 for pyruvate is possible when pyruvate is produced from oxaloacetate, which came from labelled glutamine or a glucose molecule with two labelled carbons only.

Glucose is a major metabolite used by cells to generate adenosine triphosphate (ATP). The glucose is either catabolised to lactate from pyruvate (glycolysis) or catabolised to CO_2 and water in the mitochondria for OXPHOS via the TCA cycle. However, even when oxygen is not limited, cancer cells often prefer aerobic glycolysis and secrete more lactate for cellular homeostasis. Since Otto Warburg's research on aerobic glycolysis, lactate has been extensively studied in the field of cancer. To look at the fate of glucose, labelled glucose tracing revealed accumulation of pyruvate under *siMPC1* condition in OVCAR3 cells. Over 90% of the pyruvate is predominantly derived from a labelled carbon source (figure 4.6a), i.e. [U-$^{13}C_6$] glucose, which is demonstrated by MID data corresponding to pyruvate produced from glucose (figure 4.6b). However, for cells that are grown in standard growth media supplemented with 10 mM [U-$^{13}C_3$] sodium lactate, 60% of pyruvate was derived from labelled lactate and about 40% from an unlabelled source possibly from unlabelled glucose in the media (figure 4.6c).

Pyruvate accumulation is a key advantage to cancer cells since it can act as a central metabolite to generate lactic acid, alanine, and TCA cycle intermediates like α -KG and glutamate. Therefore, supplementing lactate favours pyruvate production by cancer cells while pyruvate from glucose is not entirely abandoned, the M+0 pyruvate is derived from glucose, and M+3 pyruvate is from lactate (figure 4.6d) as summarized in pathway below (figure 4.6e). These data, together with lactate derived from glucose (figure 4.7b), suggest the occurrence for favouring of reverse Warburg effect by OVCAR3 cells when *MPC1* is depleted. To confirm this occurrence, measuring the activity of LDHA and LDHB in these cell lines would be useful. The fate of lactate is vital due to lactate being an important oncometabolite. The initial conversion of pyruvate to lactate by lactate dehydrogenase A (LDHA) is a reversible reaction whereas LDHB converts lactate back to pyruvate. Monocarboxylate transporters (MCTs), plasma membrane transporters for lactate, facilitate the transport of lactate in and out of the cell. Recent study with ^{13}C -lactate tracing has shown carbon from lactate can be used to synthesise lipids by HeLa cells (cervical cancer) and H460 (lung cancer) cell lines (Chen et al., 2016).

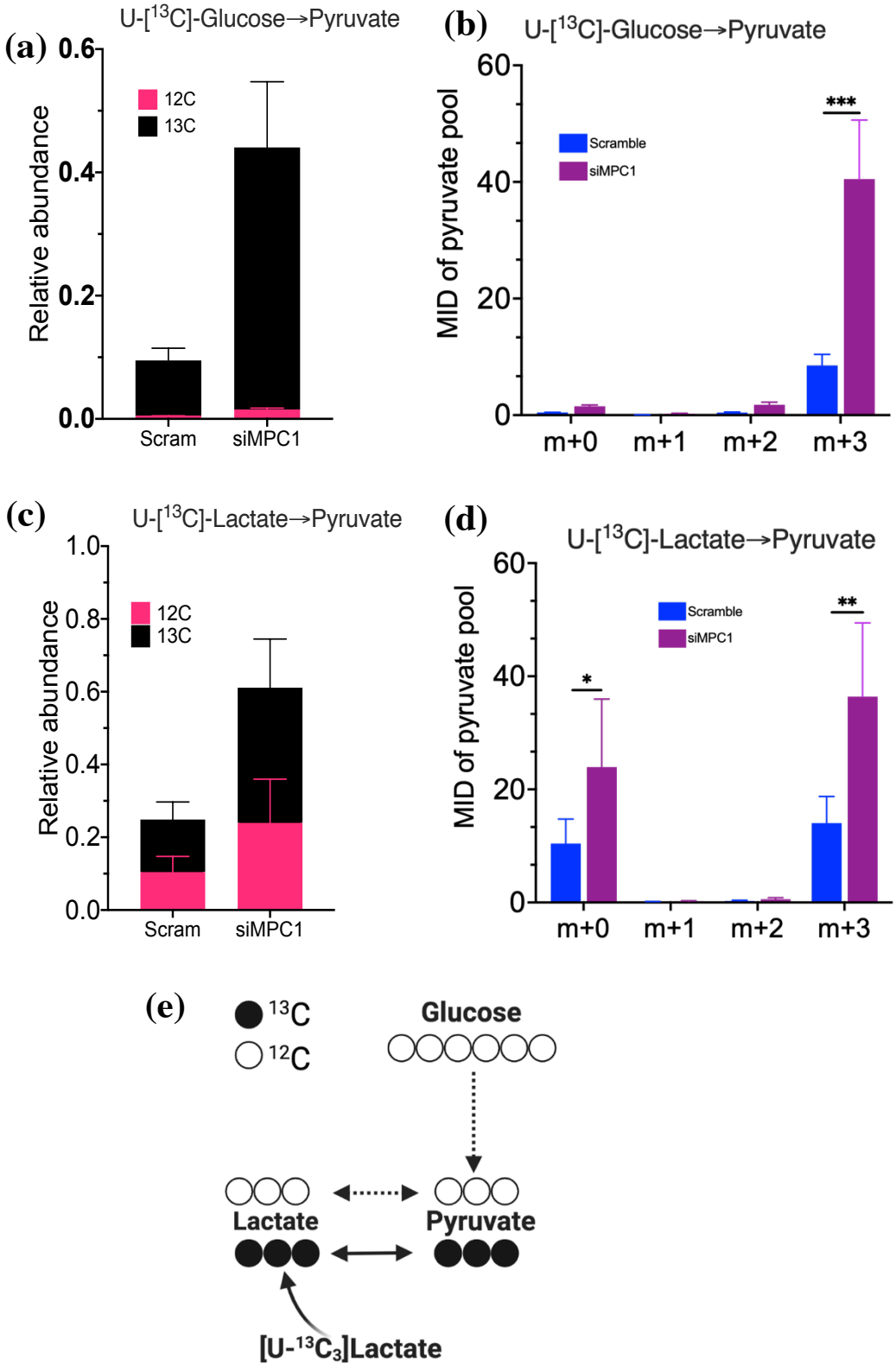
(a)
U-[13C]-Glucose→Pyruvate
Relative abundance
0.6
0.4
0.2
0.0
12C
13C
Scram
siMPC1
(b)
U-[13C]-Glucose→Pyruvate
MID of pyruvate pool
60
40
20
0
Scramble
siMPC1
***
m+0
m+1
m+2
m+3
(c)
U-[13C]-Lactate→Pyruvate
Relative abundance
1.0
0.8
0.6
0.4
0.2
0.0
12C
13C
Scram
siMPC1
(d)
U-[13C]-Lactate→Pyruvate
MID of pyruvate pool
60
40
20
0
Scramble
siMPC1
*
**
m+0
m+1
m+2
m+3
(e)
13C
12C
Glucose
Lactate
Pyruvate
[U-13C3]Lactate

Figure 4.6 Accumulation of Pyruvate produced from glucose or lactate is MPC1 dependent.
(a) Contribution of [U-$^{13}C_6$] glucose to pyruvate in OVCAR3 cells and corresponding mass isotopomer distribution (MID) of glucose to pyruvate (b). OVCAR3 cells treated with 10 mM sodium lactate and relative abundance of pyruvate produced from Lactate is shown (c) while corresponding MID of lactate to pyruvate over 72 h is (d). Figure (e) briefly illustrates the pyruvate made from labelled carbon (black circles) and unlabelled carbon source (white circles). Statistical significance was evaluated using two-way ANOVA with Sidak's multiple comparison test. Data were obtained from n=4 independent biological replicates for each experiment. Data expressed as mean + SEM; * $p \leq 0.05$, ** $p \leq 0.01$, *** $p \leq 0.001$.

4.4.4 Reverse Warburg bypass the need for MPC1

The SITA of ^{13}C-lactate has revealed vital roles of lactate in the remodelling of cancer metabolism. Studies confirm the dual function of cancer cells to produce ATP by actively combining OXPHOS and glycolysis (Santidrian et al., 2013; Zacksenhaus et al., 2017). Therefore, it's essential to look at substrates derived from the tumour microenvironment (TME), such as the oncometabolite lactate that may contribute to the cancer cell TCA cycle, thereby providing energy. The mitochondrial pyruvate carrier acts as a node between glycolysis and OXPHOS. Looking at the abundance of intracellular lactate, SITA data showed most of the lactate was derived from glucose in both scramble and *siMPC1* cells (figure 4.7a). However, MID data revealed the presence of unlabelled lactate (M+0), leading to glycolytic intermediates producing pyruvate (4.7b).

Mass isotopomer distribution of lactate in OVCAR3 cells supplemented with 10 mM sodium [U-$^{13}C_3$] lactate showed the presence of a labelled and unlabelled carbon source of lactate reflecting data obtained in figure 4.7c, while OVCAR3 cell line also proves uptake of lactate as a carbon source. Intriguingly, M+3 lactate was relatively low in *siMPC1* cells compared to scramble control (figure 4.7d). Furthermore, this observation reflects an increase in pyruvate from labelled lactate showed in figure 4.7d. To further investigate how lactate is utilized and to confirm if lactate was used for TCA cycle intermediates, I looked for substrate involved in the TCA cycle under ^{13}C-glucose and ^{13}C-lactate supplemented cells.

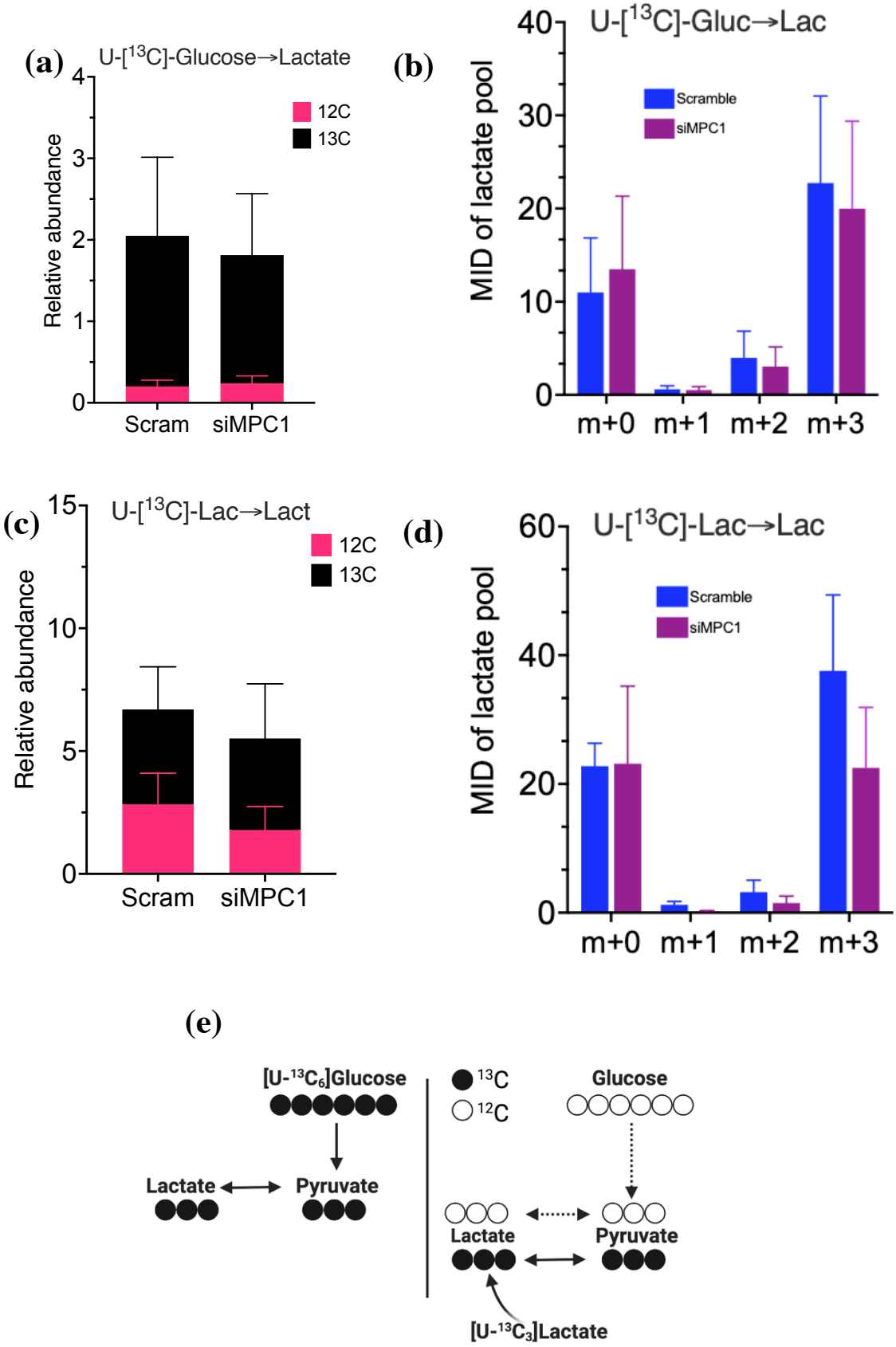
(a)
U-[13C]-Glucose→Lactate
12C
13C
Relative abundance
Scram
siMPC1
(b)
U-[13C]-Gluc→Lac
Scramble
siMPC1
MID of lactate pool
m+0
m+1
m+2
m+3
(c)
U-[13C]-Lac→Lact
12C
13C
Relative abundance
Scram
siMPC1
(d)
U-[13C]-Lac→Lac
Scramble
siMPC1
MID of lactate pool
m+0
m+1
m+2
m+3
(e)
[U-13C6]Glucose
Lactate
Pyruvate
13C
12C
Glucose
Lactate
Pyruvate
[U-13C3]Lactate

Figure 4.7 Contribution of ^{13}C-glucose and ^{13}C-Lactate to lactate MID.
(a) Contribution of [U-$^{13}C_6$] glucose to lactate in OVCAR3 cells and corresponding mass isotopomer distribution (MID) of glucose to lactate (b). OVCAR3 cells treated with 10 mM sodium lactate and relative abundance of lactate produced from glucose (^{12}C) or direct lactate (^{13}C) is shown (c) while corresponding MID for carbon distribution (d). Figure (e) briefly illustrates the pyruvate and lactate made from labelled carbon (black circles) and unlabelled carbon source (white circles). Statistical significance was evaluated using two-way ANOVA with Sidak's multiple comparison test. Data were obtained from n=4 independent biological replicates for each experiment. Data expressed as mean + SEM; * $p \leq 0.05$, ** $p \leq 0.01$, *** $p \leq 0.001$.

4.4.5 The glycolytic products pyruvate and lactate lead into TCA cycle intermediates upon *MPC1* depletion

Metabolic rewiring is crucial for proliferative cancer cells to utilise nutrients. For decades mitochondrial metabolism has been studied to target the energy utilisation by cancer cells. However, the carbon and nitrogen molecules that mediate the energy supply to drive the TCA cycle is not clearly understood. To look at the TCA cycle substrates derived from glucose or lactate, ^{13}C labelled isotopes were used to understand the distribution of carbon atoms to TCA intermediates, such as citrate and malate, which can both compensate for the loss of MPC1 via gluconeogenesis.

To further investigate on how *MPC1* depleted cells utilise glucose or lactate to produce TCA cycle intermediates, labelled glucose (without lactate) and labelled lactate (10 mM sodium lactate) in the presence of glucose were used to culture the cells. Glucose was not completely depleted under labelled lactate media. Extracellular lactate is an important source in the TME (Doherty & Cleveland, 2013). The MID data showed OVCAR3 scrambled control cells were able to use the carbon from glucose molecules to produce the TCA cycle substrate malate (figure 4.8a). Cells were able to utilise labelled glucose to make malate via pyruvate transport into the mitochondria (blue bar m+2, m+3, m+4 of figure 4.8a). Upon *MPC1* depletion, MID carbon for malate was significantly lower compared to control (figure 4.8a; m+3, m+4). When these cells were supplemented with 10 mM lactate (^{13}C labelled) to model the high lactate concentrations in the TME, a similar pattern of MID was observed. Furthermore, the total malate pool was increased in lactate supplemented cells (figure 4.8b) when compared to non-lactate supplemented cells (figure 4.8a).

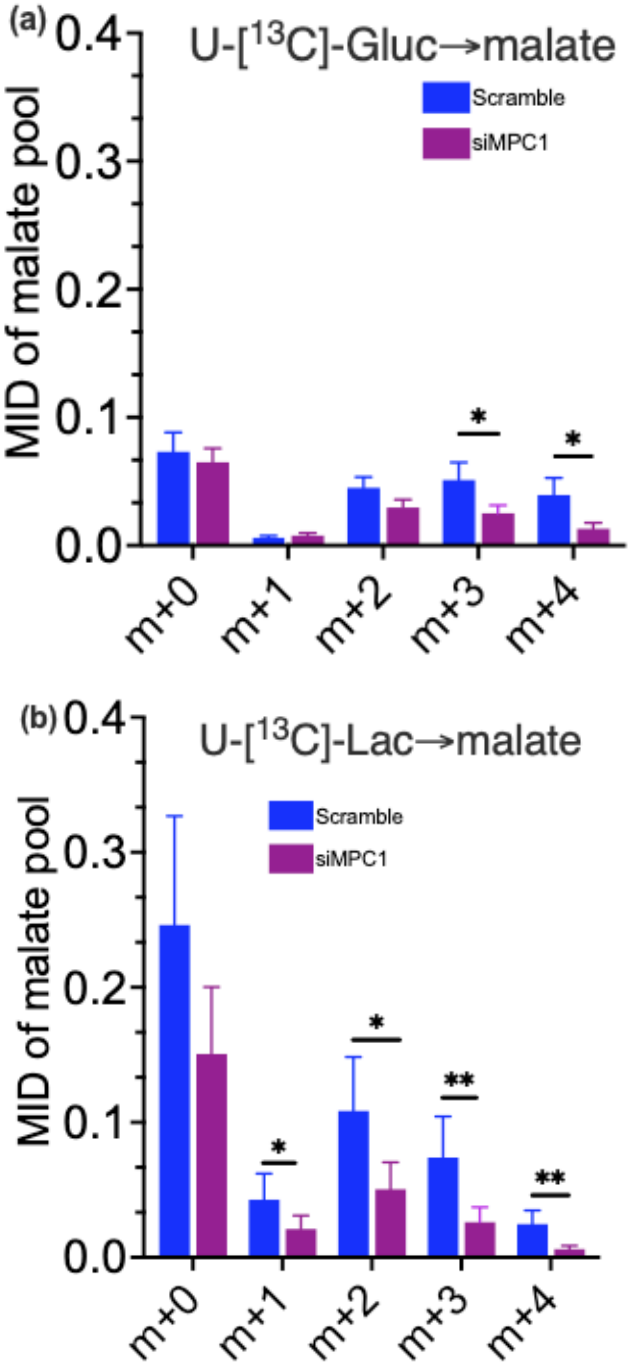

Figure 4.8 Contribution of ^{13}C-glucose and ^{13}C-Lactate to malate.
(a) malate MID derived from labelled glucose, (b) malate derived from labelled lactate in OVCAR3 cells. Statistical significance was evaluated using two-way ANOVA with Sidak's multiple comparison test. Data were obtained from n = 4 independent biological replicates for each experiment. Data expressed as mean ± SEM; * $p \leq 0.05$, ** $p \leq 0.01$, *** $p \leq 0.001$

Citrate is an essential metabolite for cells in general. Citrate is converted to isocitrate by aconitase enzyme to feed the TCA cycle, while reductive carboxylation of citrate can generate acetyl-CoA for lipid biosynthesis (Vacanti et al., 2014b). Citrate can be generated from pyruvate and α-KG (IDH2 mitochondrial and IDH1 cytosolic); hence *MPC1* depletion resulted in a significant decrease in citrate in OVCAR3 cells (figure 4.9a and figure 4.9b). Moreover, significant decreases of M+3, M+5 and M+6 in *MPC1* depleted cells suggesting of cells producing α-KG via isocitrate mediated by IDH3 (mitochondrial reduction of NAD^+ to NADH). Comparable to the data obtained for malate, supplementing lactate increased the abundance of citrate. Previous studies have shown the importance of lactate to a cancer cell's aggressive phenotype (Faubert et al., 2017; Hensley et al., 2016). In ovarian cancer patients, analysing the nutrient content of the ascites, higher levels of lactate and LDH were found (Ahmed and Stenvers, 2013; Kim et al., 2012; Kipps et al., 2013). Cancer cells utilising lactate to derive TCA cycle intermediates could be a metabolic phenomenon for therapy-resistant proliferative cells (Schneider et al., 1997; Sonveaux et al., 2008; Wilde et al., 2017).

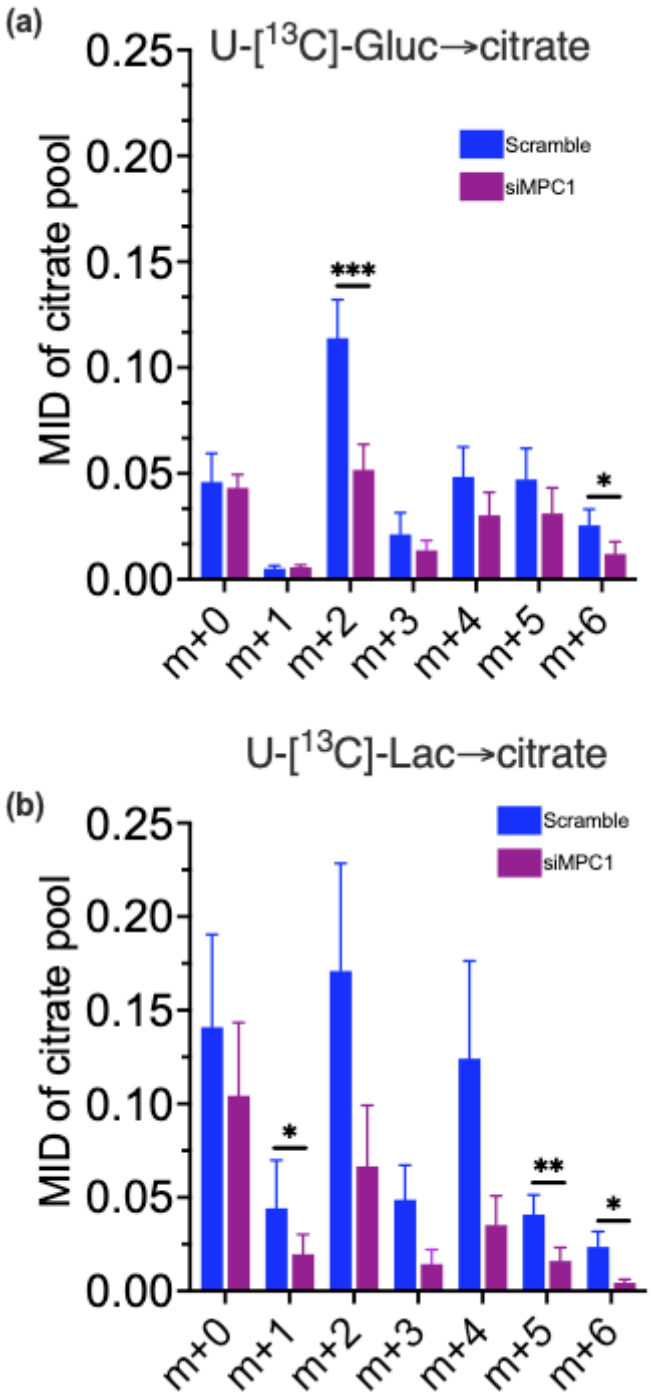

Figure 4.9 Contribution of ^{13}C-glucose and ^{13}C-Lactate to citrate.
(a) Citrate MID derived from labelled glucose, (b) citrate derived from labelled lactate in OVCAR3 cells. Statistical significance was evaluated using two-way ANOVA with Sidak's multiple comparison test. Data were obtained from n=4 independent biological replicates for each experiment. Data expressed as mean + SEM; * $p \leq 0.05$, ** $p \leq 0.01$, *** $p \leq 0.001$

Aspartate has multiple roles in cancer. Aspartate is involved in the generation of TCA cycle intermediates, nucleotide synthesis while acting as a precursor for the urea cycle for ECM remodelling (Nazemi and Rainero, 2020). Interestingly SITA analysis showed heavy labelled carbon from glucose and lactate carried over to aspartate synthesis (figure 4.10a and 4.10b). Furthermore, increased abundance of aspartate was seen in *MPC1* depleted OVCAR3 cells compared to the scramble control (figure 4.10). Cells utilising aspartate has dual advantages since it can be used as both nitrogen and carbon source. Aspartate contributes to arginine for urea cycle and purines and pyrimidines. Carbons from aspartate (M+4) contributes to citrulline to produce arginosuccinate, an intermediate of arginine for Urea cycle. Moreover, aspartate (M+2, M+3) together with α-KG is converted to oxaloacetate and glutamate by transamination.

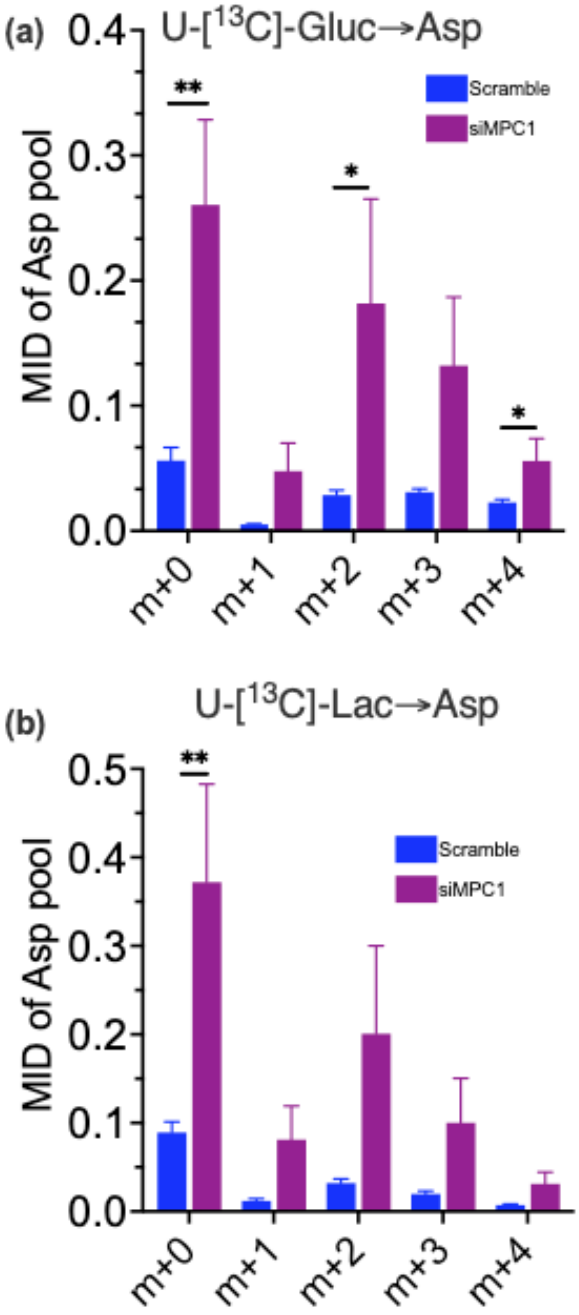

Figure 4.10 Contribution of ^{13}C-glucose and ^{13}C-Lactate to Aspartate.
(a) aspartate MID derived from labelled glucose, (b) aspartate derived from labelled lactate in OVCAR3 cells. Statistical significance was evaluated using two-way ANOVA with Sidak's multiple comparison test. Data were obtained from n = 4 independent biological replicates for each experiment. Data expressed as mean ± SEM; * $p \leq 0.05$, ** $p \leq 0.01$, *** $p \leq 0.001$

Overall, SITA studies revealed that during depletion of *MPC1* increased metabolite enrichment of amino acids (aspartate, proline, serine, asparagine, glycine) and gluconeogenesis (glycerol-3-phosphate) (figure 4.11a). Conversely, abundancies of other TCA cycle intermediates like citrate, fumarate, malate, α -KG and glutamate were relatively decreased (figure 4.11a) when *MPC1* was depleted. When the MID of TCA cycle intermediates from labelled glucose was analysed, most of the intermediates showed decreased abundance under *MPC1* depletion (figure 4.12). This alteration of amino acid metabolism upon *MPC1* inhibition agreed with glutamine being a known gluconeogenic substrate (Stark and Kibbey, 2014). Also, an increase in serine and glycine along with aspartate suggests a dual role for glutamine as a source of both carbon and nitrogen.

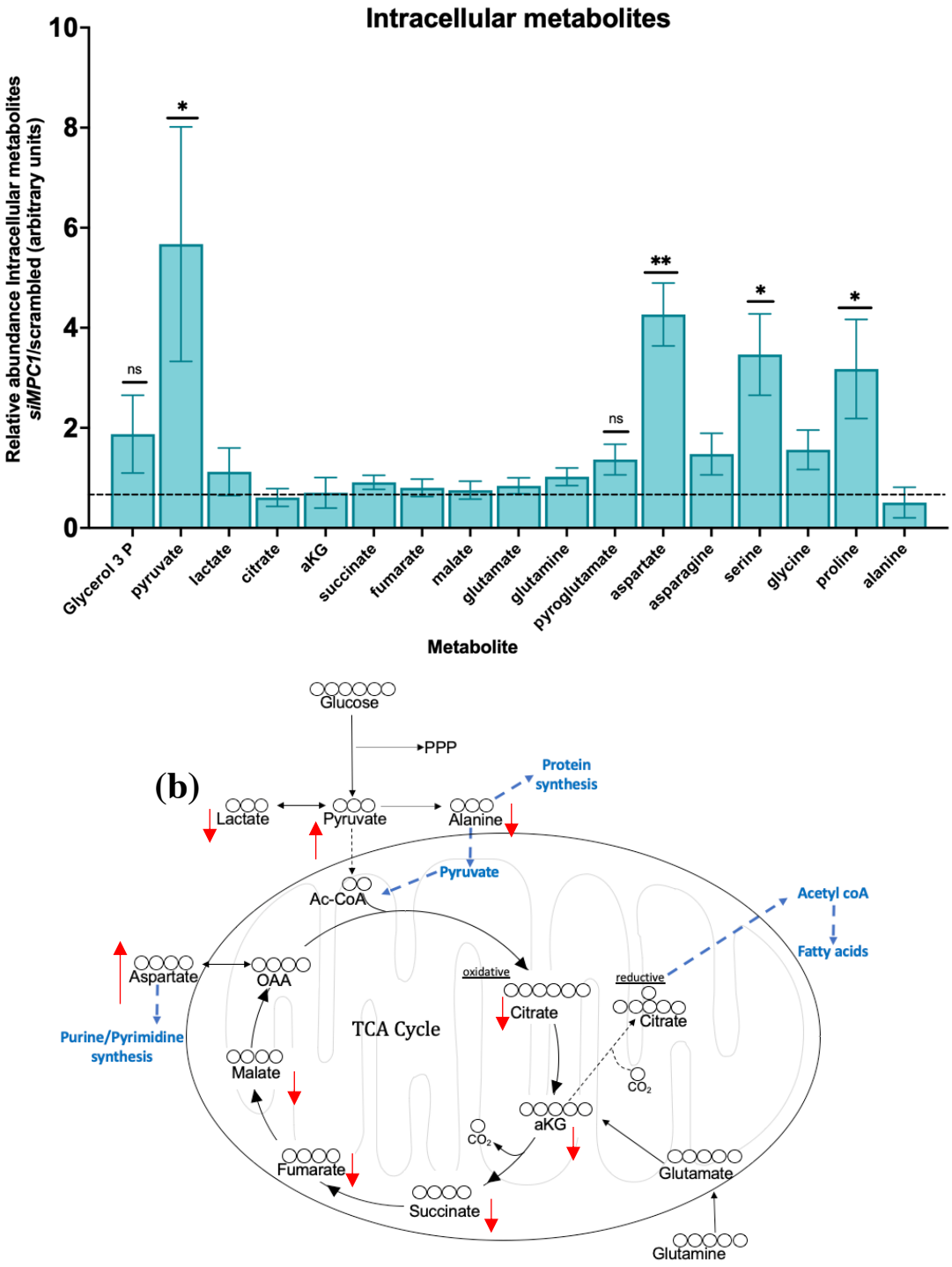

Figure 4.11 MPC1 depletion affects the glycolytic state of cells.
(a) The total metabolite pool was generated by normalising *siMPC1* cell TCA cycle intermediates to scramble control. (b) This pathway informs the usage of altered key TCA intermediates, e.g., Aspartate, Alanine, citrate. Red arrows indicate increase or decrease of metabolites. Statistical significance was evaluated using two-way ANOVA with Sidak's multiple comparison test Data were obtained from n = 4 independent biological replicates for each experiment. Data represented as mean ± SEM. Data expressed as mean ± SEM; * $p \leq 0.05$, ** $p \leq 0.01$, *** $p \leq 0.001$

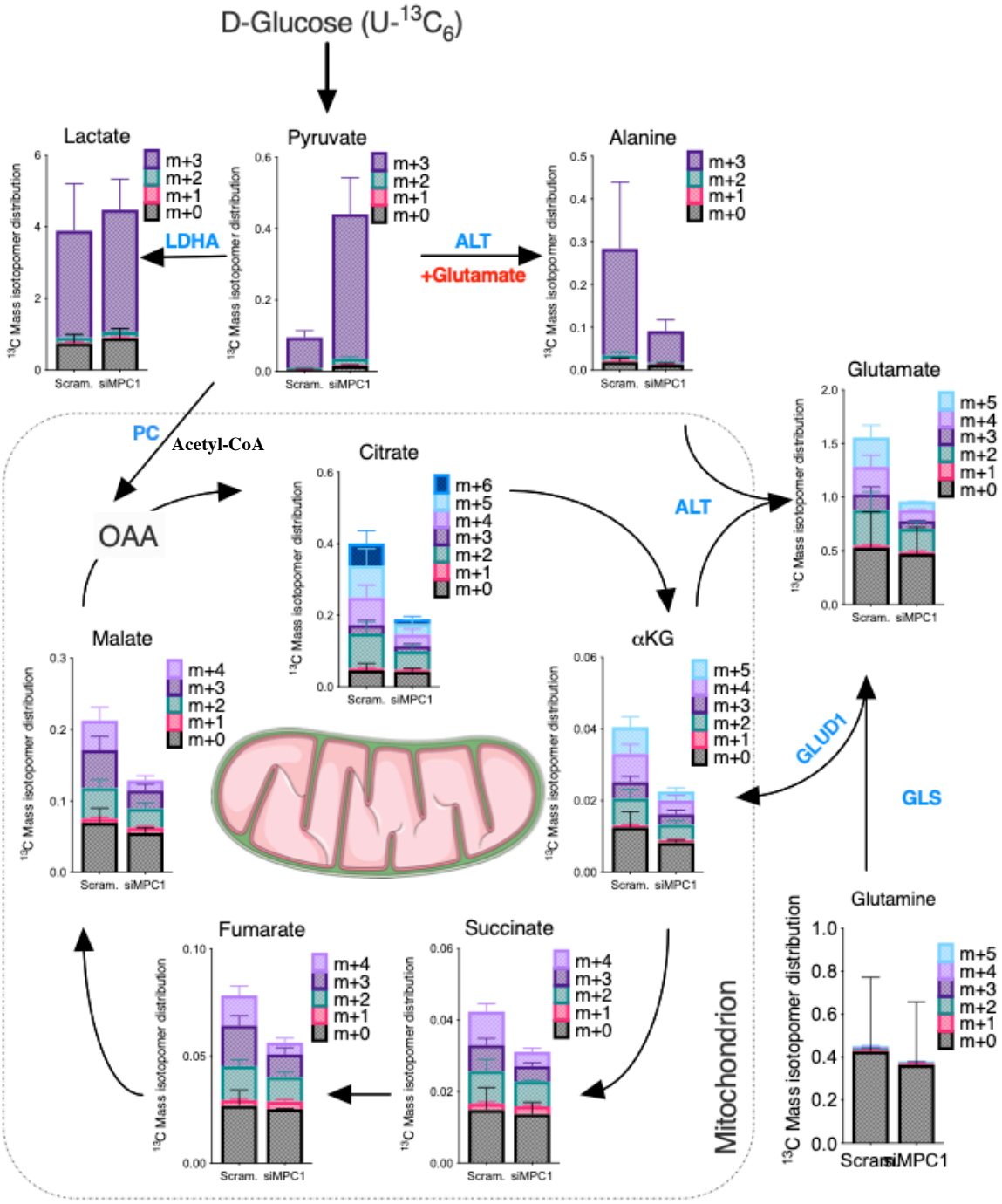

Figure 4.12 An overview of labelled glucose carbon MID through the TCA cycle. The graphs represent the mass isotopomer distribution of heavy carbon isotopes. Abbreviated enzyme names represent Lactate dehydrogenase A; LDHA, Alanine transaminase; ALT, pyruvate carboxylase; PC, glutaminase; GLS, glutamate dehydrogenase; GLUD1. Data were obtained from n = 4 independent biological replicates for each experiment. Data represented as mean ± SEM.

4.5 Discussion

The results from this Chapter show increased metabolic substrate utilisation upon *MPC1* deletion. As discussed previously, UK-5099 as a potent inhibitor of MPC complex diminish the possibility for MPC2 homodimer. However, siRNA targeting of MPC1 is specific and the real-time PCR data shows no change in MPC2 expression when MPC1 is knockdown. Loss of MPC function mimics the glucose depleted TME, initiating compensatory cellular metabolism. The MPC1 and MPC2 proteins form a hetero-oligomeric structure in the inner mitochondrial membrane. Previous studies have shown that MPC1 deletion resulted in increased tumour progression in colon, liver, breast, prostate, and lung cancer cells (Li et al., 2017a; Li et al., 2016; Schell et al., 2014b; Zhong et al., 2015). When MPC1 was re-expressed in the colon and oesophageal cancer, tumour progression was relatively reduced (Li et al., 2017b; Schell et al., 2014b). Furthermore, overexpressing MPC in Chinese hamster ovary (CHO) cells showed reduced Warburg effect (over 50% reduction in lactate levels was observed) (Bulte et al., 2020). The real-time PCR data for validating the knockdown on these cell lines show >75% successful knockdown efficiency for *MPC1*, *MPC2* and a combination of *MPC1* and *MPC2*. In order to test the hypothesis that MPC1 deletion promotes cancer proliferation and metabolic plasticity in ovarian cancer, HGSOC cell lines were used to knock down MPC. In this study, depletion of *MPC1* induced cell growth while *MPC2* depletion greatly affected cell proliferation. However, for the first time, our results show, when *MPC1* and *MPC2* were depleted simultaneously, HGSOC cell lines PEO1, PEO4 and OVCAR3 responded differently to *MPC1* knockdown. However, at different time points all three HGSOC cell lines programmed MPC1-mediated cell rescue when both MPC1 and MPC2 was targeted.

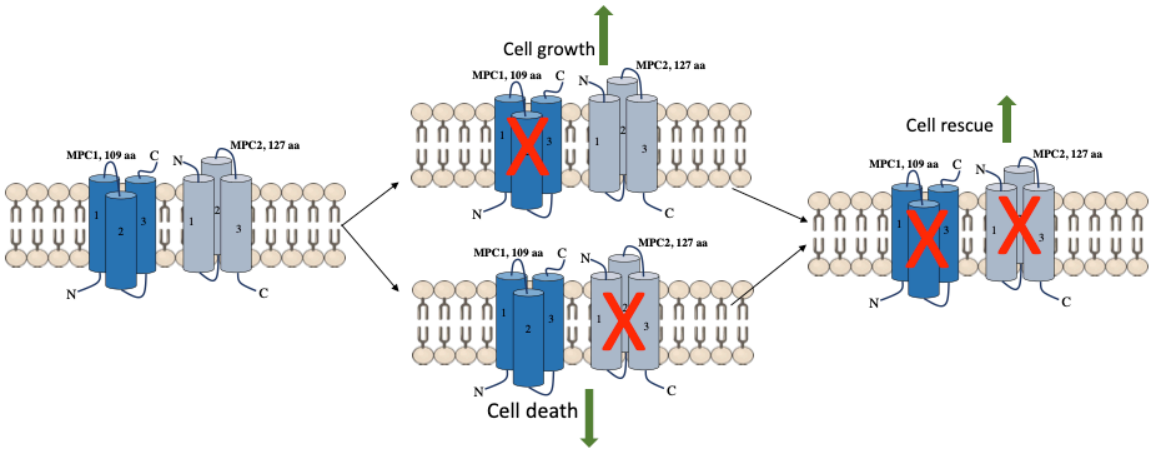

Figure 4.13 An overview of MPC1 and MPC2 depletion on cell growth.
A schematic representation of MPC1 and MPC2 heterodimer. The red cross indicates the blockage of protein expression by knocking down the MPC1 or MPC2 gene. Green arrows indicate cell growth or death. The image was developed using the Bio Render drawing tool.

The increased copy number variation for *MPC2* could indicate compensating for the loss of *MPC1*. As previously discussed in Chapter 3, OVCAR3 cells with low *MPC2* expression accumulated pyruvate, which was not evident in PEO4 cells. Conversely, our data suggest MPC2 expression in PEO4 cells was dependent on glutamine in the media. Collectively these data indicate *MPC1* depletion influences amino acid metabolism in ovarian cancer. To further investigate this assumption, we used universally labelled ^{13}C isotope to trace glucose and lactate.

Following the stable isotope tracing, an increase in intracellular pyruvate was observed in *MPC1* depleted cells. The *MPC1* knockdown increases the glycolytic rate, thereby resulting in increased activity of LDHA to produce lactate. It would be beneficial to measure the LDH activity in MPC1-deleted cells at different time points. A fall in lactate concentration (or similar intracellular lactate concentrations) could suggest the possibility of cells using the reverse Warburg's effect where cancer cells can utilise the pyruvate produced from lactate to use in the TCA cycle via MCTs without the need for MPC (Olson et al., 2016). However, current study did not measure the MCT expression under MPC1-depleted environment. Ovarian cancer patients accumulate ascites that are a pH acidic cellular fluid due to being rich in lactate and lactate

dehydrogenase. Until a recent finding of lactate utilisation for TCA cycle substrate, lactate was regarded as a waste product. The glycolytic substrate lactate is able to provide carbon atoms for the TCA cycle intermediates in human lung cancer, and these lactate utilising cells exhibited a more aggressive phenotype (Faubert et al., 2017; Hensley et al., 2016). Moreover, knocking down MCT1 and MCT4 reduced breast cancer cell migration and invasion *in vivo* (Morais-Santos et al., 2015).

Previous studies on pyruvate metabolism using ^{13}C-enriched substrates have shown reduced activity of MPC-dependent metabolic pathways (Compan et al., 2015b; Yang et al., 2014c). Conversely, our data shows *MPC1*-depleted cells utilising glucose and lactate as a precursor to producing TCA cycle intermediates. Our total metabolite pool evidently showed carbon from glycolytic end products contributing to the majority of the TCA cycle intermediates. Increased abundance of aspartate seemed to be derived from both labelled glucose and lactate, whilst the majority of it came from an unlabelled source (i.e., glutamine), which is looked into later on this thesis.

It was previously reported that an intracellular lactate shuttle operates similar to malate-aspartate shuttle (MAS) to regenerate cytosolic lactate via NAD+ reaction with LDH, not only to maintain the NAD+/NADH homeostasis but also a key event in hypoxic TME (Kane, 2014). Malate contributes to maintaining the TCA flux by being oxidised to pyruvate (NADP+ is reduced to NADPH) or being oxidising to oxaloacetate (NAD+ reduced to NADH) while maintaining the intracellular redox homeostasis. This reversible reaction is carried out by malic enzyme and malate dehydrogenase, respectively. Currently, research is being done on developing a new model of the lactate-malate-aspartate shuttle (lactate-MAS). Malate is oxidised by malate dehydrogenase in the mitochondrial matrix to produce oxaloacetate (OAA). The OAA converts to acetyl-CoA in the presence of pyruvate. When glutamate come into play, it is an added advantage to the cancer cells since it allows mitochondrial respiration via fully functioning MAS. When malate was supplemented to muscle cells to examine the oxygen consumption, malate was shown to stimulate respiration *in vitro* (Rasmussen et al., 2002).

Citrate is another major carbon compound predominantly produced by pyruvate derived acetyl-CoA. my data showed decreased citrate abundance in *MPC1* depleted cells compared to control. However, both glucose and lactate carbon were carried forward to citrate biosynthesis in the scramble control OVCAR3 cells (MPC1 present). While citrate is an intermediate for the TCA cycle, it also leads to fatty acid biosynthesis. Depleting MPC1 resulted in impaired transport of pyruvate into mitochondria, and generation of Acetyl-CoA was affected, resulting in decreased citrate levels (Herzig et al., 2012). It was previously believed that citrate could not be synthesised from extracellular space, and only intracellular substrates can lead to citrate synthesis via glucose-derived pyruvate or from glutamine (Metallo et al., 2012). Further studies also show glutamine is not necessary for the cancer cells, but it is consumed by the surrounding tissue (Marin-Valencia et al., 2012). Many studies have also shown glutamine anaplerosis under impaired glycolysis (Gonsalves et al., 2020; Yang et al., 2014c; Zhao et al., 2019).

Whether this finding is factual or not in ovarian cancer tumours, it would be beneficial to look at glutamine utilisation by cancer cells using SITA. Overall, data obtained from current research study suggest *MPC1* depletion repurposes amino acid metabolism for cancer cell survival and metastasis in HGSOC cancer cells.

Chapter Five

Loss of *MPC1* repurposes amino acid metabolism for ovarian cancer progression

5 The loss of *MPC1* repurposes amino acid metabolism for ovarian cancer progression

5.1 Introduction

Targeting cancer cell metabolism may enhance the treatment response to therapy-resistant ovarian tumours. Cancer cells switch on and off metabolically specific genes to meet increased energy demands and to maintain redox homeostasis. In addition to the use of glucose, cancer cells rely on alternative sources of nutrition when glucose becomes limited. At this stage, a major source of fuel for cancer cells is the upregulation of amino acid metabolism. Amino acids play a crucial role in tumour metabolism to provide a dual advantage to these cells by providing a carbon and nitrogen backbone to other metabolites, leading to the biosynthesis of macromolecules, energy production and glutathione biosynthesis (scavenging ROS) (Aggarwal et al., 2019; Lieu et al., 2020). To fulfil the demand for amino acids, mammalian target of rapamycin complex 1 (mTORC1) facilitates the balance between amino acid uptake and biosynthesis (Butler et al., 2021). Most of the cancers have mutated oncogenes directly involving in the upregulation or downregulation of amino acids, namely *MYC, KRAS, PI3K, PTEN, MTOR* and *ELF4* (Chalhoub and Baker, 2009; DeBerardinis and Cheng, 2010; Yang et al., 2019). Here, I focus on cancer-specific amino acid dependencies that result from loss of mitochondrial pyruvate carrier 1, driving ovarian cancer progression.

Glutamine is the most abundant amino acid in the body. Glutamine is an essential precursor for non-essential amino acid (NEAA) biosynthesis (Choi and Coloff, 2019). Furthermore, glutamine acts as the primary source of α-ketoglutarate (KG) to feed the tricarboxylic acid (TCA) cycle, whilst its intermediate glutamate is involved as an exchange factor for essential amino acids (EAA) (Butler et al., 2021). Glutamine enters the cells via solute carrier family 1 member 5 (SLC1A5) or the alanine-serine-cysteine transporter 2 (ASCT2). Glutaminolysis and *de novo* synthesis of glutamine are upregulated by the oncogenes *MYC* and *TP53* in cancer (Yang et al., 2017). An increased level of glutaminolysis has been reported in various cancers, including ovarian cancer, lung cancer, breast cancer and acute myeloid leukaemia (AML) (Vanhove et al., 2019; Yang et al., 2017). The glutamine anaplerosis to generate TCA cycle intermediates begins with the glutaminase 1 (*GLS1*) mediated catabolism of

glutamine. Though both *GLS1* and *GLS2* convert glutamine to glutamate, upregulation of mitochondrial enzyme *GLS1* expression correlates with poor prognosis in colorectal cancer, breast cancer and ovarian cancer (Qie et al., 2014; Xiang et al., 2019). Following glutamine conversion to glutamate by GLS, oxidative deamination of glutamate to α-ketoglutarate is facilitated by glutamate dehydrogenase, which generates free ammonia (NH_4^+) (Jiang et al., 2017). Increased expression of glutamate dehydrogenase was observed in hypoxic lung cancer cells mediated by hypoxia-inducible factor 1-alpha (HIF1α) with an upregulated intake of glutamine, resulting in the generation of ATP (Jiang et al., 2017). Ammonia was previously considered a toxic waste product until it was found that cancer cells can recycle ammonia to utilize nitrogen metabolism leading to the generation of key amino acids aspartate, alanine and proline (Spinelli et al., 2017).

In addition to glutamine anaplerosis, another major pathway to produce substrates for biosynthetic needs is the pyruvate carboxylation to produce oxaloacetate (OAA) via pyruvate carboxylase. Oxaloacetate contributes to aspartate biosynthesis, one of the key amino acids produced by malignant cancer cells with a high proliferative and metastatic phenotype. Aspartate is a limiting metabolite in multiple cancers (Birsoy et al., 2015a; Garcia-Bermudez et al., 2018), and an increase in mitochondrial aspartate synthesis has shown increased cellular respiration, thereby supporting cancer proliferation (Sullivan et al., 2015). Moreover, aspartate contributes to protein synthesis and purine and pyrimidine biosynthesis for nucleotides (Cheng et al., 2018; Du et al., 2013; Garcia-Bermudez et al., 2018). Similarly, the amino acid proline, either produced from the degradation of collagen proteins (shedding of extracellular matrix), from glutamate, or through the urea cycle from arginine/ornithine, has shown to play multiple roles in cancer. Proline biosynthesis mediated by collagen degradation is vital for cancer cells during epithelial-mesenchymal transition (EMT) to mesenchymal-epithelial transition (MET) and vice versa during cancer metastasis (D'Aniello et al., 2020; Elia et al., 2017a; Hollinshead et al., 2018b; Phang, 2019).

The ECM plays a crucial part in cancer cell migration and other oncogenic transformations. ECMs are a mesh of secreted proteins that provide strength and

support to cells. Likewise, degradation of ECM during cancer metastasis provides proline to generate ATP and protein synthesis. Ovarian cancer cells display increased Type VI collagen deposition during tumour formation, a factor contributing to therapy resistance in ovarian cancer (Choi et al., 2006; Sherman-Baust et al., 2003; Zhu et al., 1995). Type VI collagen is also a biomarker for pancreatic cancer and is elevated in the serum of breast cancer patients (Mazouni et al., 2008; Ohlund et al., 2009). Recently, it has been shown breast cancer cells demonstrate reliance on extracellular pyruvate in collagen-based remodelling of the ECM in the metastatic lung niche (Elia et al., 2019).

The *de novo* biosynthesis of proline occurs via Δ^1-pyrroline-5-carboxylate synthetase (P5CS/ALDH18A1) conversion of glutamate to Δ^1-pyrroline-5-carboxylate (P5C), mitochondrial PYCR1 or mitochondrial/cytosolic PYCR2 then convert P5C to proline. Alternatively, ornithine-derived P5C can also be metabolised to proline via a cytosolic PYCR3 isoform (also known as PYCRL) (Adams and Frank, 1980b; Phang et al., 2015). *PYCR1*, one of the most overexpressed metabolic genes in many cancers, is critical for the growth of breast tumours and its depletion is associated with diminished cell proliferation and tumour growth (Cai et al., 2018b; Craze et al., 2018; De Ingeniis et al., 2012; Ding et al., 2017a; Elia et al., 2017b; Kuo et al., 2016b; Loayza-Puch and Agami, 2016a; Loayza-Puch et al., 2016a; Natarajan et al., 2012; Nilsson et al., 2014; Phang et al., 2012; Phang et al., 2015). Moreover, where *PYCR1* is overexpressed in some cancers, knocking down *PYCR1* affected cell growth and metastasis (Cai et al., 2018a). In this Chapter, I have used universally heavy labelled $^{13}C_5$ isotope glutamine (figure 5.1) to trace the metabolite substrate utilization by *MPC1* depleted ovarian cancer cell lines while comparing to the substrate utilization of $^{13}C_6$ isotope glucose and $^{13}C_3$ isotope lactate that produces precursors for amino acids, nucleotides, and lipid biosynthesis, by these cells. Furthermore, the expression of proline biosynthetic pathway enzymes was measured to compare and contrast the role of proline in cancer proliferation and metastasis.

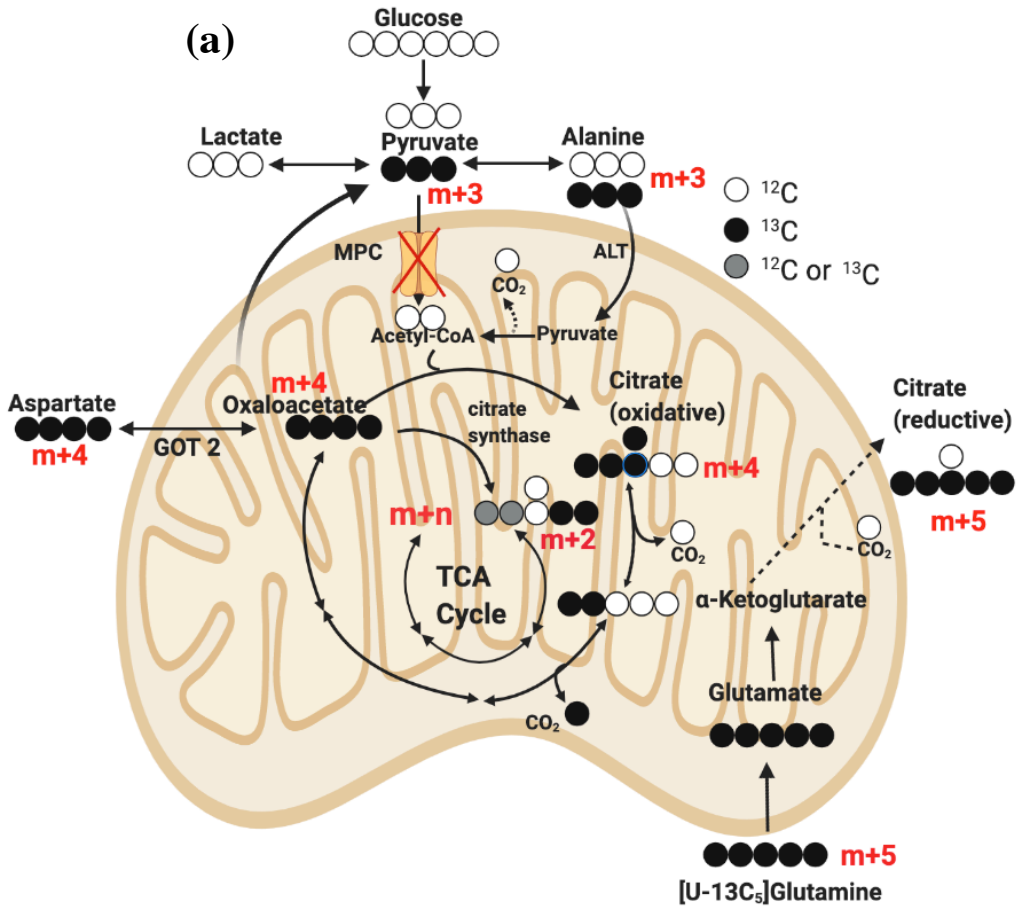
(a)
Glucose
Lactate
Pyruvate
Alanine
m+3
m+3
^{12}C
^{13}C
^{12}C or ^{13}C
MPC
ALT
CO_2
Acetyl-CoA
Pyruvate
m+4
Oxaloacetate
Aspartate
m+4
GOT 2
citrate synthase
Citrate (oxidative)
m+4
Citrate (reductive)
m+5
m+n
m+2
CO_2
CO_2
TCA Cycle
α-Ketoglutarate
Glutamate
CO_2
m+5
[U-13C5]Glutamine

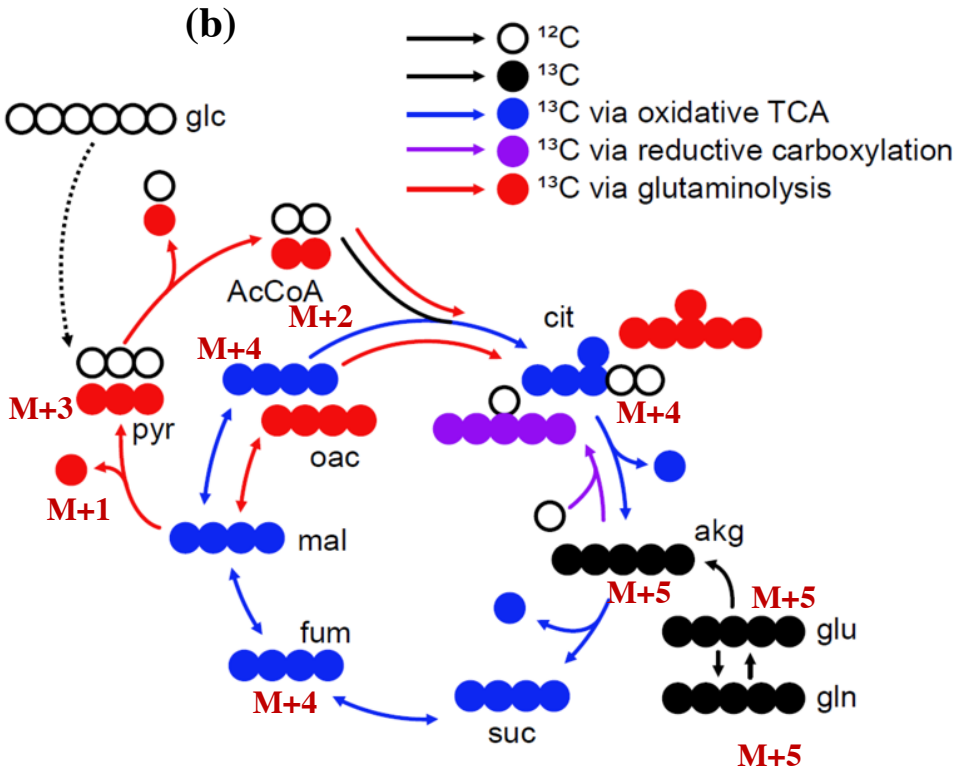
(b)
^{12}C
^{13}C
^{13}C via oxidative TCA
^{13}C via reductive carboxylation
^{13}C via glutaminolysis
glc
AcCoA
M+2
M+4
M+3
pyr
oac
M+1
mal
fum
M+4
cit
M+4
akg
M+5
M+5
glu
gln
M+5
suc

Figure 5.1 Graphical representation of labelled TCA cycle metabolites incorporated from [U-$^{13}C_5$]-glutamine.
(a) The **m+(n)** (m+5 or m+4 etc.), describes the proportion of mass isotopomer distribution (MID) for each element derived from the labelled source (i.e., glutamine). **(b)** The diagram depicts the possible TCA cycle intermediates derived from glutamine and the proposed pathway (e.g. glutamine anaplerosis or oxidative TCA) (Jeong et al., 2021).

5.2 Hypothesis

The present study tested the hypothesis that by forfeiting MPC1, epithelial ovarian cancer cells adapt amino acid metabolism for growth and metastasis. Moreover, the amino acid proline plays a vital role in promoting cancer proliferation, while proline biosynthetic enzymes biosynthesise proline for extracellular matrix formation (ECM).

5.3 Experimental Procedures

5.1.1 Cell culture

The cell line used in the following chapter is MPC1 expressing OVCAR3 cells. The cell culture method for this cell line is explained in Chapter 2, section 2.1.1. Each biological replicate is an independent passage of the cell line. Any media used for growth studies are the same as mentioned in section 2.1.1 except for siRNA cell culture, which was antibacterial, antimycotic (ABAM) free.

5.1.2 siRNA cell culture

To model, the loss of mitochondrial pyruvate carrier, *MPC1*, is deleted in ovarian cancer cells. The siRNA was set up, and the experimental design was arranged as explained in Chapter 2, section 2.3. Briefly, the cells were cultured in the recommended growth media until cells reached the desired confluency (~70% to ensure exponential growth). For siRNA depletion, 0.5 mL of Opti-MEM was added to each well of a 6-well plate. Then, 7.5 µl of RNAimax (lipofectamine) was added to each well, followed by 5 µl of targeting siRNA or scrambled control and plates incubated for 10 min at RT. Meanwhile, cells were washed with 5 mL PBS, detached using 2 mL Accutase (Merck, UK), and live cells counted using the Countess (Invitrogen Cell counter, ThermoFisher Scientific, UK). Cells were then resuspended in growth media without ABAM solution at 1 x 10^5 cells/mL. Then, 2.5 mL of cell suspension was added to the 5 mL Opti-MEM/lipofectamine/siRNA complex. Cells were incubated undisturbed for 72 h at 37 ˚C and 5% CO_2. Cells were then used immediately or reseeded as stated. Real-time qPCR was used to determine the efficacy of siRNA; 72 h was chosen as the optimal time point to achieve >70% gene knockdown.

5.1.3 Proline supplemented proliferation study

To investigate proline compensation for the loss of glutamine, OVCAR3 cells were treated with proline in a glutamine depleted environment as described in Chapter 2, section 2.7. Briefly, OVCAR3 cells were pre-incubated in complete growth media containing 5 µM UK-5099 to constantly block the MPC activity. Cells were gently washed with PBS and detached with Accutase. Cell count was recorded with a minimum of 95% viability. For the proliferation study, MPC1 inhibited OVCAR3

cells were seeded at 2,000 cells/well on a 96-well plate with differential growth media. For the current study, a medium without glutamine or proline was used as stated in *Results*. Cells were supplemented with either 2 mM glutamine or 2 mM proline. Cell culture plates were then left in the incubator at 37˚C and 5% CO_2. Following a 16-hour (to match the invasion assay) incubation, cells were washed with PBS and immediately frozen at -80˚C for DNA quantification assay (CyQUANT). Prior to performing the CyQUANT proliferation assay, cells were thawed to room temperature. The assay was performed as described in Chapter 2, section 2.6. A standard curve was generated for each plate.

5.1.4 Collagen-based invasion assay

Following a 72 h incubation in siRNA, cells were gently washed with PBS and detached with Accutase. Cell counts were recorded with a minimum of 95% viability confirmed using automated cell counter Countess™ . The invasion assay was set up as described in Chapter 2, section 2.8. Briefly, *MPC1*-depleted OVCAR3 cells were seeded onto Matrigel-coated trans well membrane. Cells were either supplemented with 2 mM glutamine or proline and incubated for 16 h. To image the cells, Giemsa cell staining protocol was used as described in Chapter 2, section 2.7.3.

5.1.5 Quantitative real-time polymerase chain reaction (qPCR)

For gene expression studies, qPCR was performed using Quantifast SYBR Green (Qiagen, UK) and the CFX connect Real-time PCR detection system (Bio-Rad, UK). All consumables were DNase/RNase-free, and the laminar flow hood was cleaned prior to using RNaseZAP wipes. The general experimental set-up included RNA extraction and cDNA synthesis, as explained in detail in Chapter 2, section 2.2. The purity of total RNA quantification was measured by Nano-drop, and 260/280 and 260/230 values were determined to be between 1.8 and 2.3. The following Chapter investigated the role of *MPC1* associated with *PYCR1, PYCR2* and *PYCR3* genes in ovarian cancer cell metabolism. The starting quantity of mRNA from the experimental sample was determined using standard curves generated from serial dilutions of pooled reference RNA with Quantifast SYBR green (Qiagen). Sample and reference genes were analysed in triplicate, and mRNA expression was normalised to housekeepers *RPL19* and *ACTB*. All the sequences for mRNA expression primers and siRNA

sequences are listed in Chapter 2, section 2.2. The gene expression data relative quantity was calculated according to Livak & Schmittgen's method (Livak and Schmittgen, 2001), and data was expressed as ΔΔCq.

5.1.6 Stable isotope tracing analysis

The current Chapter used heavy-isotope labelled glucose, glutamine, or lactate to investigate key metabolic pathways affected by the loss of the mitochondrial pyruvate carrier. The experimental set-up for stable isotope tracing analysis (SITA) is described in detail in Chapter 2, section 2.11. For stable isotope labelled glucose tracing, cells were incubated with universally labelled ^{13}C-glucose (11.1 mM; #CLM-1396. Cambridge isotope, USA) in glucose-free RPMI (#11879020, Gibco, UK) basal growth media, supplemented with dialysed FBS, glutamine (2 mM) and ABAM. For labelled lactate, cells were incubated with universally labelled sodium ^{13}C-lactate (10 mM; #CLM-1579. Cambridge isotope, USA) in glutamine free basal RPMI (#31870, Gibco, UK) growth media, supplemented with 2 mM unlabelled glutamine (ThermoFisher scientific, #25030081). For stable isotope labelled glutamine tracing, cells were incubated with universally labelled ^{13}C-glutamine (2 mM; #CLM-1822. Cambridge isotope, USA) in glutamine-free RPMI (#31870, Gibco, UK) basal growth media, supplemented with dialysed FBS and ABAM. Following 72 h exposure to siRNA, cells were reseeded in heavy-labelled media and incubated for a further period of 72 h at 37°C and 5% CO_2 in a humidified chamber. Prior to intracellular metabolite extraction, cells were washed with ice-cold saline solution and lysed in 80% methanol. Lysates were centrifuged at 12,000 x g for 10 min to remove any cell debris, and cell extracts were dried to pellets at 4°C using a speed vacuum concentrator.

Samples were run by technicians at McGill University, Canada, as a paid service. Briefly, cellular metabolites were extracted and analysed by GC-MS following a previously described protocol (Faubert et al., 2014; Vincent et al., 2015). Metabolite extracts were derived using N-(*tert*-butyldimethylsilyl)-N-methyl trifluoroacetamide (MTBSTFA) as described previously (Faubert et al., 2013). D-myristic acid (750 ng/sample) was added as an internal standard to metabolite extracts, and metabolite abundance was expressed relative to internal standards and normalised for the number of cells. GC-MS analysis was performed using an Agilent 5975C GC-MS equipped

with a DB-5MS + DG (30 m x 250 μm x 0.25 μm) capillary column (Agilent J and W, Santa Clara, CA, USA). For SITA experiments, mass isotopomer distribution was determined using a custom algorithm developed at McGill University (McGuirk et al., 2013).

5.1.7 Clonogenic assay

Single-cell cloning of *MPC1*-depleted ovarian cancer cells was observed by a clone formation assay as described in Chapter 2, section 2.9. OVCAR3 cells were depleted of *MPC1*, *PYCR1, PYCR2* or *PYCR3* individually or in combination, as stated in *Results,* for 72 h using siRNA. Cells were then gently washed in PBS and counted to achieve 800 cells/mL seeding density on a 6-well plate for Scramble control or *siMPC*1/*PYCR* conditions. Following cell seeding, cell culture plates were incubated for 21 days with refreshed media every 3-4 days whilst ensuring cells were not contaminated via intermittent observation by light microscopy. Colonies were then Giemsa stained and manually counted under a compound microscope.

5.1.8 Statistical analysis

Data are presented as mean ± SEM, with statistical analyses performed using Prism version 8.4.1. One-way ANOVA with Dunnett's multiple comparison test or Two-way ANOVA Sidak's multiple comparison test was used to compare treatment groups with the control. Majority of the experiments have a replicate size of n = 3 unless otherwise stated.

5.4 Results

5.1.9 Treating *MPC1* knockdown cells with uniformly labelled glutamine

At least 50% of the non-essential amino acids are derived from glutamine *in vitro,* and glutamine has been shown to maintain TCA cycle flux in *Mpc1*-deficient mouse liver (Gray et al., 2015; Wise and Thompson, 2010). To investigate how glutamine metabolism is utilized in response to *MPC1* depletion in human high-grade serous ovarian carcinoma, *MPC1* was knocked down in OVCAR3 cells and supplemented with 2 mM (U-$^{13}C_5$)-glutamine. To gain further insight, key TCA cycle intermediates were compared with the data I previously obtained for 11.1 mM (U-$^{13}C_6$)-glucose and 10 mM (U-$^{13}C_3$)-lactate supplementation. The experimental set-up and timing of extracting samples were identical to each other to minimise the error. Metabolic substrate utilization via stable isotope tracing of labelled glutamine (supplemented) showed intracellular metabolic changes upon MPC1 depletion at transcriptional levels. Intracellular pyruvate was significantly elevated upon *MPC1* knockdown (>5-fold). However, very few carbons or no carbon were contributed, as indicated by m+1; m+2; or m+3, from labelled glutamine to pyruvate (figure 5.2). However, a significant proportion of heavily labelled glutamine became biosynthesised into glutamate and key TCA cycle intermediates. Majority of the TCA cycle intermediates were decreased upon MPC1 depletion. Whether some of the amino acids are not produced or they have been used up by the cells is still unclear. This will have to be further verified by looking at the genes involved in these metabolic pathways or measuring the enzyme levels. However, if these TCA cycle metabolites are being used up, it would suggest an essential role for amino acid metabolism under impaired pyruvate transport in ovarian cancer cells. An overview of the glutamine substrate utilization is shown in figure 5.2. The TCA cycle intermediates are looked at further in detail in this Chapter.

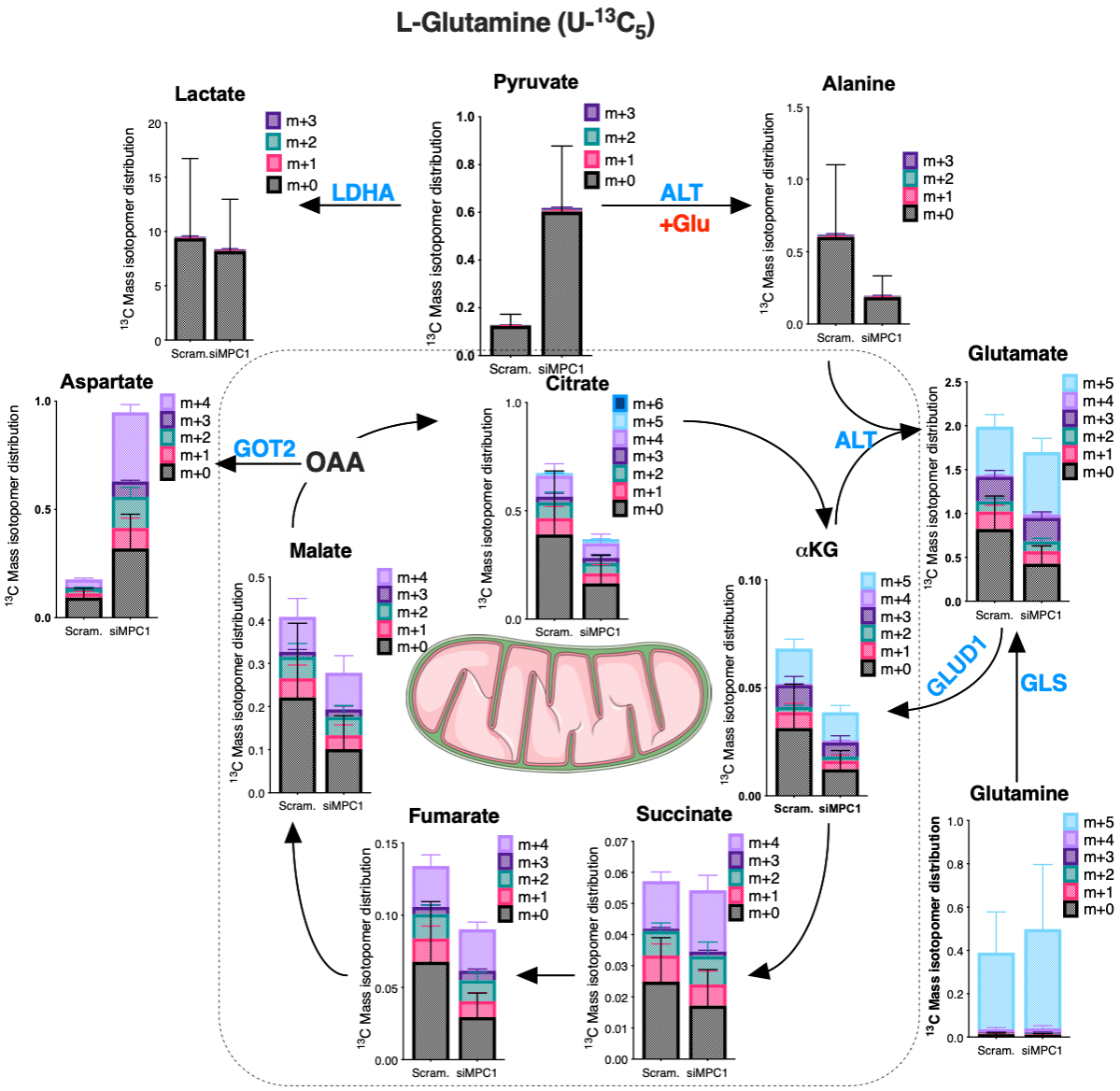

Figure 5.2 An overview of labelled glutamine carbon mass isotopologue distribution (MID) through the TCA cycle.

The graphs represent the MID of heavy carbon isotopes from labelled glutamine. Abbreviated enzyme names represent Lactate dehydrogenase A; LDHA, Alanine transaminase; ALT, pyruvate carboxylase; PC, glutaminase; GLS, glutamate dehydrogenase 1; GLUD1. Data were obtained from n=4 independent biological replicates for each experiment. Data represented as mean + SEM.

5.1.10 HGSOC cells show metabolic flexibility to sustain the biosynthesis of substrates for the TCA cycle

The primary step of glutamine metabolism is the synthesis of glutamate by glutaminase. Glutamate acts as a precursor for glutathione synthesis and many amino acid biosynthesis, including α-KG**,** proline, aspartate, and alanine. Stable isotope tracing data showed glutamate was synthesized from glucose and lactate in addition to glutamine, where the majority of the glutamate could be traced to glutamine. Moreover, glutamate utilization from a non-labelled carbon source was increased in *MPC1* lacking cells compared to Scramble control in ^{13}C-glucose supplemented cells (figure 5.3a, for ^{12}C; p = 0.02, for ^{13}C; p=0.11) and ^{13}C-lactate supplemented cells (figure 5.3b, for ^{12}C; p=0.99 and for ^{13}C; p=0.74), suggesting an increased glutamine uptake upon *MPC1* depletion. Under glutamine supplemented conditions, most of the labelled carbons were from ^{13}C-glutamine (figure 5.3c). However, abundance of glutamate was unaffected between the control or *MPC1* depleted cells (figure 5.3c, for ^{12}C; p=0.65 and for ^{13}C; p=0. 21). To further verify these findings, it would be useful to look at the enzymatic expressions regulated in these reactions but not looked into in this thesis.

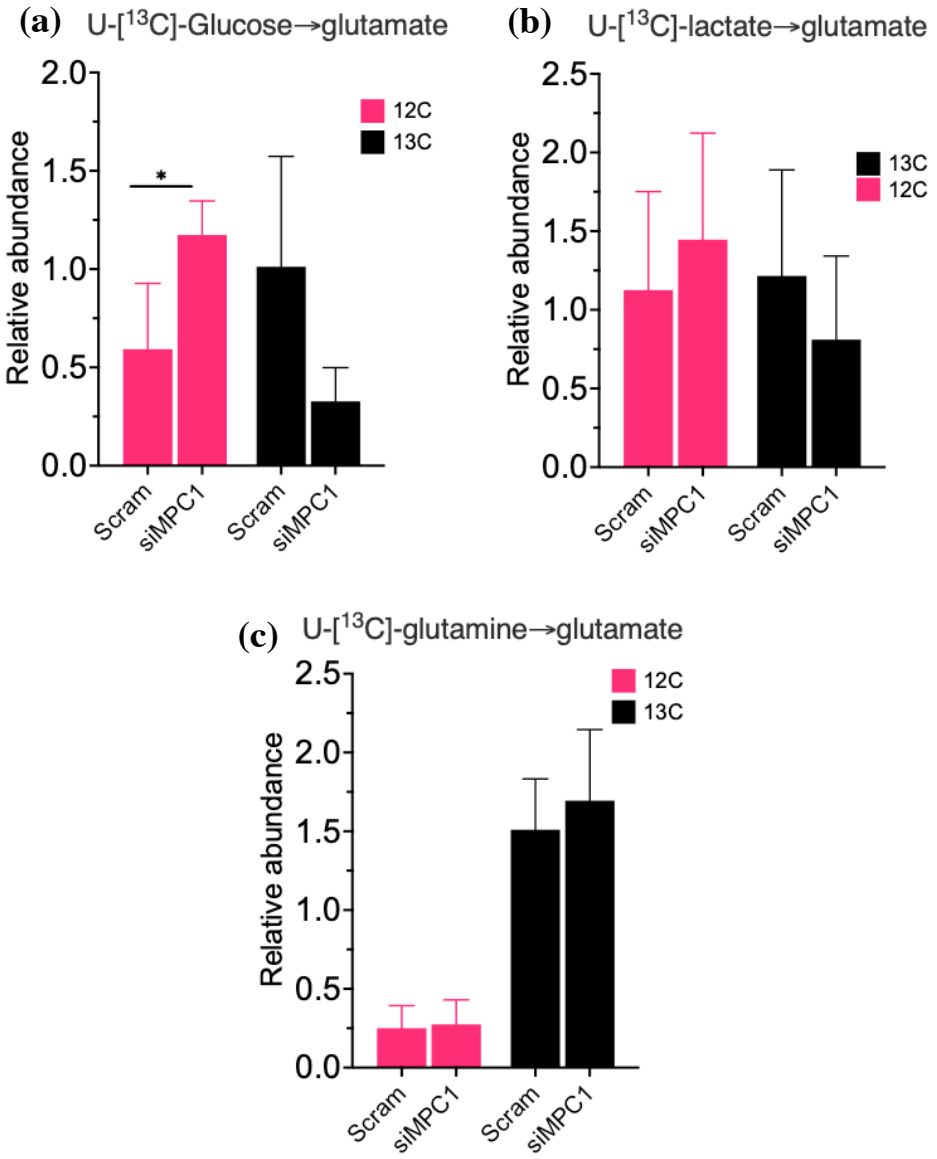

Figure 5.3 Contribution of universally-labelled ^{13}C-glucose, ^{13}C-lactate, or ^{13}C-glutamine to glutamate.
(a) glutamate MID derived from labelled glucose (black bars) compared to unlabelled glucose (pink bars), (b) glutamate derived from labelled lactate or unlabelled lactate, (c) glutamate derived from labelled or unlabelled glutamine in OVCAR3 cells. Statistical significance was evaluated using two-way ANOVA with Sidak's multiple comparison test. Data were obtained from n=4 independent biological replicates for each experiment. Data expressed as mean + SEM; * $p \leq 0.05$, ** $p \leq 0.01$, *** $p \leq 0.001$

Subsequently, glutamate is metabolised to α-KG by glutamate dehydrogenase. This conversion is crucial for cells to actively keep the TCA cycle in progress under a nutrient-depleted environment (i.e., restricted glucose). Similar to glutamate, the α-KG was produced from carbon sources of both labelled and non-labelled isotopes

(Figures 5.4a, 5.4b and 5.4c). Whilst glucose or lactate contribution to α-KG was reduced in *MPC1*-depleted cells (figure 5.4a, for ^{12}C glucose; p=0.04, for ^{13}C glucose; p=0.71; figure 5.4b, for ^{12}C lactate; p=0.86 and for ^{13}C lactate; p=0.96). However, cells depleted of *MPC1* increasingly relied on ^{13}C-glutamine to maintain α-KG (figure 5.4c, for ^{12}C; p=0.81 and for ^{13}C; p=0.27). But α-KG biosynthesis from an unlabelled carbon source is not completely abandoned, suggesting cells are able to maintain an active TCA cycle enough to meet their metabolic demands.

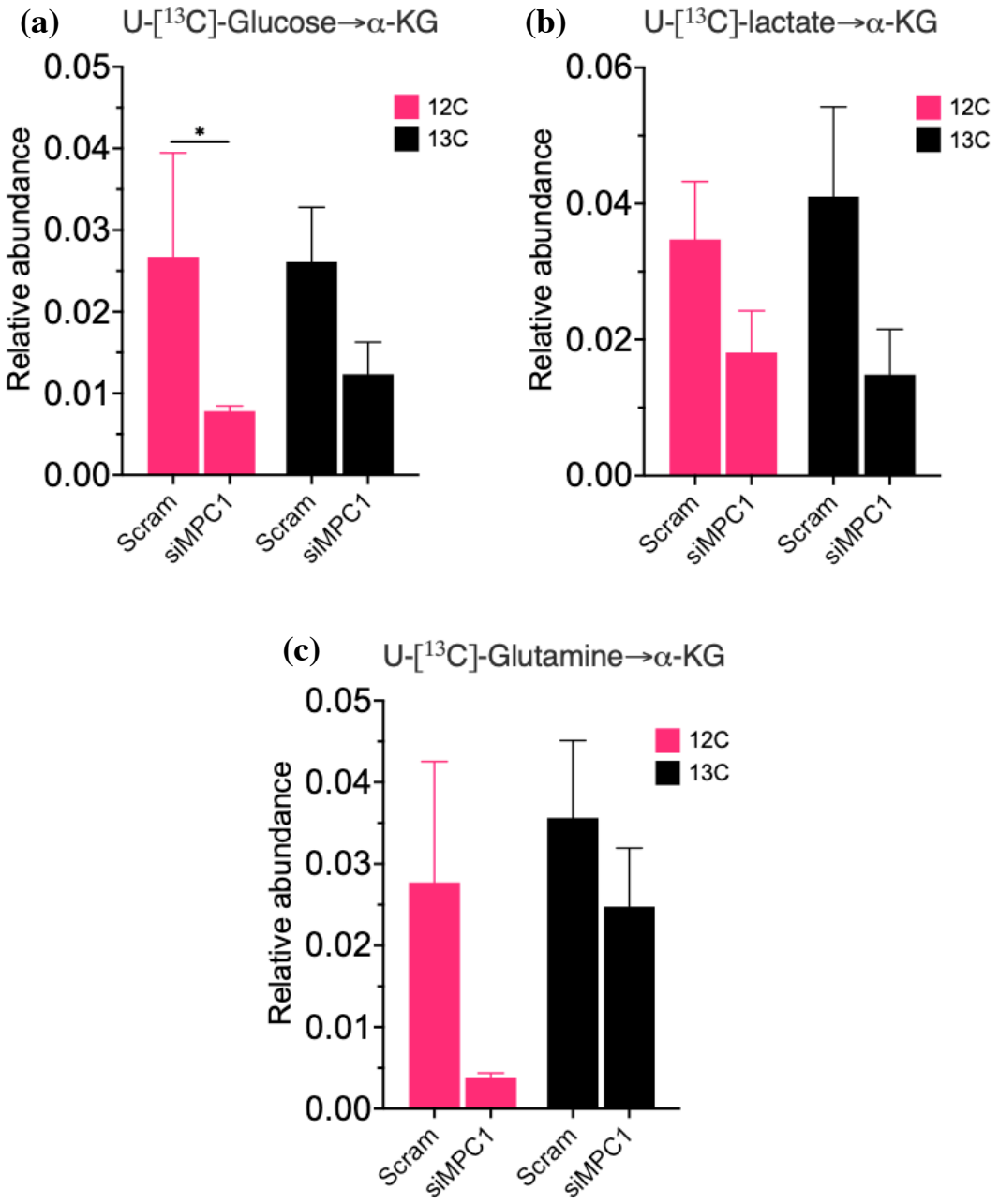

Figure 5.4 Contribution of ^{13}C-glucose, ^{13}C-glutamine, and ^{13}C-Lactate to α-ketoglutarate (α-KG).
(a) α-KG MID derived from labelled (black bars) or unlabelled (pink bars) glucose, (b) α-KG derived from labelled lactate, or (c) α-KG derived from labelled glutamine in OVCAR3 cells. Statistical significance was evaluated using two-way ANOVA with Sidak's multiple comparison test. Data were obtained from n=4 independent biological replicates for each experiment. Data expressed as mean + SEM; * $p \leq 0.05$, ** $p \leq 0.01$, *** $p \leq 0.001$

Next, I looked into pyruvate production from glutamine metabolism intermediates. A previous study on glutaminolysis in lung cancer cells showed the production of pyruvate from labelled glutamine under a glucose depleted environment via OAA mediated by phosphoenolpyruvate carboxykinase 2 (PCK2) (Vincent et al., 2015). The glycolytic end-product pyruvate, which was significantly increased upon *MPC1* depletion, barely came from the labelled carbon of glutamine in OVCAR3 cells (figure 5.5a). To further look into this, I plotted the mass isotopomer distribution (MID) data, which showed almost all pyruvate carbons, regardless of MPC1 depletion, came from a non-labelled source (i.e., pyruvate abundance was only seen in M+0, figure 5.5b). Following the accumulation of pyruvate, I looked into the abundance of citrate upon *MPC1* depletion. Citrate is primarily produced from pyruvate derived acetyl CoA (Metallo et al., 2012; Vacanti et al., 2014b; Wise and Thompson, 2010). Relatively decreased citrate levels were seen in *Mpc2* knocked down C2C12 mouse myoblasts but not *Mpc1* knocked down cells, under low pyruvate abundance (Vacanti et al., 2014b). Converse to the previous observation, pyruvate accumulation did not result in increased citrate abundance in si*MPC1* OVCAR3 cells (figure 5.5c). However, MID data for citrate showed the contribution of glutamine to citrate (abundance of M+1, M+2, M+3 and M+4) (figure 5.5d). The citrate m+2 and m+4 is produced from the reductive carboxylation of glutamine in which α-KG to citrate is then used to produce OAA and acetyl-CoA, this mechanism was shown by (Garcia-Bermudez et al., 2018), where labelled aspartate showed contribution of m+2 and m+4 to citrate. The oxidative route of α-KG to citrate would be conversion of α-KG to succinate to produce citrate by TCA cycle. The favour of oxidative or reductive route can be confirmed by measuring the enzymatic expression of IDH2.

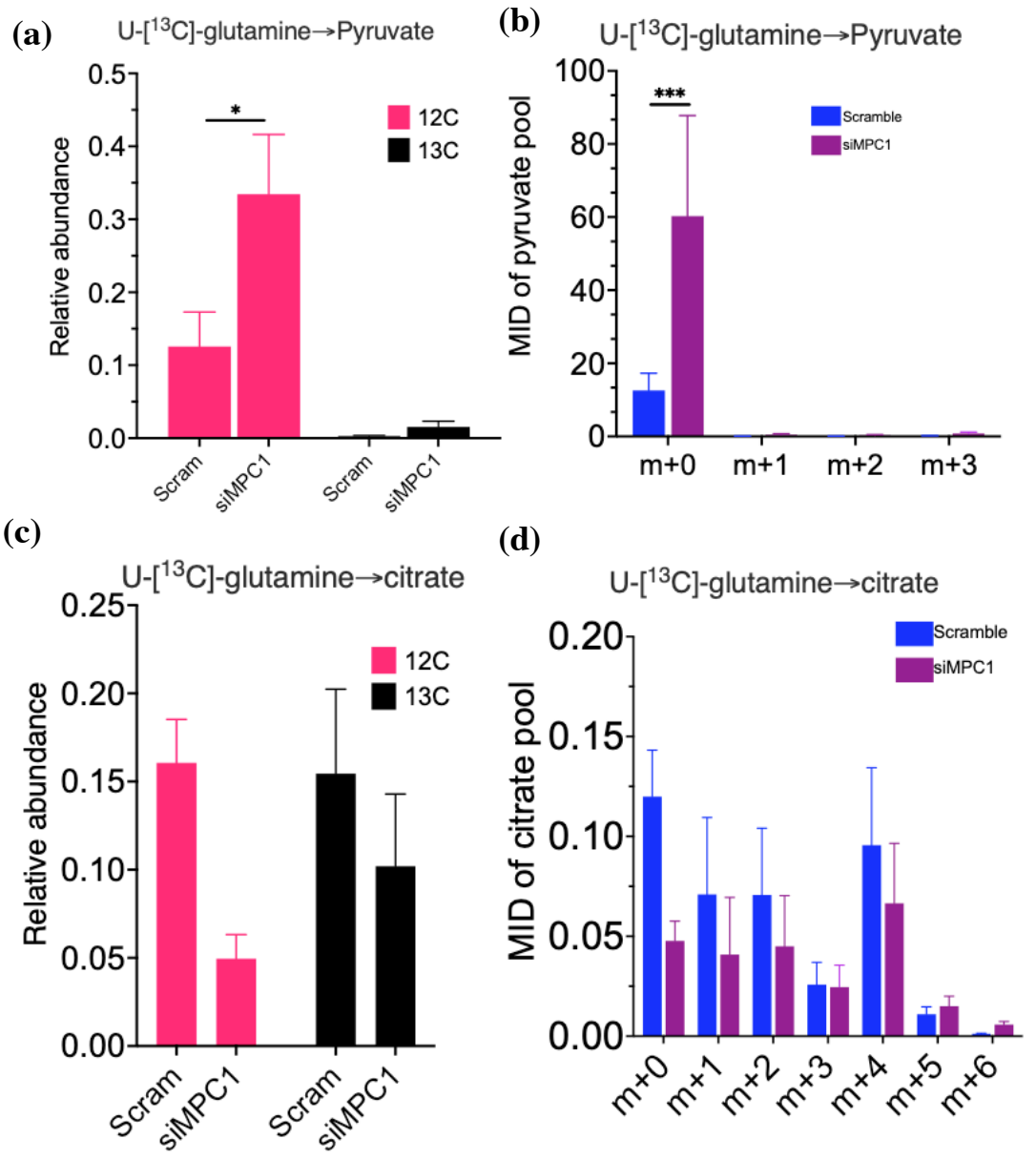

Figure 5.5 Contribution of ^{13}C-glutamine to pyruvate and citrate.
(a) 2 mM [U-$^{13}C_5$] glutamine to pyruvate in OVCAR3 cells and corresponding mass isotopomer distribution (MID) of glutamine to pyruvate (b). (c) Citrate produced from 2 mM [U-$^{13}C_5$] glutamine corresponding mass isotopomer distribution (MID) of glutamine to citrate (d). Statistical significance was evaluated using two-way ANOVA with Sidak's multiple comparison test. Data were obtained from n = 4 independent biological replicates for each experiment. Data expressed as mean ± SEM; * $p \leq 0.05$, ** $p \leq 0.01$, *** $p \leq 0.001$

The transamination of alanine yields pyruvate and glutamate. Glutamate subsequently becomes oxidatively deaminated, regenerating α-KG and yielding NH_4^+ and NAD(P)H (Altman et al., 2016). Furthermore, to the observation of pyruvate abundance from labelled glucose and lactate, the majority of the alanine abundance

was from labelled glucose (figure 5.6a) and labelled lactate (figure 5.6b), glutamine contribution to alanine was scarcely observed (figure 5.6c). However, endogenous alanine levels were relatively reduced upon *MPC1* depletion. It is unclear whether pathways leading to alanine biosynthesis are downregulated or alanine is becoming depleted to compensate from loss of MPC1-driven metabolic pathways since alanine can enter the mitochondria via alanine transporter and convert to pyruvate inside the mitochondria via alanine transaminase 2 (Bowman et al., 2016; McCommis and Finck, 2015). This can be tested in future by measuring the expression or activity of alanine transporters or enzymes involved. Alanine provides an alternative route of pyruvate carbon entry into the mitochondria and is unaffected by *Mpc2* deletion (McCommis and Finck, 2015).

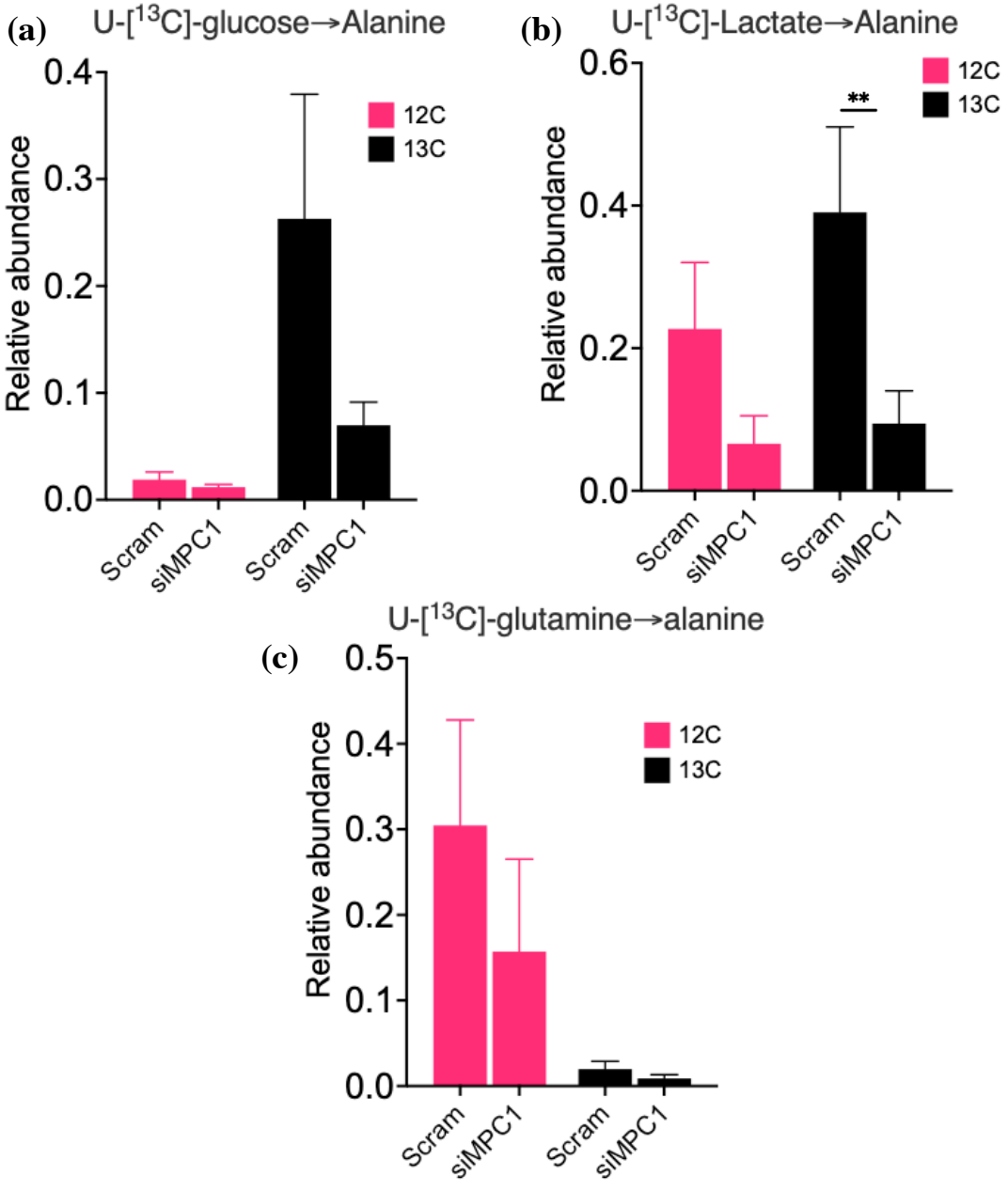

Figure 5.6 Contribution of ^{13}C-glucose, ^{13}C-glutamine, and ^{13}C-Lactate to alanine. (a) alanine derived from labelled glucose, (b) alanine derived from labelled lactate, (c) alanine derived from labelled glutamine in OVCAR3 cells. Statistical significance was evaluated using two-way ANOVA with Sidak's multiple comparison test. Data were obtained from n = 4 independent biological replicates for each experiment. Data expressed as mean ± SEM; * $p \leq 0.05$, ** $p \leq 0.01$, *** $p \leq 0.001$

These data collectively suggest, with combined data from a previous Chapter (figure 4.7 and 4.8 of chapter 4), the possibility for the reverse Warburg effect where TCA cycle intermediates are produced from glycolytic products under impaired pyruvate transport.

5.1.11 Depletion of *MPC1* in ovarian cancer cells increased aspartate metabolism

Aspartate is a NEAA predominantly derived from glutamine. *MPC* inhibition in mouse retina and mouse myoblasts resulted in the accumulation of aspartate (Du et al., 2013; Vacanti et al., 2014b). Similarly, here I show a significant increase in the abundance of aspartate in *MPC1* depleted OVCAR3 cells, although in the mouse study, knockdown of *Mpc2,* not *Mpc1,* induced this effect (Du et al., 2013; Vacanti et al., 2014b). Exogenous aspartate has poor cell permeability in non-SLC1A3-expressing cells; thus, endogenous aspartate becomes a metabolic limitation for the growth of some tumours (Sullivan et al., 2015). As OVCAR3 cells are reported to overexpress SLC1A3 (Coscia et al., 2016b), it would be interesting to understand if the increase in aspartate pool was either from an exogenous source or derived via intracellular biosynthesis. The stable isotope tracing data determined [U-$^{13}C_6$]-glucose, [U-$^{13}C_3$]-lactate and [U-$^{13}C_5$]-glutamine each contributed to majority of the endogenous pool of aspartate in *MPC1* depleted OVCAR3 cells (figures 5.7a, 5.7b and 5.7c).

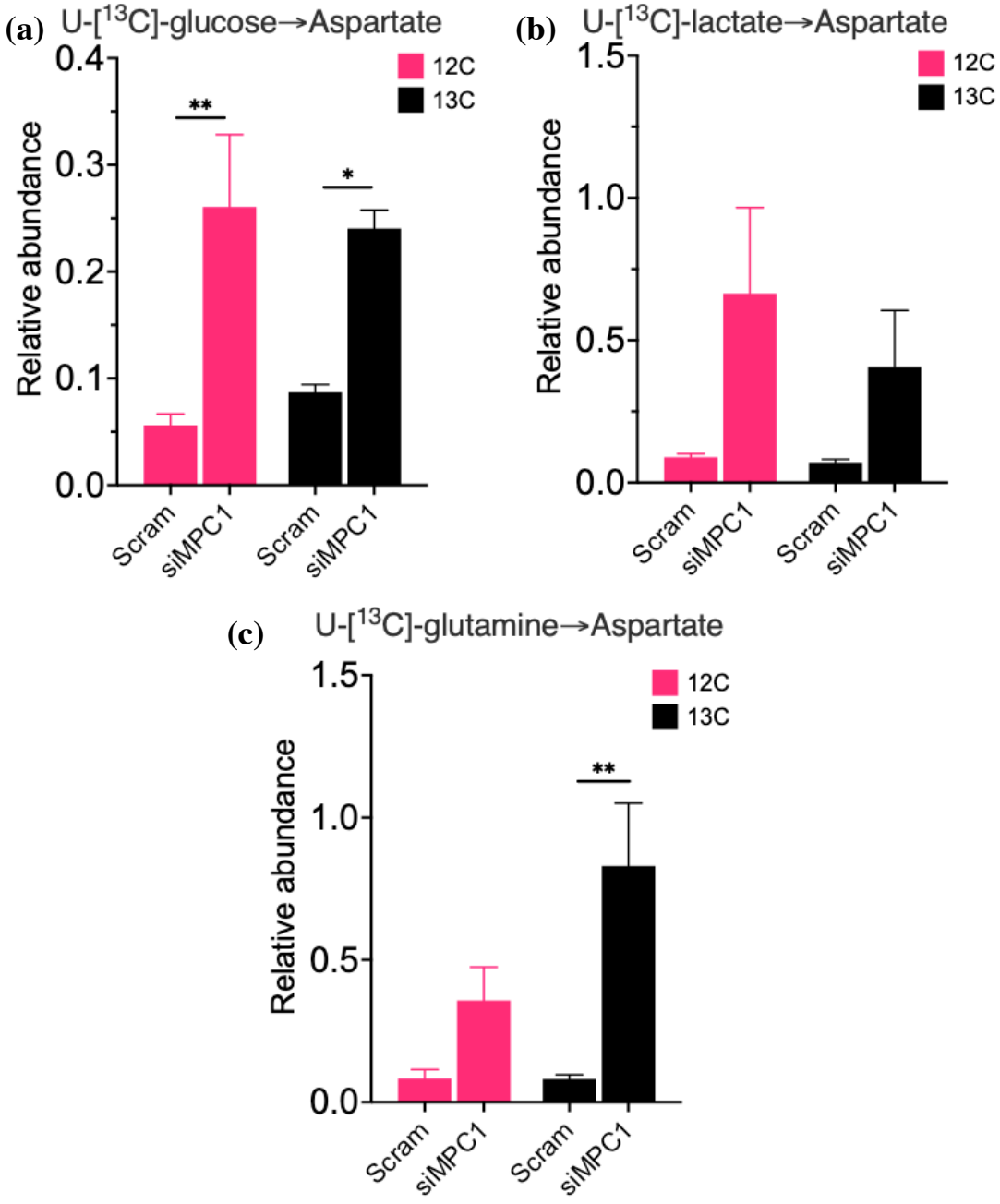

Figure 5.7 Contribution of ^{13}C-glucose, ^{13}C-glutamine, and ^{13}C-Lactate to aspartate.

(a) aspartate derived from labelled glucose, (b) aspartate derived from labelled lactate, (c) aspartate derived from labelled glutamine in OVCAR3 cells. Statistical significance was evaluated using two-way ANOVA with Sidak's multiple comparison test. Data were obtained from n = 4 independent biological replicates for each experiment. Data expressed as mean ± SEM; * $p \leq 0.05$, ** $p \leq 0.01$, *** $p \leq 0.001$

The enzymes cytosolic glutamic-oxaloacetic transaminase 1 (GOT1) and mitochondrial glutamic-oxaloacetic transaminase 2 (GOT2) facilitates the conversion of OAA to aspartate. These enzymes play an important role in linking glycolysis and OXPHOS to bring in NADH for the ETC via malate-aspartate shuttle. Moreover, the ETC also maintains the aspartate levels by importing aspartate via SLC1A3 transporter into the mitochondria. In this case, cells increase the expression of mitochondrial GOT2 to utilise certain proportion of aspartate for OAA to feed TCA cycle. The SITA data showed a significant proportion of aspartate (m+4) was derived from the oxidative metabolism of glutamine with a smaller proportion derived from reductive carboxylation (m+3) (figure 5.8c). As previously observed by Birsoy et al., 2015, glucose contributed to m+1, m+2, m+3 and m+4 of aspartate via oxidative phosphorylation (figure 5.8a) and lactate contributed to m+2 and m+3 of aspartate (figure 5.8b) (Birsoy et al., 2015b). The generation of m+4 and m+2 aspartate could also be contributing to generate citrate to replenish the TCA cycle via mitochondrial GOT2. The increased aspartate pool was observed to be derived from exogenous glucose lactate or glutamine. I measured *GOT1* and *GOT2* expression in MPC1 depleted cells. There were no significant differences seen in *GOT1/2* expression upon *MPC1* depletion. However, regardless of the presence of *MPC1*, OVCAR3 cells showed a significant increase in mitochondrial *GOT2* expression compared to cytosolic *GOT1* (figure 5.8d). These observations are consistent with previous studies in mouse retina and myeloma cells suggesting loss of MPC complex contributes to increased endogenous aspartate (Du et al., 2013; Vacanti et al., 2014b).

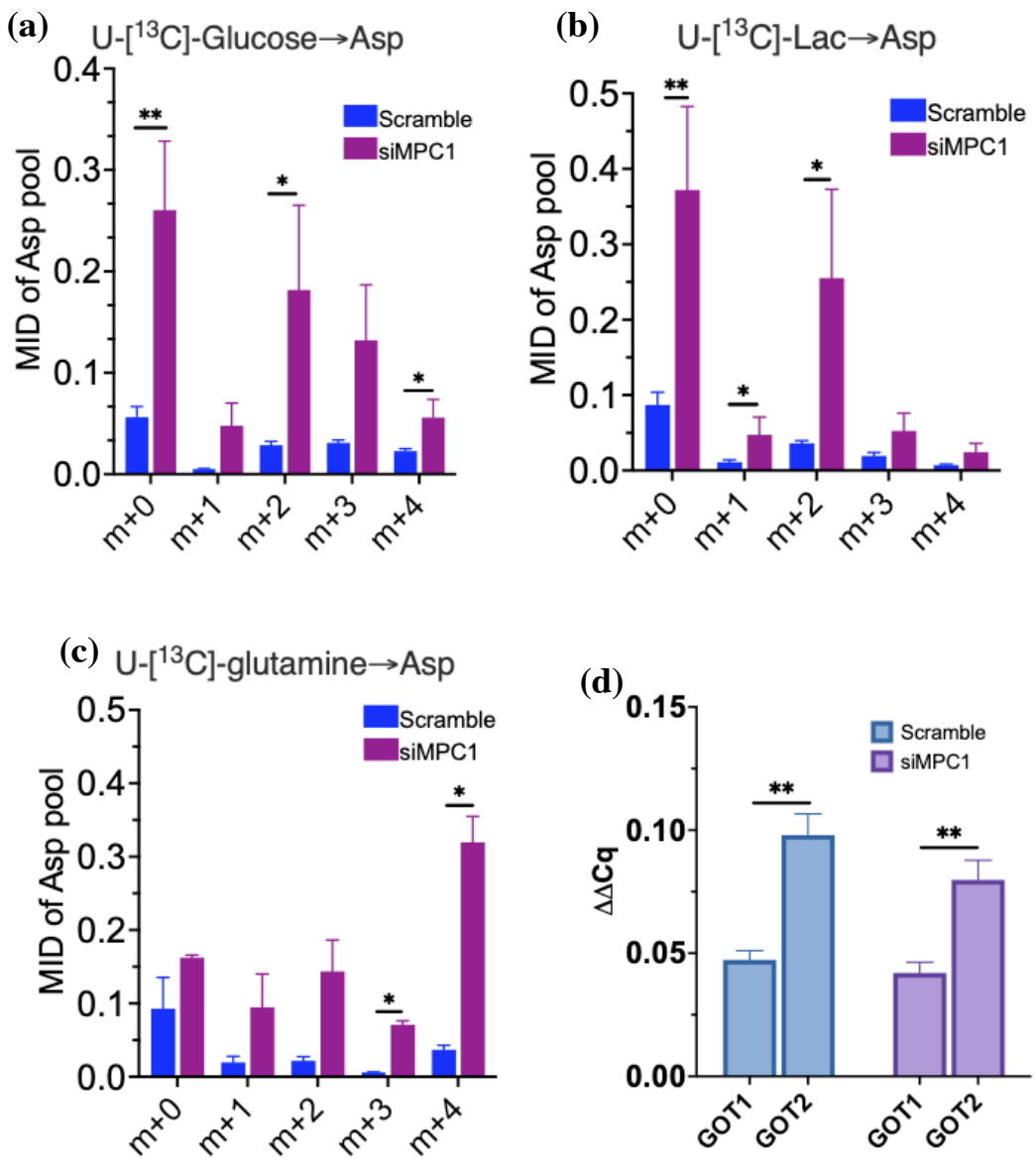

Figure 5.8 The MID of aspartate and expression of aspartate synthesising enzymes.

The MID of aspartate from (a) glucose, (b) lactate or (c) glutamine; (d) the expression of Aspartate aminotransferase 1 (aka glutamic-oxaloacetic transaminase 1; *GOT1*) or aspartate aminotransferase 2 (aka glutamic-oxaloacetic transaminase 2; *GOT2*), two enzymes involved in aspartate biosynthesis. Statistical significance was evaluated using two-way ANOVA with Sidak's multiple comparison test. Data were obtained from n=4 independent biological replicates for each experiment. Data expressed as mean + SEM; * $p \leq 0.05$, ** $p \leq 0.01$, *** $p \leq 0.001$

5.1.12 Serine and glycine levels are altered upon *MPC1* depletion.

The intermediates of one-carbon metabolism, including serine and glycine, generate essential precursors for proteins, nucleotides and lipid biosynthesis (Locasale, 2013). Here, the data from ^{13}C isotope labelling shows the accumulation of serine and glycine in *MPC1* depleted OVCAR3 cells predominantly derived from [U-$^{13}C_6$]-glucose (figure 5.9a and 5.9b) and not from [U-$^{13}C_5$]-glutamine (figure 5.9c and 5.9d). Glucose metabolism contributes ~50% of the intracellular pool of serine and [U-$^{13}C_6$]-glucose could be traced through to glycine (figure 5.9b). Furthermore, *MPC1* deletion in OVCAR3 cells resulted in a significant increase in endogenous serine and glycine (figure 5.9).

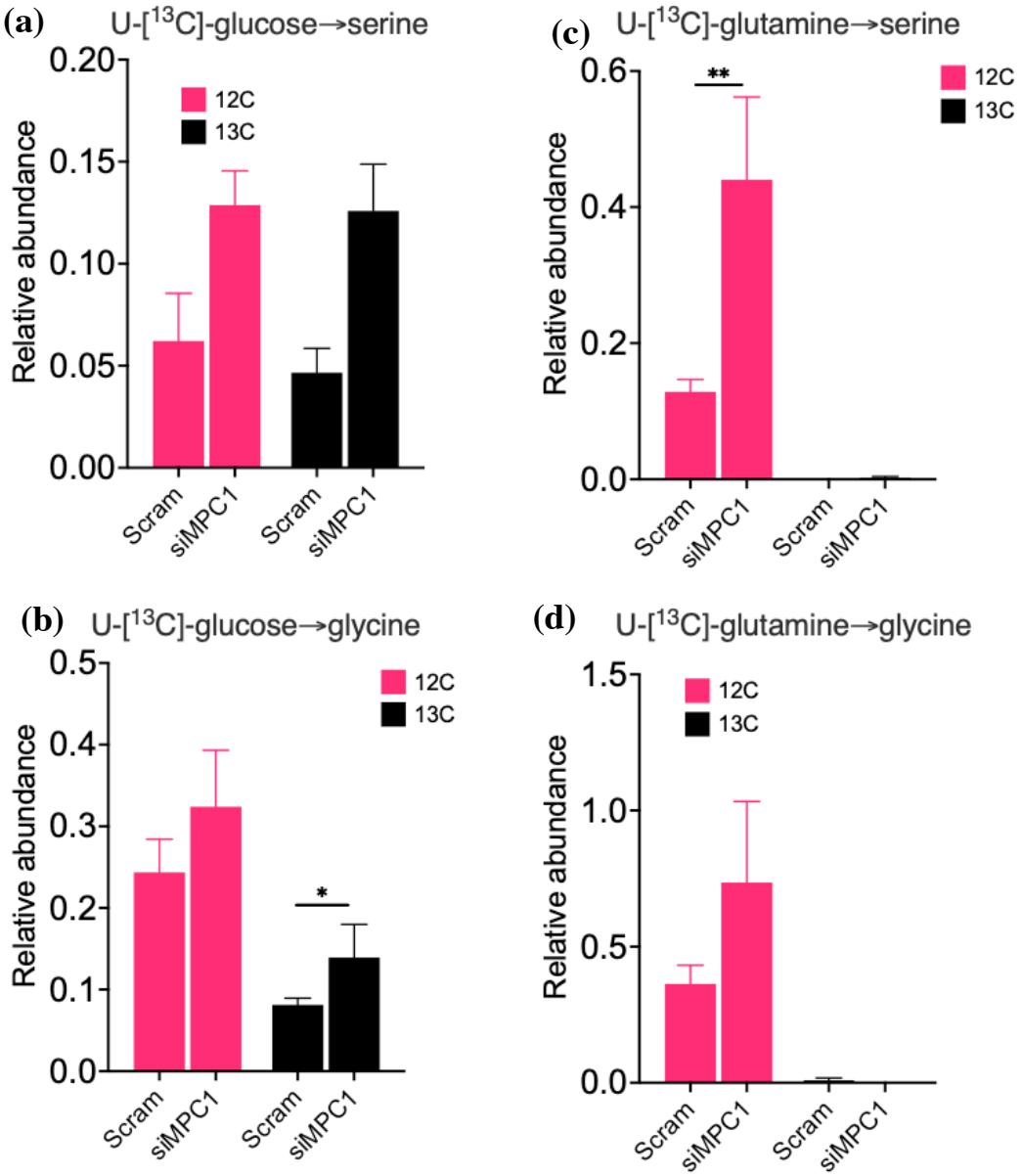

Figure 5.9 Contribution of ^{13}C-glucose or ^{13}C-glutamine to serine and glycine. (a) serine derived from labelled (black bars) or unlabelled (pink bars) glucose, (b) glycine derived from labelled or unlabelled glucose, (c) serine derived from labelled or unlabelled glutamine or glycine derived from labelled or unlabelled glutamine in OVCAR3 cells. Statistical significance was evaluated using two-way ANOVA with Sidak's multiple comparison test. Data were obtained from n=4 independent biological replicates for each experiment. Data expressed as mean + SEM; * $p \leq 0.05$, ** $p \leq 0.01$, *** $p \leq 0.001$

The serine biosynthetic pathway diverges from glycolysis, initially through the oxidation of glycolysis-derived 3-phosphoglycerate (3-PGA) via phosphoglycerate dehydrogenase (PHGDH), followed by steps involving phosphoserine aminotransferase 1 (PSAT1) and phosphoserine phosphatase (PSPH) (Phang et al., 2012). The serine biosynthesis pathway is essential in breast cancer, contributing 50% of glutamine anaplerotic flux into the TCA cycle in high *PHGDH* expressing breast cancer cells (Possemato et al., 2011b). Here, whilst *PHGDH* remained unchanged (figure 5.10a), depletion of *MPC1* reduced *PSAT1* and *PSPH* gene expression (figures 5.10b and 5.10c). Activation of the serine biosynthesis pathway, mediated by MYC, is essential for cancer progression under nutrient restricted conditions (Sun et al., 2015), and *MPC1* expression in colorectal adenocarcinomas is negatively correlated with *MYC* (Schell et al., 2014a). However, gene expression data for *MYC* showed a ~50% reduction of expression in *MPC1*-depleted cells (figure 5.10d). Taken together, this data is consistent with previous studies in cancer, where glucose-derived carbon is shown to be diverted into *de novo* serine biosynthesis, potentially contributing to the generation of α-KG from glutamate (DeNicola et al., 2015; Li and Ye, 2020; Locasale et al., 2011). However, in *MPC1* depleted ovarian cancer cells, this seems to be independent of the *MYC* oncogene.

The *de novo* synthesis of serine is also required for collagen synthesis (Nigdelioglu et al., 2016). Collagen production has been shown to play an essential role in chemotherapy resistance in ovarian cancers (Choi et al., 2006).

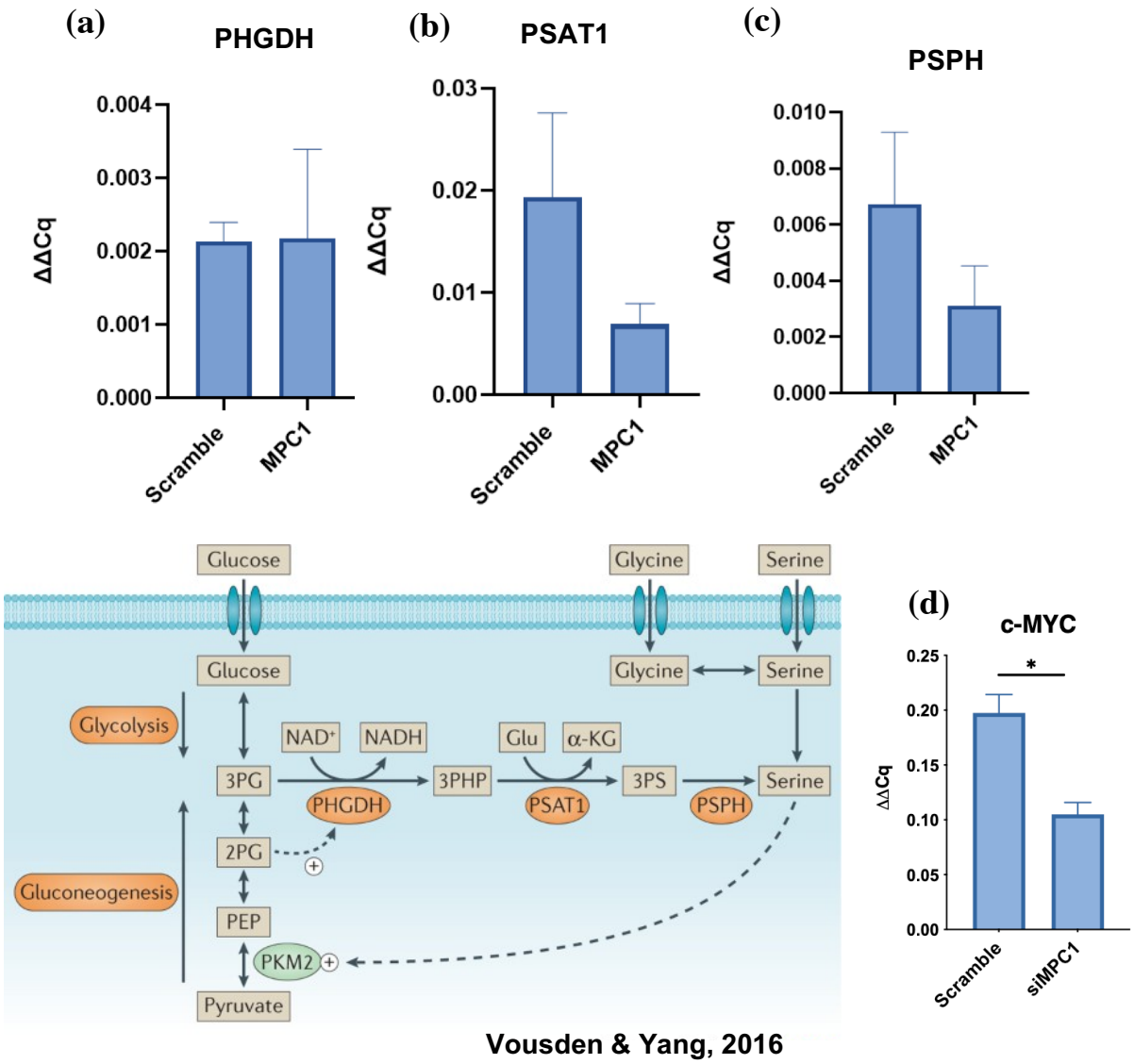

Figure 5.10 Genes involved in the serine biosynthesis pathway are altered upon *MPC1* depletion.

Gene expression data of (a) phosphoglycerate dehydrogenase (*PSPH*), (b) phosphoserine aminotransferase 1 (*PSAT1*), (c) phosphoserine phosphatase (*PSPH*) or (d) expression of *MYC* gene in *MPC1* knockdown cells. The data (a), (b) and (c) were generated by an MSci student Zack Croxford mentored by me. Statistical significance was evaluated using one-way ANOVA with Dunnett's multiple comparison test. Data were obtained from n = 3 independent biological replicates for each experiment. Data expressed as mean + SEM; * $p \leq 0.05$, ** $p \leq 0.01$, *** $p \leq 0.001$.

5.1.13 Proline may play an important role in *MPC1* depleted ovarian cancer cells.

Proline is an NEAA required for protein biosynthesis (Liang et al., 2013) and is also particularly important in the production of collagen for ECM. Moreover, increased proline metabolism is one of the most important metabolic changes in an anoikis-independent subpopulation of OVCAR3 cells (Vermeersch et al., 2015). The GC-MS data shows increased proline levels in *MPC1*-depleted cells (figure 5.10) compared to the scramble control. Proline can be synthesized from glutamate or ornithine depending on the metabolic substrate necessity (D'Aniello et al., 2020; Elia et al., 2017a; Loayza-Puch et al., 2016b). Interestingly, metabolite tracing of [U-$^{13}C_6$]-glucose, [U-$^{13}C_3$]-lactate or [U-$^{13}C_5$]-glutamine showed relatively little or no carbon contribution to proline synthesis (figure 5.11a, 5.11b and 5.11c). Furthermore, measuring ornithine aminotransferase (*OAT*) gene expression to look at the activity of ornithine metabolism, *MPC1* depletion in OVCAR3 cells showed no change in *OAT* (figure 5.11d).

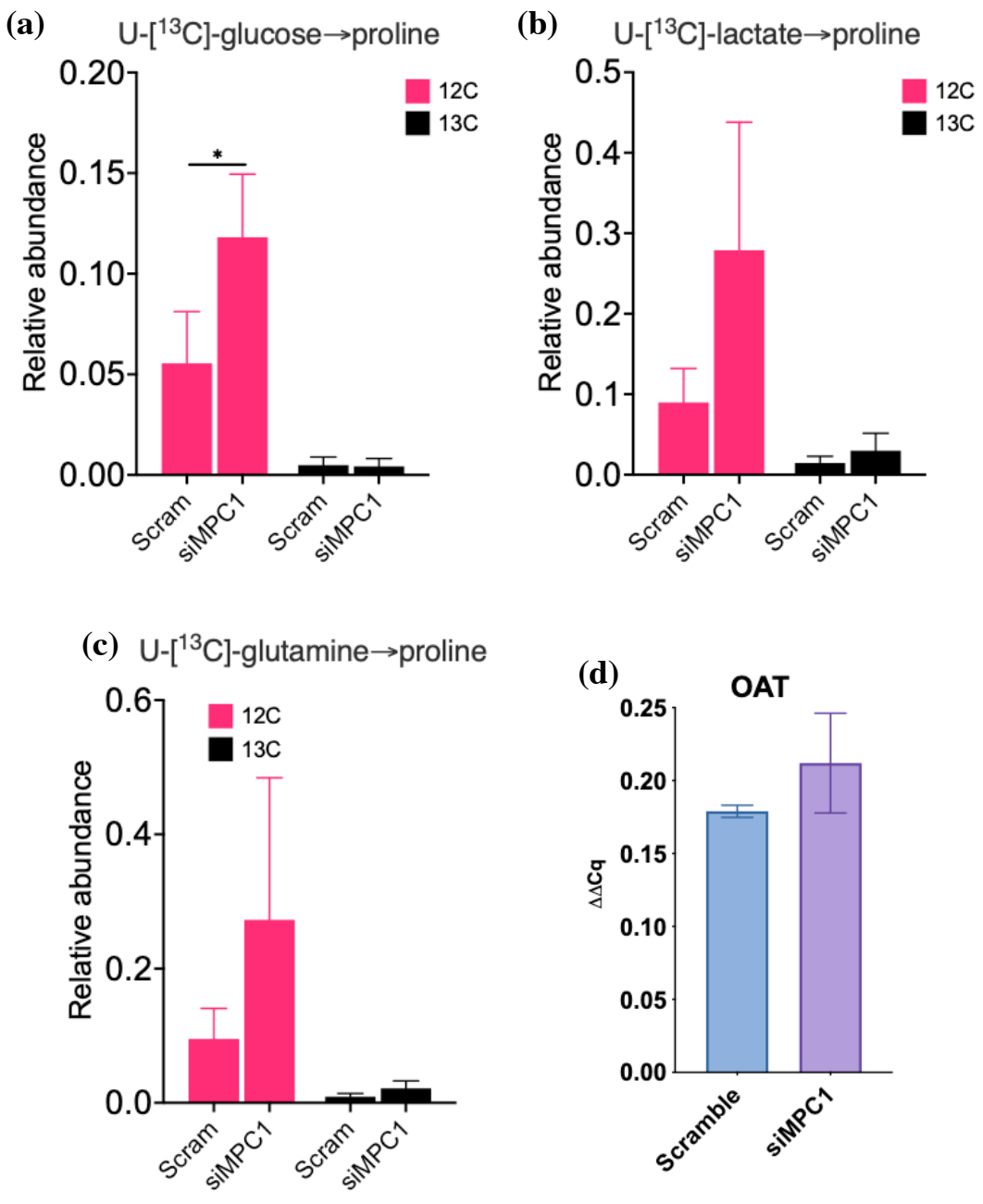

Figure 5.11 Contribution of ^{13}C-glucose, ^{13}C-Lactate, or ^{13}C-glutamine to proline biosynthesis.

(a) Proline derived from labelled (black bars) or unlabelled (pink bars) glucose, (b) proline derived from labelled or unlabelled lactate, (c) proline derived from labelled or unlabelled glutamine in OVCAR3 cells and (d) the gene expression of ornithine aminotransferase (*OAT*). Statistical significance was evaluated using two-way ANOVA with Sidak's multiple comparison test. Data were obtained from n=4 of (a), (b) and (c) while n = 3 of (d). independent biological replicates for each experiment. Data expressed as mean ± SEM; * $p \leq 0.05$, ** $p \leq 0.01$, *** $p \leq 0.001$

5.1.14 Glutamine deprivation in MPC1 lacking cells is rescued by proline.

Proline has been shown to contribute to amino acid anaplerosis in cancer, and the proline biosynthesis pathway is shown to play key roles in tumour progression involving purine, pyrimidine and protein biosynthesis, supporting cell division (Phang, 2019) and, more importantly, for cellular energy production and redox balance (Hollinshead et al., 2018b). To understand the role of proline as an anaplerotic substrate, the OVCAR3 cells were cultured with MPC inhibitor, UK-5099. The OVCAR3 cells under glutamine deprivation showed reduced DNA concentration while supplementing 2 mM proline rescued the cells with a significant increase in DNA (figure 5.12a). No changes were seen in the control whether the glutamine was depleted or the proline was supplemented in the media, suggesting a role for proline in MPC1 lacking cells when glutamine supply is limited. Moreover, supplementing exogenous proline to *MPC1*-depleted OVCAR3 cells in Matrigel resulted in cell aggregation under glutamine deprived conditions compared to the Scramble control (figure 5.12b). An increase in cell number was seen in *MPC1*-depleted OVCAR3 cells, but the presence of glutamine did not result in agglomeration of the cell on Matrigel (figure 5.12b). These data, together with proline accumulation under *MPC1* depletion in ovarian cancer cells, suggest an important role for proline in ECM biosynthesis.

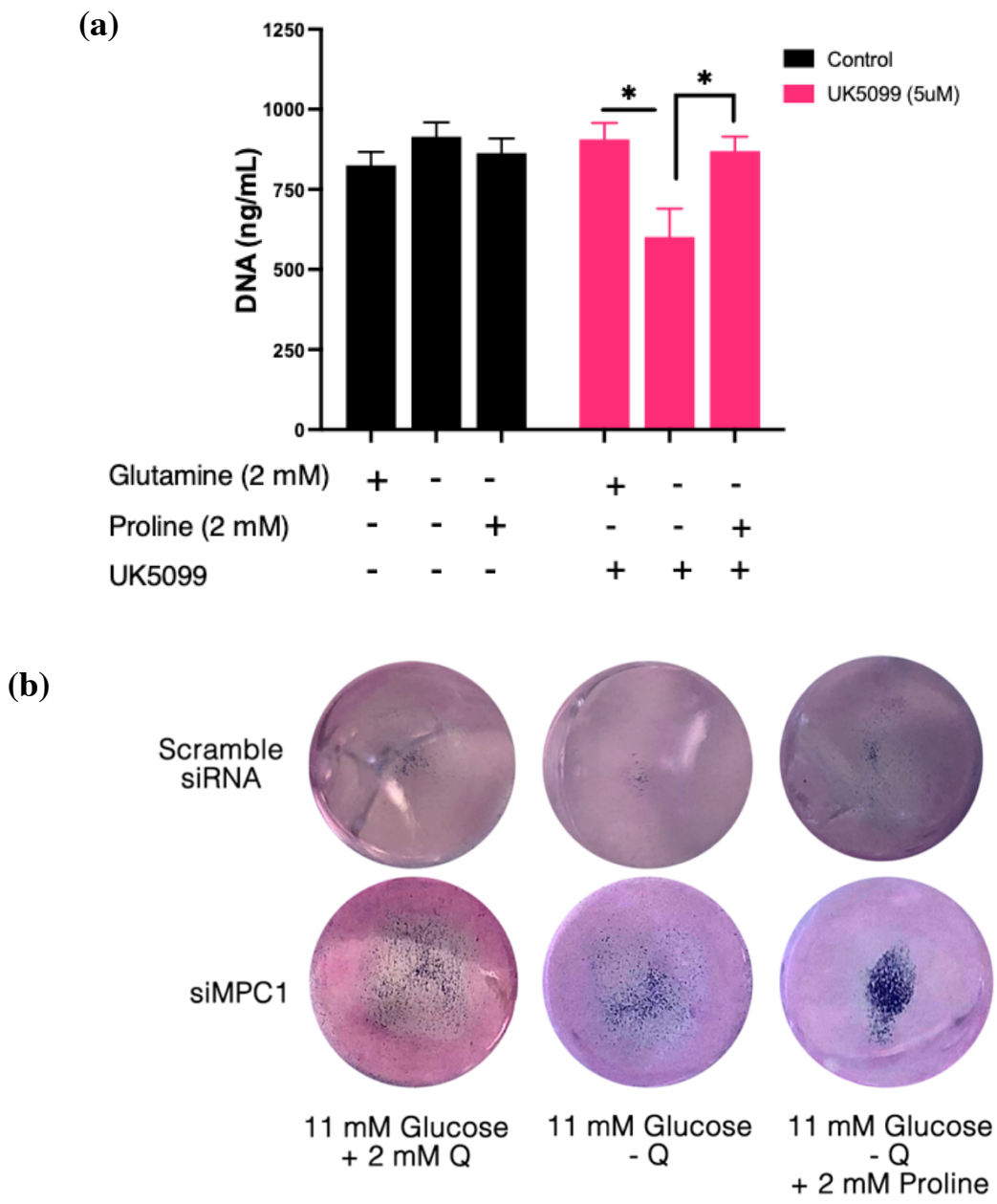

Figure 5.12 Supplementing proline to pharmacologically and genetically blocked MPC1 of OVCAR3 cells.
(a) OVCAR3 cells MPC1 pharmacologically inhibited using UK-5099 and (b) MPC1 knockdown cells (dark blue, stained using crystal violet) seeded onto a collagen-coated trans-well. Both cells were supplemented with 2 mM proline and 2 mM glutamine. Statistical significance was evaluated using two-way ANOVA with Sidak's multiple comparison test. Data was obtained from (a) n = 3 independent biological replicates for each experiment and (b) n = 1. Data expressed as mean ± SEM; * $p \leq 0.05$, ** $p \leq 0.01$, *** $p \leq 0.001$.

5.1.15 Proline biosynthesis pathway enzyme expressions were elevated upon *MPC1* depletion.

Next, I looked into the biosynthetic pathway of proline by measuring the expression of enzymes critical to the pathway. The *de novo* biosynthesis of proline occurs via pyrroline-5-carboxylate synthetase ((P5C)S) (also known as ALDH18A1) conversion of glutamate to pyrroline-5-carboxylate (P5C), mitochondrial PYCR1 or mitochondrial/cytosolic PYCR2, then convert P5C to proline. Alternatively, ornithine-derived P5C can also be metabolised to proline via a cytosolic PYCR3 isoenzyme (also known as *PYCRL*) (Adams and Frank, 1980b; Phang et al., 2015).

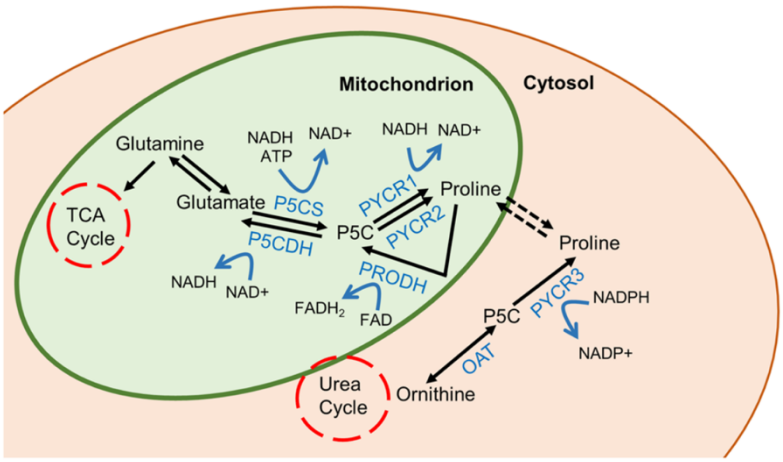

(Burke et al., 2020)

Interestingly, *MPC1* depletion in OVCAR3 cells showed a significant increase in expression of all *PYCR* isoenzymes (figure 5.13a, 5.13b, 5.13c). Furthermore, while no change in *P5C* expression was seen in *MPC1*-depleted OVCAR3 cells, the expression of (P5C)DH was relatively increased. The pyrroline-5-carboxylate dehydrogenase ((P5C)DH) (also known as *ALDH4A1*) irreversibly generates glutamate from the degradation of excess proline or ornithine to glutamate, a crucial step in interlinking the urea cycle and TCA cycle, for generating TCA cycle intermediates (Tanner et al., 2018). Mitochondrial and cytosolic oscillation of proline metabolism via *PYCR* enzymes not only produces precursors for protein biosynthesis but also leads to the maintenance of redox homeostasis. Moreover, variation in *PYCR1*, *PYCR2* and *PYCR3* upon *MPC1*-depletion gave me an interest to further look into their roles in cancer cells. Therefore, I knocked down *PYCR* isoenzymes in OVCAR3 cells to further assess their effect on ovarian cancer cell metabolism.

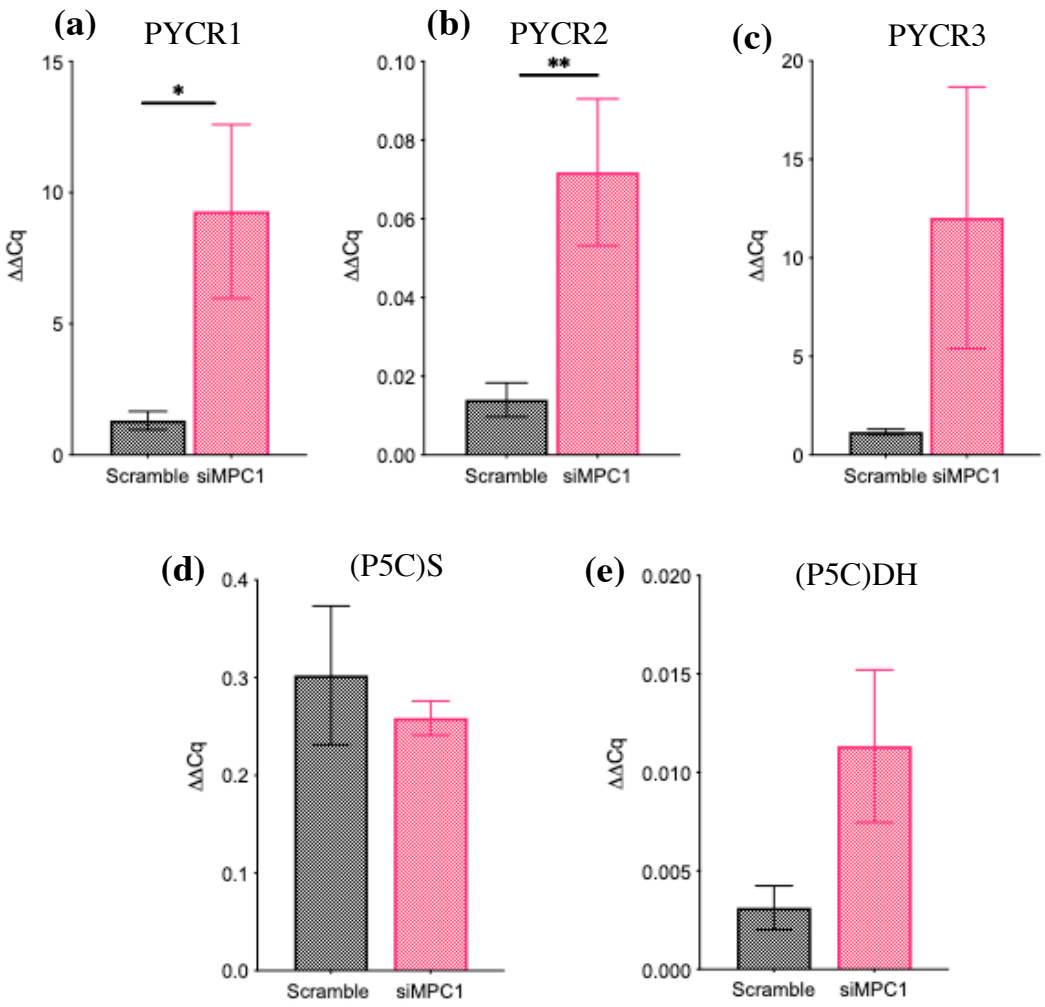

Figure 5.13 Enzymes involved in the proline biosynthesis pathway.
Real-time qPCR data showing the expression of (a) mitochondrial enzyme pyrroline-5-carboxylate reductase 1; *PYCR1*, (b) mitochondrial or cytosolic enzyme pyrroline-5-carboxylate reductase 2; *PYCR2*, (c) cytosolic pyrroline-5-carboxylate reductase 3 or L; *PYCR3*, (d) mitochondrial pyrroline-5-carboxylate synthase; (P5CS) and (e) mitochondrial pyrroline-5-carboxylate dehydrogenase; (P5CDH). Data are representative of n=3 for (a), (b) and (c) while n=4 for (c) and (d). Data set is achieved from independent biological replicates for each experiment. Data expressed as mean ± SEM; * $p \leq 0.05$, ** $p \leq 0.01$, *** $p \leq 0.001$.

5.1.16 Proline biosynthesis is essential for tumour growth and nucleotide synthesis.

To investigate the role of PYCR isoenzymes in ovarian cancer, all three isozymes *PYCR1, PYCR2* and *PYCR3,* were depleted on their own or in combination with *MPC1* in OVCAR3 cells. The knockdown efficiency at transcriptional levels showed over 80% achievement in gene silencing (figures 5.14a, 5.14b, 5.14c). Using *PYCR* depleted cells, I looked at the capability of OVCAR3 cells to form colonies. The ability of single-cell proliferation to form a colony is a crucial mechanism of proliferating cells and for metastases (Franken et al., 2006). Clonogenic assays *in vitro* have been carried out for decades to study the behaviour of cancer cells following therapeutic treatments treatment.

The *PYCR1* isoenzyme, one of the most overexpressed metabolic genes in cancer, is critical for the growth of breast tumours and its depletion is associated with diminished cell proliferation and reduced tumour growth (D'Aniello et al., 2020; Hollinshead et al., 2018b; Loayza-Puch et al., 2016b). Similarly, *PYCR1* knockout in hepatocellular carcinoma resulted in impaired tumour growth *in vivo* (Loayza-Puch et al., 2016b) and reduced growth of non-small cell carcinoma cells (Cai et al., 2018a); Converse to their data, *PYCR1* knockdown in *MPC1* expressing OVCAR3 cells did not affect the colony formation or growth (figure 5.15c), while OVCAR3 cells with combined knockdown of *MPC1 + PYCR1* resulted in reduced colony formation compared to the control (figure 5.15f). The depletion of the *PYCR2* isoenzyme, involved in the generation of mitochondrial proline from glutamate via P5C or cytosolic proline via ornithine or the depletion of the *PYCR3* isoenzyme involved in the generation of cytosolic proline via ornithine resulted in reduced OVCAR3 colony formation (figures 5.15d and 5.15e). Moreover, the combination of *siMPC1 + siPYCR2* resulted in the further reduction of colony formation compared to *siMPC1 + siPYCR3*. The *PYCR1* and *PYCR2* isoenzymes have been shown to be involved in DNA replication and repair via binding to ribonucleotide-diphosphate reductase M2B (RRM2B) (Kuo et al., 2016a). However, the role of *PYCR3* other than its role in cytosolic proline synthesis has not been extensively studied in cancer. Since *PYCR3* knockdown remarkably reduced cell growth, we further investigated the genetic dysregulation of PYCRs, mining archived patient CNV data from The Cancer Genome Atlas (TCGA). Interestingly, TCGA

mRNA data showed *PYCR2* mutation frequency was high in epithelial ovarian cancer (4th highest of all cancers profiled), whilst alteration of *PYCR3* in epithelial ovarian cancer was the highest of all cancer types profiled.

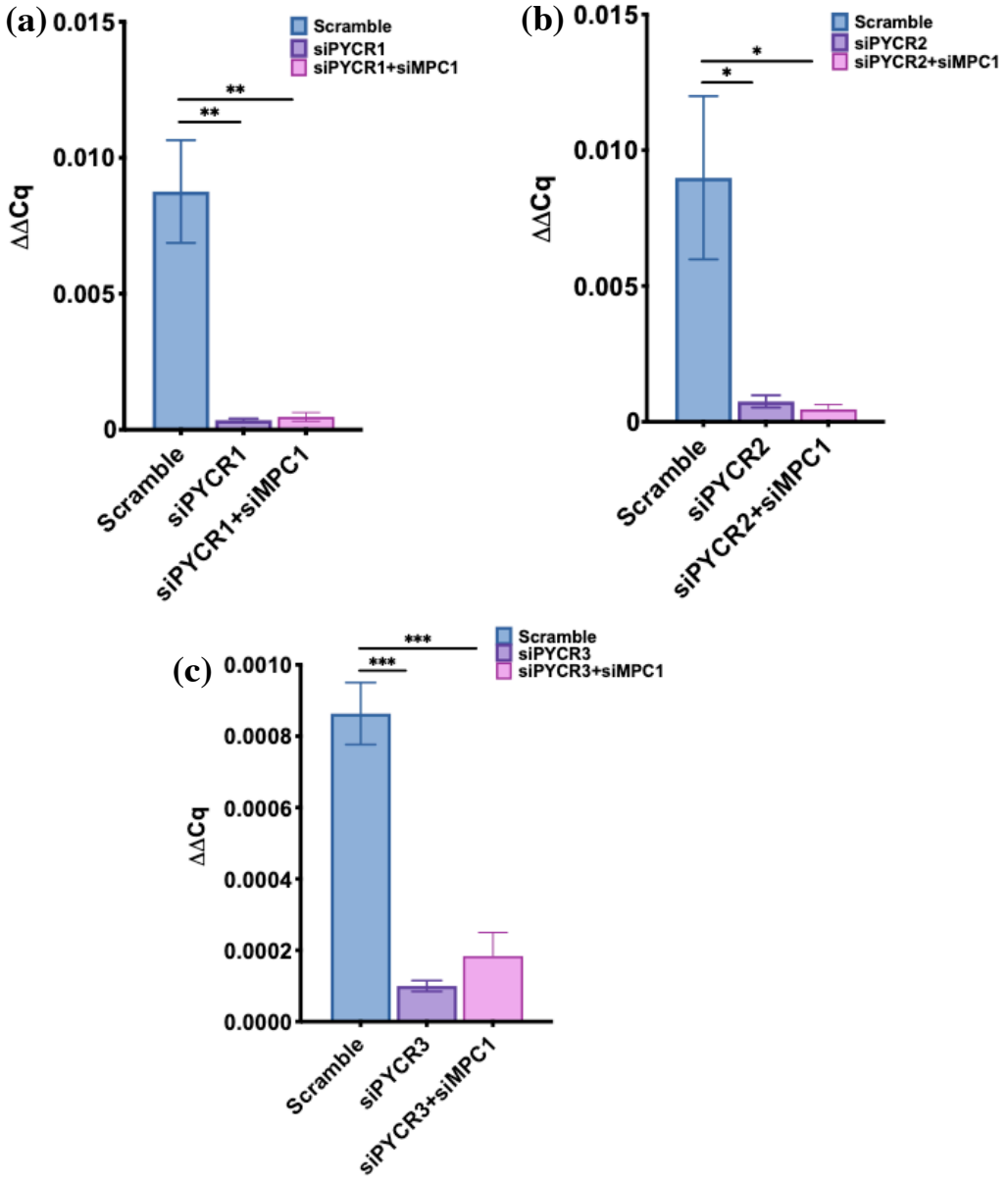

Figure 5.14 Validating gene knockdown of *PYCR* isoenzymes combined with *siMPC1* for growth study.
Real-time qPCR data showing the expression of (a) mitochondrial enzyme pyrroline-5-carboxylate reductase 1; *PYCR1*, (b) mitochondrial or cytosolic enzyme pyrroline-5-carboxylate reductase 2; *PYCR2*, or (c) cytosolic pyrroline-5-carboxylate reductase 3 or L; *PYCR3*. Statistical significance was evaluated using one-way ANOVA with Dunnett's multiple comparison test. Data were obtained from n=3 independent biological replicates for each experiment. Data expressed as mean ± SEM; * $p \leq 0.05$, ** $p \leq 0.01$, *** $p \leq 0.001$

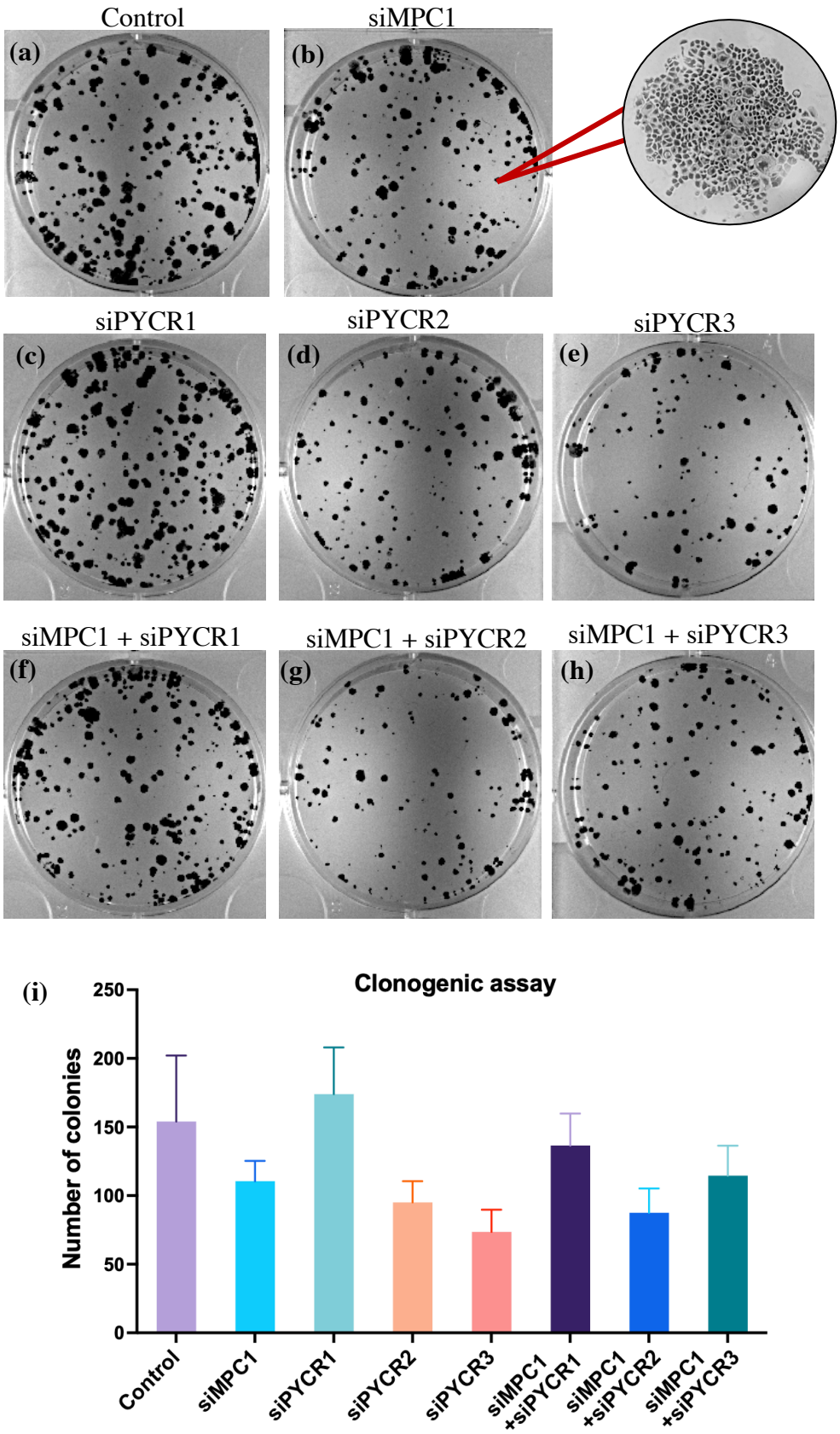

Figure 5.15 Colony formation of cells following gene knockdown of PYCR isoenzymes individually or combined with *siMPC1*.

Figures (a), (b), (c), (d), (e), (f), (g) and (h) display the colony formation by OVCAR3 cells after 14 days following siRNA. (i) shows the graph representing the colonies counted under a compound microscope. Colonies were counted manually using a clicker counter, considering ten cells or more is a colony (Franken et al., 2006). Data is obtained from n=2 independent biological replicates for each experiment.

a.

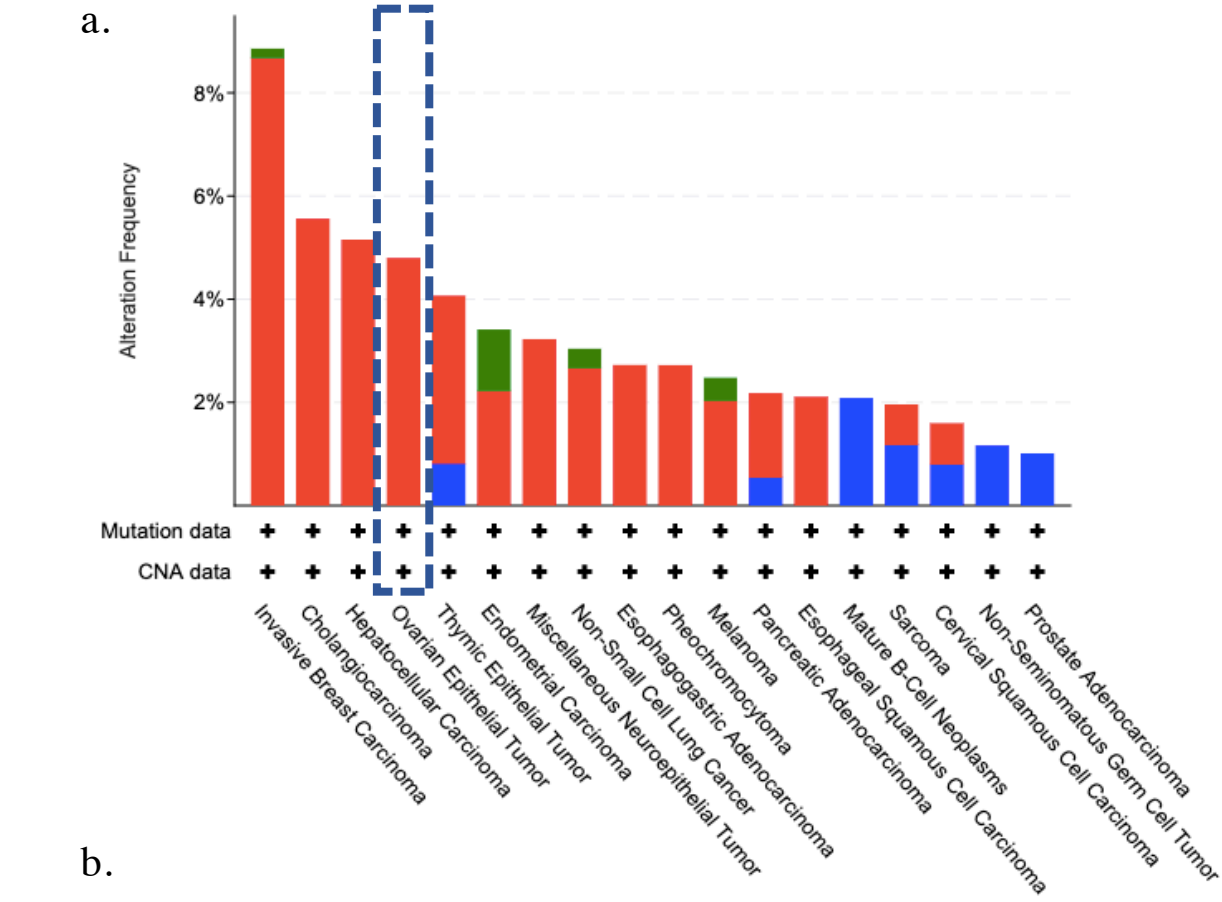
Alteration Frequency
8%
6%
4%
2%
Mutation data
CNA data
Invasive Breast Carcinoma
Cholangiocarcinoma
Hepatocellular Carcinoma
Ovarian Epithelial Tumor
Thymic Epithelial Tumor
Endometrial Carcinoma
Miscellaneous Neuroepithelial Tumor
Non-Small Cell Lung Cancer
Esophagogastric Adenocarcinoma
Pheochromocytoma
Melanoma
Pancreatic Adenocarcinoma
Esophageal Squamous Cell Carcinoma
Mature B-Cell Neoplasms
Sarcoma
Cervical Squamous Cell Carcinoma
Non-Seminomatous Germ Cell Tumor
Prostate Adenocarcinoma

b.

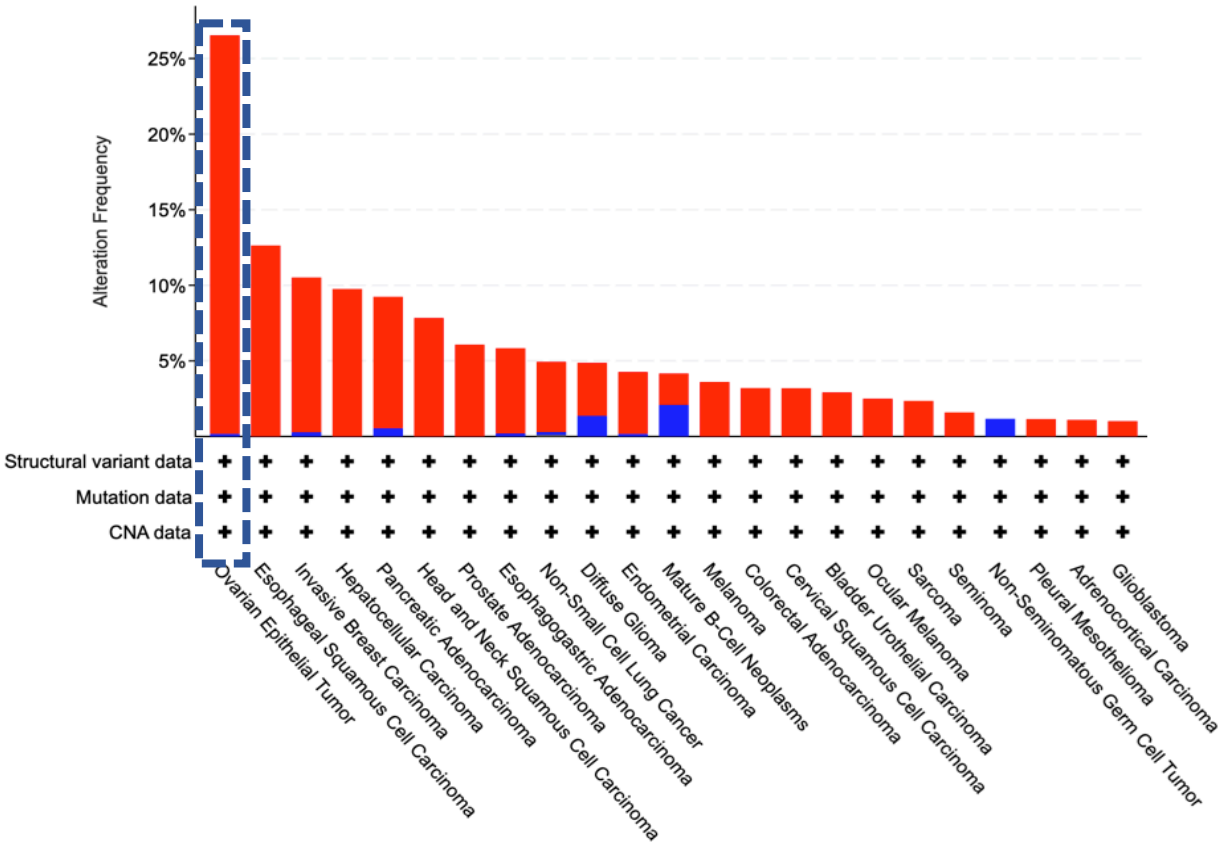
Alteration Frequency
25%
20%
15%
10%
5%
Structural variant data
Mutation data
CNA data
Ovarian Epithelial Tumor
Esophageal Squamous Cell Carcinoma
Invasive Breast Carcinoma
Hepatocellular Carcinoma
Pancreatic Adenocarcinoma
Head and Neck Squamous Cell Carcinoma
Prostate Adenocarcinoma
Esophagogastric Adenocarcinoma
Non-Small Cell Lung Cancer
Diffuse Glioma
Endometrial Carcinoma
Mature B-Cell Neoplasms
Melanoma
Colorectal Adenocarcinoma
Cervical Squamous Cell Carcinoma
Bladder Urothelial Carcinoma
Ocular Melanoma
Sarcoma
Seminoma
Non-Seminomatous Germ Cell Tumor
Pleural Mesothelioma
Adrenocortical Carcinoma
Glioblastoma

Figure 5.16 Mutation alteration frequency of PYCR2 and PYCR3 in multiple cancers.
Ovarian cancer has the 4th highest frequency of *PYCR2* (a) and highest *PYCR3* alteration (b) mutated in ovarian cancer out of all different cancer types (b). The data was generated using the cancer genome atlas (TCGA) comparing multiple patient data.

5.5 Discussion

Metabolic studies using engineered biosensors or ^{13}C-enriched substrates to monitor metabolism have shown reduced activity of MPC-dependent metabolic pathways in cancers (Compan et al., 2015a; Yang et al., 2014a). Circulating concentrations of aspartate are amongst the lowest of all the circulating amino acids. Aspartate synthesis is dependent on the electron transport chain and is an endogenous metabolic limitation in cancer cell proliferation and tumour growth (Birsoy et al., 2015a; Garcia-Bermudez et al., 2018; Sullivan et al., 2018). Here, in metabolic tracing studies, depletion of *MPC1* resulted in a 6-fold increase in endogenous aspartate and a decrease in alanine abundance, with the majority of enriched aspartate derived from ^{13}C-glutamine via the TCA cycle. Previous studies have reported increased aspartate and reduced alanine abundancies in mouse myoblasts, although this was in response to depletion of *Mpc2*, not *Mpc1* (Vacanti et al., 2014a). Furthermore, our results demonstrated no change in expression of aspartate aminotransferases in *MPC1* depleted ovarian cancer cells, in contrast to other studies showing increased aspartate dependency on oxaloacetate and GOT2 (Birsoy et al., 2015a; Yang et al., 2018).

The loss of *MPC1* resulted in *MYC* expression being reduced by half in ovarian cancer cells. The low concentrations of proline in the TME are often inadequate for maintaining high levels of protein synthesis required for highly proliferating cancer cells (Loayza-Puch and Agami, 2016b; Loayza-Puch et al., 2016a). The protooncogene *MYC* also has a role in proline metabolism, resulting in downregulation of *PRODH1* via increased expression of Mir-23b, and increased expression of *ALDH18A1* and *PYCR1* genes (Liu et al., 2012b). Human mitochondrial PYCR isoenzymes are upregulated in various cancer types, with PYCR1 reportedly being the most overexpressed metabolic enzyme, driving metastasis and tumour growth (Burke et al., 2020). Here, we demonstrate depletion of *MPC1* results in upregulation of *PYCR1*, *PYCR2* and *PYCR3* genes. In addition to reduced *MYC* expression, we showed no change in *ALDH18A1* expression in *MPC1*-depleted cells. Moreover, ^{13}C-enriched glutamine was not traced through to the increased intracellular proline observed in *MPC1* depleted ovarian cancer cells, suggesting PYCR3, the cytosolic isoform that exclusively utilises ornithine rather than glutamine for proline synthesis, may play a significant role (Nazemi and Rainero, 2020; Tanner et al., 2018). Therefore, unlike in

other cancers, where increased *PYCR1* gene expression and proline anabolism from glutamine are observed, *MPC1*-depleted ovarian cancers do not appear to be dependent on *MYC*-stimulated mitochondrial proline biosynthesis, but potentially cytosolic proline anabolism from ornithine, which remains to be explored.

Here, I demonstrated *PYCR1* depletion did not reduce colony formation in ovarian cancer cells, but lack of *PYCR2* or *PYCR3* resulted in reduced colony formation. Yet, as depletion of *MPC1* may result in a pseudo hypoxic state (increased cytosolic ratio of free NAD to NADH) for cancer cells due to reduced ETC activity, increased PYCR1 may permit the TCA cycle to progress instead of oxygen consumption and result in dissipation of electron build-up, via oxidation of NADH to NAD^+ (Hollinshead et al., 2018a), potentially explaining the observed increase in *PYCR1* upon depletion of *MPC1*. Moreover, Depletion of *PYCR1* or *PYCR2* reduces the activated mammalian target of rapamycin (mTOR) kinase via activation of AMPK kinase in cancer cells (Burke et al., 2020). Although less explored than PYCR1, previous studies employing metabolomic profiling identifies PYCR2 as the most significantly altered protein involved in amino acid metabolism in hepatocellular and oesophageal squamous cell carcinomas (Sun et al., 2019; Tang et al., 2018). As for *PYCR1*, increased expression of *PYCR2* may permit cells to cope with excessive oxidative species as a consequence of increased metabolic activity, as loss of PYCR2 is demonstrated to result in apoptosis from oxidative stress (Nakayama et al., 2015). Tumours with relatively high *PYCR2* also display upregulation of pathways involved in DNA replication (Gao et al., 2019).

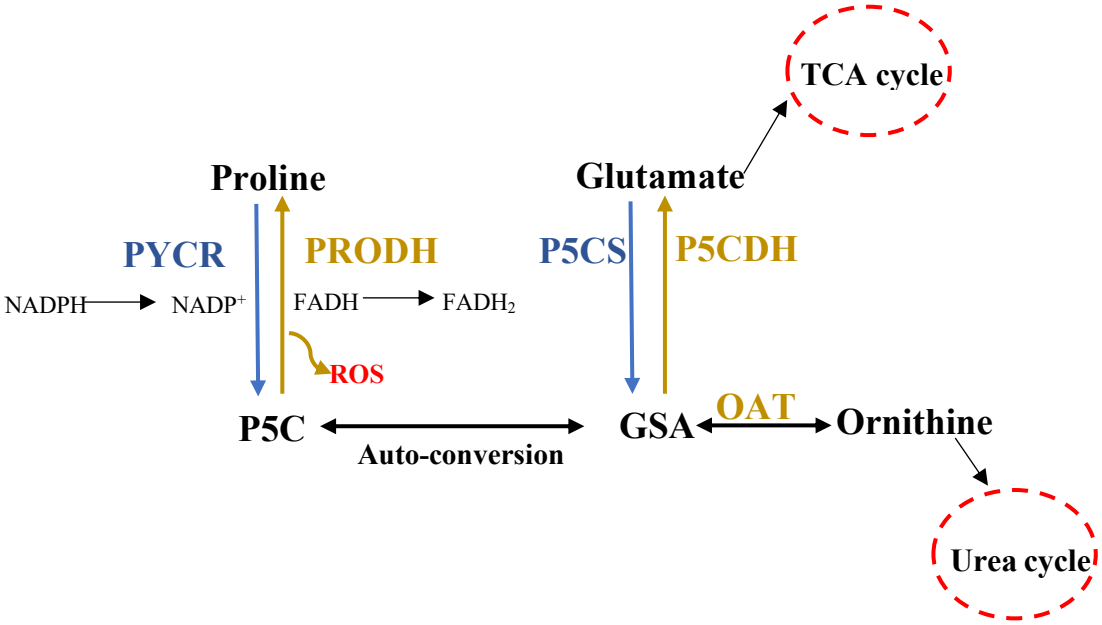

Figure 5.17 Proline biosynthesis (blue arrow) and proline catabolism (yellow arrow)

Providing exogenous proline to pharmacologically MPC inhibited cells resulted in increased concentration of DNA under glutamine deprived conditions. Moreover, *MPC1* depletion at transcriptional levels exhibited agglomeration of cells upon exogenous proline availability. Proline metabolic pathways have essential roles in collagen synthesis and ECM reprogramming (Guo et al., 2019). Increased collagen matrix formation and resultant ECM stiffening contribute to tumour development and progression (Choi et al., 2006; Levental et al., 2009). The desmoplastic subtype of HGSOC represents the poorest prognosis, highlighting the contribution of the ECM in ovarian cancer progression (Cancer Genome Atlas Research, 2011; Tothill et al., 2008). Adhesion of cancer cells to ECM enhances tumorigenicity and confers resistance to chemotherapeutic agents (Sethi et al., 1999).

The PYCR3 isoenzyme is the only cytosolic route to link proline metabolism with the urea cycle and is highly altered/mutated in epithelial ovarian cancers compared to all other cancer types profiled on The Cancer Genome Atlas. Depletion of the *PYCR3* isoenzyme greatly affected the colonization ability of single cells compared to depletion of *PYCR1*, which could be a novel therapeutic target of ovarian cancer metastasis. So far correlation between increased *PYCR3* expression and ECM

formation is poorly understood. Investigating the role of cytosolic proline mediated by PYCR3 via stable ^{15}N tracing may expose new pathways and targets for cancer therapy. In conclusion, the data generated in this chapter suggests *MPC1* depletion of OVCAR3 cells (MPC1 positive) not only repurposes amino acid metabolism for cancer cell survival but also acts as a switch between ovarian cancer cell proliferation and metastasis by employing collagen synthesizing proteins.

Chapter Six

General discussion

6 General discussion

Tumour-associated genetic alterations result in dysregulation of cancer metabolic pathways, permitting nutrient acquisition in a generally nutrient-deficient tumour microenvironment (Pavlova and Thompson, 2016). The reduced expression of MPC1 and MPC2, key orchestrators of pyruvate import into the mitochondria matrix, correlates with poor prognoses in several cancer types, including colon, lung, kidney, breast, and prostate (Li et al., 2016; Schell et al., 2014b). As the chromosomal locus for *MPC1* shows >80% loss in ovarian cancer patients, the current study investigated the role of MPC1 in ovarian cancer progression (Coscia et al., 2016a). The research conducted within this thesis aimed to provide a better understanding of key metabolic pathways in ovarian cancer progression by investigating: (a) how ovarian cancer cells regulate metabolic pathways to maintain nutrient acquisition in a nutrient-restricted tumour microenvironment; (b) metabolic substrate utilisation upon pharmacological inhibition of MPC1; or (c) inhibition of *MPC1* at the transcriptional level using siRNA to assess the effect of *MPC1*-depletion on amino acid metabolism and its contribution to ovarian cancer cell survival and metastasis. My data indicates acute loss of *MPC1* in ovarian cancer cells results in increased cell proliferation, whilst chronic depletion of *MPC1* results in increased PYCR isoenzyme expression, key enzymes involved in the proline biosynthetic pathway. Furthermore, ovarian cancer colony formation, which mimics the ability of single-cell proliferation and metastatic seeding, was dependent on the proline biosynthetic isoenzymes PYCR2 and PYCR3. According to The Cancer Genome Atlas (TCGA), a database profiling of over 10,000 cancer cases, the *PYCR3* gene is most frequently altered in ovarian cancer compared to all other tumour types profiled. Proline metabolism plays a vital role in extracellular matrix (ECM) formation and potentially in therapy-resistant cancer cells (D'Aniello et al., 2020; Sherman-Baust et al., 2003). Although, no studies have shown a correlation between loss of MPC1 and PYCR3 expression mediating cancer cell proliferation or changes in extracellular matrix (ECM).

Metabolic flexibility in ovarian cancer has been shown to drive tumour progression and resistance to chemotherapy (Cheng et al., 2018; Desbats et al., 2020; Tang et al., 2014). Glucose, the primary carbon source for proliferating cells, generates ATP

(Matulonis et al., 2016; Vincent et al., 2015). Glucose is used to generate pyruvate, which is transported into the mitochondria via the MPC1-MPC2 complex for oxidative phosphorylation (OXPHOS). Loss of MPC function increases glycolysis in cancer cells whilst initiating compensatory cellular metabolic pathways, including glutamine anaplerosis feeding the TCA cycle (Vacanti et al., 2014b). The present study was conducted on HGSOC cell lines expressing different levels of MPC. Inhibition of MPC1 resulted in a glutamine-dependent increase in cell proliferation (determined by an increase in DNA concentration) of ovarian cancer cell lines regardless of their MPC expressing levels. Moreover, MPC inhibition did not significantly affect glucose or glutamine consumption by these cell lines. However, the pyruvate produced primarily from glucose was accumulated in the supernatant of a high MPC1 expressing cell line (OVCAR3) when MPC was pharmacologically inhibited. While the TCGA analysis showed >80% copy number variance (CNV) loss of *MPC1* in ovarian cancer, about 85% of ovarian cancer patients showed CNV gain of *MPC2*, possibly indicating patient's ovarian cancer cells increased copy number of *MPC2* to compensate for the loss of *MPC1*. The expression of *MPC2* was demonstrated to be dependent on glutamine in PEO4 cells but not in OVCAR3 cells. The fate of pyruvate depends on the functional MPC complex assembled in the inner mitochondrial membrane. Interestingly, OVCAR3 cells with low MPC2 expression accumulated pyruvate, which was not evident in high MPC2 expressing PEO4 cells. Although MPC1 and MPC2 are proposed to function together as a complex (Bowman et al., 2016; Bricker et al., 2012), more recent evidence suggests MPC2 can function independently of MPC1 (Nagampalli et al., 2018), possibly suggesting PEO4 cells can adapt to the loss of MPC1 by upregulating MPC2, maintaining pyruvate import into the mitochondria, albeit at a less efficient rate.

Most of the glycolytic product pyruvate has been shown to be converted to lactate. Over 60% of ovarian cancer patients go through omental metastasis, which often leads to the build-up of ascites. Ascites is the cellular fluid containing metastasising cancer cells in multicellular aggregates (or spheroids), in addition to immune and mesothelial cells, and are shown to have an acidic environment due to being rich in lactate and lactate dehydrogenase. Increased aerobic glycolysis or the 'Warburg effect' in cancer cells was later proven to be a reversible process to utilise glycolytic by-products. This

reversed process bypasses the need for MPC and contributes to TCA cycle substrates and other essential amino acids (Faubert et al., 2013; Fu et al., 2017; Wilde et al., 2017). The observation was later known as the reverse Warburg effect. The MPC1 expressing OVCAR3 cells exhibited an increase in extracellular acidity rate upon MPC inhibition, which was not evident in PEO1 or PEO4 cells.

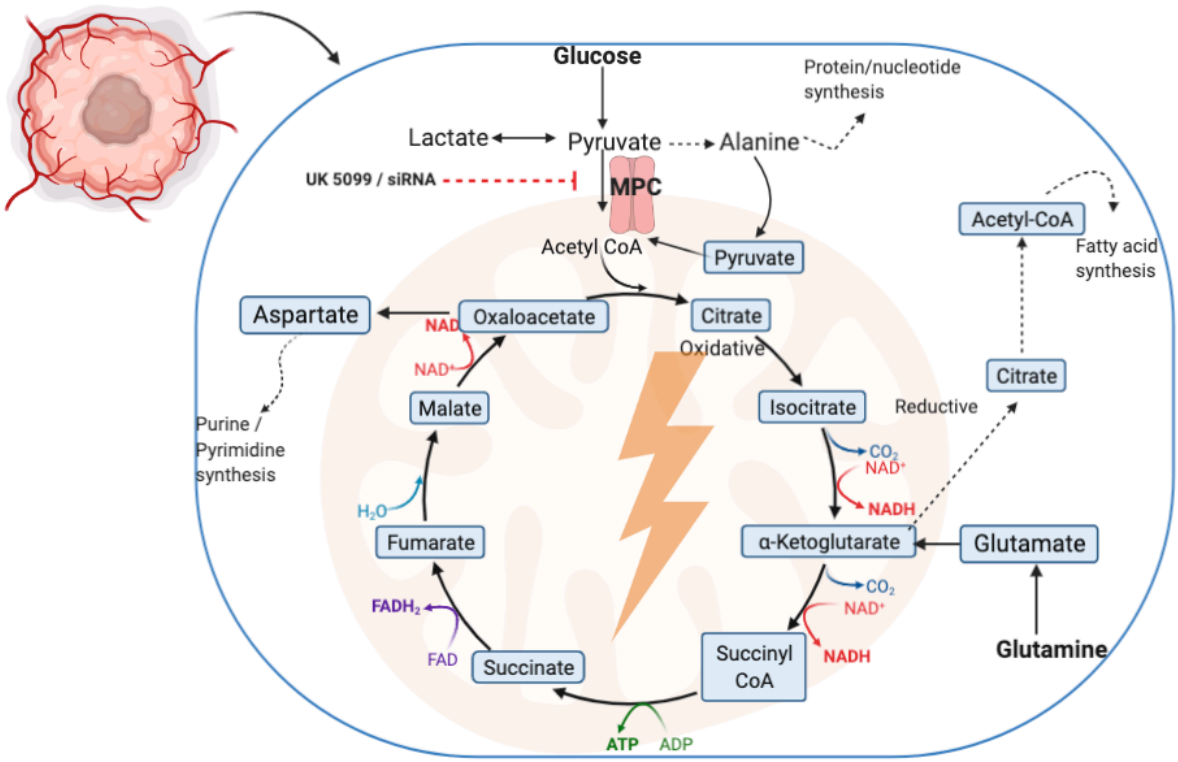

Figure 6.1 A schematic diagram of major fuelling pathways in the tumour microenvironment, including the reverse Warburg effect or glutamine anaplerosis under MPC dysregulation. The images were adapted and modified from Bio Render data base.

Cancer cells can switch the expression of metabolic specific genes depending on the tumour microenvironment (TME). Hypoxic cancer cells are more vulnerable to a nutrient-depleted TME and are able to recycle macromolecules for bioenergetic demands (Jiang et al., 2017). Glycolysis is critical for the hypoxic tumour to fulfil energy demands. The energy demand differs between the quiescent and differentiated state of cancer cells. Utilising glucose to achieve bioenergetic needs depends on which metabolic pathway cells adjust to. The MPC complex acts as a switch to aid metabolic flexibility, and the pyruvate produced from glycolysis is vital for the oncogenic switch

since it's a node between mitochondrial OXPHOS and lactate production (Ruiz-Iglesias and Manes, 2021). The statement holds true in high MPC1 expressing OVCAR3 cells. When MPC was not blocked, but glucose availability was limited (1 mM), OVCAR3 cells showed an increase in *MPC1* expression to maximise pyruvate transport into the TCA cycle, hence signalling cells to utilise more glucose. However, the MPC1 lacking or low expressing PEO1 or PEO4 cell lines did not show any change suggesting a pre-programmed metabolic state to compensate for the loss of *MPC1*. Interestingly, limiting glucose in PEO4 cells increased the expression of *MPC2*, supporting the recent finding by Nagampalli et al., 2015; expressing human recombinant MPC2 without MPC1 in yeast has shown to transport pyruvate successfully *in vitro* and *in vivo* by promoting MPC2 homodimer (Nagampalli et al., 2018). Thus, PEO4 cells may be able to form MPC2 homodimers reflecting increased OCR but not ECAR regardless of UK-5099.

The MPC1 and MPC2 isoforms have different structural features. The 12 kDa protein MPC1 has two transmembrane domains where C and N terminus directing towards the mitochondrial matrix, whereas MPC2 is a 14 kDa protein with three transmembrane domains where the N terminus is directed to the mitochondrial matrix and the C terminus is into the intermembrane space (Bender and Martinou, 2016; Bender et al., 2015). The structural features of the MPC complex may be critical to cellular function, as I show here that *MPC2* depletion at the transcriptional level reduced the DNA concentration in all three cell lines while the combination of *MPC1* and *MPC2* knockdown rescued cells from cell death. Similarly, foetus lacking MPC2 showed impaired pyruvate transport and resulted in foetal death, while in mice, MPC2 ablation resulted in hyperglycaemia (Brivet et al., 2003; Vigueira et al., 2014). This observation shows MPC2 function is critical for normal cellular function. Furthermore, the observation of MPC1 mediated cell rescue in an *MPC1-MPC2* knockdown situation agrees with the first hypothesis proposed for this thesis, *MPC1* deletion could lead to a more aggressive phenotype in epithelial ovarian cancer.

Stable isotope tracing analysis (SITA) in conjunction with metabolomics has shown promising results towards predicting pathways that may offer novel therapeutic targets (Bruntz et al., 2017; Choudhury et al., 2020; Jang et al., 2018; Yang et al., 2014c).

Current research looked at metabolic tracing studies that involved labelling of glucose, lactate, and glutamine, which are linked to glycolysis or OXPHOS. Glycolysis and OXPHOS pathways can easily be tracked via tracing heavy carbon or nitrogen isotopes. Upregulation of glycolysis generates intermediates for the *de novo* synthesis of nucleotides, amino acids, and lipids. Previous metabolic studies using engineered biosensors or ^{13}C-enriched substrates to monitor pyruvate metabolism have shown reduced activity of MPC-dependent metabolic pathways in cancers (Compan et al., 2015b; Yang et al., 2014c).

Over 90% of pyruvate carbon was from labelled glucose, whilst supplementing the media with 10 mM sodium lactate, showed lactate contributed to about 60% of pyruvate carbon. Cancer cells, instead of relying on stromal cells for nutrients, are able to generate more ATP and reducing equivalents (NADPH and NAD+) more rapidly by upregulating pyruvate to lactate pathways (Heiden et al., 2009). However, generation of NAD+ from lactate fermentation is limited due to the consumption of NAD+ during glycolysis to produce GAPDH. To overcome the deficiency in exogenous electron acceptors and to improve sufficient ATP production, cancer cells bypass the GAPDH pathway by excreting the lactate via MCTs (Sullivan et al., 2015). The *MPC1*-depleted OVCAR3 cells replicate the observation of pharmacologically MPC inhibited OVCAR3 cells by showing accumulation of pyruvate both endogenous and exogenous. Cancer cells have demonstrated increased LDHA and LDHB activity for the conversion of pyruvate to lactate and lactate to pyruvate, respectively (Chen et al., 2016; Dennison et al., 2013; Kane, 2014). The SITA revealed the abundance of amino acids derived from glucose and lactate in *MPC1*-depleted OVCAR3 cells. MPC1 lacking cells contributed carbon to amino acids in the TCA cycle, suggesting a role for the reverse Warburg effect. The MID tracing of ^{13}C-glucose and ^{13}C-Lactate revealed the contribution of glucose or lactate to TCA cycle intermediates (e.g., citrate and malate).

Cancer cells activate oncogenic pathways to undergo metabolic reprogramming for uncontrolled proliferation and cancer cell plasticity. For example, cancer cells relying on exogenous NEAAs, which contribute to a malignant phenotype by undergoing epigenetic modification (D'Aniello et al., 2020; Pavlova and Thompson, 2016).

Glutamine is the most abundant amino acid in the body, and glutamine anaplerosis is a key event seen in different cancers when the availability of glucose becomes limited (Gonsalves et al., 2020; Marin-Valencia et al., 2012; Vincent et al., 2015). The proto-oncogene *MYC* mediates glutamine metabolism in cancer, thereby leading to therapy-resistant cancer cells; hence, the majority of cancers, including ovarian cancer cells, have dysregulated *MYC* expression (DeBerardinis and Cheng, 2010; Wise and Thompson, 2010). *MYC* expression can also mediate serine and proline biosynthesis pathways, and *MPC1* expression in colorectal adenocarcinomas is negatively correlated with *MYC* (Schell et al., 2014a). Surprisingly, *MPC1* depletion resulted in more than 50% reduction of *MYC* expression in OVCAR3 cells, suggesting amino acid utilisation by ovarian cancer cells is independent of the *MYC* oncogene. Furthermore, I show an increased abundance of serine and proline via metabolite tracing study where serine was purely derived from labelled glucose or lactate but not glutamine. The serine biosynthesis pathway is essential in breast cancer, contributing 50% of glutamine anaplerotic flux into the TCA cycle in high *PHGDH* expressing breast cancer cells (Possemato et al., 2011b). However, here I showed no change in *PHGDH* while downregulation of *PSAT1* and *PSPH* in *MPC1*-depleted cells.

Circulating concentrations of aspartate are among the lowest of all the circulating amino acids. Aspartate synthesis is dependent on the electron transport chain and is an endogenous metabolic limitation in cancer cell proliferation and tumour growth (Birsoy et al., 2015a; Garcia-Bermudez et al., 2018; Sullivan et al., 2015). Intriguingly, metabolic tracing studies show *MPC1* depletion resulted in a six-fold increase in endogenous aspartate while alanine abundance was significantly reduced. Aspartate was derived from glucose and lactate, but the majority of the aspartate was derived from ^{13}C-glutamine via the TCA cycle. Previous studies have reported increased aspartate and reduced alanine abundances in mouse myoblasts, although in response to *MPC2* knockout but not *MPC1* (Vacanti et al., 2014b). Furthermore, no change in cytosolic *GOT1* (also known as aspartate aminotransferase 1) was seen in *MPC1*-depleted OVCAR3 cells. However, regardless of MPC1 expression levels, ovarian cancer cells showed increased expression of mitochondrial *GOT2* (also knowns as aspartate aminotransferase 2), which facilitates the mitochondrial conversion of OAA to aspartate. Increased aspartate dependence on oxaloacetate and *GOT2* was observed

in the retina during the use of the phosphodiesterase inhibitor, zaprinast (Du et al., 2013). Even though aspartate concentration is much reduced compared to any other circulating amino acids, it plays a major role in *de novo* purine and pyrimidine synthesis. In addition to that, aspartate has a primary role of contributing to impaired electron transport chain in proliferating cells (Birsoy et al., 2015a; Sullivan et al., 2015).

Proline has a unique structure compared to other amino acids, where its functional group (R-group) is bonded to both its central carbon atom and the amine group. Multiple research studies have reported altered proline biosynthesis, its contribution to cancer metabolism and its novel role in cancer proliferation and metastasis (D'Aniello et al., 2020; Elia et al., 2017a; Tanner et al., 2018). Insufficient concentrations of proline in the tumour microenvironment are often inadequate for maintaining high levels of protein synthesis required for proliferating cancer cells (Loayza-Puch et al., 2016b). The data obtained from the current research showed the endogenous proline was derived from neither labelled glucose, lactate, or glutamine. However, an increase in proline metabolising enzymes was seen in *MPC1*-depleted cells. Proline catabolism begins with the conversion of proline to pyrroline-5-carboxylate (P5C). The P5C is then converted to glutamate by pyrroline-5-carboxylate dehydrogenase. Glutamate derived from proline is a precursor for many biosynthetic pathways starting by conversion into α-KG and utilisation in the TCA cycle to produce ATP.

Interestingly pyrroline-5-carboxylate dehydrogenase was significantly increased in the *MPC1*-depleted ovarian cancer cell line. However, there was no change in pyrroline-5-carboxylate synthase upon *MPC1* depletion. The pyrroline-5-carboxylate synthase catalyses the conversion of glutamine-derived glutamate to P5C. Therefore, cells utilising an exogenous proline to recycle glutamate upregulates pyrroline-5-carboxylate dehydrogenase. Moreover, MPC1 deletion in ovarian cancer cells may also be a phenomenon to overcome the generation of ROS in cancer cells. Because previous studies have shown accumulation of proline can lead to higher levels of ROS, and cells are able to overcome ROS by upregulating pyrroline-5-carboxylate dehydrogenase, which converts P5C to glutamate (D'Aniello et al., 2020; Elia et al., 2017a; Phang, 2019). Furthermore, pyrroline-5-carboxylate dehydrogenase deficiency

in Drosophila resulted in swollen mitochondria and hyperprolinemia (He and DiMario, 2011). These data together suggest upregulation of pyrroline-5-carboxylate dehydrogenase is a protective mechanism against mitochondrial damage and cell death.

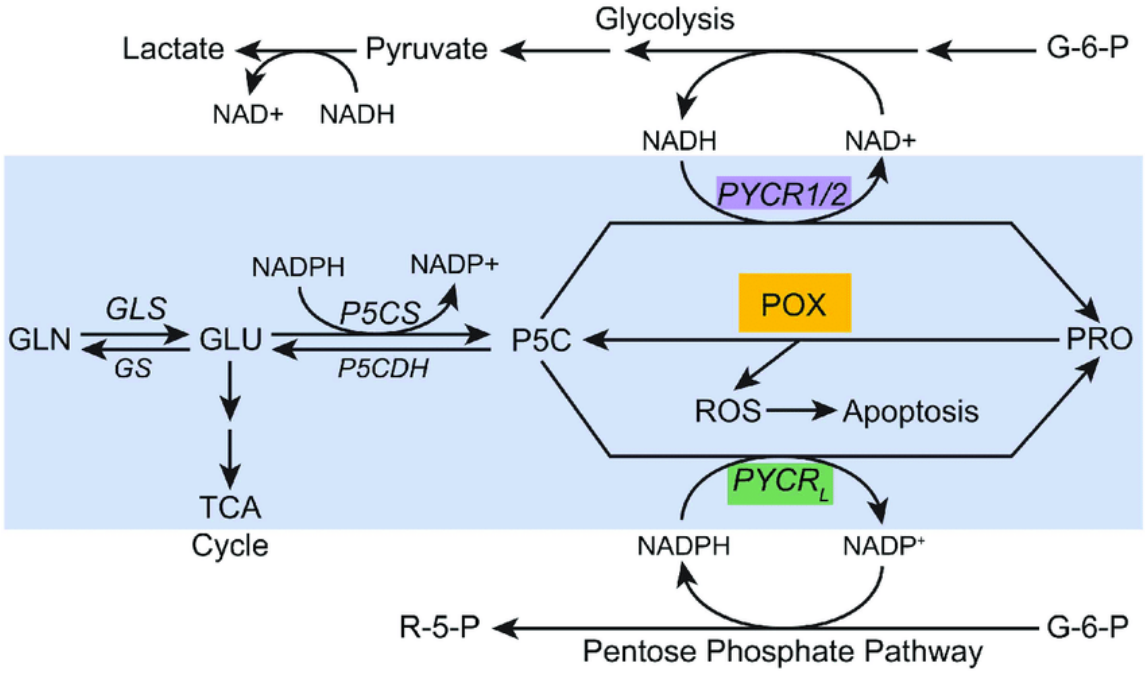

Figure 6.2 A proposed model of proline role in cancer where isozymes PYCR1, PYCR2 and PYCR3/L plays a significant role depending on their origin.
Figure adapted and modified from (Phang and Liu, 2012). The abbreviations represent Glucose 6 phosphate, G-6-P; Glutamine synthase, GS; Ribose 5 phosphate, R-5-P; Glutamine, GLN; Glutaminase, GLS.

Some of the NEAA utilised by proliferating cancer cells become conditionally essential and is achieved by utilising the abundance of ECM proteins. Extracellular matrix formation has critical roles in cancer plasticity and therapy resistance tumours, including ovarian cancer (Adams and Frank, 1980a; Elia et al., 2017a; Hollinshead et al., 2018b; Liu et al., 2015). While ECM provides colonisation and metastasis of cancer cells, ECM degradation offers an abundance of amino acids, particularly proline, glycine, and arginine. Here, I show supplementing proline to *MPC1*-depleted cells on an ECM resulted not just in increased cell number but also cell aggregation, suggesting MPC1-depletion in conjunction with endogenous proline supplementation mediated ECM formation. To further investigate the role of proline in ECM formation, I investigated the expression of key enzymes involved in ECM formation.

The three PYCR isozymes convert P5C to proline and are upregulated in many cancers. Human mitochondrial PYCR1 enzymes are upregulated in various cancer types, and recent studies show blocking of or deleting PYCR1 has been shown to suppress cancer proliferation and metastasis in lung and colorectal cancers (Gao et al., 2020; Yan et al., 2019). Converse to the finding by Gao et al., 2015; the ovarian cancer cell line OVCAR3 showed reduced colony formation under *PYCR1*-depleted condition. Moreover, higher *PYCR1* expression in breast cancer cells is shown to have increased levels of glutaminase, suggesting higher levels of proline and glutamine is a poor prognosis in human epidermal growth factor 2 negative breast cancer (Ding et al., 2017b). However, knocking down *PYCR2* and *PYCR3* in ovarian cancer cells resulted in a drastic reduction of colony growth. Looking at TCGA to compare the mRNA expression of PYCR isozymes, *PYCR2* was frequency was fourth highest of all cancers in ovarian cancer, whilst *PYCR3* is the most highly distorted in epithelial ovarian cancer compared to all other cancers profiled. Therefore, unlike other cancers where increased PYCR1 and glutamine derived proline are key orchestrators of cell proliferation and ECM formation, the *MPC1* depleted cells appear to upregulate cytosolic PYCR3 further to tumour progression, which is independent of the oncogene *MYC*. Moreover, it would be beneficial to trace labelled ^{15}N (Nitrogen-15) isotope of proline and ornithine to understand the fate of proline intermediate cytosolic P5C.

It is now evident that the observed >80% deletion of *MPC1* in HGSOCs mediates not just cancer proliferation but also therapy-resistant tumours via upregulating ECM proteins. After NEAAs, collagen proteins are the major components released during ECM degradation. The desmoplastic subtype of HGSOC represents the poorest prognosis, highlighting the contribution of the ECM in ovarian cancer progression (Cancer Genome Atlas Research, 2011; Tothill et al., 2008). Adhesion of cancer cells to ECM enhances tumorigenicity and confers resistance to chemotherapeutic agents (Sethi et al., 1999). To further look into MPC1-mediated ECM formation and cancer metastasis in therapy-resistant ovarian cancer, it would be beneficial to look at cancer-specific collagen proteins contributing to poor prognosis. Around 25% of all amino acids incorporated into collagen are proline (Guo et al., 2019). Type VI collagen (*COL6A3*) is preferentially expressed in ovarian tumour-derived epithelial cells when compared with normal human ovarian surface epithelium (Ismail et al., 2000) and

correlates with resistance to cisplatin *in vivo*. The type VI collagen (COL6A3) constitutes a major component of the desmoplastic reaction by binding to cancer-associated fibroblast type I collagen fibrils, forming thicker collagen fibres that provide structural support. Collagen VI is associated with metastasis, cell anchoring, remodelling of the ECM, metabolic dysregulation, inflammation, and cancer cell survival (Bonnans et al., 2014; Khan et al., 2009; Lohi et al., 1998; Sethi et al., 1999; Specks et al., 1992). Furthermore, mouse models demonstrate loss of collagen VI results in reduced proliferation and increased tumour cell apoptosis (Park and Scherer, 2012). The survival of cells bound to the ECM may also explain the recurrence of therapy-resistant cancer often seen clinically after chemotherapy (Galluzzi et al., 2012). For instance, the α3 chain of collagen VI (COL6A3) is one of the most highly upregulated differentially expressed genes as a result of cisplatin resistance and remodelling of the ECM through overexpression of collagen VI is associated with cisplatin resistance in ovarian cancer cells (Sherman-Baust et al., 2003; Varma et al., 2005).

In conclusion, the present thesis reports the following findings:

1. MPC1-inhibition in epithelial ovarian cancer cells promotes cell proliferation and pyruvate accumulation via upregulated glycolysis.

2. MPC1 lacking cells repurpose amino acid metabolism for cell survival and nucleotide synthesis while using less efficient MPC2 homo-oligomer for OXPHOS.

3. MPC1 deletion direct cells for proline dependency rather than glutamine. The study showed cells relying on exogenous proline.

4. Unlike the majority of the cancer type where PYCR1 is essential, the mitochondrial enzyme PYCR3 is vital for ovarian cancer proliferation and metastasis.

Even though the result from this thesis showed promising future direction on targeting amino acid metabolism to prevent cell proliferation, there are some limitation on the novelty of this work. Due to limited funding (self-funded) of this PhD research project,

initial work was conducted with four cell lines and narrowed to one cell line for metabolic studies (MPC1 expressing OVCAR3). Therefore, to argue or to prove the novelty of this research, future work must be done on *in vivo* animals models, considering positive and negative controls for MPC. Moreover, it would be beneficial to look at all the possible enzymatic expressions of pathways involved in MPC1 depleted cells. While measuring amino acids like proline is challenging due to its stability, supplementing with heavy isotope labelled both carbon and nitrogen of proline, aspartate, and serine would provide more insight knowledge of metabolic pathways favoured by HGSOC cells. Further investigating these findings in MPC1 depleted tumours in mice will give direct us to find a clinically relevant treatment option for MPC1 depleted tumours by targeting nutrient acquisition by HGSOC cells. Re-investigating the findings from this research study on multiple cells by knocking down MPC1 (including cancer cell lines and also non-cancerous cell line with an ovarian lineage) and simultaneously using animal models will surely help us find a therapeutic target for MPC1 depleted cells which contributes to over 60-70% of HGSOC patients going through relapse after surgery.

Chapter Seven

Appendices

Appendix 1. Ovarian cancer cell lines proliferation study while treated with UK-5099 for 48 h and 72 h

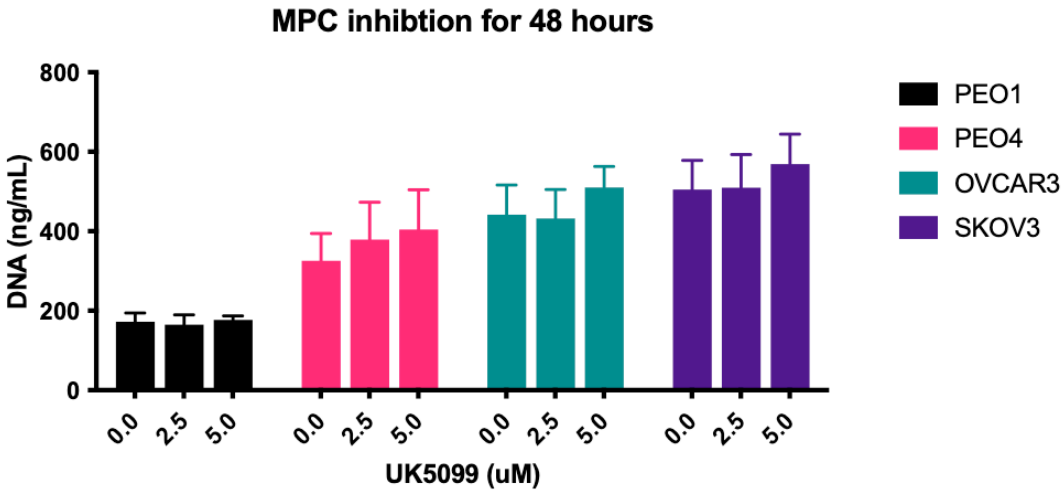

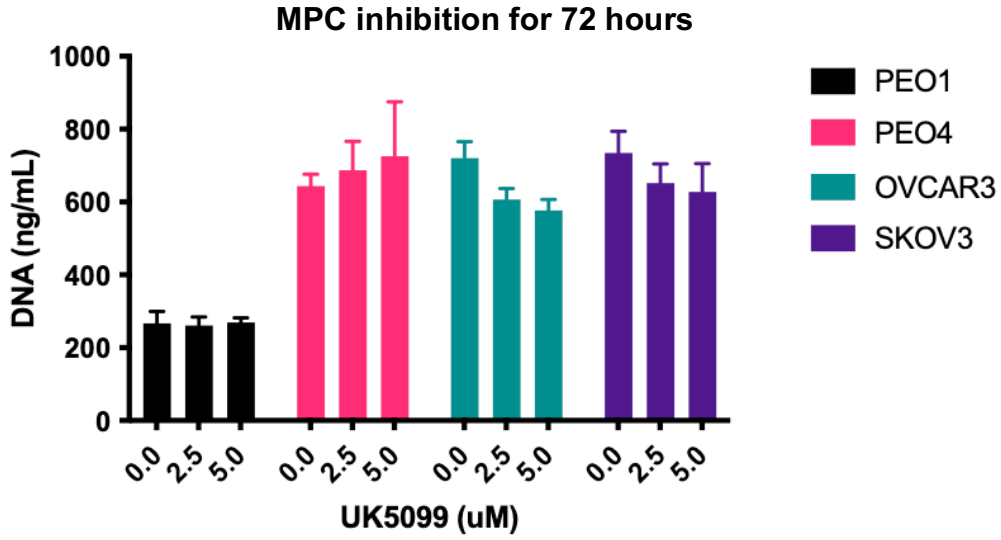

Appendix 2. Whole membrane of differential media western blotting

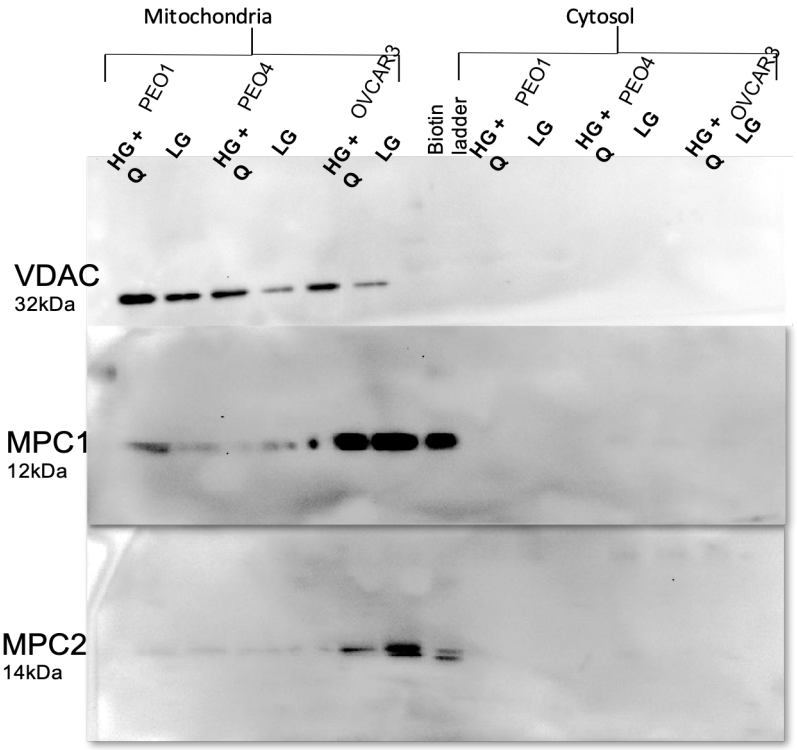

Appendix 3. Colony formation by UK-5099 treated cells

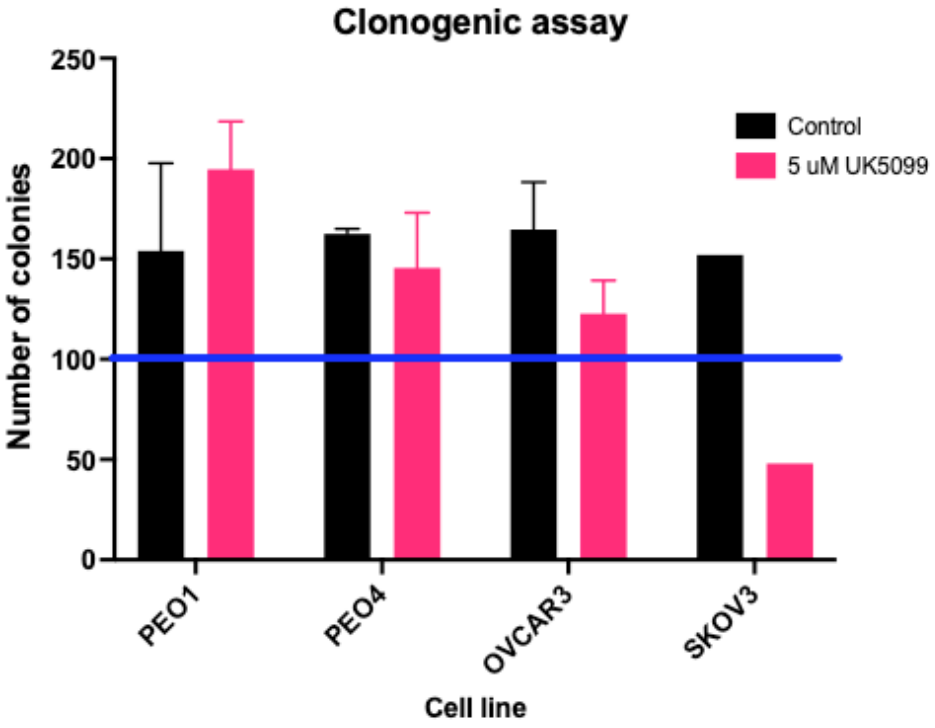

Appendix 4. OVCAR3 cells clonogenic assay whole plate template

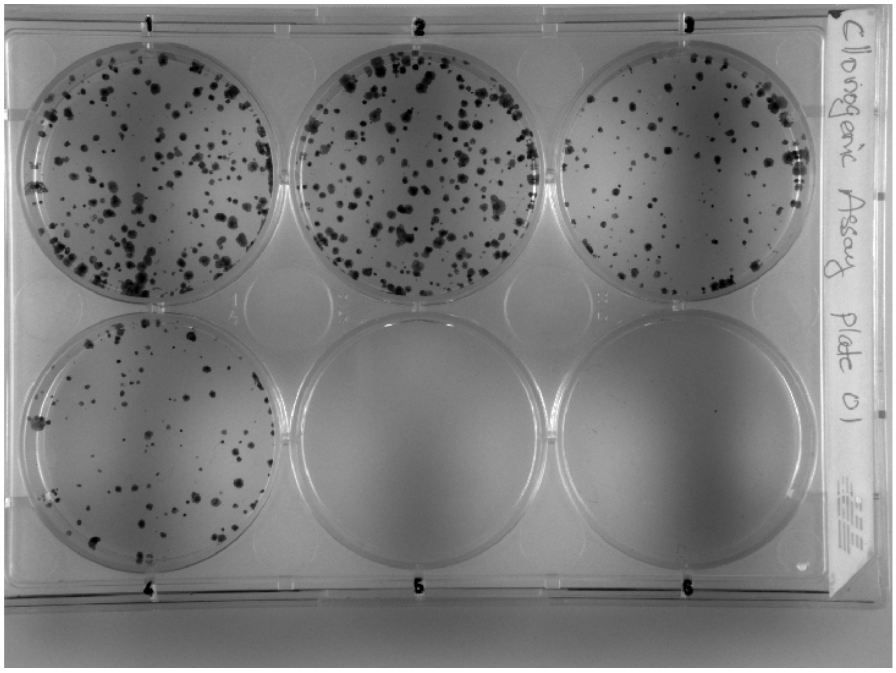

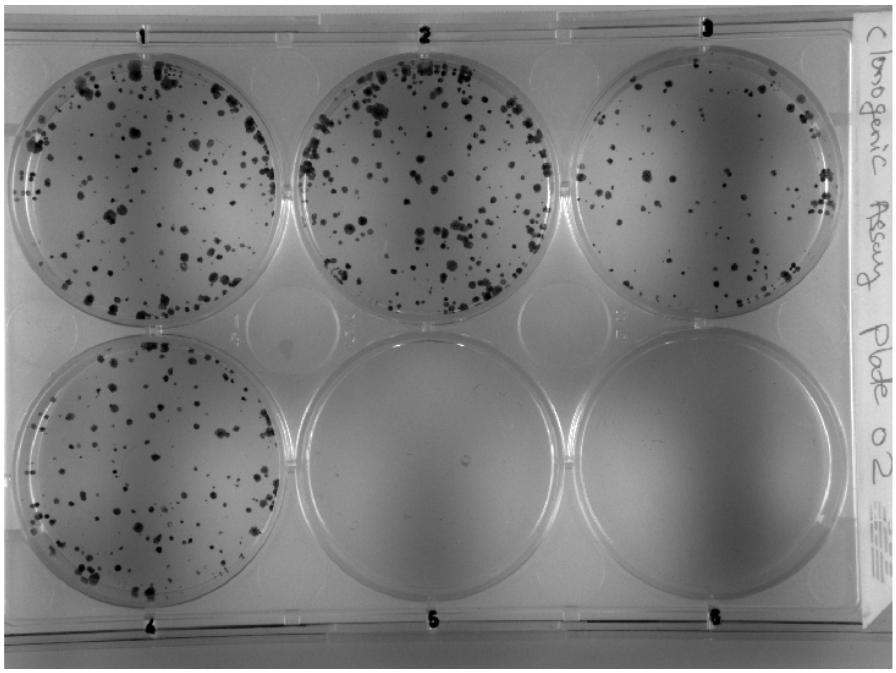

Appendix 5. Accepted and published abstract for European Association for Cancer Research conference, Amsterdam.

Loss of the mitochondrial pyruvate carrier drives 'glutamine addiction', a hallmark of aggressive ovarian cancers

MR Farook, IM Sheldon, D Gonzalez, and JG Cronin
Swansea University Medical School, Institute of Life Science, Swansea SA2 8PP, UK.
https://doi.org/10.1136/esmoopen-2018-EACR25.289

Introduction
Ovarian cancer is the sixth most common cause of cancer deaths in females in the UK. High-grade serous ovarian cancer (HGSOC) comprises 75% of epithelial ovarian carcinomas. Patients with HGSOC initially respond well to platinum-based chemotherapy, but most relapse with therapy resistant disease.
Cancer cells that adapt to their metabolic microenvironment, known as "metabolic flexibility", are more likely to proliferate, metastasise, and be resistant to therapy. In the ascitic fluid of ovarian cancer, glucose concentrations are 3 times lower than in blood, although glutamine concentrations are comparable (0.4 mM vs 0.5 mM, respectively). Consequently, aggressive ovarian cancers have adapted to use glutamine rather than glucose as a fuel source. This phenomenon is termed "glutamine addiction".
Mitochondrial pyruvate carrier (MPC) is responsible for transporting pyruvate, generated through glycolysis, into mitochondria to enable oxidative phosphorylation (OXPHOS). Up to 90% of ovarian cancers have low MPC1 expression, which correlates strongly with poor prognosis across a wide variety of cancers. We postulated that deletion of MPC may force ovarian cancer cells to use glutamine as a fuel source enabling their survival in glucose limited environments.

Materials and Method
Using ovarian cancer cell lines characterised as glutamine-addicted (SKOV3) or glutamine-independent (OVCAR3) as exemplars, the impact of MPC1 on ovarian cancer cell metabolism was investigated by quantitative PCR, Western blotting, metabolic assays, and the Seahorse XF Analyzer.

Results and Discussion
The importance of glutamine to an invasive phenotype is indicated by the observation that SKOV3 cells but not OVCAR3 cells were migratory in the presence of glutamine. The functional significance of MPC as an important link between glycolysis and OXPHOS was shown by inhibiting MPC biochemically with UK5099. UK5099 altered glutamine independent OVCAR3 cells to emulate SKOV3 cells driving a switch to glutamine metabolism for OXPHOS. Whereas non-inhibited OVCAR3 cells, even in glucose free media, did not utilise glutamine for OXPHOS.

Conclusion
The ability to model the switch from glutamine-independent to glutamine-addicted in ovarian cancer cells will allow us to investigate the metabolic and genetic changes that occur in progression from a low- to a highly invasive cancer phenotype of ovarian cancer. This in turn will provide therapeutic targets to halt or slow ovarian tumour progression.

Appendix 6. Post-Graduate conference poster presentation, Swansea university medical school.

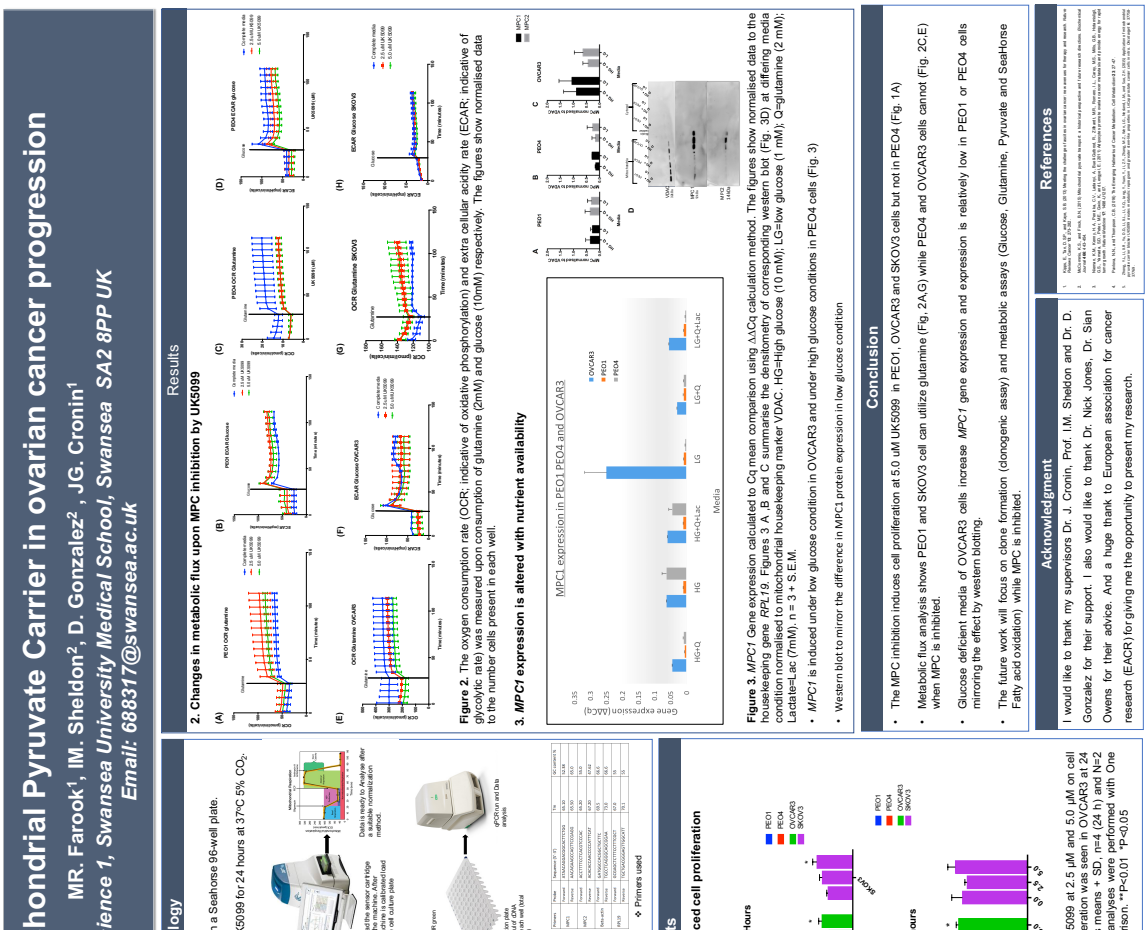

Chapter Eight

Bibliography

8 Bibliography

- Adams, E., and Frank, L. (1980). Metabolism of proline and the hydroxyprolines. Annu. Rev. Biochem. 49, 1005-1061.
- Aggarwal, V., Tuli, H.S., Varol, A., Thakral, F., Yerer, M.B., Sak, K., Varol, M., Jain, A., Khan, A., and Sethi, G. (2019). Role of Reactive Oxygen Species in Cancer Progression: Molecular Mechanisms and Recent Advancements. Biomolecules 9.
- Aguirre-Gamboa, R., Gomez-Rueda, H., Martinez-Ledesma, E., Martinez-Torteya, A., Chacolla-Huaringa, R., Rodriguez-Barrientos, A., Tamez-Pena, J.G., and Trevino, V. (2013). SurvExpress: An Online Biomarker Validation Tool and Database for Cancer Gene Expression Data Using Survival Analysis. Plos One 8.
- Al-Agha, O.M., Huwait, H.F., Chow, C., Yang, W., Senz, J., Kalloger, S.E., Huntsman, D.G., Young, R.H., and Gilks, C.B. (2011). FOXL2 Is a Sensitive and Specific Marker for Sex Cord-Stromal Tumors of the Ovary. Am. J. Surg. Pathol. 35, 484-494.
- Ahmed, N., and Stenvers, K.L. (2013). Getting to know ovarian cancer ascites: opportunities for targeted therapy-based translational research. Frontiers in oncology 3, 256-256.
- Altman, B.J., Stine, Z.E., and Dang, C.V. (2016). From Krebs to clinic: glutamine metabolism to cancer therapy. Nat Rev Cancer 16, 619-634.
- Anand, P., Kunnumakara, A.B., Sundaram, C., Harikumar, K.B., Tharakan, S.T., Lai, O.S., Sung, B.Y., and Aggarwal, B.B. (2008). Cancer is a Preventable Disease that Requires Major Lifestyle Changes. Pharmaceutical Research 25, 2097-2116.
- Anglesio, M.S., Kommoss, S., Tolcher, M.C., Clarke, B., Galletta, L., Porter, H., Damaraju, S., Fereday, S., Winterhoff, B.J., Kalloger, S.E., et al. (2013). Molecular characterization of mucinous ovarian tumours supports a stratified treatment approach with HER2 targeting in 19% of carcinomas. Journal of Pathology 229, 111-120.

- Anderson, A.S., Roberts, P.C., Frisard, M.I., Hulver, M.W., and Schmelz, E.M. (2014). Ovarian tumour-initiating cells display a flexible metabolism. Experimental Cell Research 328, 44-57.
- Angenendt, L., Mikesch, J.H., Gorlich, D., Busch, A., Arnhold, I., Rudack, C., Hartmann, W., Wardelmann, E., Berdel, W.E., Stenner, M., et al. (2018). Stromal collagen type VI associates with features of malignancy and predicts poor prognosis in salivary gland cancer. Cell Oncol (Dordr) 41, 517-525.
- Auersperg, N., Wong, A.S.T., Choi, K.C., Kang, S.K., and Leung, P.C.K. (2001). Ovarian surface epithelium: Biology, endocrinology, and pathology. Endocrine Reviews 22, 255-288.
- Bell, D., Berchuck, A., Birrer, M., Chien, J., Cramer, D.W., Dao, F., Dhir, R., DiSaia, P., Gabra, H., Glenn, P., et al. (2011). Integrated genomic analyses of ovarian carcinoma. Nature 474, 609-615.
- Bensard, C.L., Wisidigama, D.R., Olson, K.A., Berg, J.A., Krah, N.M., Schell, J.C., Nowinski, S.M., Fogarty, S., Bott, A.J., Wei, P., et al. (2019). Regulation of Tumor Initiation by the Mitochondrial Pyruvate Carrier. Cell Metab.
- Bender, T., and Martinou, J.C. (2016). The mitochondrial pyruvate carrier in health and disease: To carry or not to carry? Biochimica Et Biophysica Acta-Molecular Cell Research 1863, 2436-2442.
- Bender, T., Pena, G., and Martinou, J.C. (2015). Regulation of mitochondrial pyruvate uptake by alternative pyruvate carrier complexes. Embo Journal 34, 911-924.
- Banerjee, S., and Kaye, S.B. (2013). New Strategies in the Treatment of Ovarian Cancer: Current Clinical Perspectives and Future Potential. Clinical Cancer Research 19, 961-968.
- Bergfeldt, K., Rydh, B., Granath, F., Gronberg, H., Thalib, L., Adami, H.O., and Hall, P. (2002). Risk of ovarian cancer in breast-cancer patients with a family history of breast or ovarian cancer: a population-based cohort study. Lancet 360, 891-894.
- Berns, E., and Bowtell, D.D. (2012). The Changing View of High-Grade Serous Ovarian Cancer. Cancer Research 72, 2701-2704.
- Birsoy, K., Wang, T., Chen, W.W., Freinkman, E., Abu-Remaileh, M., and Sabatini, D.M. (2015). An Essential Role of the Mitochondrial Electron

Transport Chain in Cell Proliferation Is to Enable Aspartate Synthesis. Cell 162, 540-551.

- Boroughs, L.K., and DeBerardinis, R.J. (2015). Metabolic pathways promoting cancer cell survival and growth. Nature Cell Biology 17, 351-359.
- Bonnans, C., Chou, J., and Werb, Z. (2014). Remodelling the extracellular matrix in development and disease. Nat Rev Mol Cell Biol 15, 786-801.
- Bowman, C.E., Zhao, L., Hartung, T., and Wolfgang, M.J. (2016). Requirement for the Mitochondrial Pyruvate Carrier in Mammalian Development Revealed by a Hypomorphic Allelic Series. Molecular and Cellular Biology 36, 2089-2104.
- Bricker, D.K., Taylor, E.B., Schell, J.C., Orsak, T., Boutron, A., Chen, Y.C., Cox, J.E., Cardon, C.M., Van Vranken, J.G., Dephoure, N., et al. (2012). A Mitochondrial Pyruvate Carrier Required for Pyruvate Uptake in Yeast, Drosophila, and Humans. Science 337, 96-100.
- Brivet, M., Garcia-Cazorla, A., Lyonnet, S., Dumez, Y., Nassogne, M.C., Slama, A., Boutron, A., Touati, G., Legrand, A., and Saudubray, J.M. (2003). Impaired mitochondrial pyruvate importation in a patient and a fetus at risk. Molecular Genetics and Metabolism 78, 186-192.
- Bruntz, R.C., Lane, A.N., Higashi, R.M., and Fan, T.W.M. (2017). Exploring cancer metabolism using stable isotope-resolved metabolomics (SIRM). Journal of Biological Chemistry 292, 11601-11609.
- Bulte, D.B., Palomares, L.A., Parra, C.G., Martinez, J.A., Contreras, M.A., Noriega, L.G., and Ramirez, O.T. (2020). Overexpression of the mitochondrial pyruvate carrier reduces lactate production and increases recombinant protein productivity in CHO cells. Biotechnology and Bioengineering 117, 2633-2647.
- Butler, M., van der Meer, L.T., and van Leeuwen, F.N. (2021). Amino Acid Depletion Therapies: Starving Cancer Cells to Death. Trends in Endocrinology and Metabolism 32, 367-381.
- Cai, F., Mia, Y., Liu, C., Wu, T., Shen, S., Su, X., and Shi, Y. (2018). Pyrroline-5-carboxylate reductase 1 promotes proliferation and inhibits apoptosis in non-small cell lung cancer. Oncology Letters 15, 731-740.

- Cai, H.Y., Kumar, N., Ai, N., Gupta, S., Rath, P., and Baudis, M. (2014). Progenetix: 12 years of oncogenomic data curation. Nucleic Acids Research 42, D1055-D1062.
- Carlson, J.W., Miron, A., Jarboe, E.A., Parast, M.M., Hirsch, M.S., Lee, Y.H., Muto, M.G., Kindelberger, D., and Crum, C.P. (2008). Serous tubal Intraepithelial carcinoma: Its potential role in primary peritoneal serous carcinoma and serous cancer prevention. Journal of Clinical Oncology 26, 4160-4165.
- Cao, H.M., Sekiya, M., Ertunc, M.E., Burak, M.F., Mayers, J.R., White, A., Inouye, K., Rickey, L.M., Ercal, B.C., Furuhashi, M., et al. (2013). Adipocyte Lipid Chaperone aP2 Is a Secreted Adipokine Regulating Hepatic Glucose Production. Cell Metab. 17, 768-778.
- Catasus, L., Bussaglia, E., Rodriguez, I., Gallardo, A., Pons, C., Irving, J.A., and Prat, J. (2004). Molecular genetic alterations in endometrioid carcinomas of the ovary: Similar frequency of beta-catenin abnormalities but lower rate of microsatellite instability and PTEN alterations than in uterine endometrioid carcinomas. Human Pathology 35, 1360-1368.
- Chalhoub, N., and Baker, S.J. (2009). PTEN and the PI3-Kinase Pathway in Cancer. Annual Review of Pathology-Mechanisms of Disease 4, 127-150.
- Chen, Y.J., Mahieu, N.G., Huang, X.J., Singh, M., Crawford, P.A., Johnson, S.L., Gross, R.W., Schaefer, J., and Patti, G.J. (2016). Lactate metabolism is associated with mammalian mitochondria. Nature Chemical Biology 12, 937-+.
- Cheng, C.T., Qi, Y., Wang, Y.C., Chi, K.K., Chung, Y., Ouyang, C., Chen, Y.R., Oh, M.E., Sheng, X.P., Tang, Y.L., et al. (2018). Arginine starvation kills tumour cells through aspartate exhaustion and mitochondrial dysfunction. Communications Biology 1.
- Choudhury, F.K., Hackman, G.L., Lodi, A., and Tiziani, S. (2020). Stable Isotope Tracing Metabolomics to Investigate the Metabolic Activity of Bioactive Compounds for Cancer Prevention and Treatment. Cancers 12.
- Cho, E.S., Cha, Y.H., Kim, H.S., Kim, N.H., and Yook, J.I. (2018). The Pentose Phosphate Pathway as a Potential Target for Cancer Therapy. Biomolecules & Therapeutics 26, 29-38.

- Choi, B.H., and Coloff, J.L. (2019). The Diverse Functions of Non-Essential Amino Acids in Cancer. Cancers 11.
- Chuang, H.C., Chou, C.C., Kulp, S.K., and Chen, C.S. (2014). AMPK as a Potential Anticancer Target - Friend or Foe? Current Pharmaceutical Design 20, 2607-2618.
- Clark, R., Krishnan, V., Schoof, M., Rodriguez, I., Theriault, B., Chekmareva, M., and Rinker-Schaeffert, C. (2013). Milky Spots Promote Ovarian Cancer Metastatic Colonization of Peritoneal Adipose in Experimental Models. American Journal of Pathology 183, 576-591.
- Compan, V., Pierredon, S., Vanderperre, B., Krznar, P., Marchiq, I., Zamboni, N., Pouyssegur, J., and Martinou, J.C. (2015). Monitoring Mitochondrial Pyruvate Carrier Activity in Real Time Using a BRET-Based Biosensor: Investigation of the Warburg Effect. Molecular Cell 59, 491-501.
- Corney, D.C., Flesken-Nikitin, A., Choi, J., and Nikitin, A.Y. (2008). Role of p53 and Rb in ovarian cancer. Adv.Exp.Med.Biol. 622, 99-117.
- Coscia, F., Watters, K.M., Curtis, M., Eckert, M.A., Chiang, C.Y., Tyanova, S., Montag, A., Lastra, R.R., Lengyel, E., and Mann, M. (2016). Integrative proteomic profiling of ovarian cancer cell lines reveals precursor cell associated proteins and functional status. Nat. Commun. 7, 14.
- Craze, M.L., Cheung, H., Jewa, N., Coimbra, N.D.M., Soria, D., El-Ansari, R., Aleskandarany, M.A., Wai Cheng, K., Diez-Rodriguez, M., Nolan, C.C., et al. (2018). MYC regulation of glutamine-proline regulatory axis is key in luminal B breast cancer. Br J Cancer 118, 258-265.
- Danhier, P., Banski, P., Payen, V.L., Grasso, D., Ippolito, L., Sonveaux, P., and Porporato, P.E. (2017). Cancer metabolism in space and time: Beyond the Warburg effect. Biochimica Et Biophysica Acta-Bioenergetics 1858, 556-572.
- D'Aniello, C., Fico, A., Casalino, L., Guardiola, O., Di Napoli, G., Cermola, F., De Cesare, D., Tate, R., Cobellis, G., Patriarca, E.J., et al. (2015). A novel autoregulatory loop between the Gcn2-Atf4 pathway and L-Proline metabolism controls stem cell identity. Cell Death and Differentiation 22, 1094-1105.

- D'Aniello, C., Patriarca, E.J., Phang, J.M., and Minchiotti, G. (2020). Proline Metabolism in Tumor Growth and Metastatic Progression. Frontiers in Oncology 10, 14.
- Dashevsky, O., Varon, D., and Brill, A. (2009). Platelet-derived microparticles promote invasiveness of prostate cancer cells via upregulation of MMP-2 production. International Journal of Cancer 124, 1773-1777.
- Davidson, B., Trope, C., and Reich, R. (2012). Epithelial–Mesenchymal Transition in Ovarian Carcinoma. Frontiers in Oncology 2.
- Dawson, D.M., Goodfriend, T.L., and Kaplan, N.O. (1964). Lactic dehydrogenases: functions of the two types of rates of synthesis of the two major forms can be correlated with metabolic differentiation. Science (New York, N.Y.) 143, 929-933.
- DeBerardinis, R.J., and Cheng, T. (2010). Q's next: the diverse functions of glutamine in metabolism, cell biology and cancer. Oncogene 29, 313-324.
- Dennison, J.B., Molina, J.R., Mitra, S., Gonzalez-Angulo, A.M., Balko, J.M., Kuba, M.G., Sanders, M.E., Pinto, J.A., Gomez, H.L., Arteaga, C.L., et al. (2013). Lactate Dehydrogenase B: A Metabolic Marker of Response to Neoadjuvant Chemotherapy in Breast Cancer. Clinical Cancer Research 19, 3703-3713.
- DeNicola, G.M., Chen, P.H., Mullarky, E., Sudderth, J.A., Hu, Z., Wu, D., Tang, H., Xie, Y., Asara, J.M., Huffman, K.E., et al. (2015). NRF2 regulates serine biosynthesis in non-small cell lung cancer. Nat Genet 47, 1475-1481.
- De Ingeniis, J., Ratnikov, B., Richardson, A.D., Scott, D.A., Aza-Blanc, P., De, S.K., Kazanov, M., Pellecchia, M., Ronai, Z., Osterman, A.L., et al. (2012). Functional specialization in proline biosynthesis of melanoma. PLoS One 7, e45190.
- Desbats, M.A., Giacomini, I., Prayer-Galetti, T., and Montopoli, M. (2020). Metabolic Plasticity in Chemotherapy Resistance. Frontiers in Oncology 10, 20.
- Divakaruni, A.S., Wiley, S.E., Andreyev, A.Y., Rogers, G.W., McDonald, W.G., Colca, J.R., and Murphy, A.N. (2012). Thiazolidinediones inhibit the transport activity of the mitochondrial pyruvate carrier proteins MPC-1 and MPC-2. Biochimica Et Biophysica Acta-Bioenergetics 1817, S34-S34.

- Divakaruni, A.S., Wiley, S.E., Rogers, G.W., Andreyev, A.Y., Petrosyan, S., Loviscach, M., Wall, E.A., Yadava, N., Heuck, A.P., Ferrick, D.A., et al. (2013). Thiazolidinediones are acute, specific inhibitors of the mitochondrial pyruvate carrier. Proceedings of the National Academy of Sciences of the United States of America 110, 5422-5427.
- Ding, J., Kuo, M.L., Su, L., Xue, L., Luh, F., Zhang, H., Wang, J., Lin, T.G., Zhang, K., Chu, P., et al. (2017). Human mitochondrial pyrroline-5-carboxylate reductase 1 promotes invasiveness and impacts survival in breast cancers. Carcinogenesis 38, 519-531.
- Dixit, S.N., Seyer, J.M., and Kang, A.H. (1977). Covalent structure of collagen - amino-acid-sequence of chymotryptic peptides from carboxyl-terminal region of alpha-2-cb3 of chick-skin collagen. European Journal of Biochemistry 81, 599-607.
- Doherty, J.R., Yang, C.Y., Scott, K.E.N., Cameron, M.D., Fallahi, M., Li, W.M., Hall, M.A., Amelio, A.L., Mishra, J.K., Li, F.Z., et al. (2014). Blocking Lactate Export by Inhibiting the Myc Target MCT1 Disables Glycolysis and Glutathione Synthesis. Cancer Research 74, 908-920.
- Doherty, J.R., and Cleveland, J.L. (2013). Targeting lactate metabolism for cancer therapeutics. Journal of Clinical Investigation 123, 3685-3692.
- Du, J.H., Cleghorn, W.M., Contreras, L., Lindsay, K., Rountree, A.M., Chertov, A.O., Turner, S.J., Sahaboglu, A., Linton, J., Sadilek, M., et al. (2013). Inhibition of Mitochondrial Pyruvate Transport by Zaprinast Causes Massive Accumulation of Aspartate at the Expense of Glutamate in the Retina. Journal of Biological Chemistry 288, 36129-36140.
- Eboli, M.L., Paradies, G., Galeotti, T., and Papa, S. (1977). Pyruvate transport in tumour-cell mitochondria. Biochimica Et Biophysica Acta 460, 183-187.
- Elia, I., Broekaert, D., Christen, S., Boon, R., Radaelli, E., Orth, M.F., Verfaillie, C., Grunewald, T.G.P., and Fendt, S.M. (2017). Proline metabolism supports metastasis formation and could be inhibited to selectively target metastasizing cancer cells. Nat. Commun. 8, 11.
- Epifano, C., and Perez-Moreno, M. (2012). Crossroads of integrins and cadherins in epithelia and stroma remodeling. Cell Adhesion & Migration 6, 261-273.

- Erickson, B.K., Conner, M.G., and Landen, C.N. (2013). The role of the fallopian tube in the origin of ovarian cancer. American Journal of Obstetrics and Gynecology 209, 409-414.
- Fathalla, M.F. (1971). Incessant ovulation - factor in ovarian neoplasia. Lancet 2, 163-&.
- Fathalla, M.F. (2013). Incessant ovulation and ovarian cancer - a hypothesis re-visited. Facts, views & vision in ObGyn 5, 292-297.
- Faubert, B., Boily, G., Izreig, S., Griss, T., Samborska, B., Dong, Z.F., Dupuy, F., Chambers, C., Fuerth, B.J., Viollet, B., et al. (2013). AMPK Is a Negative Regulator of the Warburg Effect and Suppresses Tumor Growth In Vivo. Cell Metab. 17, 113-124.
- Faubert, B., Vincent, E.E., Griss, T., Samborska, B., Izreig, S., Svensson, R.U., Mamer, O.A., Avizonis, D., Shackelford, D.B., Shaw, R.J., et al. (2014). Loss of the tumour suppressor LKB1 promotes metabolic reprogramming of cancer cells via HIF-1 alpha. Proceedings of the National Academy of Sciences of the United States of America 111, 2554-2559.
- Faubert, B., Li, K.Y., Cai, L., Hensley, C.T., Kim, J., Zacharias, L.G., Yang, C.D., Do, Q.N., Doucette, S., Burguete, D., et al. (2017). Lactate Metabolism in Human Lung Tumors. Cell 171, 358-+.
- Folkins, A.K., Jarboe, E.A., Roh, M.H., and Crum, C.P. (2009). Precursors to pelvic serous carcinoma and their clinical implications. Gynecologic Oncology 113, 391-396.
- Franken, N.A.P., Rodermond, H.M., Stap, J., Haveman, J., and van Bree, C. (2006). Clonogenic assay of cells in vitro. Nat. Protoc. 1, 2315-2319.
- Fu, Y.J., Liu, S.S., Yin, S.H.L., Niu, W.H., Xiong, W., Tan, M., Li, G.Y., and Zhou, M. (2017). The reverse Warburg effect is likely to be an Achilles' heel of cancer that can be exploited for cancer therapy. Oncotarget 8, 57813-57825.
- Gangi, A., Cass, I., Paik, D., Barmparas, G., Karlan, B., Dang, C., Li, A., Walsh, C., Rimel, B.J., and Amersi, F.F. (2014). Breast Cancer Following Ovarian Cancer in BRCA Mutation Carriers. Jama Surgery 149, 1306-1313.
- Garcia-Bermudez, J., Baudrier, L., La, K., Zhu, X.G., Fidelin, J., Sviderskiy, V.O., Papagiannakopoulos, T., Molina, H., Snuderl, M., Lewis, C.A., et al. (2018). Aspartate is a limiting metabolite for cancer cell proliferation under

hypoxia and in tumours (vol 20, pg 775, 2018). Nature Cell Biology 20, 1228-1228.

- Galluzzi, L., Senovilla, L., Vitale, I., Michels, J., Martins, I., Kepp, O., Castedo, M., and Kroemer, G. (2012). Molecular mechanisms of cisplatin resistance. Oncogene 31, 1869-1883.
- Gonsalves, W.I., Jang, J.S., Jessen, E., Hitosugi, T., Evans, L.A., Jevremovic, D., Pettersson, X.M., Bush, A.G., Gransee, J., Anderson, E.I., et al. (2020). In vivo assessment of glutamine anaplerosis into the TCA cycle in human pre-malignant and malignant clonal plasma cells. Cancer & Metabolism 8.
- Gao, Y.W., Luo, L.H., Xie, Y.C., Zhao, Y., Yao, J., and Liu, X.L. (2020). PYCR1 knockdown inhibits the proliferation, migration, and invasion by affecting JAK/STAT signaling pathway in lung adenocarcinoma. Molecular Carcinogenesis 59, 503-511.
- Guo, L., Cui, C., Zhang, K., Wang, J., Wang, Y., Lu, Y., Chen, K., Yuan, J., Xiao, G., Tang, B., et al. (2019). Kindlin-2 links mechano-environment to proline synthesis and tumor growth. Nat Commun 10, 845.
- Hagedorn, C.H., and Phang, J.M. (1986). Catalytic transfer of hydride ions from nadph to oxygen by the interconversions of proline and delta-1-pyrroline-5-carboxylate. Arch. Biochem. Biophys. 248, 166-174.
- Halestrap, A.P. (1975). Mitochondrial pyruvate carrier - kinetics and specificity for substrates and inhibitors. Biochemical Journal 148, 85-96.
- Halestrap, A.P. (1976). Mechanism of inhibition of mitochondrial pyruvate transporter by alpha-cyanocinnamate derivatives. Biochemical Journal 156, 181-183.
- Halestrap, A.P., and Denton, R.M. (1974). Specific inhibition of pyruvate transport in rat-liver mitochondria and human erythrocytes by alpha-cyano-4-hydroxycinnamate. Biochemical Journal 138, 313-316.
- Hanahan, D., and Weinberg, R.A. (2000). The hallmarks of cancer. Cell 100, 57-70.
- Hanahan, D., and Weinberg, R.A. (2011). Hallmarks of Cancer: The Next Generation. Cell 144, 646-674.
- Hay, N. (2016). Reprogramming glucose metabolism in cancer: can it be exploited for cancer therapy? Nat. Rev. Cancer 16, 635-649.

- He, F., and DiMario, P.J. (2011). Drosophila delta-1-pyrroline-5-carboxylate dehydrogenase (P5CDh) is required for proline breakdown and mitochondrial integrity-Establishing a fly model for human type II hyperprolinemia. Mitochondrion 11, 397-404.
- Heiden, M.G.V., Cantley, L.C., and Thompson, C.B. (2009). Understanding the Warburg Effect: The Metabolic Requirements of Cell Proliferation. Science 324, 1029-1033.
- Hensley, C.T., Faubert, B., Yuan, Q., Lev-Cohain, N., Jin, E., Kim, J., Jiang, L., Ko, B., Skelton, R., Loudat, L., et al. (2016). Metabolic Heterogeneity in Human Lung Tumors. Cell 164, 681-694.
- Heravi-Moussavi, A., Anglesio, M.S., Cheng, S.W.G., Senz, J., Yang, W., Prentice, L., Fejes, A.P., Chow, C., Tone, A., Kalloger, S.E., et al. (2012). Recurrent Somatic DICER1 Mutations in Nonepithelial Ovarian Cancers. New England Journal of Medicine 366, 234-242.
- Herzig, S., Raemy, E., Montessuit, S., Veuthey, J.L., Zamboni, N., Westermann, B., Kunji, E.R.S., and Martinou, J.C. (2012). Identification and Functional Expression of the Mitochondrial Pyruvate Carrier. Science 337, 93-96.
- Hildyard, J.C.W., Ammala, C., Dukes, I.D., Thomson, S.A., and Halestrap, A.P. (2005). Identification and characterisation of a new class of highly specific and potent inhibitors of the mitochondrial pyruvate carrier. Biochimica Et Biophysica Acta-Bioenergetics 1707, 221-230.
- Hollinshead, K.E.R., Munford, H., Eales, K.L., Bardella, C., Li, C.J., Escribano-Gonzalez, C., Thakker, A., Nonnenmacher, Y., Kluckova, K., Jeeves, M., et al. (2018). Oncogenic IDH1 Mutations Promote Enhanced Proline Synthesis through PYCR1 to Support the Maintenance of Mitochondrial Redox Homeostasis. Cell Reports 22, 3107-3114.
- Hu, J., Liu, Z.Q., and Wang, X.P. (2013). Does TP53 mutation promote ovarian cancer metastasis to omentum by regulating lipid metabolism? Medical Hypotheses 81, 515-520.
- Huynh, T.Y.L., Zareba, I., Baszanowska, W., Lewoniewska, S., and Palka, J. (2020). Understanding the role of key amino acids in regulation of proline dehydrogenase/prolineoxidase (prodh/pox) dependent apoptosis/autophagy as

an approach to targeted cancer therapy. Molecular and Cellular Biochemistry 466, 35-44.

- Ismail, R.S., Baldwin, R.L., Fang, J., Browning, D., Karlan, B.Y., Gasson, J.C., and Chang, D.D. (2000). Differential gene expression between normal and tumor-derived ovarian epithelial cells. Cancer Res 60, 6744-6749.
- Jang, C., Chen, L., and Rabinowitz, J.D. (2018). Metabolomics and Isotope Tracing. Cell 173, 822-837.
- Jiang, M., Gu, X., Feng, X., Fan, Z., Ding, F., and Liu, Y. (2009). The molecular characterization of the brain protein 44-like (Brp44l) gene of Gekko japonicus and its expression changes in spinal cord after tail amputation. Molecular Biology Reports 36, 215-220.
- Jiang, W.G., Bryce, R.P., and Horrobin, D.F. (1998). Essential fatty acids: molecular and cellular basis of their anti-cancer action and clinical implications. Critical Reviews in Oncology Hematology 27, 179-209.
- Jiang, Z.F., Wang, M., Xu, J.L., and Ning, Y.J. (2017). Hypoxia promotes mitochondrial glutamine metabolism through HIF1 alpha-GDH pathway in human lung cancer cells. Biochemical and Biophysical Research Communications 483, 32-38.
- Jeong, H., Yu, Y., Johansson, H.J., Schroeder, F.C., Lehtio, J., and Vacanti, N.M. (2021). Correcting for Naturally Occurring Mass Isotopologue Abundances in Stable-Isotope Tracing Experiments with PolyMID. Metabolites 11.
- Kane, D.A. (2014). Lactate oxidation at the mitochondria: a lactate-malate-aspartate shuttle at work. Frontiers in Neuroscience 8.
- Khan, S.M., Funk, H.M., Thiolloy, S., Lotan, T.L., Hickson, J., Prins, G.S., Drew, A.F., and Rinker-Schaeffer, C.W. (2010). In vitro metastatic colonization of human ovarian cancer cells to the omentum. Clinical & Experimental Metastasis 27, 185-196.
- Khan, T., Muise, E.S., Iyengar, P., Wang, Z.V., Chandalia, M., Abate, N., Zhang, B.B., Bonaldo, P., Chua, S., and Scherer, P.E. (2009). Metabolic dysregulation and adipose tissue fibrosis: role of collagen VI. Mol Cell Biol 29, 1575-1591.

- Kakkad, S.M., Solaiyappan, M., O'Rourke, B., Stasinopoulos, I., Ackerstaff, E., Raman, V., Bhujwalla, Z.M., and Glunde, K. (2010). Hypoxic Tumor Microenvironments Reduce Collagen I Fiber Density. Neoplasia 12, 608-617.
- Kim, J., Coffey, D.M., Creighton, C.J., Yu, Z.F., Hawkins, S.M., and Matzuk, M.M. (2012). High-grade serous ovarian cancer arises from fallopian tube in a mouse model. Proceedings of the National Academy of Sciences of the United States of America 109, 3921-3926.
- Kim, J., Yu, L., Chen, W., Xu, Y., Wu, M., Todorova, D., Tang, Q., Feng, B., Jiang, L., He, J., et al. (2019). Wild-Type p53 Promotes Cancer Metabolic Switch by Inducing PUMA-Dependent Suppression of Oxidative Phosphorylation. Cancer Cell 35, 191-+.
- Kindelberger, D.W., Lee, Y., Miron, A., Hirsch, M.S., Feltmate, C., Medeiros, F., Callahan, M.J., Garner, E.O., Gordon, R.W., Birch, C., et al. (2007). Intraepithelial carcinoma of the fimbria and pelvic serous carcinoma: Evidence for a causal relationship. American Journal of Surgical Pathology 31, 161-169.
- Klingenb.M (1970). Mitochondria metabolite transport. Febs Letters 6, 145-&.
- Koundouros, N., and Poulogiannis, G. (2020). Reprogramming of fatty acid metabolism in cancer. British Journal of Cancer 122, 4-22.
- Kuo, M.L., Lee, M.B., Tang, M., den Besten, W., Hu, S., Sweredoski, M.J., Hess, S., Chou, C.M., Changou, C.A., Su, M., et al. (2016). PYCR1 and PYCR2 Interact and Collaborate with RRM2B to Protect Cells from Overt Oxidative Stress. Sci Rep 6, 18846.
- Kyriazi, S., Kaye, S.B., and deSouza, N.M. (2010). Imaging ovarian cancer and peritoneal metastases-current and emerging techniques. Nature Reviews Clinical Oncology 7, 381-393.
- Lafleur, M.A., Drew, A.F., de Sousa, E.L., Blick, T., Bills, M., Walker, E.C., Williams, E.D., Waltham, M., and Thompson, E.W. (2005). Upregulation of matrix metalloproteinases (MMPs) in breast cancer xenografts: A major induction of stromal MMP-13. International Journal of Cancer 114, 544-554.
- Landen, C.N., Birrer, M.J., and Sood, A.K. (2008). Early events in the pathogenesis of epithelial ovarian cancer. Journal of Clinical Oncology 26, 995-1005.

- Langdon, S.P., Lawrie, S.S., Hay, F.G., Hawkes, M.M., McDonald, A., Hayward, I.P., Schol, D.J., Hilgers, J., Leonard, R.C.F., and Smyth, J.F. (1988). Characterization and properties of 9 human ovarian adenocarcinoma cell-lines. Cancer Research 48, 6166-6172.
- Langyel, E. (2010). Ovarian Cancer Development and Metastasis. American Journal of Pathology 177, 1053-1064.
- Le, A., Lane, A.N., Hamaker, M., Bose, S., Gouw, A., Barbi, J., Tsukamoto, T., Rojas, C.J., Slusher, B.S., Zhang, H.X., et al. (2012). Glucose-Independent Glutamine Metabolism via TCA Cycling for Proliferation and Survival in B Cells. Cell Metab. 15, 110-121.
- Lee, Y., Miron, A., Drapkin, R., Nucci, M.R., Medeiros, F., Saleemuddin, A., Garder, J., Birch, C., Mou, H., Gordon, R.W., et al. (2007). A candidate precursor to serous carcinoma that originates in the distal fallopian tube. Journal of Pathology 211, 26-35.
- Li, X.L., Han, G.Y., Li, X.R., Kan, Q.C., Fan, Z.R., Li, Y.Q., Ji, Y.S., Zhao, J., Zhang, M.Z., Grigalavicius, M., et al. (2017a). Mitochondrial pyruvate carrier function determines cell stemness and metabolic reprogramming in cancer cells. Oncotarget 8, 46363-46380.
- Li, Y.Q., Li, X.R., Kan, Q.C., Zhang, M.Z., Li, X.L., Xu, R.P., Wang, J.S., Yu, D.D., Goscinski, M.A., Wen, J.G., et al. (2017b). Mitochondrial pyruvate carrier function is negatively linked to Warburg phenotype in vitro and malignant features in esophageal squamous cell carcinomas. Oncotarget 8, 1058-1073.
- Li, X.L., Ji, Y.S., Han, G.Y., Li, X.R., Fan, Z.R., Li, Y.Q., Zhong, Y.L., Cao, J., Zhao, J., Zhang, M.Z., et al. (2016). MPC1 and MPC2 expressions are associated with favorable clinical outcomes in prostate cancer. BMC Cancer 16, 12.
- Li, D., Wang, C.Q., Mal, P.F., Yu, Q.G., Gu, M.Q., Dong, L.Q., Jiang, W.J., Pan, S.H., Xie, C.M., Han, J.H., et al. (2018). PGC1 alpha promotes cholangiocarcinoma metastasis by upregulating PDHA1 and MPC1 expression to reverse the Warburg effect. Cell Death & Disease 9.
- Li, A.M., and Ye, J. (2020). The PHGDH enigma: Do cancer cells only need serine or also a redox modulator? Cancer Lett 476, 97-105.

- Lieu, E.L., Nguyen, T., Rhyne, S., and Kim, J. (2020). Amino acids in cancer. Experimental and Molecular Medicine 52, 15-30.
- Liu, W., Hancock, C.N., Fischer, J.W., Harman, M., and Phang, J.M. (2015). Proline biosynthesis augments tumour cell growth and aerobic glycolysis: involvement of pyridine nucleotides. Scientific Reports 5.
- Lisio, M.A., Fu, L.L., Goyeneche, A., Gao, Z.H., and Telleria, C. (2019). High-Grade Serous Ovarian Cancer: Basic Sciences, Clinical and Therapeutic Standpoints. International Journal of Molecular Sciences 20.
- Liu, W., Le, A., Hancock, C., Lane, A.N., Dang, C.V., Fan, T.W.M., and Phang, J.M. (2012). Reprogramming of proline and glutamine metabolism contributes to the proliferative and metabolic responses regulated by oncogenic transcription factor c-MYC. Proceedings of the National Academy of Sciences of the United States of America 109, 8983-8988.
- Livak, K.J., and Schmittgen, T.D. (2001). Analysis of relative gene expression data using real-time quantitative PCR and the 2(T)(-Delta C) method. Methods 25, 402-408.
- Loayza-Puch, F., Rooijers, K., Buil, L.C.M., Zijlstra, J., Vrielink, J.F.O., Lopes, R., Ugalde, A.P., van Breugel, P., Hofland, I., Wesseling, J., et al. (2016). Tumour-specific proline vulnerability uncovered by differential ribosome codon reading. Nature 530, 490-+.
- Locasale, J.W. (2013). Serine, glycine, and one-carbon units: cancer metabolism in full circle. Nature Reviews Cancer 13, 572-583.
- Lohi, J., Leivo, I., Oivula, J., Lehto, V.P., and Virtanen, I. (1998). Extracellular matrix in renal cell carcinomas. Histol Histopathol 13, 785-796.
- Lu, F.I., Gilks, C.B., Mulligan, A.M., Ryan, P., Allo, G., Sy, K., Shaw, P.A., Pollett, A., and Clarke, B.A. (2012). Prevalence of Loss of Expression of DNA Mismatch Repair Proteins in Primary Epithelial Ovarian Tumors. International Journal of Gynecological Pathology 31, 524-531.
- Mangili, G., Bergamini, A., Taccagni, G., Gentile, C., Panina, P., Vigano, P., and Candiani, M. (2012). Unraveling the two entities of endometrioid ovarian cancer: A single center clinical experience. Gynecologic Oncology 126, 403-407.

- Marin-Valencia, I., Yang, C.D., Mashimo, T., Cho, S., Baek, H., Yang, X.L., Rajagopalan, K.N., Maddie, M., Vemireddy, V., Zhao, Z.Z., et al. (2012). Analysis of Tumor Metabolism Reveals Mitochondrial Glucose Oxidation in Genetically Diverse Human Glioblastomas in the Mouse Brain In Vivo. Cell Metab. 15, 827-837.
- Matulonis, U.A., Sood, A.K., Fallowfield, L., Howitt, B.E., Sehouli, J., and Karlan, B.Y. (2016). Ovarian cancer. Nature Reviews Disease Primers 2, 22.
- McCleland, M.L., Adler, A.S., Shang, Y.L., Hunsaker, T., Truong, T., Peterson, D., Torres, E., Li, L., Haley, B., Stephan, J.P., et al. (2012). An Integrated Genomic Screen Identifies LDHB as an Essential Gene for Triple-Negative Breast Cancer. Cancer Research 72, 5812-5823.
- McGuirk, S., Gravel, S.-P., Deblois, G., Papadopoli, D.J., Faubert, B., Wegner, A., Hiller, K., Avizonis, D., Akavia, U.D., Jones, R.G., et al. (2013). PGC-1alpha supports glutamine metabolism in breast cancer. Cancer & metabolism 1, 22-22.
- McCommis, K.S., and Finck, B.N. (2015). Mitochondrial pyruvate transport: a historical perspective and future research directions. Biochem. J. 466, 443-454.
- McConechy, M.K., Anglesio, M.S., Kalloger, S.E., Yang, W., Senz, J., Chow, C., Heravi-Moussavi, A., Morin, G.B., Mes-Masson, A.M., Carey, M.S., et al. (2011). Subtype-specific mutation of PPP2R1A in endometrial and ovarian carcinomas. Journal of Pathology 223, 567-573.
- Medicine, I.o., National Academies of Sciences, E., and Medicine (2016). Ovarian Cancers: Evolving Paradigms in Research and Care. (Washington, DC: The National Academies Press).
- Mendesmourao, J., Halestrap, A.P., Crisp, D.M., and Pogson, C.I. (1975). involvement of mitochondrial pyruvate transport in pathways of gluconeogenesis from serine and alanine in isolated rat and mouse-liver cells. Febs Letters 53, 29-32.
- Metallo, C.M., Gameiro, P.A., Bell, E.L., Mattaini, K.R., Yang, J.J., Hiller, K., Jewell, C.M., Johnson, Z.R., Irvine, D.J., Guarente, L., et al. (2012). Reductive glutamine metabolism by IDH1 mediates lipogenesis under hypoxia. Nature 481, 380-U166.

- Mukherjee, A., Chiang, C., Daifotis, H., Nieman, K., Fahrmann, J., Lastra, R., Romero, I., Fiehn, O. and Lengyel, E., 2020. Adipocyte-Induced FABP4 Expression in Ovarian Cancer Cells Promotes Metastasis and Mediates Carboplatin Resistance. Cancer Research 80, 1748-1761.
- Naora, H. (2005). Developmental Patterning in the wrong context - The paradox of epithelial ovarian cancers. Cell Cycle 4, 1033-1035.
- Nazemi, M., and Rainero, E. (2020). Cross-Talk Between the Tumor Microenvironment, Extracellular Matrix, and Cell Metabolism in Cancer. Frontiers in Oncology 10, 7.
- Nagampalli, R.S.K., Quesnay, J.E.N., Adamoski, D., Islam, Z., Birch, J., Sebinelli, H.G., Girard, R., Ascencao, C.F.R., Fala, A.M., Pauletti, B.A., et al. (2018). Human mitochondrial pyruvate carrier 2 as an autonomous membrane transporter. Scientific Reports 8.
- Nakayama, T., Al-Maawali, A., El-Quessny, M., Rajab, A., Khalil, S., Stoler, J.M., Tan, W.H., Nasir, R., Schmitz-Abe, K., Hill, R.S., et al. (2015). Mutations in PYCR2, Encoding Pyrroline-5-Carboxylate Reductase 2, Cause Microcephaly and Hypomyelination. Am J Hum Genet 96, 709-719.
- Natarajan, S.K., Zhu, W., Liang, X., Zhang, L., Demers, A.J., Zimmerman, M.C., Simpson, M.A., and Becker, D.F. (2012). Proline dehydrogenase is essential for proline protection against hydrogen peroxide-induced cell death. Free Radic Biol Med 53, 1181-1191.
- Nicholson, L.J., Smith, P.R., Hiller, L., Szlosarek, P.W., Kimberley, C., Sehouli, J., Koensgen, D., Mustea, A., Schmid, P., and Crook, T. (2009). Epigenetic silencing of argininosuccinate synthetase confers resistance to platinum-induced cell death but collateral sensitivity to arginine auxotrophy in ovarian cancer. International Journal of Cancer 125, 1454-1463.
- Nieman, K.M., Kenny, H.A., Penicka, C.V., Ladanyi, A., Buell-Gutbrod, R., Zillhardt, M.R., Romero, I.L., Carey, M.S., Mills, G.B., Hotamisligil, G.S., et al. (2011). Adipocytes promote ovarian cancer metastasis and provide energy for rapid tumour growth. Nature Medicine 17, 1498-U1207.
- Nigdelioglu, R., Hamanaka, R.B., Meliton, A.Y., O'Leary, E., Witt, L.J., Cho, T., Sun, K., Bonham, C., Wu, D., Woods, P.S., et al. (2016). Transforming

Growth Factor (TGF)-beta Promotes de Novo Serine Synthesis for Collagen Production. J Biol Chem 291, 27239-27251.

- Nilsson, R., Jain, M., Madhusudhan, N., Sheppard, N.G., Strittmatter, L., Kampf, C., Huang, J., Asplund, A., and Mootha, V.K. (2014). Metabolic enzyme expression highlights a key role for MTHFD2 and the mitochondrial folate pathway in cancer. Nat Commun 5, 3128.
- Otto, A.M. (2016). Warburg effect(s)-a biographical sketch of Otto Warburg and his impacts on tumour metabolism. Cancer & Metabolism 4.
- Papa, S., Francavilla, A., Paradies, G., and Meduri, B. (1971). Transport of pyruvate in rat liver mitochondria. Febs Letters 12, 285-+.
- Pandhare, J., Donald, S.P., Cooper, S.K., and Phang, J.M. (2009). Regulation and Function of Proline Oxidase Under Nutrient Stress. Journal of Cellular Biochemistry 107, 759-768.
- Paradies, G., Capuano, F., Palombini, G., Galeotti, T., and Papa, S. (1983). Transport of pyruvate in mitochondria from different tumour-cells. Cancer Research 43, 5068-5071.
- Park, S., Safi, R., Liu, X.J., Baldi, R., Liu, W., Liu, J., Locasale, J.W., Chang, C.Y., and McDonnell, D.P. (2019). Inhibition of ERR alpha Prevents Mitochondrial Pyruvate Uptake Exposing NADPH-Generating Pathways as Targetable Vulnerabilities in Breast Cancer. Cell Reports 27, 3587-+.
- Patch, A.M., Christie, E.L., Etemadmoghadam, D., Garsed, D.W., George, J., Fereday, S., Nones, K., Cowin, P., Alsop, K., Bailey, P.J., et al. (2015). Whole-genome characterization of chemoresistant ovarian cancer. Nature 521, 489-494.
- Patra, K.C., and Hay, N. (2014). The pentose phosphate pathway and cancer. Trends in Biochemical Sciences 39, 347-354.
- Pavlova, N.N., and Thompson, C.B. (2016). The Emerging Hallmarks of Cancer Metabolism. Cell Metabolism 23, 27-47.
- Phang, J.M. (1985). The regulatory functions of proline and pyrroline-5-carboxylic acid. Curr. Top. Cell. Regul. 25, 91-132.
- Phang, J.M. (2019). Proline Metabolism in Cell Regulation and Cancer Biology: Recent Advances and Hypotheses. Antioxid. Redox Signal. 30, 635-649.

- Phang, J.M., Liu, W., Hancock, C., and Christian, K.J. (2012). The proline regulatory axis and cancer. Front Oncol 2, 60.
- Phang, J.M., Liu, W., Hancock, C.N., and Fischer, J.W. (2015). Proline metabolism and cancer: emerging links to glutamine and collagen. Curr Opin Clin Nutr Metab Care 18, 71-77.
- Possemato, R., Marks, K.M., Shaul, Y.D., Pacold, M.E., Kim, D., Birsoy, K., Sethumadhavan, S., Woo, H.K., Jang, H.G., Jha, A.K., et al. (2011). Functional genomics reveal that the serine synthesis pathway is essential in breast cancer. Nature 476, 346-U119.
- Potter, M., Newport, E., and Morten, K.J. (2016). The Warburg effect: 80 years on. Biochemical Society Transactions 44, 1499-1505.
- Prat, J., Ribe, A., and Gallardo, A. (2005). Hereditary ovarian cancer. Human Pathology 36, 861-870.
- Pradeep, S., Kim, S.W., Wu, S.Y., Nishimura, M., Chaluvally-Raghavan, P., Miyake, T., Pecot, C.V., Kim, S.J., Choi, H.J., Bischoff, F.Z., et al. (2014). Hematogenous Metastasis of Ovarian Cancer: Rethinking Mode of Spread. Cancer Cell 26, 77-91.
- Przybycin, C.G., Kurman, R.J., Ronnett, B.M., Shih, I.M., and Vang, R. (2010). Are All Pelvic (Nonuterine) Serous Carcinomas of Tubal Origin? American Journal of Surgical Pathology 34, 1407-1416.
- Qie, S., Chu, C., Li, W.H., Wang, C.G., and Sang, N.L. (2014). ErbB2 Activation Upregulates Glutaminase 1 Expression Which Promotes Breast Cancer Cell Proliferation. Journal of Cellular Biochemistry 115, 498-509.
- Rasmussen, H.N., van Hall, G., and Rasmussen, U.F. (2002). Lactate dehydrogenase is not a mitochondrial enzyme in human and mouse vastus lateralis muscle. Journal of Physiology-London 541, 575-580.
- Rauckhorst, A.J., and Taylor, E.B. (2016). Mitochondrial pyruvate carrier function and cancer metabolism. Current Opinion in Genetics & Development 38, 102-109.
- Reid, B.M., Permuth, J.B., and Sellers, T.A. (2017). Epidemiology of ovarian cancer: a review. Cancer Biol. Med. 14, 9-32.
- Rintoul, R.C., and Sethi, T. (2001). The role of extracellular matrix in small-cell lung cancer. Lancet Oncol 2, 437-442.

- Ruiz-Iglesias, A., and Manes, S. (2021). The Importance of Mitochondrial Pyruvate Carrier in Cancer Cell Metabolism and Tumorigenesis. Cancers 13.
- Ryan, N.A.J., Evans, D.G., Green, K., and Crosbie, E.J. (2017). Pathological features and clinical behavior of Lynch syndrome-associated ovarian cancer. Gynecologic Oncology 144, 491-495.
- Salani, R., Backes, F.J., Fung, M.F.K., Holschneider, C.H., Parker, L.P., Bristow, R.E., and Goff, B.A. (2011). Posttreatment surveillance and diagnosis of recurrence in women with gynecologic malignancies: Society of Gynecologic Oncologists recommendations. American Journal of Obstetrics and Gynecology 204, 466-478.
- Santidrian, A.F., Matsuno-Yagi, A., Ritland, M., Seo, B.B., Leboeuf, S.E., Gay, L.J., Yagi, T., and Felding-Habermann, B. (2013). Mitochondrial complex I activity and NAD+/NADH balance regulate breast cancer progression. Journal of Clinical Investigation 123, 1068-1081.
- Sandulache, V.C., Ow, T.J., Pickering, C.R., Frederick, M.J., Zhou, G., Fokt, I., Davis-Malesevich, M., Priebe, W., and Myers, J.N. (2011). Glucose, Not Glutamine, Is the Dominant Energy Source Required for Proliferation and Survival of Head and Neck Squamous Carcinoma Cells. Cancer 117, 2926-2938.
- Schell, J.C., Olson, K.A., Jiang, L., Hawkins, A.J., Van Vranken, J.G., Xie, J.X., Egnatchik, R.A., Earl, E.G., DeBerardinis, R.J., and Rutter, J. (2014). A Role for the Mitochondrial Pyruvate Carrier as a Repressor of the Warburg Effect and Colon Cancer Cell Growth. Molecular Cell 56, 400-413.
- Schneider, D., Halperin, R., Langer, R., Bukovsky, I., and Herman, A. (1997). Peritoneal fluid lactate dehydrogenase in ovarian cancer. Gynecol. Oncol. 66, 399-404.
- Sethi, T., Rintoul, R.C., Moore, S.M., MacKinnon, A.C., Salter, D., Choo, C., Chilvers, E.R., Dransfield, I., Donnelly, S.C., Strieter, R., et al. (1999). Extracellular matrix proteins protect small cell lung cancer cells against apoptosis: a mechanism for small cell lung cancer growth and drug resistance in vivo. Nat Med 5, 662-668.
- Sherman-Baust, C.A., Weeraratna, A.T., Rangel, L.B., Pizer, E.S., Cho, K.R., Schwartz, D.R., Shock, T., and Morin, P.J. (2003). Remodeling of the

extracellular matrix through overexpression of collagen VI contributes to cisplatin resistance in ovarian cancer cells. Cancer Cell 3, 377-386.

- Seidman, J.D., Horkayne-Szakaly, I., Haiba, M., Boice, C.R., Kurman, R.J., and Ronnett, B.M. (2004). The histologic type and stage distribution of ovarian carcinomas of surface epithelial origin. International Journal of Gynecological Pathology 23, 41-44.
- Shaw, P.A., Rouzbahman, M., Pizer, E.S., Pintilie, M., and Begley, H. (2009). Candidate serous cancer precursors in fallopian tube epithelium of BRCA1/2 mutation carriers. Mod. Pathol. 22, 1133-1138.
- Siegel, R.L., Miller, K.D., and Jemal, A. (2016). Cancer Statistics, 2016. Ca-a Cancer Journal for Clinicians 66, 7-30.
- Singh, N., Gilks, C.B., Wilkinson, N., and McCluggage, W.G. (2015). Assessment of a new system for primary site assignment in high-grade serous carcinoma of the fallopian tube, ovary, and peritoneum. Histopathology 67, 331-337.
- Singer, G., Oldt, R., Cohen, Y., Wang, B.G., Sidransky, D., Kurman, R.J., and Shih, I.M. (2003). Mutations in BRAF and KRAS characterize the development of low-grade ovarian serous carcinoma. Journal of the National Cancer Institute 95, 484-486.
- Son, J., Lyssiotis, C.A., Ying, H.Q., Wang, X.X., Hua, S.J., Ligorio, M., Perera, R.M., Ferrone, C.R., Mullarky, E., Shyh-Chang, N., et al. (2013). Glutamine supports pancreatic cancer growth through a KRAS-regulated metabolic pathway (vol 496, pg 101, 2013). Nature 499.
- Sonveaux, P., Vegran, F., Schroeder, T., Wergin, M.C., Verrax, J., Rabbani, Z.N., De Saedeleer, C.J., Kennedy, K.M., Diepart, C., Jordan, B.F., et al. (2008). Targeting lactate-fueled respiration selectively kills hypoxic tumour cells in mice. Journal of Clinical Investigation 118, 3930-3942.
- Souba, W.W. (1993). Glutamine and cancer. Annals of Surgery 218, 715-728.
- Spinelli, J.B., Yoon, H., Ringel, A.E., Jeanfavre, S., Clish, C.B., and Haigis, M.C. (2017). Metabolic recycling of ammonia via glutamate dehydrogenase supports breast cancer biomass. Science 358, 941-946.
- Stark, R., and Kibbey, R.G. (2014). The mitochondrial isoform of phosphoenolpyruvate carboxykinase (PEPCK-M) and glucose homeostasis:

Has it been overlooked? Biochimica Et Biophysica Acta-General Subjects 1840, 1313-1330.

- Stallings-Mann, M., and Radisky, D. (2007). Matrix metalloproteinase-induced malignancy in mammary epithelial cells. Cells Tissues Organs 185, 104-110.
- Still, E.R., and Yuneva, M.O. (2019). Hopefully devoted to Q: targeting glutamine addiction in cancer (vol 116, pg 1375, 2017). British Journal of Cancer 120, 957-957.
- Sullivan, L.B., Gui, D.Y., Hosios, A.M., Bush, L.N., Freinkman, E., and Vander Heiden, M.G. (2015). Supporting Aspartate Biosynthesis Is an Essential Function of Respiration in Proliferating Cells. Cell 162, 552-563.
- Sun, L., Song, L., Wan, Q., Wu, G., Li, X., Wang, Y., Wang, J., Liu, Z., Zhong, X., He, X., et al. (2015). cMyc-mediated activation of serine biosynthesis pathway is critical for cancer progression under nutrient deprivation conditions. Cell Res 25, 429-444.
- Szlosarek, P.W., Grimshaw, M.J., Wilbanks, G.D., Hagemann, T., Wilson, J.L., Burke, F., Stamp, G., and Balkwill, F.R. (2007). Aberrant regulation of argininosuccinate synthetase by TNF-alpha in human epithelial ovarian cancer. International Journal of Cancer 121, 6-11.
- Tanner, J.J., Fendt, S.M., and Becker, D.F. (2018). The Proline Cycle As a Potential Cancer Therapy Target. Biochemistry 57, 3433-3444.
- Tang, L., Zeng, J., Geng, P., Fang, C., Wang, Y., Sun, M., Wang, C., Wang, J., Yin, P., Hu, C., et al. (2018). Global Metabolic Profiling Identifies a Pivotal Role of Proline and Hydroxyproline Metabolism in Supporting Hypoxic Response in Hepatocellular Carcinoma. Clin Cancer Res 24, 474-485.
- Tang, C., Jardim, D.L., and Hong, D. (2014). MET in ovarian cancer Metastasis and resistance? Cell Cycle 13, 1220-1221.
- Tibiletti, M.G., Trubia, M., Ponti, E., Sessa, L., Acquati, F., Furlan, D., Bernasconi, B., Fichera, M., Mihalich, A., Ziegler, A., et al. (1998). Physical map of the D6S149-D6S193 region on chromosome 6q27 and its involvement in benign surface epithelial ovarian tumours. Oncogene 16, 1639-1642.
- Tothill, R.W., Tinker, A.V., George, J., Brown, R., Fox, S.B., Lade, S., Johnson, D.S., Trivett, M.K., Etemadmoghadam, D., Locandro, B., et al.

(2008). Novel molecular subtypes of serous and endometrioid ovarian cancer linked to clinical outcome. Clin Cancer Res 14, 5198-5208.

- Usher-Smith, J.A., Fraser, J.A., Bailey, P.S.J., Griffin, J.L., and Huang, C.L.H. (2006). The influence of intracellular lactate and H+ on cell volume in amphibian skeletal muscle. Journal of Physiology-London 573, 799-818.
- Uysal, K.T., Scheja, L., Wiesbrock, S.M., Bonner-Weir, S., and Hotamisligil, G.S. (2000). Improved glucose and lipid metabolism in genetically obese mice lacking aP2. Endocrinology 141, 3388-3396.
- Vacanti, N.M., Divakaruni, A.S., Green, C.R., Parker, S.J., Henry, R.R., Ciaraldi, T.P., Murphy, A.N., and Metallo, C.M. (2014). Regulation of Substrate Utilization by the Mitochondrial Pyruvate Carrier. Molecular Cell 56, 425-435.
- Vang, R., Shih, I.M., and Kurman, R.J. (2009). Ovarian Low-grade and High-grade Serous Carcinoma Pathogenesis, Clinicopathologic and Molecular Biologic Features, and Diagnostic Problems. Advances in Anatomic Pathology 16, 267-282.
- Vanhove, K., Derveaux, E., Graulus, G.J., Mesotten, L., Thomeer, M., Noben, J.P., Guedens, W., and Adriaensens, P. (2019). Glutamine Addiction and Therapeutic Strategies in Lung Cancer. International Journal of Molecular Sciences 20.
- Varma, R.R., Hector, S.M., Clark, K., Greco, W.R., Hawthorn, L., and Pendyala, L. (2005). Gene expression profiling of a clonal isolate of oxaliplatin-resistant ovarian carcinoma cell line A2780/C10. Oncol Rep 14, 925-932.
- Vaughan, S., Coward, J.I., Bast, R.C., Berchuck, A., Berek, J.S., Brenton, J.D., Coukos, G., Crum, C.C., Drapkin, R., Etemadmoghadam, D., et al. (2011). Rethinking ovarian cancer: recommendations for improving outcomes. Nature Reviews Cancer 11, 719-725.
- Vincent, E.E., Sergushichev, A., Griss, T., Gingras, M.C., Samborska, B., Ntimbane, T., Coelho, P.P., Blagih, J., Raissi, T.C., Choiniere, L., et al. (2015). Mitochondrial Phosphoenolpyruvate Carboxykinase Regulates Metabolic Adaptation and Enables Glucose-Independent Tumor Growth. Molecular Cell 60, 195-207.

- Vigueira, P.A., McCommis, K.S., Schweitzer, G.G., Remedi, M.S., Chambers, K.T., Fu, X.R., McDonald, W.G., Cole, S.L., Colca, J.R., Kletzien, R.F., et al. (2014). Mitochondrial Pyruvate Carrier 2 Hypomorphism in Mice Leads to Defects in Glucose-Stimulated Insulin Secretion. Cell Reports 7, 2042-2053.
- Wang, L.M., Xu, M.F., Qin, J., Lin, S.C., Lee, H.J., Tsai, S.Y., and Tsai, M.J. (2016). MPC1, a key gene in cancer metabolism, is regulated by COUP-TFII in human prostate cancer. Oncotarget 7, 14673-14683.
- Wang, Y., Nicholes, K., and Shih, I.M. (2020). The Origin and Pathogenesis of Endometriosis. In Annual Review of Pathology: Mechanisms of Disease, Vol 15, 2020.
- Warburg, O., Wind, F., and Negelein, E. (1927). The metabolism of tumours in the body. The Journal of general physiology 8, 519-530.
- Wei, P., Dove, K.K., Bensard, C., Schell, J.C., and Rutter, J. (2018). The Force Is Strong with This One: Metabolism (Over) powers Stem Cell Fate. Trends in Cell Biology 28, 551-559.
- Wilde, L., Roche, M., Domingo-Vidal, M., Tanson, K., Philp, N., Curry, J., and Martinez-Outschoorn, U. (2017). Metabolic coupling and the Reverse Warburg Effect in cancer: Implications for novel biomarker and anticancer agent development. Seminars in Oncology 44, 198-203.
- Wiegand, K.C., Shah, S.P., Al-Agha, O.M., Zhao, Y.J., Tse, K., Zeng, T., Senz, J., McConechy, M.K., Anglesio, M.S., Kalloger, S.E., et al. (2010). ARID1A Mutations in Endometriosis-Associated Ovarian Carcinomas. New England Journal of Medicine 363, 1532-1543.
- Wiberg, C., Hedbom, E., Khairullina, A., Lamande, S.R., Oldberg, A., Timpl, R., Morgelin, M., and Heinegard, D. (2001). Biglycan and decorin bind close to the n-terminal region of the collagen VI triple helix. J Biol Chem 276, 18947-18952.
- Xiang, L.S., Mou, J., Shao, B., Wei, Y.Q., Liang, H.J., Takano, N., Semenza, G.L., and Xie, G.F. (2019). Glutaminase 1 expression in colorectal cancer cells is induced by hypoxia and required for tumour growth, invasion, and metastatic colonization. Cell Death & Disease 10.
- Yan, K., Xu, X., Wu, T., Li, J., Cao, G., Li, Y.M., and Ji, Z.Z. (2019). Knockdown of PYCR1 inhibits proliferation, drug resistance and EMT in

colorectal cancer cells by regulating STAT3-Mediated p38 MAPK and NF-kappa B signalling pathway. Biochemical and Biophysical Research Communications 520, 486-491.

- Yang, J., Nie, J., Ma, X.L., Wei, Y.Q., Peng, Y., and Wei, X.W. (2019). Targeting PI3K in cancer: mechanisms and advances in clinical trials. Molecular Cancer 18.
- Yang, C.D., Sudderth, J., Dang, T.Y., Bachoo, R.G., McDonald, J.G., and DeBerardinis, R.J. (2009). Glioblastoma Cells Require Glutamate Dehydrogenase to Survive Impairments of Glucose Metabolism or Akt Signaling. Cancer Research 69, 7986-7993.
- Yang, L.F., Moss, T., Mangala, L.S., Marini, J., Zhao, H.Y., Wahlig, S., Armaiz-Pena, G., Jiang, D.H., Achreja, A., Win, J., et al. (2014). Metabolic shifts toward glutamine regulate tumour growth, invasion, and bioenergetics in ovarian cancer. Molecular Systems Biology 10, 23.
- Yang, L.F., Venneti, S., and Nagrath, D. (2017). Glutaminolysis: A Hallmark of Cancer Metabolism. Annual Review of Biomedical Engineering, Vol 19 19, 163-194.
- Yang, S., Hwang, S., Kim, M., Seo, S.B., Lee, J.H., and Jeong, S.M. (2018). Mitochondrial glutamine metabolism via GOT2 supports pancreatic cancer growth through senescence inhibition. Cell Death & Disease 9.
- Yoo, H.C., Yu, Y.C., Sung, Y., and Han, J.M. (2020). Glutamine reliance in cell metabolism. Experimental & molecular medicine.
- Zacksenhaus, E., Shrestha, M., Liu, J.C., Vorobieva, I., Chung, P.E.D., Ju, Y.J., Nir, U., and Jiang, Z. (2017). Mitochondrial OXPHOS Induced by RB1 Deficiency in Breast Cancer: Implications for Anabolic Metabolism, Stemness, and Metastasis. Trends in Cancer 3, 768-779.
- Zhao, Y.Q., Zhao, X., Chen, V., Feng, Y., Wang, L., Croniger, C., Conlon, R.A., Markowitz, S., Fearon, E., Puchowicz, M., et al. (2019). Colorectal cancers utilize glutamine as an anaplerotic substrate of the TCA cycle in vivo. Scientific Reports 9.
- Zhong, Y.L., Li, X.R., Yu, D.D., Li, X.L., Li, Y.Q., Long, Y., Yuan, Y., Ji, Z.Y., Zhang, M.Z., Wen, J.G., et al. (2015). Application of mitochondrial pyruvate carrier blocker UK-5099 creates metabolic reprogram and greater

stem-like properties in LnCap prostate cancer cells in vitro. Oncotarget 6, 37758-37769.

- Zhou, X., Xiong, Z.J., Xiao, S.M., Zhou, J., Ding, Z., Tang, L.C., Chen, X.D., Xu, R., and Zhao, P. (2017). Overexpression of MPC1 inhibits the proliferation, migration, invasion, and stem cell-like properties of gastric cancer cells. Oncotargets and Therapy 10, 5151-5163.